

Microbially-mediated transformation and mobilization of Fe-organic associations in the soil

Von der Naturwissenschaftlichen Fakultät der
Gottfried Wilhelm Leibniz Universität Hannover

zur Erlangung des Grades
Doktorin der Naturwissenschaften (Dr. rer. nat.)

genehmigte Dissertation

von

Christine Poggenburg, Dipl.- Geow.

2018

Referent: Prof. Dr. rer. nat. habil. Georg Guggenberger

Korreferent: Prof. Dr. rer. nat. habil. Robert Mikutta

Korreferent: Prof. Dr. Ruben Kretzschmar

Tag der Promotion: 07.12.2017

This thesis was written using 100 % recycled words.

Abstract

Iron (Fe) oxyhydroxides are important constituents of the soil mineral phase known to stabilize organic matter (OM) under oxic conditions. In an anoxic milieu, however, these Fe-organic associations are exposed to microbial reduction, releasing OM and associated contaminants into the soil solution and exposing OM to decomposition, thus causing the release of greenhouse gases (CO₂, CH₄, N₂O). At present, only few studies have addressed the influence of adsorbed natural OM (NOM) on the reactivity of Fe-organic associations. The overall aim of this thesis was to systematically assess the impact of the composition and concentration of both adsorbed and coprecipitated naturally occurring OM on microbial, ligand-promoted, and electrochemical reduction and dissolution of Fe-organic associations, regarding (i) electron shuttling, (ii) complexation of Fe(II,III), (iii) surface site coverage and/or pore blockage, (iv) aggregation, and (v) crystallinity.

Adsorption complexes and coprecipitates with varying carbon loadings were synthesized combining different Fe oxyhydroxides (ferrihydrite, lepidocrocite, goethite, hematite, magnetite) with NOM of different origin (extracellular polymeric substances from *Bacillus subtilis*, OM extracted from soil Oi and Oa horizons). The samples were characterized by nuclear magnetic resonance spectroscopy (NMR), X-ray diffraction (XRD), Fourier transform infrared spectroscopy (FTIR), X-ray photoelectron spectroscopy (XPS), N₂ gas adsorption, electrophoretic mobility and particle size measurements, OM desorption, and mediated electrochemical reduction (MER). Incubation experiments under anaerobic conditions were conducted for 16 days comparing two different strains of dissimilatory Fe(III)-reducing bacteria (*Shewanella putrefaciens*, *Geobacter metallireducens*).

Microbial reduction of the pure Fe oxyhydroxides was controlled by the specific surface area (SSA) and solubility of the minerals. For *Shewanella putrefaciens*, the Fe reduction of adsorption complexes strongly correlated with the concentration of potentially usable electron-shuttling molecules for NOM concentrations < 2 mg C L⁻¹, whereas for *Geobacter metallireducens*, Fe reduction depended on the particle size and thus aggregation of the adsorption complexes.

Similarly, Fe-OM coprecipitate reduction by *Shewanella putrefaciens* was influenced by the amount of available electron shuttling molecules provided by the NOM, whereas the Fe(III) reduction by *Geobacter metallireducens* as well as abiotic Fe(III) reduction was influenced by particle size and NOM-induced aggregation. The specific surface area proved to be a poor predictor of Fe reduction of Fe-OM coprecipitates.

Siderophore-mediated dissolution experiments with desferrioxamine-B (DFOB) were conducted at both pH 4 and pH 7. At pH 4, adsorbed OM provided a more effective protection against DFOB due to its larger sorption affinity. At pH 7, the surface site blockage by adsorbed OM at comparable C loadings was less effective, while less aggregated particles were more prone to dissolution. The accelerating and inhibiting influence of OM coprecipitated with Fe on DFOB-promoted dissolution largely varied with its composition.

These diverging results suggest that the influence of OM on the stability of Fe-organic associations in soils cannot easily be assessed without considering the heterogeneous composition of soil OM and the microbial soil community. Understanding environmental Fe and C cycling, therefore, requires experimental approaches extending beyond the use of pure Fe oxyhydroxides and model organisms.

Key words: soil organic matter; iron oxyhydroxides; microbial reduction

Zusammenfassung

Organische Substanz (OM) im Boden, die in einem oxischen Milieu durch Adsorption an Eisenoxidhydroxide stabilisiert wird, kann unter anoxischen Bedingungen durch mikrobielle Reduktion mobilisiert werden. Dieses führt zur Abbau der OM, der daraus resultierenden Emission von Treibhausgasen (CO_2 , CH_4 , N_2O) und Freisetzung assoziierter Schwermetalle und organischer Schadstoffe. Der mögliche Einfluss natürlicher adsorbierter natürlicher OM auf die Reaktivität eisenorganischer Assoziationen wurde bisher jedoch nur unzureichend erforscht. Das übergeordnete Ziel der Arbeit bestand deshalb darin, systematisch den Einfluss der Zusammensetzung und Konzentration adsorbierter und kopräzipitierter natürlich vorkommender OM auf die mikrobielle, Ligand-induzierte und elektrochemische Reduktion und Auflösung eisenorganischer Assoziationen zu untersuchen, speziell im Hinblick auf (i) Elektronenshuttling, (ii) Komplexierung von Fe(II,III), (iii) Blockierung der Oberflächen und/oder Poren, (iv) Aggregation und (v) Kristallinität.

Adsorptionskomplexe und Kopräzipitate mit unterschiedlichen C-Gehalten wurden aus verschiedenen Eisenoxyhydroxiden (Ferrihydrit, Lepidokrokit, Goethit, Hämatit, Magnetit) und OM unterschiedlicher Herkunft (extrazelluläre polymere Substanz isoliert aus *Bacillus subtilis*, wasserlösliche OM eines L- und eines Oh-Horizontes) hergestellt. Die Proben wurden mit nuclearmagnetischer Resonanzspektroskopie (NMR), Röntgendiffraktometrie (XRD), Fourier transformierter Infrarotspektroskopie (FTIR), Röntgenphotoelektronenspektroskopie (XPS), N_2 Gas Adsorption, Messungen der electrophoretischen Mobilität und Partikelgröße, OM Desorption und medierter elektrochemischer Reduktion (MER) charakterisiert. Anschließend wurden diese mit zwei verschiedenen eisenreduzierenden Bakterienarten (*Shewanella putrefaciens*, *Geobacter metallireducens*) beimpft und 16 Tage lang unter anaeroben Bedingungen inkubiert.

Die mikrobielle Reduktion der reinen Fe oxyhydroxide wurde durch die spezifische Oberfläche (SSA) und die Löslichkeit der Minerale gesteuert. Bei *Shewanella putrefaciens* korrelierte die Fe-Reduktion der Adsorptionskomplexe stark mit der Konzentration potentiell nutzbarer Elektronenshuttlingmoleküle für OM Konzentrationen $< 2 \text{ mg C L}^{-1}$, wohingegen die Fe-Reduktion durch *Geobacter metallireducens* von der Partikelgröße und damit der Aggregation der Adsorptionskomplexe abhing.

Ähnlicherweise hing die Reduktion der Fe-OM-Kopräzipitate durch *Shewanella putrefaciens* von der Menge vorhandener OM-bürtiger Elektronenshuttlingmoleküle ab, wohingegen sowohl die Fe-Reduktion durch *Geobacter metallireducens* als auch die abiotische Fe-Reduktion durch die Partikelgröße und OM-gesteuerte Aggregation beeinflusst wurde. Die spezifische Oberfläche stellte sich als ungeeignet heraus, um die Fe-Reduktion von Fe-OM-Kopräzipitaten vorherzusagen.

Siderophor-medierte Auflösungsexperimente mit desferrioxamine-B (DFOB) wurden bei pH 4 und pH 7 durchgeführt. Bei pH 4 bot die adsorbierte OM auf Grund ihrer größeren Sorptionsaffinität einen effektiven Schutz gegen DFOB. Bei pH 7 war die Oberflächenblockierung bei vergleichbaren C Gehalten weniger effektiv, wobei weniger aggregierte Partikel gleichzeitig anfälliger gegenüber Auflösung waren. Der beschleunigende und hemmende Einfluss der mit Fe kopräzipitierten OM auf DFOB-gesteuerte Auflösung variierte stark mit deren Zusammensetzung.

Diese stark voneinander abweichenden Ergebnisse suggerieren, dass der Einfluss von OM auf die Stabilität eisenorganischer Assoziationen in Böden nicht ohne gleichzeitige Betrachtung der heterogenen Zusammensetzung der organischen Bodensubstanz und der mikrobiellen Gemeinschaft bestimmt werden kann. Das Verständnis der Kreisläufe von Fe und C in der Umwelt setzt demnach experimentelle Ansätze voraus, die weit über die Anwendung reiner Eisenoxyhydroxide und Modellorganismen hinausgehen.

Stichwörter: Organische Bodensubstanz; Eisenoxyhydroxide; Mikrobielle Reduktion

Table of Contents

Abstract	I
Zusammenfassung	III
Table of Contents	V
List of Tables	VI
List of Figures	VII
Abbreviations	X
1 GENERAL INTRODUCTION	1
1.1 Fe-organic associations	1
1.1.1 Fe oxyhydroxides	1
1.1.2 Soil organic matter	3
1.1.3 Adsorption vs. coprecipitation	4
1.1.4 Environmental significance	7
1.2 Microbial Fe reduction	7
1.2.1 General introduction	7
1.2.2 Shewanella and Geobacter	9
1.3 Influence of soil organic matter on microbial Fe reduction	11
1.4 Siderophore-promoted dissolution	14
1.5 Electrochemical reduction	16
1.6 Motivation and hypotheses	17
1.7 References	22
2 Study I	29
3 Study II	85
4 Study III	166
5 SYNTHESIS	198
5.1 Variability of characteristics of Fe-organic associations	198
5.2 Enhancement of microbial Fe reduction by organic matter	199
5.3 Inhibition of microbial Fe reduction by organic matter	201
5.4 Impact of organic matter on Fe oxyhydroxide transformation	203
5.5 Impact of adsorption vs. coprecipitation	204
5.6 Impact of electron transfer mechanism on microbial Fe reduction	206
5.7 Ligand-promoted dissolution	208
5.8 Microbial reduction vs. mediated electrochemical reduction	210
6 CONCLUSIONS AND OUTLOOK	213
Acknowledgements	220
Lebenslauf	221
Publications	222

List of Tables

STUDY I

Table 1 Bulk element composition, BET-derived specific surface area (SSA) and C constants, and pore volumina of ferrihydrite (Fh) and coprecipitates (coprec.). Values in parentheses depict the standard deviation of at least triplicate measurements. Feorg = organically complexed Fe, ND = not detected. 46

Table 2 Band assignments in ATR-FTIR spectra of beech Oi and spruce Oa as well as respective coprecipitates (Coprec.) according to Scheel et al. (2008) and Omoike and Chorover (2006). 48

Table 3 Distribution of functional groups in NOM and EPS as revealed by solid-state ^{13}C -NMR spectroscopy. 48

Table 4 Surface element composition of freeze-dried NOM, EPS, and coprecipitates (coprec.) derived from XPS survey spectra and surface carbon speciation derived from C1s XPS detail spectra. Values in parentheses depict the standard deviation of at least triplicate measurements. The different types of carbon were assigned as follows: (i) aliphatic and aromatic carbon displaying bonds to carbon and hydrogen (C-C, C=C, C-H; at 285.0 ± 0.1 eV), (ii) carbon displaying a single bond to oxygen or nitrogen as in carbohydrates and amines (C-O, C-N; at 286.5 ± 0.2 eV), (iii) carbon displaying two bonds to oxygen as in aldehydes, ketones, and amides (C=O, O-C-O, O=C-N; at 288.0 ± 0.1 eV), and (iv) carboxylic carbon displaying three bonds to oxygen (O-C=O; at 289.1 ± 0.2 eV). 53

STUDY III

Table 1 Carbon (C) content, organic carbon (OC) desorbed in 10 mM KCl, and XPS-derived surface carbon content of adsorption complexes and coprecipitates derived from extracellular polymeric substances (EPS) and two types of plant-derived natural organic matter (NOM) extracted from an Oi horizon under beech and an Oa horizon under spruce. Values in parentheses depict the standard deviation of at least triplicate measurements. 177

Table 2 Particle size (determined in 10 mM KCl at pH 4 and pH 7) and specific surface area (SSA)-based initial dissolution rates of ferrihydrite, adsorption complexes, and coprecipitates derived from extracellular polymeric substances (EPS) and two types of plant-derived natural organic matter (NOM) extracted from an Oi horizon under beech and an Oa horizon under spruce. Values in parentheses depict the standard deviation of at least 10 measurements. 184

List of Figures

Fig. 1.1 Possible arrangement of poorly crystalline minerals (e.g., ferrihydrite; Fh) and organic matter (OM) in adsorption complexes and coprecipitates. In contrast to adsorption complexes, coprecipitates contain more OM depending on the initial metal-to-carbon (M/C) ratio (A ¼ higher M/C; B ¼ lower M/C) with the mineral and organic components being more “evenly mixed” than in adsorption complexes. During coprecipitation a portion of OM might become occluded in ferrihydrite clusters (oOM). A certain portion of associated OM prevails as insoluble metal – organic complexes as indicated by the dots representing monomeric to oligomeric Fe and Al species (Kleber et al., 2015). 6

Fig. 1.2 Microbial strategies mediating electron transfer to insoluble Fe(III) oxides. Three primary strategies have been proposed to facilitate the electron transfer between microorganisms and solid Fe(III) oxide surfaces. **a** | In *Geobacter* spp. direct contact with the oxide surface is required. The production of ‘nanowires’, conductive extracellular appendages, facilitates electron transfer by functioning as an electrical conduit to the Fe(III) oxide surface. **b** | An endogenously or exogenously produced electron shuttle mediates electron transfer to solid-phase Fe(III) oxides. **c** | The production of complexing ligands as in the case of *Geothrix* sp. aids in the dissolution of the solid-phase Fe(III) oxide providing a soluble Fe(III) form more readily available to the microorganism. Although these strategies have only been demonstrated for Fe(III)-reducing microorganisms, similar strategies might be used by Fe(II)-oxidizing microorganisms that are utilizing solid-phase Fe(II) electron donors. e^- , electrons; L, ligand (Weber et al., 2006). 9

STUDY I

Fig. 1 ATR-FTIR spectra of freeze-dried NOM and EPS before and after coprecipitation with Fe(III). 47

Fig. 2 Detail C1s spectra of freeze-dried NOM, EPS and coprecipitates derived from XPS measurements. Black lines represent measured data, grey areas represent subpeaks of different carbon species as determined by peak deconvolution, dark grey lines represent the sum curve of the latter. Different types of carbon were assigned as follows: (i) aliphatic and aromatic carbon displaying bonds to carbon and hydrogen (C-C, C=C, C-H; at 285.0 ± 0.1 eV), (ii) bond to oxygen carbon displaying a single or nitrogen as in carbohydrates and amines (C-O, C-N; at 286.5 ± 0.2 eV), (iii) carbon displaying two bonds to oxygen as in aldehydes, ketones, and amides (C=O, O-C-O, O=C-N; at 288.0 ± 0.1 eV), and (iv) carboxylic carbon displaying three bonds to oxygen (O-C=O; at 289.1 ± 0.2 eV). 52

Fig. 3 XRD diagrams of ferrihydrite and the coprecipitates. 55

Fig. 4 Electron acceptor capacity (EAC) of ferrihydrite (Fh) and coprecipitates determined with four different electron transfer mediators in relation to the Fe(III) content of the sample (a), relationship between electron transfer rates and the initial particle size of the samples (10 mM KCl, pH 7) (b), relationship between electron transfer rates and organic carbon (OC) contents of different spruce Oa coprecipitates (c), relationship between electron transfer rates and electron acceptor capacity (Diquat) of each respective NOM or EPS (d). Different colors of the symbols refer to the type of sample, different shapes of the symbols refer to the type of electron transfer mediator that was used for each experiment. Error bars represent standard deviation of at least duplicate measurements. 56

Fig. 5 Microbial reduction of ferrihydrite and coprecipitates by *Shewanella putrefaciens* (a) and *Geobacter metallireducens* (b), $Fe(II)_{total}$ contents were determined after complete acidic digestion. Error bars represent the standard deviation of triplicate experiments. Please note the different scales of the y-axis. 60

LIST OF FIGURES

- Fig. 6** Relationship between initial microbial reduction rates of ferrihydrite and coprecipitates and the SUVA (specific UV absorbance) at 280 nm of desorbed NOM and EPS in each respective microbial medium (a, c), relationship between initial microbial reduction rates and the initial particle size (in *Shewanella* or *Geobacter* medium, pH 7) of each sample (b, d). Error bars represent the standard deviation of triplicate experiments ($\text{Fe(II)}_{\text{total}}$) or measurements. 61
- STUDY II**
- Fig. 1** ATR-FTIR spectra of freeze-dried NOM (dashed line) and adsorption complexes (solid lines). Numbers next to solid lines represent carbon loadings (mg C g^{-1} Fe oxide) of adsorption complexes. 103
- Fig. 2** XPS-derived carbon surface concentration in relation to the carbon content of the adsorption complexes. Error bars depict the standard deviation of at least triplicate measurements. 104
- Fig. 3** Distribution of different carbon species of freeze-dried NOM and adsorption complexes derived from detail XPS C1s measurements. 105
- Fig. 4** Relationship between the BET-derived specific surface area (SSA) and the micropore volume, the small and large mesopore volume, and the carbon content of pure Fe oxides and adsorption complexes. Error bars depict the standard deviation of at least duplicate measurements. 109
- Fig. 5** Microbial reduction of the pure Fe oxides by *Shewanella putrefaciens* and *Geobacter metallireducens*. $\text{Fe(II)}_{\text{total}}$ contents were determined after acidic digestion of the adsorption complexes. Error bars represent the standard deviation of triplicate experiments. 110
- Fig. 6a** Microbial reduction of the ferrihydrite, lepidocrocite, and goethite adsorption complexes by *Shewanella putrefaciens*. $\text{Fe(II)}_{\text{total}}$ contents were determined after acidic digestion of the adsorption complexes. Error bars represent the standard deviation of triplicate experiments. 115
- Fig. 6b** Microbial reduction of the hematite and magnetite adsorption complexes by *Shewanella putrefaciens*. $\text{Fe(II)}_{\text{total}}$ contents were determined after acidic digestion of the adsorption complexes. Error bars represent the standard deviation of triplicate experiments. 116
- Fig. 7a** Microbial reduction of the ferrihydrite, lepidocrocite, and goethite adsorption complexes by *Geobacter metallireducens*. $\text{Fe(II)}_{\text{total}}$ contents were determined after acidic digestion of the adsorption complexes. Error bars represent the standard deviation of triplicate experiments. 117
- Fig. 7b** Microbial reduction of the hematite and magnetite adsorption complexes by *Geobacter metallireducens*. $\text{Fe(II)}_{\text{total}}$ contents were determined after acidic digestion of the adsorption complexes. Error bars represent the standard deviation of triplicate experiments. 118
- Fig. 8** Microbial reduction of dissolved EPS, Beech Oi, and Spruce Oa by *Shewanella putrefaciens* and *Geobacter metallireducens*. Error bars represent the standard deviation of triplicate experiments. 119
- Fig. 9** Relationship between the initial microbial reduction rates of the adsorption complexes and the desorbed organic carbon (OC) of NOM and EPS for *Shewanella putrefaciens* and the relationship between the initial microbial reduction rates and the initial particle size for *Geobacter metallireducens*. Error bars represent the standard deviation of triplicate experiments or measurements. 126
- Fig. 10** Relationship between the initial microbial reduction rates of the adsorption complexes and the BET-derived specific surface area (SSA) for *Shewanella putrefaciens* and *Geobacter metallireducens*. Error bars represent the standard deviation of triplicate experiments or measurements. 127

STUDY III

Fig. 1 Different carbon species of freeze-dried EPS (extracellular polymeric substances), NOM (natural organic matter extracted from an Oi horizon under beech and an Oa horizon under spruce), adsorption complexes, and coprecipitates derived from detail XPS C1s spectra. Different types of carbon were assigned as follows: (i) aliphatic and aromatic carbon displaying bonds to carbon and hydrogen (C-C, C=C, C-H; at 285.0 ± 0.1 eV), (ii) bond to oxygen carbon displaying a single or nitrogen as in carbohydrates and amines (C-O, C-N; at 286.5 ± 0.2 eV), (iii) carbon displaying two bonds to oxygen as in aldehydes, ketones, and amides (C=O, O-C-O, O=C-N; at 288.0 ± 0.1 eV), and (iv) carboxylic carbon displaying three bonds to oxygen (O-C=O; at 289.1 ± 0.2 eV). 179

Fig. 2 Relationship between the BET-derived specific surface area (SSA) and the micropore volume, the small and large mesopore volume, and the carbon content of pure ferrihydrite, adsorption complexes, and coprecipitates derived from extracellular polymeric substances (EPS) and two types of plant-derived natural organic matter (NOM) extracted from an Oi horizon under beech and an Oa horizon under spruce. Error bars depict the standard deviation of at least duplicate measurements. 183

Fig. 3 Electrophoretic mobility (EM) in 10 mM KCl in relation to pH for ferrihydrite, adsorption complexes, and coprecipitates (coprec) derived from extracellular polymeric substances (EPS) and two types of plant-derived natural organic matter (NOM) extracted from an Oi horizon under beech and an Oa horizon under spruce. Error bars depict the standard deviation of 10 circles of measurement. 185

Fig. 4 Dissolution of ferrihydrite, adsorption complexes, and coprecipitates (coprec) by $50 \mu\text{M}$ DFOB in 10 mM KCl at pH 7. Organic matter (OM) was extracted from extracellular polymeric substances (EPS) and two types of plant-derived natural OM (NOM) derived from an Oi horizon under beech and an Oa horizon under spruce. Error bars depict the standard deviation of triplicate measurements. Please note the different scale of the y-axis for the coprecipitates. 189

Fig. 5 Dissolution of ferrihydrite, adsorption complexes, and coprecipitates (coprec) by $50 \mu\text{M}$ DFOB in 10 mM KCl at pH 4. Organic matter (OM) was extracted from extracellular polymeric substances (EPS) and two types of plant-derived natural OM (NOM) derived from an Oi horizon under beech and an Oa horizon under spruce. Error bars depict the standard deviation of triplicate measurements. 190

Abbreviations

AQDS	anthraquinone-2,6-disulfonic acid
BET	Brunauer-Emmett-Teller
C	carbon
CV	cyanoviologen (1,1'-bis(cyanomethyl)-4,4'-bipyridyl)
DFOB	desferrioxamine-B
DOM	dissolved organic matter
DQ	diquat dibromide monohydrate (1,1'-ethylene-2,2'-bipyridyl)
EAC	electron acceptor capacity
EM	electrophoretic mobility
EPS	extracellular polymeric substances
Fe	iron
Fh	ferrihydrite
FTIR	Fourier transform infrared spectroscopy
HEPES	4-(2-hydroxyethyl)-1-piperazineethanesulfonic acid
IC	ion chromatography
ICP-OES	inductively coupled plasma optical emission spectroscopy
LMWO	low molecular weight organic
MER	mediated electrochemical reduction
MOPS	3-morpholinopropane-1-sulfonic acid
N	nitrogen
NMR	nuclear magnetic resonance
NOM	natural organic matter
OC	organic carbon
OM	organic matter
RF	riboflavin 5'-monophosphate sodium salt
SOM	soil organic matter
SSA	specific surface area
SUVA	specific ultraviolet absorbance
TN	total nitrogen
TOC	total organic carbon
UV-Vis	ultraviolet-visible spectrometry
XPS	x-ray photoelectron spectroscopy
XRD	x-ray diffraction
ZiV	zwitterionic viologen (4,4'-bipyridinium-1,1'-bis(2-ethylsulfonate))

1 GENERAL INTRODUCTION

1.1 Fe-organic associations

1.1.1 Fe oxyhydroxides

Fe oxyhydroxides are ubiquitously found in nature and are particularly widespread in soils (Schwertmann and Cornell, 2000). (The term Fe oxyhydroxides henceforth encompasses Fe oxides, Fe hydroxides, and Fe oxyhydroxides unless explicitly stated otherwise.) With the exception of magnetite, Fe oxyhydroxides are formed by weathering of primary igneous rocks like pyroxenes, amphiboles, biotites and olivines (Schwertmann and Cornell, 2000). A typical weathering reaction can be found in goethite being precipitated from fayalite (an end-member of olivine) following oxidation of Fe(II) and subsequent hydrolysis of Fe(III) (Schwertmann and Cornell, 2000):



All Fe oxyhydroxides are composed of octahedrons representing the basic structural unit. The latter comprises an Fe atom surrounded by either six O or by both O^{2-} and OH^- ions. The differences between the Fe oxyhydroxides are derived from the arrangements of the octahedral units and the linkages between them (Kämpf et al., 2000). Isomorphic substitution may replace the Fe^{3+} in the center of the octahedron with, e.g., Al^{3+} , Mn^{3+} , Cr^{3+} , or V^{3+} . Furthermore, Fe oxyhydroxides have been reported to be coprecipitated with several heavy metals, including Ni^{2+} , Co^{3+} , Zn^{2+} , Cd^{2+} , Pb^{4+} , and Cu^{2+} (Schwertmann and Cornell, 2000). Fe oxyhydroxides thus provide a huge variety of minerals differing in their structure, crystallinity, surface area, particle size and reactivity.

The most important Fe oxyhydroxides found in soils are goethite ($\alpha\text{-FeOOH}$), hematite ($\alpha\text{-Fe}_2\text{O}_3$), lepidocrocite ($\gamma\text{-FeOOH}$), ferrihydrite ($\text{Fe}_{8.2}\text{O}_{8.5}(\text{OH})_{7.43} \cdot 3\text{H}_2\text{O}$) (Michel et al.,

2010), magnetite (Fe_3O_4), and maghemite ($\gamma\text{-Fe}_2\text{O}_3$) with minor occurrences of akaganeite ($\beta\text{-FeOOH}$) and feroxyhyte ($\delta'\text{-FeOOH}$) (Schwertmann and Cornell, 2000).

Goethite is the most common Fe oxyhydroxide in soils. It can be found in both aerobic and anaerobic soils all around the world with a predominant occurrence in cool to temperate, humid climates (Schwertmann, 1985). Goethite is either formed via direct precipitation of slowly oxidized Fe(II) or via slow transformation of ferrihydrite (Cornell and Schwertmann, 2003).

The Fe oxide hematite is the second most common Fe oxyhydroxide in soils, almost exclusively found in aerobic soils of subtropical, Mediterranean, and humic to subhumic tropical regions, since its formation is favored by mean annual temperatures $> 15\text{ }^\circ\text{C}$ and reduced water activity (Schwertmann and Cornell, 2000). It typically occurs in lateritic and plinthitic soils, red Mediterranean soils, oxisols, and ultisols (Cornell and Schwertmann, 2003). Unlike goethite, hematite does not precipitate directly from Fe(III) provided by the soil solution, but requires crystallization from ferrihydrite (Schwertmann and Cornell, 2000).

Lepidocrocite is most frequently found in redoximorphic environments, which are characterized by displaying alternating reducing and oxidizing conditions. Its formation is suppressed by both carbonate and Al and generally constraint to anaerobic, clayey, non-calcareous soils of cooler and temperate regions (Cornell and Schwertmann, 2003).

Ferrihydrite is a metastable Fe oxyhydroxide only exhibiting short-range order, whose exact structure is still a matter of intense research (Michel et al., 2010). Its occurrence is therefore confined to either young Holocene soils or environments, in which the transformation to more stable minerals like goethite or hematite is inhibited by, e.g., organic matter (OM). Its formation is further enhanced in favor of goethite or hematite by a rapid oxidation of Fe(II) and thus a large rate of Fe(III) supply. Environments meeting the requirements of ferrihydrite formation include groundwater and stagnant water soils like gleys and pseudogleys, podzols of temperate and cool regions, and paddy soils (Childs, 1992).

Magnetite occupies a special position among the Fe oxyhydroxides. Firstly, it is a mixed-valent Fe oxide containing both structural Fe(II) and Fe(III) and secondly, it is not built by weathering of primary minerals like the other Fe oxyhydroxides. Lithogenic magnetite in soils can be found as remnant of igneous rocks (Cornell and Schwertmann, 2003), whereas pedogenic magnetite is generated either biologically controlled by magnetotactic bacteria or by microbial dissimilatory Fe reduction (section 1.2) and oxidation (Bazylinski et al., 2007).

Maghemite is most commonly formed via aerial oxidation of lithogenic magnetite or via conversion of other Fe oxyhydroxides initiated by huge amounts of heat generated during bush or forest fires (Schwertmann and Cornell, 2000). It is mainly found in the aerobic soils of the tropics and subtropics (Cornell and Schwertmann, 2003).

The formation of akaganeite requires the presence of chloride and temperatures above 60 °C and is thus most commonly formed around hot brines and springs (Schwertmann and Cornell, 2000).

Feroxyhyte is only rarely found in natural soils and thus little is known about the requirements of formation beyond the assumption of a rapid Fe(II) oxidation process (Schwertmann and Cornell, 2000).

1.1.2 Soil organic matter

The exact definition of soil organic matter (SOM) is still a topic of ongoing dispute and far from having reached a consensus among soil scientists (Kleber et al., 2015). Resolving and describing the complete chemical structure of complex, heterogeneous, polymeric, and polydispersive SOM remains a challenge to this day.

Traditionally, SOM is referred to as humus, which encompasses all organic compounds in the soil minus undecayed plant and animal tissues, their partial decomposition products, and the living soil biomass (Stevenson, 1994). Humus can be divided into humic substances and

nonhumic substances. The latter consist of compounds which are identifiable as a recognized class of biochemistry, like amino acids, carbohydrates, fats, waxes, resins, and organic acids, whereas humic substances can further be divided into humins, humic acids, and fulvic acids. Humins are operationally defined as the fraction of humic substances, which is soluble in neither NaOH nor HCl. Humic acids are soluble in NaOH, but not in HCl, whereas fulvic acids remain in solution during addition of NaOH with a subsequent addition of HCl (Stevenson, 1994).

OM in the soil solution can be found as either dissolved OM (DOM) or particulate OM. Latter encompasses particles and aggregates, which are suspended in solution and may thus be mobilized without being actually dissolved in solution (Kleber et al., 2015). DOM is traditionally defined as dissolved molecules and particles passing through a filter with a pore size $<0.45 \mu\text{m}$ (Kalbitz et al., 2000) and therefore comprises both truly dissolved molecules and organic colloids. Furthermore, OM can build mineral-organic associations, as discussed in more detail in section 1.1.3.

1.1.3 Adsorption vs. coprecipitation

Association of OM with Fe oxyhydroxides may occur via adsorption or coprecipitation (Kleber et al., 2015). Adsorption to mineral surfaces can take place via “innersphere complexation” featuring the formation of polar covalent bonds between atoms at the mineral surface and OM (also referred to as chemisorption) (Luo, 2007) or via “outersphere complexation” featuring OM being electrostatically held at the mineral surface by Coulomb forces (also referred to as physisorption) while at least partially retaining its hydration shell (Essington, 2004). Physisorption includes adsorption via H-bond formation, Van-der-Waals interactions, and hydrophobic interactions (Berg et al., 2002). The covalent bonds provided by adsorption via innersphere complexation are stronger than the ones provided via outersphere

complexation by several magnitudes (Luo, 2007). A binding mechanisms transitioning between innersphere and outersphere complexation is provided by cation bridging (Lützwow et al., 2006) and involves the coordination of both OM-derived functional groups and mineral-derived hydroxyl groups by polyvalent cations. Mikutta et al. (2007) identified the adsorption of OM to goethite to be governed by ligand-exchange, with cation-bridging and Van-der-Waals interactions contributing less than 10 % to the process of adsorption. Ligand-exchange resembles a type of innersphere complexation and thus results in OM bound tightly to the mineral surface.

The most abundant mineral phase in Fe-OM coprecipitates is usually ferrihydrite (Kleber et al., 2015). A slow oxidation of Fe(II) during precipitation may also result in lepidocrocite making up the main mineral phase of Fe-OM coprecipitates (Pédrot et al., 2011). Coprecipitation of Fe in the presence of OM involves several concomitant and interlinked processes, including the complexation of hydrolyzed Fe(II) and Fe(III) by OM, precipitation of insoluble Fe-organic complexes, adsorption of OM to ferrihydrite, and occlusion of pure OM into newly formed ferrihydrite aggregates (Fig. 1.1; Kleber et al., 2015). In comparison to ferrihydrite forming in the absence of OM and mineral-organic associations that form exclusively by OM adsorption to preexisting pure ferrihydrite surfaces, coprecipitation with organic constituents yields smaller crystal sizes with a more defective crystallographic structure (Cismasu et al., 2011; Eusterhues et al., 2008; Schwertmann et al., 2005), as well as different aggregation states (Mikutta et al., 2012). Fe-OM coprecipitation can occur in soils displaying very different conditions, such as well drained soils (Dolfing et al., 1999), temporarily waterlogged paddy soils (Kögel-Knabner et al., 2010), or acidic mineral soils (Nierop et al., 2002) like Spodosols (Wagai and Mayer, 2007). It may also be found in engineered settings such as acid mine drainage (Cheng et al., 2009), or industrial coagulation water treatment landfills (Bachand et al., 2000; Downing et al., 2008; Henneberry et al., 2011). Coprecipitation of organic compounds with Fe is not constraint to plant-derived NOM

leached from organic soil layers, but has been found to be initiated by OM of microbial origin, such as extracellular polymeric substances (EPS), too (Rancourt et al., 2005; Marschner et al., 2008; Mikutta et al., 2009), which are found in biofilms originating from both living and dead microbial cells (Beveridge et al., 1997).

Despite Fe-OM coprecipitation generally being assumed to be a widespread process in soils (Cismasu et al., 2011; Eusterhues et al., 2011), a proper estimation of its contribution to Fe-organic associations has not been successful so far due to the lack of suitable quantification techniques (Kleber et al., 2015).

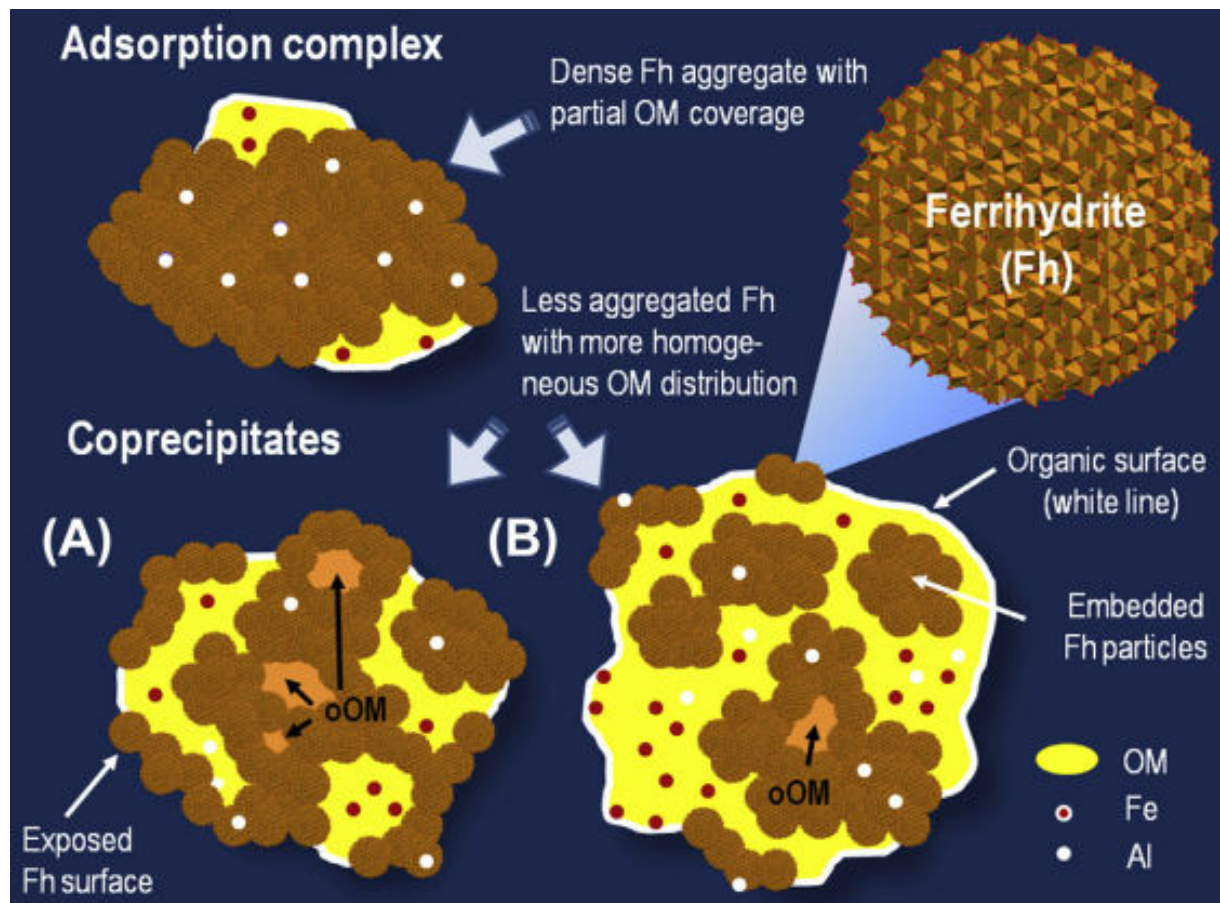


Fig. 1.1 Possible arrangement of poorly crystalline minerals (e.g., ferrihydrite; Fh) and organic matter (OM) in adsorption complexes and coprecipitates. In contrast to adsorption complexes, coprecipitates contain more OM depending on the initial metal metal-to-carbon (M/C) ratio (A $\frac{1}{4}$ higher M/C; B $\frac{1}{4}$ lower M/C) with the mineral and organic components being more “evenly mixed” than in adsorption complexes. During coprecipitation a portion of OM might become occluded in ferrihydrite clusters (oOM). A certain portion of associated OM prevails as insoluble metal – organic complexes as indicated by the dots representing monomeric to oligomeric Fe and Al species (Kleber et al., 2015).

1.1.4 Environmental significance

The long-term stability of SOM under oxic conditions has been linked to its preservation by association with Fe oxyhydroxides, particularly with poorly crystalline phases such as ferrihydrite (Kaiser and Guggenberger, 2007; Mikutta et al., 2006). The stabilizing effect of Fe oxyhydroxides on OM may, however, be lessened by a number of processes. First, OM may be desorbed under both oxic and anoxic conditions, thus increasing the bioavailability of carbon (Hanke et al., 2013; Mikutta et al., 2007). Under anoxic conditions, microbial reduction of Fe-OM associations may additionally mobilize OM (Glasauer et al., 2003; Lovley et al., 2004; Weiss et al., 2004), thus counteracting the stabilizing effect of Fe compounds. Dissimilatory Fe(III) reduction can further account for the release of other oxide-associated compounds into the soil solution and groundwater such as organic contaminants (Lovley and Anderson, 2000), heavy metals (Brümmer et al., 2013; Perelomov et al., 2011; Violante et al., 2003), or oxyanions (Mesuere and Fish, 1999; Sannino et al., 2009). Apart from the process of podzolisation, Fe oxyhydroxides and Fe-organic associations can generally be mobilized by protonation, reduction, and complexation (Schwertmann, 1991). While the influence of proton-promoted dissolution Fe oxyhydroxides in soils displaying pH values > 4 is usually negligible (Kraemer, 2004), microbial reduction will be discussed in chapter 1.2 and ligand-promoted dissolution via complexation will be explored in more detail in chapter 1.4.

1.2 Microbial Fe reduction

1.2.1 General introduction

Iron respiration was most likely among the earliest types of microbial metabolism to evolve on earth and thus predates the utilization of O_2 , NO_3^- , and SO_4^{2-} as respiratory terminal electron acceptors (Vargas et al., 1998). Today it can be found among both domains of Archaea and Bacteria inhabiting a diverse variety of different environments, with identified

extremophiles ranging from acidophilic (<pH 6) to alkaliphilic (pH 9 – pH 11) as well as from psychrophilic (-20 – 10 °C) over thermophilic (45 – 80 °C) to hyperthermophilic (>80 °C) microorganisms (Weber et al, 2006). The reductive mobilization of Fe(III) oxides in modern sedimentary environments is generally controlled by microbial Fe(III) reduction, with the exception of sulphidogenic environments (Lovley et al., 2004). Latter are characterized by the abiotic reduction of Fe oxyhydroxides with hydrogen sulphide (H₂S) acting as electron donor (Canfield, 1989). Overall, Fe-reducing microorganisms are estimated to oxidize 90 % of the organic matter in both marine and terrestrial sediments (Canfield et al., 1993).

Under O₂-deficiency, the enzymatic reduction of Fe(III) can be coupled to the complete oxidation of organic compounds to carbon dioxide (CO₂), which provides enough energy to support cell growth (Lovley and Phillips, 1988). During this process, Fe(III) is partly reduced to Fe(II), partly reprecipitated and partly converted to other Fe oxyhydroxides.

Due to their low solubility at pH values above 4 (Schwertmann, 1991), pure Fe oxyhydroxides as well as mineral-organic associations are not able to pass the microbial outer cell membrane in order to be reduced. Fe-reducing bacteria overcame this constraint by developing different electron transfer pathways for Fe(III) to be reduced in the extracellular space (Fig. 1.2; Weber et al., 2006). These include (i) direct transfer of electrons via redox-enzymes anchored in the outer bacterial membrane (Myers and Nealson, 1988; K P Nevin and Lovley, 2000) or (ii) conductive cellular nanowires (El-Naggar et al., 2010; Gorby et al., 2006; Reguera et al., 2005) and pili providing both attachment and conductive features, (iii) mediated electron transfer to the mineral by using Fe-chelating compounds (Kraemer, 2004; Lovley et al., 1994; Nevin and Lovley, 2002), and (iv) endogenous electron shuttling molecules like secreted flavins (Marsili et al., 2008; Nevin and Lovley, 2002; Newman and Kolter, 2000; von Canstein et al., 2008), and/or exogenous electron shuttling compounds as provided by NOM (Lovley et al., 1996). While the electron transfer via direct contact between the mineral and the cell can transport electrons over a distance of only 2 nm (Gray and

Winkler, 2010), the other transfer mechanisms provide strategies to transport electrons over distances in the μm range (Melton et al., 2014). In biofilms, electrons have even been reported to be transported over a distance of several centimeters via multistep electron hopping between redox-active cofactors, before finally being transferred to an Fe oxyhydroxide (Lovley et al., 1996; Nielsen et al., 2010).

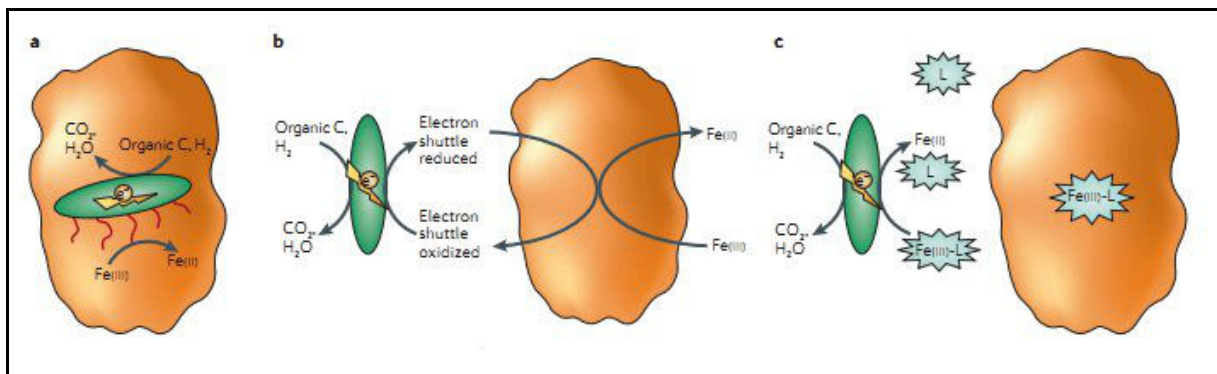


Fig. 1.2 Microbial strategies mediating electron transfer to insoluble Fe(III) oxides. Three primary strategies have been proposed to facilitate the electron transfer between microorganisms and solid Fe(III) oxide surfaces. **a** | In *Geobacter* spp. direct contact with the oxide surface is required. The production of ‘nanowires’, conductive extracellular appendages, facilitates electron transfer by functioning as an electrical conduit to the Fe(III) oxide surface. **b** | An endogenously or exogenously produced electron shuttle mediates electron transfer to solid-phase Fe(III) oxides. **c** | The production of complexing ligands as in the case of *Geothrix* sp. aids in the dissolution of the solid-phase Fe(III) oxide providing a soluble Fe(III) form more readily available to the microorganism. Although these strategies have only been demonstrated for Fe(III)-reducing microorganisms, similar strategies might be used by Fe(II)-oxidizing microorganisms that are utilizing solid-phase Fe(II) electron donors. e^- , electrons; L, ligand (Weber et al., 2006).

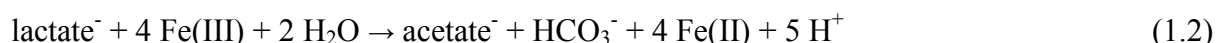
1.2.2 *Shewanella* and *Geobacter*

Shewanellaceae and *Geobacteraceae* are regarded as two of the most common families of Fe-reducing microorganisms under circumneutral conditions (Thamdrup, 2000). Especially *Geobacteraceae* are found in many soils and sediments (Lovley et al., 2011, 2004), even though doubts arose as to whether estimations of the abundance of these types of microorganisms might be attributed to the culture enrichment procedures rather than to their actual natural occurrences (Piepenbrock et al., 2014).

Both *Shewanella* and *Geobacter* species employ *c*-type cytochromes, which are proteins partly located in the outer membrane of the cell and partly located in the periplasm between

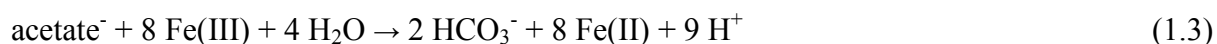
the outer membrane and the cytoplasmic membrane (Liang et al., 2009). Electrons are transferred from the intracellular cytoplasm via a dehydrogenase located in the cytoplasmic membrane to the periplasm, where electron transfer is mediated by a quinone pool consisting of different ubiquinones and menaquinones. Finally, electrons are transferred from the quinone pool to either a *c*-type cytochrome or an Fe(III) reductase, which catalyse the transfer to an electron acceptor like an Fe oxyhydroxide in the extracellular space (Weber et al., 2006).

Shewanella species have been shown to excrete molecules acting as electron shuttles rather than transferring electrons via direct contact to the mineral (Kotloski and Gralnick, 2013; von Canstein et al., 2008). Marsili et al. (2008) identified those redox-active molecules to be a mixture of riboflavin and riboflavin-5'-phosphate with the mixture shifting to > 90 % riboflavin in biofilms. Despite the observation of *Shewanella oneidensis* growing different types of pili under electron acceptor limitation, the conductive nature or involvement in surface attachment of those appendages is still a matter of discussion (Reguera et al., 2005). So far, the ability to transport electrons along those nanowires has only been confirmed for *Shewanella oneidensis* strain MR-1 (El-Naggar et al., 2010). Electron donors that can be coupled to Fe(III) reduction by *Shewanella* species include lactate, pyruvate, formate, and hydrogen (Lovley et al., 1989). A well studied example can be found in the incomplete oxidation of lactate to acetate and carbon dioxide by *Shewanella putrefaciens* (Lovley et al., 1989):



While both direct contact and electron transfer via conductive nanowires have been suggested for *Geobacter* species (Boesen and Nielsen, 2013; Malvankar et al., 2011), the bacterium itself does not produce endogenous electron-shuttling molecules or chelators

(Nevin and Lovley, 2000). The first *Geobacter* species and microorganism in general, which was found to display complete oxidation of organic compounds to carbon dioxide coupled with enzymatic reduction of Fe(III) was *Geobacter metallireducens* (Lovley et al., 1993), formerly known as GS-15 (Lovley et al., 2004):



Apart from acetate, *Geobacter metallireducens* is able to use a variety of different electron donors like propionate, butyrate, valerate, pyruvate, and ethanol. The list further includes a range of aromatic compounds, which are also common anthropogenic contaminants and thus especially environmentally significant, such as toluene, phenol, *p*-cresol, benzoate, benzylalcohol, benzaldehyde, *p*-hydroxybenzoate, *p*-hydroxybenzylalcohol, and *p*-hydroxybenzaldehyde (Lovley et al., 2004).

1.3 Influence of soil organic matter on microbial Fe reduction

The microbial reduction of pure Fe oxyhydroxides has been proposed to be controlled by their specific surface area (Roden, 2003), their solubility (Bonneville et al., 2006), and their particle size for particles < 1 μm (Schwertmann, 1991). Adding OM to the system provides several additional factors potentially influencing both the rate and extent of microbial Fe reduction. On the one hand, OM may accelerate microbial reduction and thereby solubilization of Fe oxyhydroxides by (i) complexing Fe(II), thereby increasing the thermodynamic driving force for Fe(III) reduction (Royer et al., 2002), (ii) acting as a ligand towards Fe(III) thereby promoting solubilization (Jones et al., 2009), (iii) mediating electron transfer from dissimilatory Fe-reducing bacteria to the mineral by shuttling electrons through redox active moieties in the OM structure (Amstaetter et al., 2012; Jiang and Kappler, 2008; Lovley et al., 1996), and (iv) increasing the solubility by inducing smaller crystal sizes and a

more defective crystallographic structure during the process of coprecipitation (Cismasu et al., 2011; Eusterhues et al., 2008; Schwertmann et al., 2005). On the other hand, OM may also decelerate the reduction of coprecipitates by (i) blocking surface sites on the mineral and (ii) initiating aggregation upon adsorption (Amstaetter et al., 2012; Kaiser and Guggenberger, 2003).

The OM-derived Fe reduction enhancing factor studied most intensively in the past was mediating electron transfer by providing exogenous electron shuttling compounds. Organic compounds that electron shuttling abilities have been attributed to include humic acids (Lovley et al., 1996), plant exudates (Nevin and Lovley, 2000), antibiotics (Hernandez et al., 2004), and biochar (Kappler et al., 2014). The impact of OM on microbial Fe reduction is expected to depend on its origin, which affects the structural complexity and chemical composition of the material. So far, this complexity of OM has hardly been addressed in previous studies on microbial Fe reduction, the majority of which used either specific OM fractions like purified humic acid (Amstaetter et al., 2012; Shimizu et al., 2013) or defined low molecular weight organic (LMWO) compounds like quinones (Liu et al., 2007; Zachara et al., 2011; Zhu et al., 2013). Among the latter, anthraquinone-2,6-disulfonic acid (AQDS) is the most frequently used, serving as a model compound with excellent electron shuttle properties by reversibly accepting and donating electrons via its quinone/hydroquinone moieties. Lovley and Blunt-Harris (1999) and Scott et al. (1998) suggested such quinone/hydroquinone structures in OM to play a major role in electron shuttling in soils. Electron shuttling is, however, likely not restricted to this redox couple. Chen et al. (2003) attributed accelerated Fe(III) reduction to electron shuttling by humic acid-derived high-molecular weight aromatic structures and, to a smaller but still considerable extent, to NOM-derived low-molecular weight polyphenolic compounds. Plant debris-derived phenolic compounds providing electron shuttles were proposed by Lovley et al. (1998), too.

Moreover, Wolf et al. (2009) showed that AQDS had a smaller sorption affinity towards ferrihydrite amongst several tested quinones of various composition with the sorption affinity of AQDS being 10-fold smaller than those of fulvic and humic acids. Experiments using AQDS as OM analogon, therefore, contain an easily available electron shuttling compound and do not capture effects resulting from strong and preferential sorption of complex aromatic NOM constituents in soils with electron shuttling properties (Chorover and Amistadi, 2001; Kalbitz et al., 2005; Scheel et al., 2007). Sorptive fractionation of OM itself varies with OM composition and concentration, which hugely impacts aggregation, bioavailable surface area, and thus the kinetics of microbial Fe reduction.

Microbial reduction of Fe(III) oxyhydroxides and coprecipitates by *Shewanella* species can be enhanced by model quinones (Newman and Kolter, 2000) and humic acids (Amstaetter et al., 2012; Shimizu et al., 2013) if the amount of dissolved organic carbon exceeds a threshold of 5-10 mg C L⁻¹ (Jiang and Kappler, 2008) and the amount of Fe oxyhydroxide is sufficiently small for the degree of induced aggregation to not outweigh the processes accelerating Fe reduction (Amstaetter et al., 2012). Nevertheless, microbial reduction by *Shewanella putrefaciens* in relation to the particle size of Fe-organic associations has not been explored systematically so far.

Geobacteraceae have been reported to couple the oxidation of acetate to the reduction of extracellular quinone moieties (Coates et al., 1998), while both *Geobacter metallireducens* (Lovley et al., 1996; Scott et al., 1998) and *Geobacter sulfurreducens* (Jiang and Kappler, 2008) were able to reduce humic acids when no Fe was present. However, Eusterhues et al. (2014) found decreased Fe reduction rates by *Geobacter bremensis* when NOM extracted from a forest floor was added to pure ferrihydrite by adsorption or coprecipitation. These observations do not support a major impact of *Geobacter* using external electron shuttles in systems containing both NOM and Fe.

1.4 Siderophore-promoted dissolution

The strategy of releasing Fe-chelating compounds into the soil solution to promote Fe solubilization (Lovley et al., 1994; Nevin and Lovley, 2002) is not exclusive to Fe reducing bacteria. Since Fe does not only serve as terminal electron acceptor, but also as essential micronutrient for many organisms, several bacteria, fungi and graminaceous plants exude Fe-chelating siderophores (Neilands, 1957; Roemheld, 1991; Takagi, 1976; Winkelmann, 1992) to increase the availability of otherwise poorly soluble Fe oxyhydroxides. Siderophores are defined as LMWO ligands exhibiting a large specificity and selectivity towards Fe(III) displaying a huge variety of chemical structures (Kraemer, 2004). Fe-chelating functional groups of microbial siderophores feature α -hydroxycarboxylate, hydroxamate, catecholate, and carboxylate, whereas plant siderophores are characterized by carboxalate, hydroxal, and amine groups (Kraemer, 2006). Typical concentrations of siderophores found in soils range between 10^{-7} and 10^{-8} M (Powell et al., 1980).

Ligand-controlled dissolution is assumed to take place in three steps by i) fast surface complex formation via ligand exchange by replacement of surface hydroxal groups or water, ii) slow, rate determining detachment of the surface metal center, and iii) fast regeneration of the mineral surface (Furrer and Stumm, 1986). The ligand adsorbs to the surface and forms a precursor complex, which polarizes the bond between the Fe and the O of the crystal lattice, thus weakening the bond and facilitating the bond breaking. Ligand-promoted dissolution has been found particularly effective for ligands building mononuclear multidentate surface complexes (Furrer and Stumm, 1986; Ludwig et al., 1995). Multinuclear complexes rather inhibit dissolution of Fe, since the coordination of several surface sites per molecule prevents the detachment of the Fe atom due to the simultaneous detachment of several atoms by the same ligand being thermodynamically unfavorable (Bondietti et al., 1993).

While the siderophore-promoted dissolution of pure Fe oxyhydroxides has been investigated meticulously (Kraemer, 2004), studies examining Fe oxyhydroxides coated with

adsorbed OM or Fe-OM coprecipitates have been sparse (Goebel et al., 2017; Mikutta and Kretzschmar, 2008). Combining LMWO acids like oxalate, citrate, malonate and ascorbate with the siderophore desferrioxamine-B (DFOB) has been reported to increase dissolution rates of Fe oxyhydroxides due to synergistic effects (Cheah et al., 2003; Reichard et al., 2007; Wang et al., 2015). However, the effect of more complex, heterogeneous natural organic matter adsorbed to Fe oxyhydroxide has not been addressed systematically so far.

The abiotic reduction of Fe oxyhydroxides has repeatedly been reported to depend on their specific surface area (SSA) and the underlying crystal order (Larsen and Postma, 2001; Roden, 2003). Since both adsorbed and coprecipitated OM decrease the SSA by blocking surface sites on the ferrihydrite surfaces and initiating aggregation (Eusterhues et al., 2011; Kaiser and Guggenberger, 2007, 2003), sorbed OM is expected to decelerate the abiotic dissolution of both adsorption complexes and coprecipitates. Nevertheless, Mikutta and Kretzschmar (2008) reported increased siderophore-induced Fe dissolution rates of polygalacturonic acid-derived Fe coprecipitates in comparison to pure ferrihydrite. The increased dissolution of the same coprecipitates was attributed to smaller and less aggregated particles induced by greater charged-derived repulsive forces, with only a minor influence of their crystallinity.

Furthermore, the only study examining the siderophore-promoted dissolution of Fe-organic associations published so far (Mikutta and Kretzschmar, 2008) conducted their experiments at circumneutral pH. Particularly the rhizosphere, however, usually exhibits lower pH values, as organic acids and protons are released into the soil via plant roots (April and Keller, 1990; Bonneville et al., 2011; Brantley et al., 2011). The pH affects the charge and therefore particle size and aggregation of Fe-organic associations (Alvarez-Puebla and Garrido, 2005; Angelico et al., 2014; Siéliéchi et al., 2008) and ultimately the sorption and desorption behaviour of OM (Kaiser and Zech, 1999) and thus requires further attention as well.

1.5 Electrochemical reduction

A common problem when determining microbial as well as abiotic Fe reduction kinetics lies in the necessity of applying indirect measurements to quantify Fe(II) contents and thus decoupling the quantification of the reduced species from the actual experiment. A possible solution to this dilemma is offered by the technique of mediated electrochemical reduction (MER), which allows for continuous monitoring of the changing electron acceptor capacity during sample reduction at a constant redox potential (Sander et al., 2015). The redox state of Fe oxyhydroxides can thus be determined without the obligation to separate dissolved Fe(II) from the suspended sample and without the problem of oxidation during sampling or further reduction during acidification for certain quantification methods, like, e.g. the ferrozine assay (Stookey, 1970).

A typical practical approach to conduct MER is described by Klüpfel et al. (2014). Analyses are conducted in an electrochemical cell, which consists of a glassy carbon cylinder serving both as working electrode and reaction vessel, a Ag/AgCl reference electrode, and a counter electrode made of coiled platinum wire, which is separated from the carbon cylinder by a porous glass frit. The cell is filled with KCl serving as background electrolyte and buffered at a pH 7 with either HEPES or MOPS. The working electrode is equilibrated to a certain reduction potential E_h , which is optimized to allow fast reduction of the dissolved electron transfer mediator. Latter is added to ensure a fast electron transfer and a fast redox calibration of the sample. The electron accepting capacities (EAC; defined as the number of electrons transferred to a mass unit of analyte) are obtained by integrating the baseline-corrected reductive current peaks resulting from each sample according to Sander et al. (2015):

$$\text{EAC} = \frac{\int \frac{I_{\text{Red}}}{F} dt}{m_{\text{sample}}} \quad (1.4)$$

Here, I_{Red} (A) represents the baseline-corrected reductive current, F the Faraday constant (96,485 C mol⁻¹), and m_{sample} (g) the mass of each respective added sample. The term $\int \frac{I_{Red}}{F} dt$ corresponds to the number of electrons transferred. Electron transfer rates for each sample can be calculated by assuming a pseudo-first-order rate law. Despite all of its benefits, MER has not been used for characterization of Fe-organic associations yet.

1.6 Motivation and hypotheses

Reviewing the research conducted so far, several gaps of knowledge arose, which are addressed in the following:

- (I) When examining the stimulating effect of organic compounds like humic acids on microbial Fe reduction, it is common practice to add them to a suspension of a certain Fe oxyhydroxide and review the compound concentration of the whole system without differentiating between adsorbed and dissolved C (Jiang and Kappler, 2008). A study providing adsorption complexes with defined C contents and quantifying both adsorbed and easily desorbable C is lacking so far.
- (II) Humic acid imposed aggregation has been suggested to influence the microbial ferrihydrite aggregation (Amstaetter et al., 2012). Nevertheless, a systematic assessment of the particle size in suspension or the specific surface area of adsorption complexes in relation to microbial reduction has not been conducted so far.
- (III) The majority of previous studies on microbial Fe reduction used either specific OM fractions like purified humic acid (Amstaetter et al., 2012; Shimizu et al., 2013) or defined LMWO compounds like quinones (Liu et al., 2007; Zachara et al., 2011; Zhu et al., 2013). While the latter serve as excellent electron shuttles, they do not reflect the sorptive properties of natural OM. During the extraction of humic and fulvic acids, the organic compounds are exposed to extremely acidic and alkaline pH values not commonly found in soils (Stevenson, 1994), thus potentially triggering irreversible conformational and structural changes. The resulting compounds may therefore not

exhibit the same properties as the original humic substances. Nevertheless, studies investigating the impact of naturally plant-derived organic matter on microbial reduction are sparse. The same is true for OM expected to contain little amounts of electron-shuttling molecules like extracellular polymeric substances (EPS) derived from biofilms.

- (IV) Since the research on Fe-OM coprecipitates has only been established fairly recently (Cismasu et al., 2011; Eusterhues et al., 2008), comparatively little is known about the impact of natural OM on the microbial reduction of Fe-OM coprecipitates (Pédrot et al., 2011; Henneberry et al., 2012; Shimizu et al., 2013; Eusterhues et al., 2014). Among the cited studies, only the last one was conducted using naturally derived OM. Further research is thus required to assess the impact of coprecipitated OM on microbial reduction with regard to its composition and in comparison to adsorbed OM.
- (V) Even though the microbial Fe reduction by *Shewanella* and *Geobacter* species has been suggested to be affected by OM to differing degrees due to their difference in electron transfer mechanisms (Eusterhues et al., 2014), studies exposing the same samples to reduction by both species applying the same experimental conditions have not been published so far.
- (VI) Combining LMWO acids like oxalate, citrate, malonate and ascorbate with the siderophore DFOB has been reported to increase dissolution rates of Fe oxyhydroxides due to synergistic effects (Cheah et al., 2003; Reichard et al., 2007; Wang et al., 2015). However, the effect of more complex, heterogeneous natural organic matter adsorbed to Fe oxyhydroxide has not been addressed systematically so far.
- (VII) MER offers a method of continuously monitoring the changing electron acceptor capacity of Fe oxyhydroxides during reduction at a constant redox potential (Sander et al., 2015). Nevertheless, MER has not been used for characterization of Fe-organic associations so far.

The overall aim of this thesis was therefore to systematically assess the impact of the composition and concentration of both adsorbed and coprecipitated naturally occurring OM on microbial, ligand-promoted, and electrochemical reduction and dissolution of Fe-organic associations, regarding (i) electron shuttling, (ii) complexation of Fe(II,III), (iii) surface site coverage and/or pore blockage, (iv) aggregation, and (v) crystallinity. Specifically, the following hypotheses were addressed:

- H1** Dissolved organic matter enhances microbial reduction of Fe oxyhydroxides by complexation of Fe(II, III) and by providing redox active electron-shuttling compounds.
- H2** Adsorbed and coprecipitated OM inhibits microbial reduction of Fe oxyhydroxides by blocking surface sites and inducing aggregation.
- H3** Organic matter inhibits the transformation of Fe oxyhydroxides during microbial Fe reduction in comparison to pure Fe oxyhydroxides.
- H4** Ferrihydrite-OM coprecipitates are more prone to microbial reduction than ferrihydrite-OM adsorption complexes due to their more defective crystal structure.
- H5** Fe-reducing bacteria using different electron transfer mechanisms are affected by adsorbed and coprecipitated OM to differing degrees.
- H6** Ligand-promoted dissolution of ferrihydrite is inhibited by adsorbed and coprecipitated organic matter via surface site blockage and aggregation.
- H7** Mediated electrochemical reduction assesses both the redox state of ferrihydrite and ferrihydrite-organic matter coprecipitates and their stability against reductive mobilization.

In order to assess these hypotheses, the following studies were conducted:

I. Microbial Reduction of Ferrihydrite-Organic Matter Coprecipitates by *Shewanella putrefaciens* and *Geobacter metallireducens* in Comparison to Mediated Electrochemical Reduction

Study I aimed to systematically assess the effect of coprecipitated OM on the microbial reduction of Fe-OM coprecipitates with regard to (i) the composition of OM, (ii) easily desorbable compounds, (iii) the surface site coverage and/or pore blockage by OM, and (iv) aggregation states. Pure ferrihydrite and Fe-OM coprecipitates were synthesized using three different types of OM (extracellular polymeric substances extracted from *Bacillus subtilis* (EPS), OM extracted from the Oi horizon of a Cambisol under beech (beech Oi), and OM extracted from the Oa horizon of a Podzol under spruce (spruce Oa)). These phases were characterized by N₂ gas adsorption, nuclear magnetic resonance spectroscopy (NMR), Fourier transform infrared spectroscopy (FTIR), X-ray diffraction (XRD), X-ray photoelectron spectroscopy (XPS), NOM desorption experiments, and mediated electrochemical reduction (MER). Iron(III) reduction under anaerobic conditions was monitored for 16 days using two different strains of dissimilatory Fe(III)-reducing bacteria (*Shewanella putrefaciens*, *Geobacter metallireducens*). Mineral transformation during reduction was determined by XRD and FTIR of the solid post-incubation phases.

II. Impact of Natural Organic Matter Coatings on the Microbial Reduction of Iron Oxides

Study II examined the impact of both the composition and concentration of adsorbed OM on microbial Fe reduction with regard to (i) electron shuttling, (ii) complexation of Fe(II,III), (iii) surface site coverage and/or pore blockage, and (iv) aggregation. Adsorption complexes with varying carbon loadings were synthesized combining different Fe oxyhydroxides (ferrihydrite, lepidocrocite, goethite, hematite, magnetite) with OM of different origin (EPS, beech Oi and spruce Oa). The adsorption complexes were characterized by XRD, FTIR, XPS, N₂ gas adsorption, electrophoretic mobility and particle size measurements, and OM desorption. Incubation experiments under anaerobic conditions were conducted for 16 days comparing two different strains of dissimilatory Fe(III)-reducing bacteria (*Shewanella putrefaciens*, *Geobacter metallireducens*). Mineral transformation during reduction was assessed via XRD and FTIR.

III. Siderophore-promoted dissolution of ferrihydrite associated with adsorbed and coprecipitated natural organic matter

Study III explored the impact of the composition of both adsorbed and coprecipitated OM on the siderophore-promoted dissolution of ferrihydrite in relation to (i) surface site coverage and pore blockage, (ii) aggregation state, (iii) charge characteristics, and (iv) crystallinity with additional consideration of the pH. Ferrihydrite-OM adsorption complexes and Fe-OM coprecipitates were synthesized in addition to pure ferrihydrite using OM of different origin (EPS, beech Oi and spruce Oa). The Fe-organic associations were characterized by N₂ gas adsorption, XPS, electrophoretic mobility, particle size measurements and desorption experiments. Siderophore-mediated dissolution experiments with desferrioxamine-B (DFOB) were conducted at both pH 4 and pH 7.

1.7 References

- Alvarez-Puebla, R.A., Garrido, J.J., 2005. Effect of pH on the aggregation of a gray humic acid in colloidal and solid states. *Chemosphere* 59, 659–667. doi:10.1016/j.chemosphere.2004.10.021
- Amstaetter, K., Borch, T., Kappler, A., 2012. Influence of humic acid imposed changes of ferrihydrite aggregation on microbial Fe(III) reduction. *Geochim. Cosmochim. Acta* 85, 326–341. doi:10.1016/j.gca.2012.02.003
- Angelico, R., Ceglie, A., He, J.Z., Liu, Y.R., Palumbo, G., Colombo, C., 2014. Particle size, charge and colloidal stability of humic acids coprecipitated with ferrihydrite. *Chemosphere* 99, 239–247. doi:10.1016/j.chemosphere.2013.10.092
- April, R., Keller, D., 1990. Mineralogy of the rhizosphere in forest soils of the eastern United States. *Biogeochemistry*. doi:10.1007/BF00002714
- Bachand, P.A.M., Richardson, C.J., Vaithyanathan, P., 2000. Phase II low intensity chemical dosing (LICD): Development of management practices. Final report submitted to Florida Department of Environmental Protection in fulfillment of Contract No. WM720.
- Bazylinski, D.A., Frankel, R.B., Konhauser, K.O., 2007. Modes of biomineralization of magnetite by microbes. *Geomicrobiol. J.* 24, 465–475. doi:10.1080/01490450701572259
- Berg, J.M., Tymoczko, J.L., Stryer, L., 2002. *Biochemistry*, 5th ed. W. H. Freeman, New York, USA.
- Beveridge, T.J., Makin, S.A., Kadurugamuwa, J.L., Li, Z., 1997. Interactions between biofilms and the environment. *FEMS Microbiol. Rev.* 20, 291–303. doi:10.1016/S0168-6445(97)00012-0
- Boesen, T., Nielsen, P., 2013. Molecular dissection of bacterial nanowires. *MBio* 4, e00270-13. doi:10.1128/mBio.00270-13.Copyright
- Bondietti, G., Sinniger, J., Stumm, W., 1993. The reactivity of Fe(III) (hydr)oxides - Effects of ligands in inhibiting the dissolution. *Colloids Surfaces A Physicochem. Eng. Asp.* 79, 157–167.
- Bonneville, S., Behrends, T., Cappellen, P. Van, Hyacinthe, C., Röling, W.F.M., 2006. Reduction of Fe(III) colloids by *Shewanella putrefaciens*: A kinetic model. *Geochim. Cosmochim. Acta* 70, 5842–5854. doi:10.1016/j.gca.2006.04.029
- Bonneville, S., Morgan, D.J., Schmalenberger, A., Bray, A., Brown, A., Banwart, S.A., Benning, L.G., 2011. Tree-mycorrhiza symbiosis accelerate mineral weathering: Evidences from nanometer-scale elemental fluxes at the hypha-mineral interface. *Geochim. Cosmochim. Acta* 75, 6988–7005. doi:10.1016/j.gca.2011.08.041
- Brantley, S.L., Magonigal, J.P., Scatena, F.N., Balogh-Brunstad, Z., Barnes, R.T., Bruns, M.A., Van Cappellen, P., Dontsova, K., Hartnett, H.E., Hartshorn, A.S., Heimsath, A., Herndon, E., Jin, L., Keller, C.K., Leake, J.R., Mcdowell, W.H., Meinzer, F.C., Mozdzer, T.J., Petsch, S., Pett-Ridge, J., Pregitzer, K.S., Raymond, P.A., Riebe, C.S., Shumaker, K., Sutton-Grier, A., Walter, R., Yoo, K., 2011. Twelve testable hypotheses on the geobiology of weathering. *Geobiology* 9, 140–165. doi:10.1111/j.1472-4669.2010.00264.x
- Brümmer, G.W., Barrow, N.J., Fischer, L., 2013. Effect of porosity of goethite on the sorption of six heavy metal ions. *Eur. J. Soil Sci.* 64, 805–813. doi:10.1111/ejss.12091
- Canfield, D.E., 1989. Reactive iron in marine sediments. *Geochim. Cosmochim. Acta* 53, 619–632. doi:10.1016/0016-7037(89)90005-7
- Canfield, D.E., Jorgensen, B.B., Fossing, H., Glud, R., Gundersen, J., Ramsing, N.B., Thamdrup, B., Hansen, J.W., Nielsen, L.P., Hall, P.O.J., 1993. Pathways of organic carbon oxidation in three continental margin sediments. *Mar. Geol.* 113, 27–40.
- Cheah, S.-F., Kraemer, S.M., Cervini-Silva, J., Sposito, G., 2003. Steady-state dissolution kinetics of goethite in the presence of desferrioxamine B and oxalate ligands: implications for the microbial acquisition of iron. *Chem. Geol.* 198, 63–75.

- doi:10.1016/S0009-2541(02)00421-7
- Chen, J., Gu, B., Royer, R.A., Burgos, W.D., 2003. The roles of natural organic matter in chemical and microbial reduction of ferric iron. *Sci. Total Environment* 307, 167–78. doi:10.1016/S0048-9697(02)00538-7
- Cheng, H., Hu, Y., Luo, J., Xu, B., Zhao, J., 2009. Geochemical processes controlling fate and transport of arsenic in acid mine drainage (AMD) and natural systems. *J. Hazard. Mater.* 165, 13–26. doi:10.1016/j.jhazmat.2008.10.070
- Childs, C.W., 1992. Ferrihydrite: A review of structure, properties, and occurrence in relation to soils. *J. Plant Nutr. Soil Sci.* 155, 441–448. doi:10.1002/jpln.19921550515
- Chorover, J., Amistadi, M.K., 2001. Reaction of forest floor organic matter at goethite, birnessite and smectite surfaces. *Geochim. Cosmochim. Acta* 65, 95–109.
- Cismasu, A.C., Michel, F.M., Tcaciuc, A. P., Tyliszczak, T., Brown, Jr, G.E., 2011. Composition and structural aspects of naturally occurring ferrihydrite. *Comptes Rendus Geosci.* 343, 210–218. doi:10.1016/j.crte.2010.11.001
- Coates, J.D., Ellis, D.J., Roden, E., Gaw, K., Blunt-Harris, E.L., Lovley, D.R., 1998. Recovery of humics-reducing bacteria from a diversity of sedimentary environments. *Appl. Environ. Microbiol.* 64, 1504–1509.
- Cornell, R.M., Schwertmann, U., 2003. *The iron oxides*, 2nd ed. Wiley-VCH. doi:10.1002/3527602097
- Dolfing, J., Chardon, W.J., Japenga, J., 1999. Association between colloidal iron, aluminum, phosphorus, and humic acids. *Soil Sci.* 164, 171–179. doi:10.1097/00010694-199903000-00003
- Downing, B.D., Bergamaschi, B.A., Evans, D.G., Boss, E., 2008. Assessing contribution of DOC from sediments to a drinking-water reservoir using optical profiling. *Lake Reserv. Manag.* 24, 381–391. doi:10.1080/07438140809354848
- El-Naggar, M.Y., Wanger, G., Leung, K.M., Yuzvinsky, T.D., Southam, G., Yang, J., Lau, W.M., Nealson, K.H., Gorby, Y.A., 2010. Electrical transport along bacterial nanowires from *Shewanella oneidensis* MR-1. *Proc. Natl. Acad. Sci. U. S. A.* 107, 18127–31. doi:10.1073/pnas.1004880107
- Essington, M.E., 2004. *Soil and water chemistry: an integrated approach*. CRC Press, Boca Raton, Florida, USA.
- Eusterhues, K., Hädrich, A., Neidhardt, J., Küsel, K., Keller, T.F., Jandt, K.D., Totsche, K.U., 2014. Reduction of ferrihydrite with adsorbed and coprecipitated organic matter: microbial reduction by *Geobacter bremensis* vs. abiotic reduction by Na-dithionite. *Biogeosciences* 11, 4953–4966. doi:10.5194/bg-11-4953-2014
- Eusterhues, K., Rennert, T., Knicker, H., Kögel-Knabner, I., Totsche, K.U., Schwertmann, U., 2011. Fractionation of organic matter due to reaction with ferrihydrite: coprecipitation versus adsorption. *Environ. Sci. Technol.* 45, 527–33. doi:10.1021/es1023898
- Eusterhues, K., Wagner, F.E., Häusler, W., Hanzlik, M., Knicker, H., Totsche, K.U., Kögel-Knabner, I., Schwertmann, U., 2008. Characterization of ferrihydrite-soil organic matter coprecipitates by X-ray diffraction and Mössbauer spectroscopy. *Environ. Sci. Technol.* 42, 7891–7.
- Furrer, G., Stumm, W., 1986. The coordination chemistry of weathering: I. Dissolution kinetics of δ -Al₂O₃ and BeO. *Geochim. Cosmochim. Acta* 50, 1847–1860. doi:10.1016/0016-7037(86)90243-7
- Glasauer, S., Weidler, P.G., Langley, S., Beveridge, T.J., 2003. Controls on Fe reduction and mineral formation by a subsurface bacterium. *Geochim. Cosmochim. Acta* 67, 1277–1288. doi:10.1016/S0016-7037(00)01199-7
- Goebel, M.-O., Adams, F., Boy, J., Guggenberger, G., Mikutta, R., 2017. Mobilization of glucose-6-phosphate from ferrihydrite by ligand-promoted dissolution is higher than of orthophosphate. *J. Plant Nutr. Soil Sci.* 180, 279–282. doi:10.1002/jpln.201600479

- Gorby, Y., Yanina, S., McLean, J.S., Rosso, K.M., Moyles, D., Dohnalkova, A., Beveridge, T.J., Chang, I.S., Kim, B.H., Kim, K.S., Culley, D.E., Reed, S.B., Romine, M.F., Saffarini, D.A., Hill, E.A., Shi, L., Elias, D.A., Kennedy, D.W., Pinchuk, G., Watanabe, K., Ishii, S., Logan, B., Nealson, K.H., Fredrickson, J.K., 2006. Correction for Lygeros et al., Stochastic hybrid modeling of DNA replication across a complete genome. *Proc. Natl. Acad. Sci. U.S.A.* 103, 11358–11363. doi:10.1073/pnas.0905246106
- Gray, H.B., Winkler, J.R., 2010. Electron flow through metalloproteins. *Biochim. Biophys. Acta - Bioenerg.* 1797, 1563–1572. doi:10.1016/j.bbabi.2010.05.001
- Hanke, A., Cerli, C., Muhr, J., Borken, W., Kalbitz, K., 2013. Redox control on carbon mineralization and dissolved organic matter along a chronosequence of paddy soils. *Eur. J. Soil Sci.* 64, 476–487. doi:10.1111/ejss.12042
- Henneberry, Y.K., Kraus, T.E.C., Fleck, J.A., Krabbenhoft, D.P., Bachand, P.M., Horwath, W.R., 2011. Removal of inorganic mercury and methylmercury from surface waters following coagulation of dissolved organic matter with metal-based salts. *Sci. Total Environ.* 409, 631–637. doi:10.1016/j.scitotenv.2010.10.030
- Henneberry, Y.K., Kraus, T.E.C., Nico, P.S., Horwath, W.R., 2012. Structural stability of coprecipitated natural organic matter and ferric iron under reducing conditions. *Org. Geochem.* 48, 81–89. doi:10.1016/j.orggeochem.2012.04.005
- Hernandez, M.E., Kappler, A., Newman, D.K., 2004. Phenazines and other redox-active antibiotics promote microbial mineral reduction. *Appl. Environ. Microbiol.* 70, 921–928. doi:10.1128/AEM.70.2.921
- Jiang, J., Kappler, A., 2008. Kinetics of microbial and chemical reduction of humic substances: implications for electron shuttling. *Environ. Sci. Technol.* 42, 3563–9.
- Jones, A.M., Collins, R.N., Rose, J., Waite, T.D., 2009. The effect of silica and natural organic matter on the Fe(II)-catalysed transformation and reactivity of Fe(III) minerals. *Geochim. Cosmochim. Acta* 73, 4409–4422. doi:10.1016/j.gca.2009.04.025
- Kaiser, K., Guggenberger, G., 2007. Sorptive stabilization of organic matter by microporous goethite: sorption into small pores vs. surface complexation. *Eur. J. Soil Sci.* 58, 45–59. doi:10.1111/j.1365-2389.2006.00799.x
- Kaiser, K., Guggenberger, G., 2003. Mineral surfaces and soil organic matter. *Eur. J. Soil Sci.* 54, 219–236.
- Kaiser, K., Zech, W., 1999. Release of natural organic matter sorbed to oxides and a subsoil. *Soil Sci. Soc. Am. J.* 63, 1157–1166.
- Kalbitz, K., Schwesig, D., Rethemeyer, J., Matzner, E., 2005. Stabilization of dissolved organic matter by sorption to the mineral soil. *Soil Biol. Biochem.* 37, 1319–1331. doi:10.1016/j.soilbio.2004.11.028
- Kalbitz, K., Solinger, S., Park, J.-H., Michalzik, B., Matzner, E., 2000. Controls on the Dynamics of Dissolved Organic Matter in Soils: a Review. *Soil Sci.* 165, 277–304. doi:10.1097/00010694-200004000-00001
- Kämpf, N., Scheinost, A.L., Schulze, D.G., 2000. *Oxide minerals*. CRC Press, Boca Raton, Florida, USA.
- Kappler, A., Wuestner, M.L., Ruecker, A., Harter, J., Halama, M., Behrens, S., 2014. Biochar as an Electron Shuttle between Bacteria and Fe(III) Minerals. *Environ. Sci. Technol.* 1, 339–344. doi:10.1021/ez5002209
- Kleber, M., Eusterhues, K., Keiluweit, M., Mikutta, C., Mikutta, R., Nico, P.S., 2015. Mineral–organic associations: formation, properties, and relevance in soil environments. *Adv. Agron.* 130. doi:10.1016/bs.agron.2014.10.005
- Klüpfel, L., Keiluweit, M., Kleber, M., Sander, M., 2014. Redox properties of plant biomass-derived black carbon (biochar). *Environ. Sci. Technol.* 48, 5601–5611. doi:10.1021/es500906d
- Kögel-Knabner, I., Amelung, W., Cao, Z., Fiedler, S., Frenzel, P., Jahn, R., Kalbitz, K.,

- Kölbl, A., Schloter, M., 2010. Biogeochemistry of paddy soils. *Geoderma* 157, 1–14. doi:10.1016/j.geoderma.2010.03.009
- Kotloski, N.J., Gralnick, J.A., 2013. Flavin electron shuttles dominate extracellular electron transfer by *Shewanella oneidensis*. *MBio* 4, 10–13. doi:10.1128/mBio.00553-12
- Kraemer, S.M., 2004. Iron oxide dissolution and solubility in the presence of siderophores. *Aquat. Sci. - Res. Across Boundaries* 66, 3–18. doi:10.1007/s00027-003-0690-5
- Kraemer S. M., Crowley D. E. and Kretzschmar R., 2006. Geochemical aspects of phytosiderophore-promoted iron acquisition by plants. *Adv. Agron.* 91, 1–46.
- Larsen, O., Postma, D., 2001. Kinetics of reductive bulk dissolution of lepidocrocite, ferrihydrite, and goethite. *Geochim. Cosmochim. Acta* 65, 1367–1379. doi:10.1016/S0016-7037(00)00623-2
- Liang, S., David, J.R., Zheming, W., Sebastien, N.K., Kevin, M.R., John, M.Z., James, K.F., 2009. The roles of outer membrane cytochromes of *Shewanella* and *Geobacter* in extracellular electron transfer. *Environ. Microbiol. Rep.* 1, 220–227. doi:10.1111/j.1758-2229.2009.00035.x
- Liu, C., Zachara, J.M., Foster, N., Strickland, J., 2007. Kinetics of reductive dissolution of hematite by bio-reduced anthraquinone-2,6-disulfonate 1–7.
- Lovley, D.R., Anderson, R.T., 2000. Influence of dissimilatory metal reduction on fate of organic and metal contaminants in the subsurface. *Hydrogeol. J.* 8, 77–88.
- Lovley, D.R., Blunt-Harris, E.L., 1999. Role of humic-bound iron as an electron transfer agent in dissimilatory Fe (III) reduction. *Appl. Environ. Microbiol.* 65, 4252–4254.
- Lovley, D.R., Coates, J.D., Blunt-Harris, E.L., Phillips, E.J.P., Woodward, J.C., 1996. Humic substances as electron acceptors for microbial respiration. *Nature* 382, 445–448.
- Lovley, D.R., Fraga, J.L., Hayes, L.A., Phillips, E.J.P., Coates, J.D., 1998. Humic Substances as a Mediator for Microbially Catalyzed Metal Reduction. *Acta Hydrochim. Hydrobiol.* 26, 152–157.
- Lovley, D.R., Giovannoni, S.J., White, D.C., Champine, J.E., Phillips, E.J.P., Gorby, Y.A., Goodwin, S., 1993. *Geobacter metallireducens* gen. nov. sp. nov., a microorganism capable of coupling the complete oxidation of organic compounds to the reduction of iron and other metals. *Arch. Microbiol.* 159, 336–344.
- Lovley, D.R., Holmes, D.E., Nevin, K.P., 2004. Dissimilatory Fe(III) and Mn(IV) reduction. *Adv. Microb. Physiol.* 49, 219–86. doi:10.1016/S0065-2911(04)49005-5
- Lovley, D.R., Phillips, E.J.P., 1988. Novel mode of microbial energy metabolism: organic carbon oxidation coupled to dissimilatory reduction of iron or manganese. *Appl. Environ. Microbiol.* 54, 1472–80.
- Lovley, D.R., Phillips, E.J.P., Lonergan, D.J., 1989. Hydrogen and formate oxidation coupled to dissimilatory reduction of iron or manganese by *Alteromonas putrefaciens*. *Appl. Environ. Microbiol.* 55, 700–706.
- Lovley, D.R., Ueki, T., Zhang, T., Malvankar, N.S., Shrestha, P.M., Flanagan, K.A., Aklujkar, M., Butler, J.E., Giloteaux, L., Rotaru, A.-E., Holmes, D.E., Franks, A.E., Orellana, R., Risso, C., Nevin, K.P., 2011. *Geobacter*, in: Poole, R.K. (Ed.), *Advances in Microbial Physiology*. Elsevier, Amsterdam, pp. 1–100. doi:10.1016/B978-0-12-387661-4.00004-5
- Lovley, D.R., Woodward, J.C., Chappelle, F.H., 1994. Stimulated anoxic biodegradation of aromatic hydrocarbons using Fe(III) ligands. *Nature* 370, 128–131.
- Ludwig, C., Casey, W.H., Rock, P.A., 1995. Prediction of ligand-promoted dissolution rates from the reactivities of aqueous complexes. *Nature*. doi:10.1038/375044a0
- Luo, Y.R., 2007. *Comprehensive handbook of chemical bond energies*. CRC Press, Boca Raton, Florida, USA.
- Lützow, M. V., Kögel-Knabner, I., Ekschmitt, K., Matzner, E., Guggenberger, G., Marschner, B., Flessa, H., 2006. Stabilization of organic matter in temperate soils: Mechanisms and

- their relevance under different soil conditions - A review. *Eur. J. Soil Sci.* 57, 426–445. doi:10.1111/j.1365-2389.2006.00809.x
- Malvankar, N.S., Vargas, M., Nevin, K.P., Franks, A.E., Leang, C., Kim, B.-C., Inoue, K., Mester, T., Covalla, S.F., Johnson, J.P., Rotello, V.M., Tuominen, M.T., Lovley, D.R., 2011. Tunable metallic-like conductivity in microbial nanowire networks. *Nat. Nanotechnol.* 6, 573–579. doi:10.1038/nnano.2011.119
- Marsili, E., Baron, D.B., Shikhare, I.D., Coursolle, D., Gralnick, J.A., Bond, D.R., 2008. *Shewanella* secretes flavins that mediate extracellular electron transfer. *Proc. Natl. Acad. Sci. U. S. A.* 105, 3968–73. doi:10.1073/pnas.0710525105
- Melton, E.D., Swanner, E.D., Behrens, S., Schmidt, C., Kappler, A., 2014. The interplay of microbially mediated and abiotic reactions in the biogeochemical Fe cycle. *Nat. Rev. Microbiol.* 12, 797–808. doi:10.1038/nrmicro3347
- Mesuere, K., Fish, W., 1999. Chromate and oxalate adsorption on goethite. 2. Surface complexation modeling of competitive adsorption. *Environ. Sci. Technol.* 26, 2365–2370.
- Michel, F.M., Barrón, V., Torrent, J., Morales, M.P., Serna, C.J., Boily, J.-F., Liu, Q., Ambrosini, A., Cismasu, A. C., Brown, G.E., 2010. Ordered ferrimagnetic form of ferrihydrite reveals links among structure, composition, and magnetism. *Proc. Natl. Acad. Sci. U. S. A.* 107, 2787–92. doi:10.1073/pnas.0910170107
- Mikutta, C., Kretzschmar, R., 2008. Synthetic coprecipitates of exopolysaccharides and ferrihydrite. Part II: Siderophore-promoted dissolution. *Geochim. Cosmochim. Acta* 72, 1128–1142. doi:10.1016/j.gca.2007.11.034
- Mikutta, R., Baumgärtner, A., Schippers, A., Haumaier, L., Guggenberger, G., 2012. Extracellular polymeric substances from *Bacillus subtilis* associated with minerals modify the extent and rate of heavy metal sorption. *Environ. Sci. Technol.* 46, 3866–73. doi:10.1021/es204471x
- Mikutta, R., Kleber, M., Torn, M.S., Jahn, R., 2006. Stabilization of soil organic matter: association with minerals or chemical recalcitrance? *Biogeochemistry* 77, 25–56. doi:10.1007/s10533-005-0712-6
- Mikutta, R., Mikutta, C., Kalbitz, K., Scheel, T., Kaiser, K., Jahn, R., 2007. Biodegradation of forest floor organic matter bound to minerals via different binding mechanisms. *Geochim. Cosmochim. Acta* 71, 2569–2590. doi:10.1016/j.gca.2007.03.002
- Myers, C.R., Nealson, K.H., 1988. Bacterial manganese reduction and growth with manganese oxide as the sole electron acceptor. *Science* 240, 1319–21. doi:10.1126/science.240.4857.1319
- Neilands, J.B., 1957. Some aspects of microbial iron metabolism. *Anal. Biochem.* 21, 220–230.
- Nevin, K.P., Lovley, D.R., 2002. Mechanisms for accessing insoluble Fe(III) oxide during dissimilatory Fe(III) reduction by *Geothrix fermentans*. *Appl. Environ. Microbiol.* 68, 2294–2299. doi:10.1128/AEM.68.5.2294
- Nevin, K.P., Lovley, D.R., 2000. Lack of production of electron-shuttling compounds or solubilization of Fe(III) during reduction of insoluble Fe(III) oxide by *Geobacter metallireducens*. *Appl. Environ. Microbiol.* 66, 2248–51.
- Nevin, K.P., Lovley, D.R., 2000. Potential for nonenzymatic reduction of Fe(III) via electron shuttling in subsurface sediments. *Environ. Sci. Technol.* 34, 2472–2478. doi:10.1021/es991181b
- Newman, D.K., Kolter, R., 2000. A role for excreted quinones in extracellular electron transfer. *Nature* 405, 94–7. doi:10.1038/35011098
- Nielsen, L.P., Risgaard-Petersen, N., Fossing, H., Christensen, P.B., Sayama, M., 2010. Electric currents couple spatially separated biogeochemical processes in marine sediment. *Nature* 463, 1071–1074. doi:10.1038/nature08790

- Nierop, K.G.J., Jansen, B., Verstraten, J.M., 2002. Dissolved organic matter, aluminium and iron interactions: Precipitation induced by metal/carbon ratio, pH and competition. *Sci. Total Environ.* 300, 201–211. doi:10.1016/S0048-9697(02)00254-1
- Pédrot, M., Le Boudec, A., Davranche, M., Dia, A., Henin, O., 2011. How does organic matter constrain the nature, size and availability of Fe nanoparticles for biological reduction? *J. Colloid Interface Sci.* 359, 75–85. doi:10.1016/j.jcis.2011.03.067
- Perelomov, L. V., Pinskiy, D.L., Violante, A., 2011. Effect of organic acids on the adsorption of copper, lead, and zinc by goethite. *Eurasian Soil Sci.* 44, 22–28. doi:10.1134/S1064229311010091
- Piepenbrock, A., Behrens, S., Kappler, A., 2014. Comparison of humic substance- and Fe (III)- reducing microbial communities in anoxic aquifers. *Geomicrobiol. J.* 31, 917–928. doi:10.1080/01490451.2014.911994
- Powell, P.E., Cline, G.R., Reid, C.P.P., Szaniszlo, P.J., 1980. Occurrence of hydroxamate siderophore iron chelators in soils. *Nature.* doi:10.1038/287833a0
- Rancourt, D.G., Thibault, P.J., Mavrocordatos, D., Lamarche, G., 2005. Hydrous ferric oxide precipitation in the presence of nonmetabolizing bacteria: Constraints on the mechanism of a biotic effect. *Geochim. Cosmochim. Acta* 69, 553–577. doi:10.1016/j.gca.2004.07.018
- Reguera, G., McCarthy, K.D., Mehta, T., Nicoll, J.S., Tuominen, M.T., Lovley, D.R., 2005. Extracellular electron transfer via microbial nanowires. *Nature* 435, 1098–101. doi:10.1038/nature03661
- Reichard, P.U., Kretzschmar, R., Kraemer, S.M., 2007. Dissolution mechanisms of goethite in the presence of siderophores and organic acids. *Geochim. Cosmochim. Acta* 71, 5635–5650. doi:10.1016/j.gca.2006.12.022
- Roden, E.E., 2003. Fe(III) oxide reactivity toward biological versus chemical reduction. *Environ. Sci. Technol.* 37, 1319–1324. doi:10.1021/es026038o
- Roemheld, V., 1991. The Role of phytosiderophores in aquisition of iron and other micronutrients in graminaceous species: an ecological approach. *Plant Soil* 130, 127–134.
- Royer, R.A., Burgos, W.D., Fisher, A.S., Jeon, B.-H., Unz, R.F., Dempsey, B. a, 2002. Enhancement of hematite bioreduction by natural organic matter. *Environ. Sci. Technol.* 36, 2897–904. doi:10.1021/es015735y
- Sander, M., Hofstetter, T.B., Gorski, C.A., 2015. Electrochemical analyses of redox-active iron minerals: A review of non-mediated and mediated approaches. *Environ. Sci. Technol.* 49, 5862–5878. doi:10.1021/acs.est.5b00006
- Sannino, F., De Martino, A., Pigna, M., Violante, A., Di Leo, P., Mesto, E., Capasso, R., 2009. Sorption of arsenate and dichromate on polymerin, Fe(OH)_x-polymerin complex and ferrihydrite. *J. Hazard. Mater.* 166, 1174–9. doi:10.1016/j.jhazmat.2008.12.015
- Scheel, T., Dörfel, C., Kalbitz, K., 2007. Precipitation of dissolved organic matter by aluminum stabilizes carbon in acidic forest soils. *Soil Sci. Soc. Am. J.* 71, 64–74. doi:10.2136/sssaj2006.0111
- Schwertmann, U., 1991. Solubility and dissolution of iron oxides. *Plant Soil* 130, 1–25.
- Schwertmann, U., 1985. The effect of pedogenic environments on iron oxide minerals, in: *Advances in Soil Science.* pp. 171–200.
- Schwertmann, U., Cornell, R.M., 2000. *Iron Oxides in the Laboratory: Preparation and Characterization*, 2nd ed. Wiley-VCH, Weinheim, Germany.
- Schwertmann, U., Wagner, F., Knicker, H., 2005. Ferrihydrite–humic associations: magnetic hyperfine interactions. *Soil Sci. Soc. Am. J.* 69, 1009–1015. doi:10.2136/sssaj2004.0274
- Scott, D.T., McKnight, D.M., Blunt-Harris, E.L., Kolesar, S.E., Lovley, D.R., 1998. Quinone moieties act as electron acceptors in the reduction of humic substances by humics-reducing microorganisms. *Environ. Sci. Technol.* 32, 2984–2989.

- doi:10.1021/es980272q
- Shimizu, M., Zhou, J., Schröder, C., Obst, M., Kappler, A., Borch, T., 2013. Dissimilatory reduction and transformation of ferrihydrite-humic acid coprecipitates. *Environ. Sci. Technol.* 47, 13375–84. doi:10.1021/es402812j
- Siéliéchi, J.M., Lartiges, B.S., Kayem, G.J., Hupont, S., Frochot, C., Thieme, J., Ghanbaja, J., d’Espinose de la Caillerie, J.B., Barrès, O., Kamga, R., Levitz, P., Michot, L.J., 2008. Changes in humic acid conformation during coagulation with ferric chloride: Implications for drinking water treatment. *Water Res.* 42, 2111–2123. doi:10.1016/j.watres.2007.11.017
- Stevenson, F.J., 1994. *Humus chemistry - genesis, composition, reactions*, 2nd ed. John Wiley & Sons, New York.
- Stookey, L.L., 1970. Ferrozine - a new spectrophotometric reagent for iron. *Anal. Chem.* 42, 779–781. doi:10.1021/ac60289a016
- Takagi, S., 1976. Naturally occurring iron-chelating compounds in oat- and rice-root washings. *Soil Sci. Plant Nutr.* 22, 423–433. doi:10.1080/00380768.1976.10433004
- Thamdrup B., 2000. *Bacterial manganese and iron reduction in aquatic sediments*. Adv. Microb. Ecol. Kluwer Academic/ Plenum Publishers, New York.
- Vargas, M., Kashefi, K., Blunt-Harris, E.L., Lovley, D.R., 1998. Microbiological evidence for Fe(III) reduction on early Earth. *Nature* 395, 65–67. doi:10.1038/25720
- Violante, A., Ricciardella, M., Pigna, M., 2003. Adsorption of heavy metals on mixed Fe-Al oxides in the absence or presence of organic ligands. *Water. Air. Soil Pollut.* 143, 289–306.
- von Canstein, H., Ogawa, J., Shimizu, S., Lloyd, J.R., 2008. Secretion of flavins by *Shewanella* species and their role in extracellular electron transfer. *Appl. Environ. Microbiol.* 74, 615–23. doi:10.1128/AEM.01387-07
- Wagai, R., Mayer, L.M., 2007. Sorptive stabilization of organic matter in soils by hydrous iron oxides. *Geochim. Cosmochim. Acta* 71, 25–35. doi:10.1016/j.gca.2006.08.047
- Wang, Z., Schenkeveld, W.D.C., Kraemer, S.M., Giammar, D.E., 2015. Synergistic effect of reductive and ligand-promoted dissolution of goethite. *Environ. Sci. Technol.* 49, 7236–7244. doi:10.1021/acs.est.5b01191
- Weber, K.A., Achenbach, L.A., Coates, J.D., 2006. Microorganisms pumping iron: anaerobic microbial iron oxidation and reduction. *Nat. Rev. Microbiol.* 4, 752–64. doi:10.1038/nrmicro1490
- Weiss, J. V., Emerson, D., Megonigal, J.P., 2004. Geochemical control of microbial Fe(III) reduction potential in wetlands: comparison of the rhizosphere to non-rhizosphere soil. *FEMS Microbiol. Ecol.* 48, 89–100. doi:10.1016/j.femsec.2003.12.014
- Winkelmann, G., 1992. Structures and functions of fungal siderophores containing hydroxamate and complexone type iron binding ligands. *Mycol. Res.* 96, 529–534. doi:10.1016/S0953-7562(09)80976-3
- Wolf, M., Kappler, A., Jiang, J., Meckenstock, R.U., 2009. Effects of humic substances and quinones at low concentrations on ferrihydrite reduction by *Geobacter metallireducens*. *Environ. Sci. Technol.* 43, 5679–85.
- Zachara, J.M., Kukkadapu, R.K., Peretyazhko, T., Bowden, M., Wang, C., Kennedy, D.W., Moore, D., Arey, B., 2011. The mineralogic transformation of ferrihydrite induced by heterogeneous reaction with bio-reduced anthraquinone disulfonate (AQDS) and the role of phosphate. *Geochim. Cosmochim. Acta* 75, 6330–6349. doi:10.1016/j.gca.2011.06.030
- Zhu, W., Nan, Y., Huang, T., Wu, F., 2013. The mechanism, thermodynamic and kinetic characteristics of the microbial reduction of goethite mediated by anthraquinone-2-sulfonate. *Geomicrobiol. J.* 30, 928–940. doi:10.1080/01490451.2013.791356

2 Study I

**Microbial Reduction of Ferrihydrite-Organic Matter Coprecipitates by
Shewanella putrefaciens and *Geobacter metallireducens* in Comparison to
Mediated Electrochemical Reduction**

Contribution: I was involved in designing the experiments, prepared the Fe-organic associations, conducted the laboratory experiments and most of the analyses, collected and evaluated the data, compiled the tables and graphs, and wrote the manuscript.

Published in *Chemical Geology* 447 (2016) 133-147.

DOI: 10.1016/j.chemgeo.2016.09.031.

**Microbial Reduction of Ferrihydrite-Organic Matter Coprecipitates by
Shewanella putrefaciens and *Geobacter metallireducens* in Comparison to
Mediated Electrochemical Reduction**

Christine Poggenburg^{1,2,*}, Robert Mikutta³, Michael Sander⁴, Axel Schippers⁵,
Alexander Marchanka^{6,7}, Reiner Dohrmann^{5,8}, Georg Guggenberger^{1,2}

¹ Institute of Soil Science, Leibniz University Hannover,
Herrenhäuser Straße 2, 30419 Hannover, Germany

² Centre for Solid State Chemistry and New Materials, Leibniz University Hannover,
Callinstraße 3, 30167 Hannover, Germany

³ Soil Science and Soil Protection, Martin Luther University Halle-Wittenberg,
Von-Seckendorff-Platz 3, 06210 Halle (Saale), Germany

⁴ Institute of Biogeochemistry and Pollutant Dynamics, Swiss Federal Institute of Technology,
Universitätstrasse 16, 8029 Zurich, Switzerland

⁵ Bundesanstalt für Geowissenschaften und Rohstoffe (BGR),
Stilleweg 2, 30655 Hannover, Germany

⁶ Institute of Organic Chemistry, Leibniz University Hannover,
Schneiderberg 1B, 30167 Hannover, Germany

⁷ Centre of Biomolecular Drug Research (BMWZ), Leibniz University Hannover,
Schneiderberg 38, 30167 Hannover, Germany

⁸ Landesamt für Bergbau, Energie und Geologie (LBEG),
Stilleweg 2, 30655 Hannover, Germany

*Corresponding author: poggenburg@ifbk.uni-hannover.de, +49 5117622625

Abstract

Despite numerous studies seeking to elucidate the effect of various specific organic compounds on the reactivity and stability of Fe oxyhydroxides in soil, studies examining the effect of natural organic matter (NOM) on the microbial reduction of Fe-organic matter (OM) coprecipitates are still rare. In this study, pure ferrihydrite (Fh) and Fe-OM coprecipitates were synthesized using three different types of NOM (extracellular polymeric substances extracted from *Bacillus subtilis*, OM extracted from the Oi horizon of a Cambisol, and OM extracted from the Oa horizon of a Podzol). These phases were characterized by N₂ gas adsorption, nuclear magnetic resonance spectroscopy (NMR), Fourier transform infrared spectroscopy (FTIR), X-ray diffraction (XRD), X-ray photoelectron spectroscopy (XPS), NOM desorption experiments, and mediated electrochemical reduction (MER). Iron(III) reduction under anaerobic conditions was monitored for 16 days using two different strains of dissimilatory Fe(III)-reducing bacteria (*Shewanella putrefaciens*, *Geobacter metallireducens*). Mineral transformation during reduction was determined by XRD and FTIR of the solid post-incubation phases. Fe(III) reduction by *Shewanella putrefaciens* was influenced by the amount of available electron shuttling molecules provided by the NOM, whereas the Fe(III) reduction by *Geobacter metallireducens* as well as abiotic Fe(III) reduction was influenced by particle size and NOM-induced aggregation. The specific surface area proved to be a poor predictor of Fe reduction of Fe-OM coprecipitates. This study emphasizes that certain physicochemical properties of natural Fe oxyhydroxides (composition of sorbed NOM and aggregation state) impact the Fe reduction by distinct microorganisms to differing degrees. Understanding environmental Fe and C cycling, therefore, requires experimental approaches extending beyond the use of pure Fe oxyhydroxides and model organisms.

Key Words: iron oxyhydroxides; natural organic matter; extracellular polymeric substances; *Shewanella putrefaciens*; *Geobacter metallireducens*; mediated electrochemical reduction

1 INTRODUCTION

The long-term stability of soil organic matter (OM) under oxic conditions has been linked to its preservation by association with iron (Fe) oxyhydroxides, particularly with poorly crystalline phases such as ferrihydrite (Kaiser and Guggenberger, 2007; Mikutta et al., 2006). The stabilizing effect of (Fe) oxyhydroxides on OM may, however, be lessened by a number of processes. First, OM may become desorbed under both oxic and anoxic conditions, thus increasing the bioavailability of carbon (Hanke et al., 2013; Mikutta et al., 2007). Under anoxic conditions, microbial reduction of Fe-OM associations may additionally mobilize OM (Glasauer et al., 2003; Lovley et al., 2004; Weiss et al., 2004), thus counteracting the stabilizing effect of Fe compounds. Dissimilatory Fe(III) reduction can further account for the release of other oxide-associated compounds into the soil solution and groundwater such as organic contaminants (Lovley and Anderson, 2000), heavy metals (Brümmer et al., 2013; Perelomov et al., 2011; Violante et al., 2003), or oxyanions (Mesuere and Fish, 1999; Sannino et al., 2009). Organic substances are known to strongly influence the magnitude of Fe(III) reduction — a circumstance addressed by a number of studies examining the effects of different specific organic compounds (quinones, humic acids) on the reactivity and stability of Fe oxyhydroxides in soil (e.g., Amstaetter et al., 2012; Liu et al., 2007; Zachara et al., 2011; Zhu et al., 2013). At present, however, comparatively little is known about the impact of natural OM (NOM) on the microbial reduction of Fe-OM coprecipitates (Pédrot et al., 2011; Henneberry et al., 2012; Shimizu et al., 2013; Eusterhues et al., 2014).

Fe-OM coprecipitation can occur in soils with very different conditions, such as well drained soils (Dolfing et al., 1999), temporarily waterlogged paddy soils (Kögel-Knabner et al., 2010), or acidic mineral soils (Nierop et al., 2002) like Spodosols (Wagai and Mayer, 2007). It may also be found in engineered settings such as acid mine drainage (Cheng et al., 2009), or industrial coagulation water treatment landfills (Bachand et al., 2000; Downing et al., 2008; Henneberry et al., 2011). Apart from plant-derived NOM leached from organic soil

layers, coprecipitated organic compounds can also be of microbial origin such as extracellular polymeric substances (Rancourt et al., 2005; Marschner et al., 2008; Mikutta et al., 2009). Assessing the reactivity of Fe-OM coprecipitates towards microbial reduction is confounded by the fact that coprecipitates may largely differ in their physicochemical properties. While ferrihydrite (Fh) typically is the most abundant mineral phase in Fe-OM coprecipitates (Kleber et al., 2015), the properties can vary strongly depending on the conditions under which the coprecipitates were formed. Coprecipitation of Fe in the presence of NOM can involve several concomitant and interlinked processes, including the complexation of hydrolyzed Fe(II) and Fe(III) by NOM, precipitation of insoluble Fe-organic complexes, adsorption of NOM to Fh, and occlusion of pure NOM into newly formed Fh aggregates (Kleber et al., 2015). In comparison to Fh forming in the absence of NOM and mineral-organic associations that form exclusively by OM adsorption to preexisting pure Fh surfaces, coprecipitation with organic constituents yields smaller crystal sizes with a more defective crystallographic structure (Cismasu et al., 2011; Eusterhues et al., 2008; Schwertmann et al., 2005), as well as different aggregation states (Mikutta et al., 2012). This, in turn, can directly affect the extent of microbial Fe reduction. Previous studies showed that OM may accelerate microbial reduction and thereby solubilization of Fe oxyhydroxides by (i) complexing Fe(II), thereby increasing the thermodynamic driving force for Fe(III) reduction (Royer et al., 2002), (ii) acting as a ligand towards Fe(III) thereby promoting solubilization (Jones et al., 2009), and (iii) mediating electron transfer from dissimilatory Fe-reducing bacteria to the mineral by shuttling electrons through redox active moieties in the OM structure (Amstaetter et al., 2012; Jiang and Kappler, 2008; Lovley et al., 1996). Conversely, OM may also decelerate the reduction of coprecipitates by (i) blocking surface sites on the mineral and (ii) initiating aggregation upon adsorption (Amstaetter et al., 2012; Kaiser and Guggenberger, 2003).

The relative importance that NOM plays in these processes is expected to depend on its origin, which affects the structural complexity and chemical composition of the material. So

far, this complexity of NOM has been little addressed in previous studies on microbial Fe reduction that used either specific NOM fractions (e.g., purified humic acid; Amstetter et al., 2012; Shimizu et al., 2013) or defined low-molecular weight organic compounds (e.g., quinones; Liu et al., 2007; Zachara et al., 2011; Zhu et al., 2013). Among the latter, anthraquinone-2,6-disulfonic acid (AQDS) is the most frequently used, serving as a model compound with excellent electron shuttle properties by reversibly accepting and donating electrons via its quinone/hydroquinone moieties. Lovley and Blunt-Harris (1999) suggest that such quinone/hydroquinone structures in NOM also play a major role in electron shuttling in soils. Electron shuttling is, however, likely not restricted to this redox couple. Chen et al. (2003) attributed accelerated Fe(III) reduction to electron shuttling by humic acid-derived high-molecular weight aromatic structures and, to a smaller but still considerable extent, to NOM-derived low-molecular weight polyphenolic compounds. Moreover, Wolf et al. (2009) showed that AQDS had a smaller sorption affinity towards Fh amongst several tested quinones of various composition with the sorption affinity of AQDS being 10-fold smaller than those of fulvic and humic acids. Experiments using AQDS, therefore, contain an easily available electron shuttling compound and do not capture effects resulting from strong and preferential sorption of complex aromatic NOM constituents in soils with electron shuttling properties (Chorover and Amistadi, 2001; Kalbitz et al., 2005; Scheel et al., 2007). Sorptive fractionation of OM itself varies with NOM composition and concentration, which hugely impacts aggregation, bioavailable surface area, and thus the kinetics of microbial Fe reduction.

In addition to the properties of Fe-OM coprecipitates, including the type of OM present, the microbial reduction of the coprecipitates may further depend on the Fe-reducing bacteria and their Fe respiration pathways. Pure Fe oxyhydroxides as well as mineral-organic associations cannot pass the outer cell membrane of Fe-reducing bacteria and hence need to be reduced in the extracellular space. To this end, different electron transfer pathways were developed (Weber et al., 2006). These include (i) direct transfer of electrons via redox-

enzymes anchored in the outer bacterial membrane (Myers and Nealson, 1988; Nevin and Lovley, 2000) or conductive cellular nanowires (El-Naggar et al., 2010; Gorby et al., 2006; Reguera et al., 2005) and (ii) mediated electron transfer to the mineral by using Fe-chelating compounds (Kraemer, 2004; Lovley et al., 1994; Nevin and Lovley, 2002), endogenous electron shuttling molecules like secreted flavins (Marsili et al., 2008; Nevin and Lovley, 2002; Newman and Kolter, 2000; von Canstein et al., 2008), and/or exogenous electron shuttling compounds as provided by NOM (Lovley et al., 1996).

Shewanella species have been shown to excrete flavins acting as electron shuttling molecules rather than transferring electrons via direct contact (Kotloski and Gralnick, 2013; von Canstein et al., 2008). Furthermore, microbial reduction of Fe(III) in oxyhydroxides and coprecipitates by *Shewanella* species can be enhanced by model quinones (Newman and Kolter, 2000) and humic acids (Amstaetter et al., 2012; Shimizu et al., 2013) if the amount of dissolved organic carbon exceeds a threshold of 5-10 mg C L⁻¹ (Jiang and Kappler, 2008) and the amount of Fe oxyhydroxide is sufficiently small that the degree of induced aggregation does not outweigh processes accelerating Fe reduction (Amstaetter et al., 2012).

Geobacteraceae represent one of the most common families of Fe-reducing microorganisms and are found in many soils and sediments (Lovley et al., 2011, 2004). While both direct contact and electron transfer via conduction nanowires have been suggested for *Geobacter* species (Boesen and Nielsen, 2013; Malvankar et al., 2011), the bacterium itself does not produce endogenous electron-shuttling molecules or chelators (Nevin and Lovley, 2000). Despite the ability of *Geobacter* species to reduce extracellular quinone moieties (Scott et al., 1998) and humic acid (Jiang and Kappler, 2008; Lovley et al., 1996) when no Fe is present, Eusterhues et al. (2014) found decreased Fe reduction rates by *Geobacter bremensis* when NOM extracted from a forest floor was added to pure Fh by adsorption or coprecipitation. The findings of Eusterhues et al. (2014) therefore do not point towards *Geobacter* using external electron shuttles in systems containing both NOM and Fe, thus

contradicting the previously implied rather minor impact of the electron transfer mechanism or the microorganism involved.

The aim of this study was therefore to systematically assess the effect of coprecipitated NOM on the microbial reduction of Fe-OM coprecipitates with regard to (i) the composition of OM, (ii) easily desorbable compounds, (iii) the surface site coverage and/or pore blockage by OM, and (iv) aggregation states. To address these questions, Fe-OM coprecipitates with NOM of different origin were synthesized using microbially derived OM (i.e., extracellular polymeric substances extracted from *Bacillus subtilis*) and two different types of plant-derived NOM (i.e., OM extracted from the Oi horizon of a Cambisol and the Oa horizon of a Podzol). In a first step, pure Fh and the coprecipitates were characterized by mediated electrochemical reduction (MER). In a second step, these materials were incubated under anoxic conditions for 16 days in the presence of two different strains of dissimilatory Fe(III)-reducing bacteria (*Shewanella putrefaciens*, *Geobacter metallireducens*), which differed in their favored extracellular electron transfer pathways. Mineral transformation during reduction was determined by XRD and FTIR of the phases collected after incubation. The results of the microbial reduction experiments of the Fe-OM coprecipitates were discussed in relation to their abiotic reduction in electrochemical cells containing defined electron transfer mediators (Sander et al., 2015). As such, the electrochemical measurements served as a reference for the microbial Fe reduction and allowed the reactivity of the coprecipitates to be assessed under very well defined conditions.

2 MATERIAL AND METHODS

2.1 Extraction of Extracellular Polymeric Substances and Natural Organic Matter

Extraction of extracellular polymeric substances (EPS) was carried out according to de Brouwer et al. (2002) and Omoike and Chorover (2006): A freeze-dried culture of *Bacillus subtilis* (ATCC 7003; BCCMTM/LMG Bacteria Collection) was activated aerobically in LB-

Lennox medium (yeast extract, 5 g L⁻¹; trypton, 10 g L⁻¹; NaCl, 5 g L⁻¹) at 303 K for 24 h. An inoculum of 1 mL was transferred to 500 mL of the same medium in a 1-L flask with air-conductive aluminum caps and incubated at 303 K and 120 rpm on a horizontal shaker until the early stationary growth phase was reached. After removal of bacterial cells by centrifuging the suspension at 5,000 g and 277 K for 15 min, residual cell components were removed by centrifugation of the decanted supernatant at 10,000 g for 50 min. EPS were precipitated from the collected supernatant with 277 K cold ethanol at a ratio of 1:3 (v/v supernatant/ethanol). After storage at 248 K for 18 h, the mixture was centrifuged at 10,000 g for 50 min. To remove residual medium and ethanol, the obtained EPS pellet was re-suspended in sterile water (filtered <100 nm) and dialyzed for 72 h (Spectra/Por 7, 1000 MWCO) with two changes of sterile water per day. Finally, the solution containing the purified EPS was freeze-dried. The amount of residual cells in the purified EPS was determined by fluorescence microscopy (Zeiss Axiophot Fluorescence Microscope, Carl Zeiss AG, Jena, Germany) after embedding an EPS aliquot in Moviol-Mounting medium and staining with SYBR-Green. This analysis revealed that the freeze-dried EPS contained approximately 7.85×10^6 cells mg⁻¹ EPS.

Material for NOM extraction was collected from the Oi horizon of a Eutric Cambisol under European beech (*Fagus sylvatica* L.) in the Deister Mountains (Germany) and from the Oa horizon of a Haplic Podzol under Norway spruce (*Picea abies* (L.) Karst.) in the Fichtelgebirge Mountains (Germany). Air-dried litter was crushed manually, mixed with doubly deionized water (1/10 w/v), and stirred for 15 min, before the suspension was equilibrated at 298 K for 16 h. Oa material was extracted with doubly deionized water (1/5 w/v) and equilibrated on a horizontal shaker at 1,000 rpm at 298 K for 16 h. After pre-filtration through 0.7- μ m glass fiber filters (GF 92, Whatman GmbH, Dassel, Germany), the solution was filtered through 0.45- μ m cellulose nitrate membrane filters (G, Sartorius AG, Göttingen, Germany). Dissolved total organic carbon (TOC) and total nitrogen (TN) were

quantified using a TOC/TN_b-Analyzer (liqui TOC II, Elementar Analysensysteme GmbH, Hanau, Germany).

2.2 Preparation of Ferrihydrite and Coprecipitates

Two-line Fh was synthesized by titrating a solution of 0.2 M FeCl₃ to a pH of 7.0 using 1 M NaOH (Schwertmann and Cornell, 2000). For coprecipitation, solutions of FeCl₃ and each respective NOM were rapidly mixed to obtain initial Fe(III) and OC concentrations of 4.17 mM and an Fe(III)/C ratio of 1.0. This step was followed by immediate titration to a pH of 7.0 to minimize aggregation of OM due to the initially acidic conditions (Angelico et al., 2014; Mikutta et al., 2014). In order to avoid centrifugation-induced structural change and aggregation, the suspensions were dialyzed against doubly deionized water (Spectra/Por 7, 1,000 MWCO) until the electric conductivity was <10 $\mu\text{S cm}^{-1}$. The precipitates were frozen in liquid nitrogen at 77 K, freeze-dried, and sieved to a size <200 μm .

2.3 Characterization of Organic Matter, Ferrihydrite, and Coprecipitates

The organic source materials and Fe hydrolysis products were characterized by multiple methods, detailed information about each analytical procedure is provided in Appendix A.

Freeze-dried and homogenized material of each type of NOM was characterized by solid-state cross-polarization magic angle spinning ¹³C NMR (nuclear magnetic resonance) spectroscopy performed on a 600 MHz SB Bruker Avance III spectrometer (Bruker, Billerica, MA, USA). Chemical shift regions were assigned according to Kögel-Knabner (2000) and quantified by peak integration.

The OC and total N contents of Fh and the coprecipitates were quantified with a CN analyzer (Vario EL III, Elementar GmbH, Hanau, Germany). Fe, P, and S contents of Fh and the coprecipitates were determined with inductively coupled plasma optical emission spectroscopy (ICP-OES, Varian 725-ES, Varian Inc., Palo Alto, CA, USA) after dissolution

of approximately 5 mg of the freeze-dried solids in 2.5 mL of 10 M HCl and subsequent tenfold dilution with 0.1 M HCl. Fe(II) contents of the Fe-OM coprecipitates were quantified using the ferrozine assay (Stookey, 1970) adapted according to Lovley and Phillips (1987). Organically complexed Fe(III) was quantified after extraction by pyrophosphate and subsequent measurement of Fe contents with ICP-OES.

Powder samples of Fh and the coprecipitates were analyzed by X-ray diffraction (XRD, Siemens D500, Siemens AG/Bruker AXS GmbH, Karlsruhe, Germany) using $\text{CuK}\alpha$ radiation and scanned from 2° to 80° 2θ with a step size of 0.05° and a step time of 10 s.

X-ray photoelectron (XPS) spectra of the freeze-dried unreacted NOM, Fh, and the coprecipitates were acquired with a Kratos Axis Ultra DLD spectrometer (Kratos Analytical, Manchester, UK) recording survey spectra and C1s high resolution spectra. To quantify the relative contributions of different carbon oxidation states, the following subpeaks were assigned to the C1s peak according to Gerin et al. (2003), Omoike and Chorover (2004), and Leone et al. (2006): (i) aliphatic and aromatic carbon displaying bonds to carbon and hydrogen (C-C, C=C, C-H; at 285.0 ± 0.1 eV), (ii) carbon displaying a single bond to oxygen or nitrogen as in carbohydrates and amines (C-O, C-N; at 286.5 ± 0.2 eV), (iii) carbon displaying two bonds to oxygen as in aldehydes, ketones, and amides (C=O, O-C-O, O=C-N; at 288.0 ± 0.1 eV), (iv) carboxylic carbon displaying three bonds to oxygen (O-C=O; at 289.1 ± 0.2 eV).

Fourier transform infrared (FTIR) spectra were recorded for the freeze-dried NOM, Fh, and coprecipitates using the attenuated total reflectance (ATR) mode (TENSOR 27, Bruker, Bremen, Germany).

The specific surface area (SSA) of Fh and the coprecipitates was determined in duplicate with an Autosorb-1 surface area analyzer (Quantachrome Instruments, Boynton Beach, FL, USA). After degassing under vacuum at 313 K for 24 h, N_2 was adsorbed to the minerals at 77 K. The Brunauer-Emmett-Teller (BET) equation was applied to the adsorption data in the

relative pressure range of 0.05 to 0.3 P/P_0 (Brunauer et al., 1938). The total pore volume (TPV) was determined using the last data point of the adsorption branch of the isotherm at 0.995 P/P_0 . The micropore volume (<2 nm) was quantified by applying the Dubinin-Radushkevich (DR) method (Gregg and Sing, 1982) to adsorption points <0.01 P/P_0 . The mesopore volume (2-50 nm) was determined by applying the Barrett-Joyner-Halenda (BJH) method (Barrett et al., 1951). Differentiation between small (2-10 nm) and large (10-50 nm) mesopores was achieved by linear interpolation.

The pH-dependent electrophoretic mobility (EM) and particle size of the Fh and coprecipitates were determined in 10 mM KCl background electrolyte and, in addition, for both types of microbial media used in the reduction experiments, as described in section 2.4 and 2.5, using a ZetaPALS Zeta Potential Analyzer (Brookhaven Instruments Corp., Holtsville, USA).

In order to determine the chemical fractionation of NOM and EPS during coprecipitation, the initial solutions and the supernatants of the post-precipitation solution were analyzed for OC and total N with a TOC/TN_b-Analyzer. Additionally, Na, K, Mg, Ca, Fe, Mn, Al, Si, P, and S in the initial and post-reaction solutions were measured with ICP-OES, and NH_4^+ , NO_3^- , SO_4^{2-} , and PO_4^{3-} with ion chromatography (Dionex ICS-90 Ion Chromatography System, Dionex Corporation, Sunnyvale, CA, United States). The UV absorbance at 280 nm was determined for the initial NOM and EPS solution and post-reaction solutions using a UV-Visible Spectrophotometer (Cary 50 Scan, Varian Inc., Mulgrave, Victoria, Australia) and a 1-cm quartz cuvette. The OC-normalized specific UV absorbance (SUVA) at 280 nm increases proportionally to the aromaticity of OM. A decrease in SUVA after coprecipitation relative to the OM solution prior to coprecipitation thus signifies a preferential sorption of aromatic OM moieties (Chorover and Amistadi, 2001; Scheel et al., 2007).

To link microbial Fe reduction to the amount of bioavailable NOM and EPS, easily desorbable OC was quantified in separate desorption experiments using the same solid to

solution ratios and nutrient solutions as used in the reduction experiments but excluding HEPES and lactate or acetate (see 2.5). Each set-up was prepared in triplicate. The suspensions were adjusted to a pH of 7.0 using 1 M NaOH and equilibrated on an end-over-end shaker for 24 h at 298 K. After centrifugation for 1 h at 6,000 g, the supernatants were filtered <math><0.45 \mu\text{m}</math> and analyzed for OC with a TOC/TN_b-Analyzer.

2.4 Mediated Electrochemical Reduction

All electrochemical analyses were conducted in a glovebox under N₂ atmosphere (O₂ <math><0.1 \text{ ppm}</math>). Prior to use, all solutions were purged with N₂ for 1 h at 353 K and for 1 h at room temperature. Mediated electrochemical reduction (MER) was conducted at two different reduction potentials E_h (-0.49 V and -0.28 V) to examine whether Fe(III) reduction rates increased with decreasing E_h . Furthermore, to assess potential effects of the chemical properties of the electron transfer mediator on reduction rates, four different mediators were tested: cyanoviologen (1,1'-bis(cyanomethyl)-4,4'-bipyridyl) (CV) was synthesized according to Gorski et al. (2012), riboflavin 5'-monophosphate sodium salt (RF) was purchased from TCI (>93 %), diquat dibromide monohydrate (1,1'-ethylene-2,2'-bipyridyl) (DQ) was purchased from Supelco (analytical grade), and zwitterionic viologen (4,4'-bipyridinium-1,1'-bis(2-ethylsulfonate)) (ZiV) was synthesized according to Gorski et al. (2013). This reference also contains a more detailed characterization of the electron transfer mediators used. An excess concentration of the electron transfer mediator relative to the added Fe was used in all measurements to ensure pseudo-first-order rate conditions. In addition to the coprecipitates described above, two additional coprecipitates were examined. They were obtained from a spruce Oa and Fe(III) mixture with initial Fe/C ratios of 1.0 and 0.1 and titrated to a pH of 4 using 1 M NaOH as described in detail by Mikutta et al. (2014).

MER of the Fh, coprecipitates, and freeze-dried NOM and EPS was conducted according to Klüpfel et al. (2014). Briefly, the electrochemical cell used in this study consisted of a

glassy carbon cylinder (Sigradur G, HTW, Germany) serving both as working electrode and reaction vessel, a Ag/AgCl reference electrode (Bioanalytical Systems Inc., USA), and a counter electrode made of coiled platinum wire, which was separated from the carbon cylinder by a porous glass frit. The cell was filled with 5.5 mL of 0.1 M KCl buffered at a pH 7 with HEPES or MOPS (0.01 M). The working electrode was equilibrated to a reduction potential E_h of -0.49 V for DQ and ZiV and to a reduction potential E_h of -0.28 V for CV and RF. After addition of 130 μL electron transfer mediator solution (10 mM) and reestablishment of constant background currents, 20 μL of sample suspensions containing 1 g sample L^{-1} were spiked to the cell. The electron accepting capacities (EAC; i.e., the number of electrons transferred to a mass unit of analyte) were obtained by integrating the baseline-corrected reductive current peaks resulting from each sample according to Sander et al. (2015):

$$\text{EAC} = \frac{\int \frac{I_{Red}}{F} dt}{m_{sample}} \quad (1)$$

Here, I_{Red} (A) represents the baseline-corrected reductive current, F the Faraday constant (96,485 C mol^{-1}), and m_{sample} (g) the mass of each respective added sample. The term $\int \frac{I_{Red}}{F} dt$ corresponds to the number of electrons transferred. Electron transfer rates for each sample were calculated by assuming a pseudo-first-order rate law (for more information, please see Appendix B). As the reduction rates of Fh and Fe-OM coprecipitates did not show noticeable differences between solutions buffered with MOPS and HEPES, only results obtained from solutions containing HEPES buffer are discussed.

2.5 Microbial Reduction Experiments

Liquid cultures of *Shewanella putrefaciens* (DSM-6067) and *Geobacter metallireducens* (DSM-7210) were purchased from the Leibniz Institute DSMZ-German Collection of Microorganisms and Cell Cultures. A sterile 100-mL flask with an air-conductive aluminum cap containing 50 mL of altered medium DSM 948 (meat extract, 1.0 g L^{-1} ; yeast extract,

2.0 g L⁻¹; casein peptone, 5.0 g L⁻¹; NaCl 5.0 g L⁻¹) was inoculated with 500 μL of the *Shewanella putrefaciens* culture and incubated on a horizontal shaker at 303 K and 120 rpm for 72 h. An inoculum for the reduction experiments was prepared by transferring 1 mL of the aerobic culture into a sterile flask containing 100 mL initially oxic DSM 948 medium, which was incubated on a horizontal shaker at 303 K and 120 rpm. After 16 h the culture had reached the late exponential growth phase with cells starting to engage in anaerobic metabolism (Lies et al., 2005). Reduction experiments with *Shewanella putrefaciens* were conducted in inorganic nutrient solution containing CaCl₂ · 2H₂O, 0.1 g L⁻¹; KCl, 0.1 g L⁻¹; NH₄Cl, 1.5 g L⁻¹; NaH₂PO₄ · H₂O, 0.6 g L⁻¹; NaCl, 0.1 g L⁻¹; MgCl₂ · 6H₂O, 0.1 g L⁻¹; MgSO₄ · 7H₂O, 0.1 g L⁻¹; MnCl₂ · 4H₂O, 0.005 g L⁻¹; NaMoO₄ · 2H₂O, 0.001 g L⁻¹ (Lovley and Phillips, 1988) with 5 mmol L⁻¹ Na-lactate (0.56 g L⁻¹) as electron donor.

Ten milliliters of the *Geobacter metallireducens* culture were transferred with a syringe into a sterile, crimp sealed 150-mL serum flask containing 100 mL anoxic *Geobacter* medium DSM 579 (Fe(III)-citrate, 13.70 g L⁻¹; NaHCO₃, 2.50 g L⁻¹; NH₄Cl, 1.50 g L⁻¹; NaH₂PO₄, 0.60 g L⁻¹; KCl, 0.10 g L⁻¹; Na-acetate, 2.50 g L⁻¹; trace element solution (DSMZ medium 141, Table C.1), 10.00 mL L⁻¹; vitamin solution (DSMZ medium 141, Table C.2), 10.00 mL L⁻¹; Na₂WO₄ · 2H₂O, 0.25 mg L⁻¹). After incubation on a horizontal shaker at 303 K and 120 rpm for 5 days, the Fe(III)-citrate had been visibly reduced. These steps were repeated with fresh medium to prepare an inoculum for the Fh and coprecipitate reduction experiments with *Geobacter metallireducens* described below. For those experiments, Fe(III)-citrate and NaHCO₃ were omitted from the *Geobacter* medium described above and 5 mmol L⁻¹ Na-acetate (0.41 g L⁻¹) served as electron donor.

To avoid media-induced precipitation of siderite and vivianite and minimize phosphate-induced desorption of NOM and EPS from the coprecipitates, HEPES was used to buffer the solutions in reduction experiments to a pH of 7. HEPES was chosen as it showed the least sorption affinity to Fh of all tested common buffers (BisTris, HEPES, MOPS, PIPES,

bicarbonate, phosphate, data not shown). Additional sorption tests conducted with lactate and acetate revealed that they did not sorb to Fh to detectable extents. Each solution was sterilized either in an autoclave or by filtration (Supor R-200, Pall Corporation, Ann Arbor, MI, USA) and made anoxic by flushing with N₂ for 1 h while cooling down after autoclaving.

Approximately 30-40 mg of Fh or coprecipitate corresponding to 10 mM Fe(III) were weighed into sterile 50-mL serum flasks before adding 30 mL of nutrient solution. After crimp sealing the flasks with butyl rubber stoppers, the suspensions were bubbled with N₂ (containing 20 % CO₂ for set-ups with *Geobacter metallireducens*) for 30 min once more and left to equilibrate for 24 h. Flasks were either inoculated with the pre-culture of *Shewanella putrefaciens* to obtain a final cell concentration of 2 x 10⁵ cells mL⁻¹ or with the pre-culture of *Geobacter metallireducens* to obtain a final cell concentration of 1 x 10⁷ cells mL⁻¹. Cell counts were determined as described in section 2.1. Pre-tests had shown that *Geobacter* did not grow as fast as *Shewanella* when each of the cultures were inoculated into medium containing the same nutrients and dissolved Fe(III). Furthermore, at initial cell concentrations below 1 x 10⁷ cells mL⁻¹, no reduction of Fe oxyhydroxides by *Geobacter* could be detected at all. In addition, we aimed to keep up the comparability to several studies published in the past, which usually featured smaller initial cell densities for *Shewanella* (e.g., Amstaetter et al., 2012) and larger initial cell densities for *Geobacter* (e.g. Wolf et al., 2009). The decision to work with different initial cell concentrations was, therefore, derived from the attempt to compromise between these issues.

The suspensions were incubated at 303 K in the dark for 16 days. Samples were taken after 1, 3, 6, 10, and 16 days to quantify Fe(II) and Fe_{total} contents. For that purpose, 1 mL of the suspension was sampled with a syringe and instantly acidified with 20 μL of 5 M H₂SO₄. For quantification of dissolved Fe(II) and Fe(III), samples were filtered through 0.025-μm PES membrane filters (Anotop 25, Whatman GmbH, Dassel, Germany). To determine total Fe(II) concentrations, samples were completely dissolved in 0.5 M H₂SO₄ before

applying the ferrozine assay (see section 2.3). Despite the attempt to quantify both dissolved and total Fe(II) concentrations, reduction rates are discussed for the latter only (see also Appendix C.1). Control samples containing no bacteria showed no release of Fe(II) apart from the amount produced during the preparation of the coprecipitates. The possibility of Fe(III) reduction by desorbed NOM, lactate, or acetate during acidic dissolution of the samples was ruled out by pretests conducted with FeCl₃.

After 16 days, the solid post-incubation phases were separated by centrifugation for 1 h at 6,000 g, dried and stored under N₂ atmosphere, and characterized by FTIR applying the same parameters as listed in section 2.3. For XRD analysis, ca. 10 mg of the solid phase were resuspended in 1 mL of anoxic 4 μM HgCl₂ to suppress microbial activity. The suspension was transferred to and dried on glass slides of 25 mm diameter. After drying, the specimens were transferred from the glove box to the XRD chamber in sealed bottles filled with N₂ and analyzed in the absence of oxygen. (For a more detailed description, please see Appendix D.) Microbial Fe reduction kinetics could neither be properly described by the model developed by Christoffersen and Christoffersen (1976) nor by pseudo-first order (Lagergren, 1898) or pseudo-second order models (Ho and McKay, 1998). While Fe(III) reduction by *Shewanella putrefaciens* probably did not reach its full extent after 16 days, parameters exerting an influence on reduction by *Geobacter metallireducens* might be too complex for description by models commonly applied to these type of experiments.

2.6 Statistics

Two-sided t-tests for unpaired samples with a significance level of $\alpha = 0.05$ were performed for the results of the different methods of characterization and the microbial reduction experiments to compare the means of the different experimental variables using the software GNU R 3.1.1 (R Development Core Team, 2015). In case of different variances, which were determined by a preceding F-test, Welch's variation of the t-test was applied.

STUDY I

Table 1 Bulk element composition, BET-derived specific surface area (SSA) and C constants, and pore volumina of ferrihydrite (Fh) and coprecipitates (coprec.). Values in parentheses depict the standard deviation of at least triplicate measurements. Fe_{org} = organically complexed Fe, ND = not detected.

Sample	Fe _{total} (mg g ⁻¹)	Fe(II) (mg g ⁻¹)	Fe _{org} (%)	OC (mg g ⁻¹)	N (mg g ⁻¹)	P (mg g ⁻¹)	S (mg g ⁻¹)
Fh	503.4 (7.9)	ND	ND	0.1 (0.0)	ND	ND	ND
EPS coprec.	350.9 (5.2)	4.1 (0.4)	0.8 (0.1)	138.7 (0.0)	18.7 (0.1)	2.1 (0.2)	0.3 (0.0)
Beech Oi coprec.	421.8 (5.4)	4.7 (0.2)	1.2 (0.1)	83.8 (0.0)	4.4 (0.2)	1.6 (0.1)	0.2 (0.0)
Spruce Oa coprec.	336.2 (6.3)	20.2 (6.2)	4.9 (0.6)	151.0 (0.4)	4.7 (0.2)	1.0 (0.1)	0.3 (0.0)

Sample	SSA (m ² g ⁻¹)	BET-C	MIV ^a (mm ³ g ⁻¹)	MEV ^b		TPV ^c (mm ³ g ⁻¹)	EM ^d (10 ⁻⁸ m ² V ⁻¹ S ⁻¹)
				2-10 nm (mm ³ g ⁻¹)	10-50 nm (mm ³ g ⁻¹)		
Fh	359.7 (12.9)	187.8 (21.5)	127.5 (19.0)	72.0 (1.7)	12.0 (1.3)	251.4 (9.2)	-3.1 (0.3)
EPS coprec.	26.8 (1.3)	13.5 (0.3)	6.0 (0.0)	21.0 (0.8)	13.6 (0.4)	59.7 (3.3)	-2.1 (0.2)
Beech Oi coprec.	144.8 (2.8)	111.4 (1.6)	51.0 (1.4)	33.9 (2.9)	10.8 (0.2)	119.1 (1.4)	-3.1 (0.3)
Spruce Oa coprec.	24.9 (2.7)	11.9 (0.1)	5.5 (0.7)	19.1 (1.6)	12.8 (0.7)	60.0 (1.0)	-3.3 (0.1)

^a MIV, micropore volume; ^b MEV, mesopore volume; ^c TPV, total pore volume; ^d EM, electrophoretic mobility in inorganic nutrient solution.

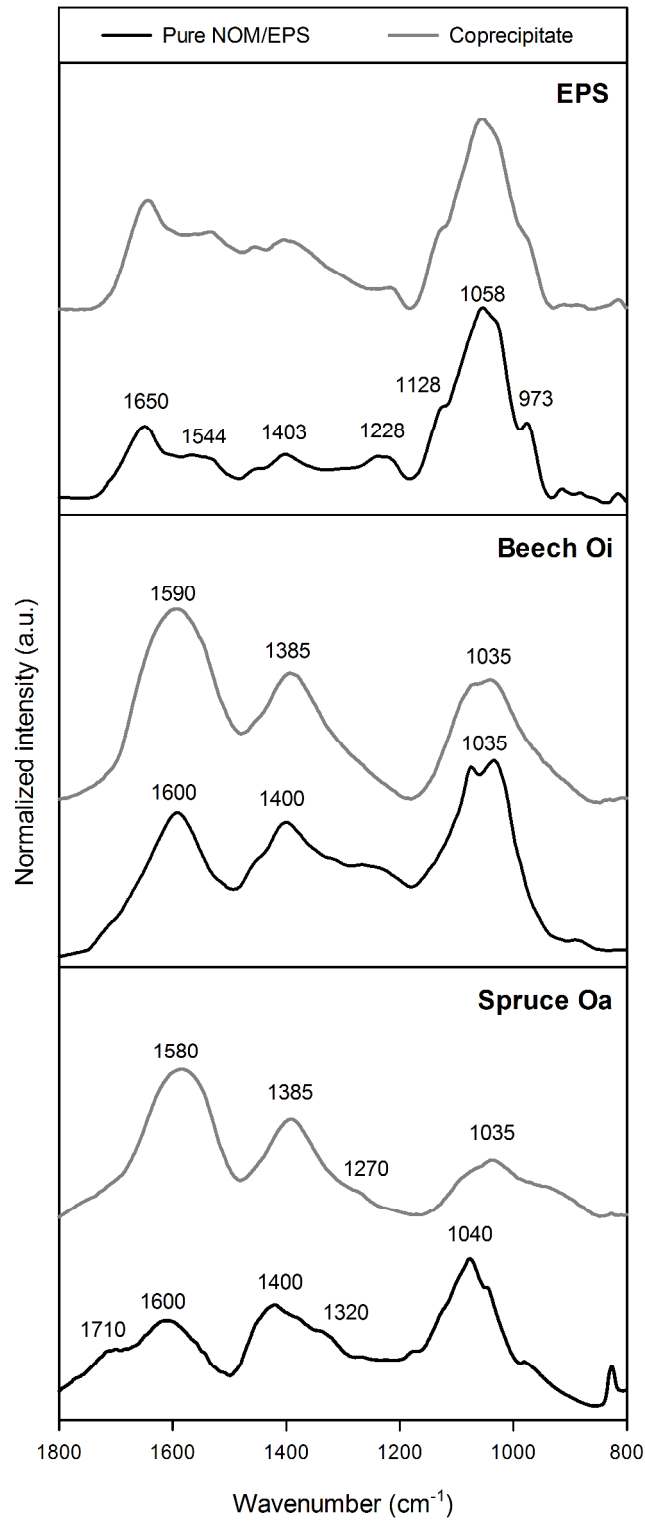


Fig. 1 ATR-FTIR spectra of freeze-dried NOM and EPS before and after coprecipitation with Fe(III).

STUDY I

Table 2 Band assignments in ATR-FTIR spectra of beech Oi and spruce Oa as well as respective coprecipitates (Coprec.) according to Scheel et al. (2008) and Omoike and Chorover (2006).

EPS	Beech Oi	Spruce Oa	Coprec.	Band assignment
		1710		protonated carboxylic groups
		1600-1640		C=O stretching of deprotonated carboxylic groups
		1456		carboxylate stretching vibration overlapping with asymmetric C-C deformation
		1400		complexed carboxylic groups (chelates or binding of metals)
		1320		C-O stretching of deprotonated carboxylic groups
		1270		C-O stretching of phenolic groups
		1040		C-O stretching of polysaccharides
1660				C=O stretching of amides associated with proteins (amide I)
1544				N-H deformation and C-N stretching in -CO-NH- of proteins (amide II)
1449				symmetric CH ₂ deformation and C-OH deformation
1404				symmetric C-O stretching of COO ⁻ groups
1242				asymmetric P=O stretching of phosphodiester backbone of nucleic acid (DNA and RNA); may also be due to phosphorylated proteins
1127				O-H deformation, C-O stretching, ring vibrations of polysaccharides
1078				symmetric P=O stretching of phosphodiester backbone of nucleic acid (DNA and RNA), C-O-C and C-O-P. Also phosphorylated proteins and C-OH stretching
920				Asymmetric ester O-P-O stretching modes from nucleic acids
			1153	P-O-Fe stretching
			1028	P-O-Fe stretching

Table 3 Distribution of functional groups in NOM and EPS as revealed by solid-state ¹³C-NMR spectroscopy.

Sample	Carboxyl-/ carbonyl-C 160-210 ppm	Aryl C 110-160 ppm	O-Alkyl C 50-110 ppm	Alkyl-C 0-50 ppm
EPS	6	4	77	12
Beech Oi	7	11	61	21
Spruce Oa	15	18	42	25

3 RESULTS AND DISCUSSION

3.1 Properties of Ferrihydrite and Coprecipitates

3.1.1 Bulk and surface element contents

Pure Fh had the largest Fe content with 503.4 mg Fe g⁻¹ (Table 1), followed by the beech Oi coprecipitate (421.8 mg Fe g⁻¹) and EPS and spruce Oa coprecipitates (350.9 and 336.3 mg Fe g⁻¹, respectively). Consistently, the OC content of the beech Oi coprecipitate was considerably smaller (83.8 mg C g⁻¹) than the OC contents of the EPS and spruce Oa coprecipitates (138.8 and 151.0 mg C g⁻¹, respectively). The EPS coprecipitate exhibited the largest N content (18.7 mg N g⁻¹), whereas the N contents of the beech Oi and spruce Oa coprecipitates were considerably smaller (4.1 and 4.7 mg N g⁻¹, respectively) and did not differ significantly from each other. For a more detailed discussion, please see Appendix E1. Only the spruce Oa-derived coprecipitate showed a considerable amount of ferrous Fe (2 % of total Fe; Table 1), suggesting partial reduction of Fe(III) by reduced moieties originally present in the NOM solutions (Mikutta, 2011). Despite their differing total OC contents, the coprecipitates exhibited similar surface C contents as revealed by XPS (Table 4). The C/Fe weight ratios at the surface of the coprecipitates increased 40 to 80-fold in comparison to the bulk samples, resulting in surfaces dominated by organic moieties.

3.1.2 Bulk and surface carbon speciation

The FTIR spectrum of pure EPS exhibited broad signals that were consistent with vibrations of amide bonds in proteins (amide I, 1650 cm⁻¹), deformation vibrations of N-H and valence vibrations of C-N in -CO-NH- of proteins (amide II, 1544 cm⁻¹), symmetric C-O vibrations of carboxylic groups in complexes (1403 cm⁻¹), and overlapping C-O stretching vibrations of polysaccharides with symmetric stretching vibrations of P=O in the phosphodiester backbone of nucleic acids (1058 cm⁻¹, Table 2, Fig. 1). Upon precipitation, the intensity ratio of amide I to polysaccharides increased from 0.38 in the pure EPS to 0.59 in

the coprecipitates, indicating preferential uptake of protein structures into the coprecipitates. This finding is in agreement with previous studies on EPS adsorption to goethite (Omoike and Chorover, 2006). Conversely, Mikutta et al. (2011) found polysaccharides to be the dominant EPS component incorporated into Al coprecipitates, which suggests differences in their reactivity during coprecipitation between Fe and Al. Characterization of the EPS solution by SUVA at 280 nm before and after precipitation revealed small and similar contents of aromatic moieties in the initial EPS along with negligible fractionation during coprecipitation. These observations are in agreement with the solid-state ^{13}C -NMR spectrum revealing less than 5 % of aromatic C for pure EPS with O-alkyl C representing the dominant functional group with 77 % (Table 3).

The main peaks in the FTIR spectra of spruce Oa- and beech Oi-derived NOM were assigned to C=O stretching of deprotonated carboxylic groups (1600 cm^{-1}), carboxylic groups in complexes (1400 cm^{-1}), and C-O stretching of polysaccharides (1035 cm^{-1} , Table 2, Fig. 1) with the last one being the dominant group. Additional shoulders in the absorbance peaks of the spruce Oa at 1710 cm^{-1} and 1320 cm^{-1} were indicative of protonated carboxylic groups and C-O stretching of deprotonated carboxylic groups. Consistent with the results of the FTIR analysis, solid-state ^{13}C -NMR spectroscopy revealed that spruce Oa-derived NOM exhibited the largest relative amount of carboxylic and aryl C (15 % and 18 %, respectively), followed by beech Oi-derived NOM (7 and 11 %, Table 3). Analogous to the trend seen for EPS, O-alkyl C made up the largest part of OC for both types of plant-derived NOM (42 % for spruce Oa, 61 % for beech Oi). Similar to the study by Scheel et al. (2008) working with Al coprecipitates, differences in the composition between primarily plant-derived NOM of different origin seemed to disappear during precipitation with Fe, as the ratio of the FTIR peak heights at 1600 cm^{-1} and 1400 cm^{-1} was equivalently 1.6. Despite this finding and the suggestion that mainly organic molecules with carboxylic groups attached to aromatic rings are precipitated (Scheel et al., 2008), the FTIR spectrum of the spruce Oa coprecipitate

exhibited an additional shoulder at 1270, pointing towards C-O stretching of phenolic groups. Furthermore, after coprecipitation with Fe(III), the SUVA of spruce Oa-derived NOM remaining in solution decreased by 83 % compared to the initial NOM solution, whereas coprecipitation with beech Oi-derived NOM resulted in a smaller decrease of 67 %. Thus, preferential coprecipitation of aromatic moieties was more pronounced for spruce Oa-derived NOM than for beech Oi-derived NOM. The decreased peak intensity of carboxylic groups in complexes upon coprecipitation in comparison to the original NOM is in agreement with the small amount of organically bound Fe(III), which was 1.2 % in the case of the beech Oi coprecipitate and 4.9 % in the case of the spruce Oa coprecipitate (Table 1). Compared to the initial NOM, both coprecipitates exhibited considerably reduced peak intensities at 1035 cm⁻¹ indicating negligible coprecipitation of polysaccharides. The larger absorbance intensity at this wavenumber measured in the beech Oi coprecipitate in comparison to the spruce Oa coprecipitate might be attributed to the larger phosphate content.

Unlike both types of plant-derived NOM, the C1s XPS detail spectrum of EPS revealed a considerable contribution of carbon displaying two bonds to oxygen, such as O=C-N (Fig. 2, Table 4), which is in agreement with the results of EPS bulk characterization by FTIR. Upon coprecipitation, however, amide C considerably decreased along with carbon displaying a single bond to oxygen as primarily found in carbohydrates, leaving the uppermost 1–10 nm of the coprecipitate surfaces to be dominated by aliphatic C with increased carboxylic C contents. Because both the SUVA at 280 nm and the NMR-derived data (Table 3) suggested very small contents of aromatic C in the original EPS, the contribution of aromatic C to the subpeak at 285 eV is most likely negligible. Thus, the data suggests that both aliphatic and carboxylic C found in proteins seem to be oriented towards the surface of the EPS coprecipitate. The considerably decreased contents of carbohydrate C in the coprecipitates supported the results obtained by FTIR. The aforementioned disappearance of differences in the structural composition of plant-derived NOM during coprecipitation was also evident in

the C1s XPS spectra of the coprecipitates (Fig. 2, Table 4). For both beech Oi and spruce Oa coprecipitates, aliphatic and aromatic carbon represented the dominant carbon species on the coprecipitate surfaces, while carbon displaying a single bond to oxygen, as in carbohydrates, decreased in comparison to the corresponding NOM, analogous to the bulk measurements conducted with FTIR. Given the error in the quantification of carboxylic carbon by XPS (Table 2), there was no significant change with respect to its contribution to the source NOM.

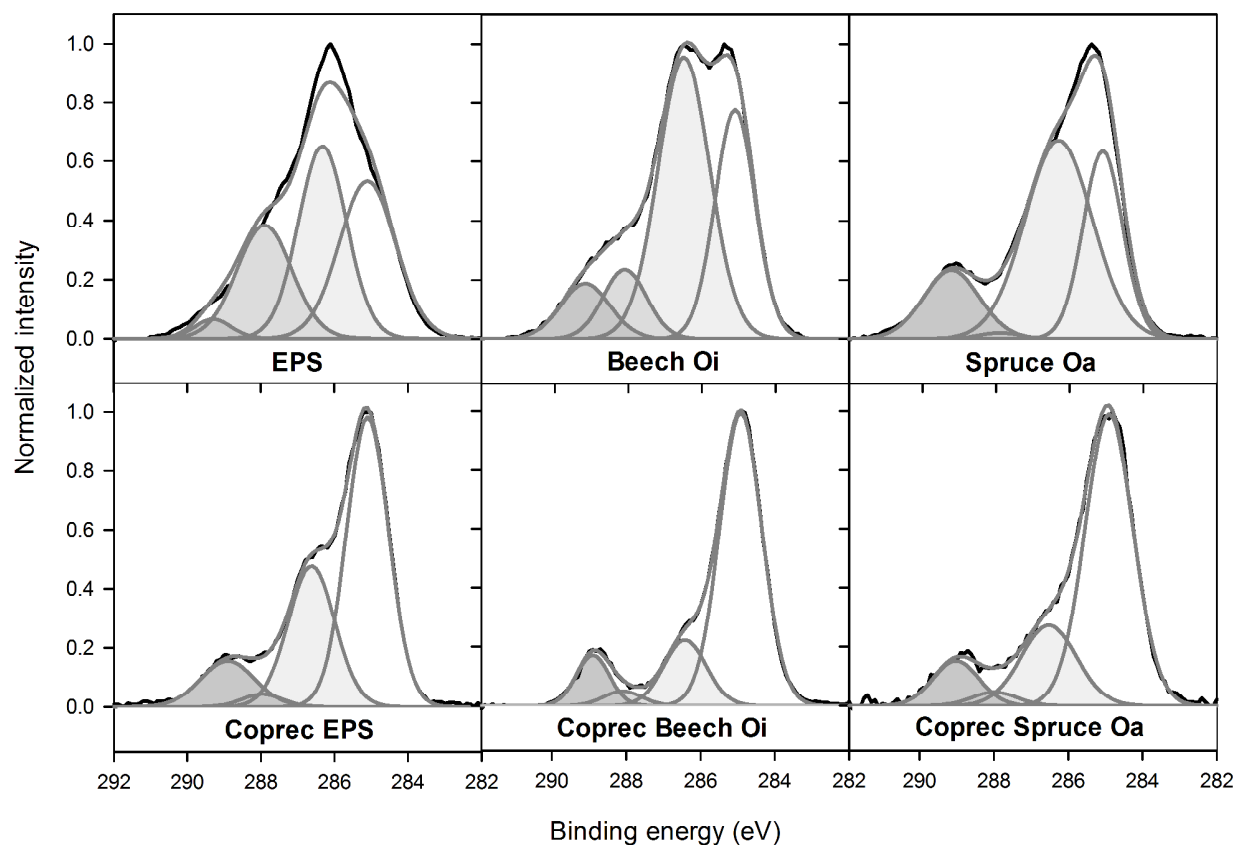


Fig. 2 Detail C1s spectra of freeze-dried NOM, EPS and coprecipitates derived from XPS measurements. Black lines represent measured data, grey areas represent subpeaks of different carbon species as determined by peak deconvolution, dark grey lines represent the sum curve of the latter. Different types of carbon were assigned as follows: (i) aliphatic and aromatic carbon displaying bonds to carbon and hydrogen (C-C, C=C, C-H; at 285.0 ± 0.1 eV), (ii) bond to oxygen carbon displaying a single or nitrogen as in carbohydrates and amines (C-O, C-N; at 286.5 ± 0.2 eV), (iii) carbon displaying two bonds to oxygen as in aldehydes, ketones, and amides (C=O, O-C-O, O=C-N; at 288.0 ± 0.1 eV), and (iv) carboxylic carbon displaying three bonds to oxygen (O-C=O; at 289.1 ± 0.2 eV).

STUDY I

Table 4 Surface element composition of freeze-dried NOM, EPS, and coprecipitates (coprec.) derived from XPS survey spectra and surface carbon speciation derived from C1s XPS detail spectra. Values in parentheses depict the standard deviation of at least triplicate measurements. The different types of carbon were assigned as follows: (i) aliphatic and aromatic carbon displaying bonds to carbon and hydrogen (C-C, C=C, C-H; at 285.0 ± 0.1 eV), (ii) carbon displaying a single bond to oxygen or nitrogen as in carbohydrates and amines (C-O, C-N; at 286.5 ± 0.2 eV), (iii) carbon displaying two bonds to oxygen as in aldehydes, ketones, and amides (C=O, O-C-O, O=C-N; at 288.0 ± 0.1 eV), and (iv) carboxylic carbon displaying three bonds to oxygen (O-C=O; at 289.1 ± 0.2 eV).

Sample	C 1s (atom %)	N 1s (atom %)	O 1s (atom %)	Fe 2p (atom %)	P 2p (atom %)	S 2p (atom %)
EPS	65.3 (1.3)	3.4 (0.5)	28.4 (0.7)	ND	2.4 (0.3)	ND
Beech Oi NOM	64.8 (0.5)	2.7 (0.5)	30.2 (0.9)	ND	2.1 (0.4)	0.2 (0.0)
Spruce Oa NOM	68.6 (2.1)	1.6 (0.3)	27.6 (1.6)	ND	1.0 (0.1)	1.1 (0.2)
EPS coprec.	68.2 (0.6)	1.7 (0.1)	27.2 (1.4)	4.2 (1.0)	0.7 (0.2)	ND
Beech Oi coprec.	63.1 (2.1)	0.0 (0.0)	30.3 (0.8)	4.0 (1.5)	0.5 (0.4)	0.1 (0.0)
Spruce Oa coprec.	69.4 (1.6)	0.2 (0.2)	26.8 (1.6)	2.8 (0.4)	0.8 (0.4)	0.1 (0.0)

Sample	C-C, C=C, C-H (%)	C-O, C-N (%)	C=O, O-C-O (%)	O-C=O, O=C-N (%)
EPS	37.3 (3.1)	35.6 (3.9)	24.0 (1.2)	3.1 (0.9)
Beech Oi NOM	32.1 (6.1)	46.9 (10.6)	13.4 (6.5)	7.6 (2.1)
Spruce Oa NOM	32.3 (3.0)	43.4 (9.6)	5.8 (4.6)	18.5 (8.1)
EPS coprec.	48.8 (0.9)	32.6 (2.9)	10.0 (4.8)	8.6 (1.0)
Beech Oi coprec.	71.7 (0.9)	15.5 (1.3)	3.2 (1.2)	9.6 (0.7)
Spruce Oa coprec.	63.7 (2.3)	19.9 (1.9)	6.8 (3.4)	9.6 (1.9)

3.1.3 Crystallinity, surface area, and porosity

The XRD pattern of Fh revealed two characteristically broad peaks at 0.25 and 0.15 nm (Fig. 3, Schwertmann et al., 2005). The latter was less pronounced in the XRD patterns of the coprecipitates, while the signal at 0.25 nm broadened and shifted towards smaller 2θ values. Cross-linking of $\text{Fe}(\text{O},\text{OH})_6$ octahedra chains during coprecipitation may have been disturbed to some extent by NOM and EPS molecules resulting in slightly less crystalline structures in comparison to pure Fh (Eusterhues et al., 2008; Waychunas et al., 1993). Nevertheless, two-line Fh seemed to be the dominant mineral phase in all samples.

The pure Fh exhibited a SSA of $359.7 \text{ m}^2 \text{ g}^{-1}$ (Table 1), which lies within the range of values previously reported for Fh (e.g. Eusterhues et al., 2008; Mikutta et al., 2014; Schwertmann and Cornell, 2000). Analogous to their similar Fe and C contents, the EPS and spruce Oa coprecipitate showed a similar decrease in SSA in comparison to pure Fh by 93 %. The SSA of the beech Oi coprecipitate decreased by only 60 %. These findings are consistent with previous studies examining Fe-OM coprecipitates with similar initial Fe/C ratios (Eusterhues et al., 2008; Mikutta et al., 2014; Shimizu et al., 2013). Fifty per cent of the total pore volume (TPV) of Fh was located within micropores, which were nearly completely undetectable for the EPS and spruce Oa coprecipitate and were decreased by 60 % in the case of the beech Oi coprecipitate. Similar trends were found for the small mesopores. Conversely, the large mesopores hardly differed among the samples. The ratio of $\text{SSA}_{\text{coprecipitate}}/\text{SSA}_{\text{pureFh}}$ was 0.07 for both the EPS and spruce Oa coprecipitate, thus indicating significant particle aggregation. The beech Oi-induced aggregation was smaller (i.e., ratio of 0.4) but still significant. In line with the XPS measurements, the small BET-derived C constants and the negative surface charge characteristics deduced from electrophoretic mobility measurements confirmed the prevalence of organic moieties on the surface of the coprecipitates (Table 1).

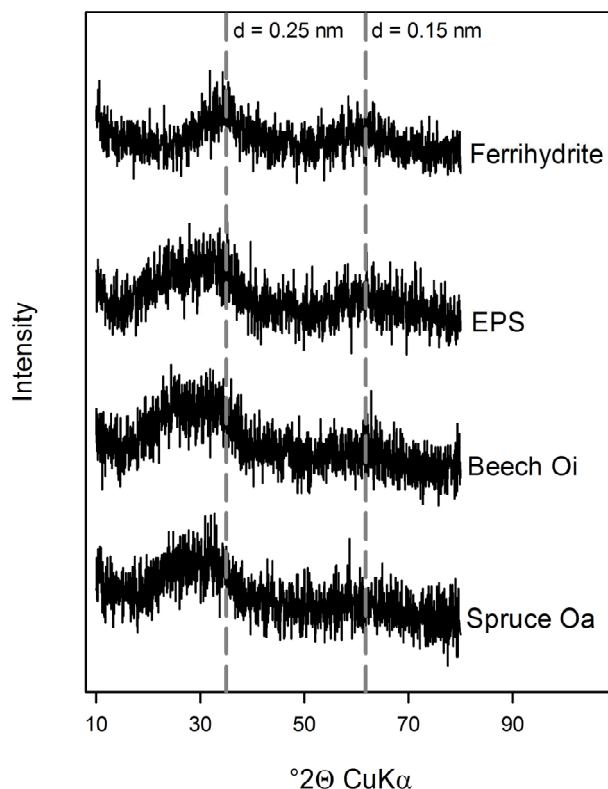


Fig. 3 XRD diagrams of ferrihydrite and the coprecipitates.

3.2 Electrochemical Reduction

3.2.1 Electron accepting capacity

The electron accepting capacity (EAC) of Fh and the coprecipitates were approximately equal to the Fe(III) content determined by acidic digestion within an error range of 10 % (Fig. 4a). Ratios of EAC/Fe(III) of coprecipitates larger than unity may have resulted from electron transfer to reducible moieties in the NOM and EPS. Additional deviations from unity and overall variability may have resulted from non-uniform distribution of Fh and coprecipitate aggregates in the suspensions from which samples were pipette-transferred to the electrochemical cells. Re-association of Fe(II) formed during the reduction with the coprecipitates, a process that may block surface reduction sites (Liu et al., 2001; Roden and Urrutia, 1999) and therefore result in an underestimation of Fe(III), seems unlikely considering the overall fast reduction rates (see section 3.2.2) and EAC values of approximately unity. As each of the samples was completely reduced within 30 min, surface

passivation by OM did not affect the absolute amount of electrons transferred to the coprecipitates.

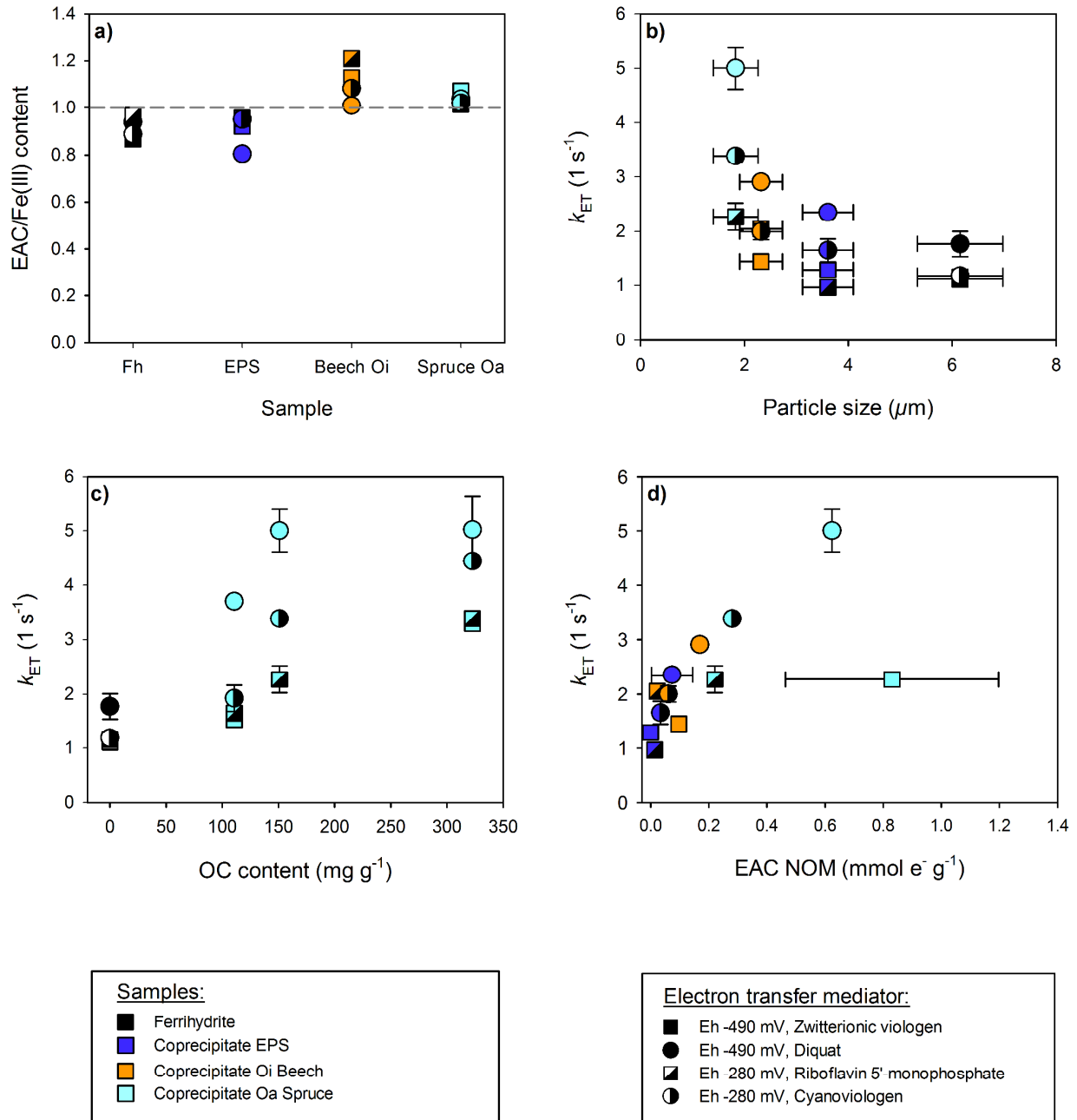


Fig. 4 Electron acceptor capacity (EAC) of ferrihydrite (Fh) and coprecipitates determined with four different electron transfer mediators in relation to the Fe(III) content of the sample (a), relationship between electron transfer rates and the initial particle size of the samples (10 mM KCl, pH 7) (b), relationship between electron transfer rates and organic carbon (OC) contents of different spruce Oa coprecipitates (c), relationship between electron transfer rates and electron acceptor capacity (Diquat) of each respective NOM or EPS (d). Different colors of the symbols refer to the type of sample, different shapes of the symbols refer to the type of electron transfer mediator that was used for each experiment. Error bars represent standard deviation of at least duplicate measurements.

3.2.2 Rates of electron transfer

The overall rate at which electrons were transferred across the working electrode in the electrochemical cell may have been limited by the rate at which (i) the mediator was reduced at the working electrode, (ii) the reduced mediator was transferred to a reactive site at the surface of the Fh or coprecipitates, (iii) the electron was transferred from the reduced mediator to the analyte, and/or (iv) the oxidized mediator was transferred back to the working electrode (Sander et al., 2015). As the electrochemical cells were continuously stirred during the analyses and pseudo-first-order rate constants measured for the reduction of the electron transfer mediators were on average at least 5 times larger than the rates measured upon addition of Fh or the coprecipitates, electron transfer from the reduced mediator to the analyte (Fh or the coprecipitates) most likely dominated the overall reduction rates and hence the current responses measured. Furthermore, the amount of mediator added was large enough to exclude restrictive dependencies on its concentration (data not shown). Therefore, the measured reductive currents reflected the reactivity of the samples towards abiotic reduction (Larsen and Postma, 2001).

Electron transfer rates of all coprecipitates were larger than those of pure Fh (Fig. 4b, c, and d). This observation is in agreement with previous studies on abiotic reduction using desferrioxamine to dissolve Fe(III)-polygalacturonic acid coprecipitates (Mikutta and Kretzschmar, 2008) and Na-dithionite to dissolve Fe(III)-NOM coprecipitates (Eusterhues et al., 2014). Pseudo-first-order reduction rates measured in the electrochemical cell showed no correlation with the SSA, TPV, or specific pore sizes of the coprecipitates (data not shown). Instead, the rates of electron transfer decreased in an exponential manner with increasing particle sizes of the coprecipitates (Fig. 4b). This trend indicates that the electron transfer rate of the coprecipitates was dictated by the aggregate size and not related to SSA, which integrates over physically less accessible surfaces in pore domains such as micropores. About 50 % of the TPV of ferrihydrite was located in micropores <2 nm, thus restricting access of

the electron transfer mediators to a large fraction of the total surface area. Our results therefore stand in apparent contrast to findings of Roden (2003), who reported that the abiotic dissolution of OM-free Fe oxides did not depend on particle aggregation but on their SSA, which correlated to oxide crystal order. For those organic-free systems, which are virtually non-existent in soils or sediments, Larsen and Postma (2001) argued that a simple relationship between the BET-derived SSA and abiotic reduction rates of Fe oxides was only valid for minerals with a similar crystal structure. Similar to our data, Mikutta and Kretzschmar (2008) also reported an inverse correlation of initial abiotic dissolution rates of polygalacturonic acid-derived Fe(III) coprecipitates and their particle size as polygalacturonate lead to smaller, less aggregated particles.

However, in our experiments, the rates of electron transfer to coprecipitates containing a larger amount of OM were no longer correlated to their particle size. Even though the particle size of the Oa spruce coprecipitate with an initial Fe/C ratio of 0.1 ($322.7 \text{ mg C g}^{-1}$) was twice as large as the one of the Oa spruce coprecipitate with an initial Fe/C ratio of 1.0 titrated to pH 7 ($151.0 \text{ mg C g}^{-1}$), the electron transfer rates did not decrease accordingly. Instead, for Oa spruce coprecipitates synthesized at different pH and with different initial C contents, the electron transfer rates seemed to increase with decreasing Fe/C ratio (Fig. 4c). The increased reduction rates can therefore probably be attributed to the more defective crystal structure, which is induced by increasing NOM contents as discussed in section 3.1.3. The only sample-mediator combination not following this trend was the DQ-mediated reduction of the coprecipitate with an initial Fe/C ratio of 0.1 (For more details on the different mediators refer to section 3.2.3). This exception was probably due to the large electron transfer rates no longer being solely governed by the rate of electron transfer from the mediator to the sample but also by the rate of reduction of the mediator itself, i.e., the electron transfer from the reduced mediator to the sample was no longer the only rate-determining step. Both aggregation state and crystallinity thus seemed to affect the rate of electrochemical reduction

of Fe-OM coprecipitates. Noteworthy, rates of electron transfer seemed to correlate with the EAC of each respective NOM used for coprecipitate synthesis (Fig. 4d). While this correlation may suggest accelerated reduction due to the presence of additional electron shuttling moieties in the desorbed NOM, the NOMs with larger EACs also coincided with smaller particle sizes of the corresponding coprecipitates (Fig. 4b and d). Moreover, the mediator concentration in the cell (0.3 mM) considerably exceeded the amount of initially desorbed NOM and EPS, which were below the detection limit in 10 mM KCl solution. Thus, electron shuttling of desorbed NOM and EPS was most likely negligible compared to shuttling via the mediators. However, OM associated with the coprecipitates (i.e., not dissolved) may have been involved in the electron transfer to the Fe(III) oxides to some extent.

3.2.3 Influence of different electron transfer mediators

The potentials applied to the working electrode in MER of -0.28 V and -0.49 V were set to be within the redox buffering range of the respective mediators (i.e., -0.28 V for CV and RF with standard reduction potentials of $E_h^0 = -0.14\text{V}$ and -0.18V , respectively and -0.49 V for DQ and the ZiV mediator with $E_h^0 = -0.35\text{V}$ and -0.41V , respectively) (Sander et al., 2015). Even though the difference between the potential applied to the working electrode and the E_h^0 of the mediator at pH 7 was set to be the same in each set-up, the difference between each respective standard potential of the coprecipitates and the electron transfer mediator would have been largest for DQ and ZiV making them the stronger reducing agents of all mediators engaged. Electron transfer was generally fastest in cells with DQ as the mediator (Fig. 4 b, c, and d), likely reflecting the low potential that was applied in these measurements (-0.49V) in combination with the larger concentration of reduced mediator species as compared to ZiV (i.e., a larger difference between applied potential and E_h^0 for DQ than the zwitterionic mediator). Compared to DQ at the same applied potential, electrochemical

reduction mediated by ZiV might have been additionally slowed down by the sorption of sulfonate groups to the coprecipitate surfaces or by repulsion of the negatively charged mediator by the negative surface charge of the coprecipitates. As the surface charge of Fh was near the point of zero charge (PZC 7.4), the differences between the electron transfer mediators were less pronounced (Fig. 4b). Electrochemical reduction mediated by RF might have been slowed down by the sorption of the phosphate group to Fh surfaces (Stumm, 1997). Overall, however, the reduction rates of the coprecipitates were comparable (difference less than a factor of three) in all MER treatments, despite different mediators and applied reduction potentials (i.e., $E_h = -0.49$ or -0.28 V). We conclude that reduction potentials higher than -0.28 V would likely have been sufficient to reduce Fe(III) in Fh and the coprecipitates.

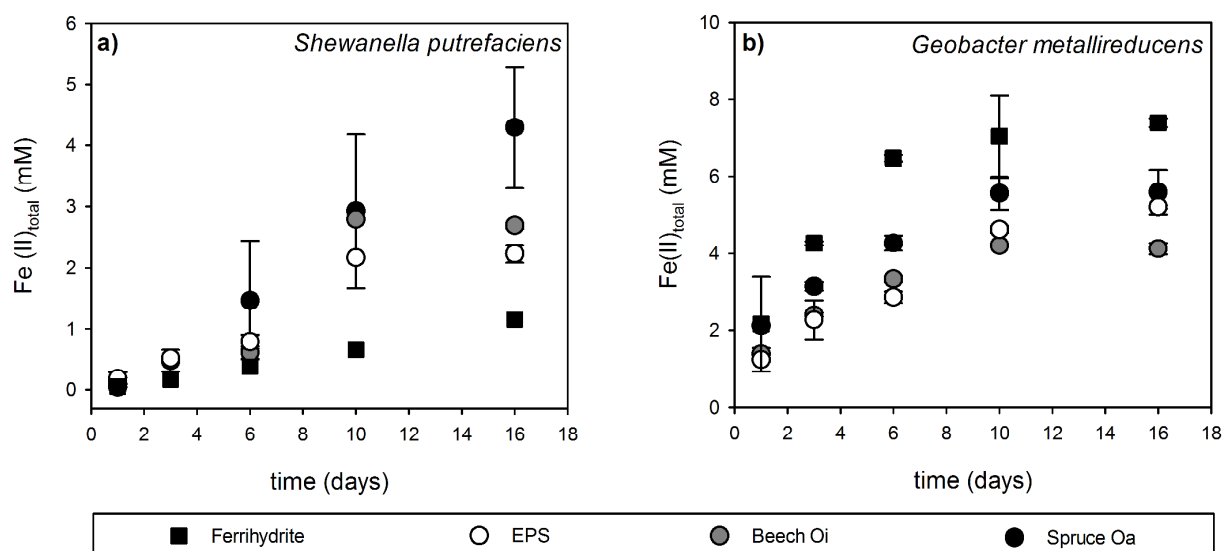


Fig. 5 Microbial reduction of ferrihydrite and coprecipitates by *Shewanella putrefaciens* (a) and *Geobacter metallireducens* (b), Fe(II)_{total} contents were determined after complete acidic digestion. Error bars represent the standard deviation of triplicate experiments. Please note the different scales of the y-axis.

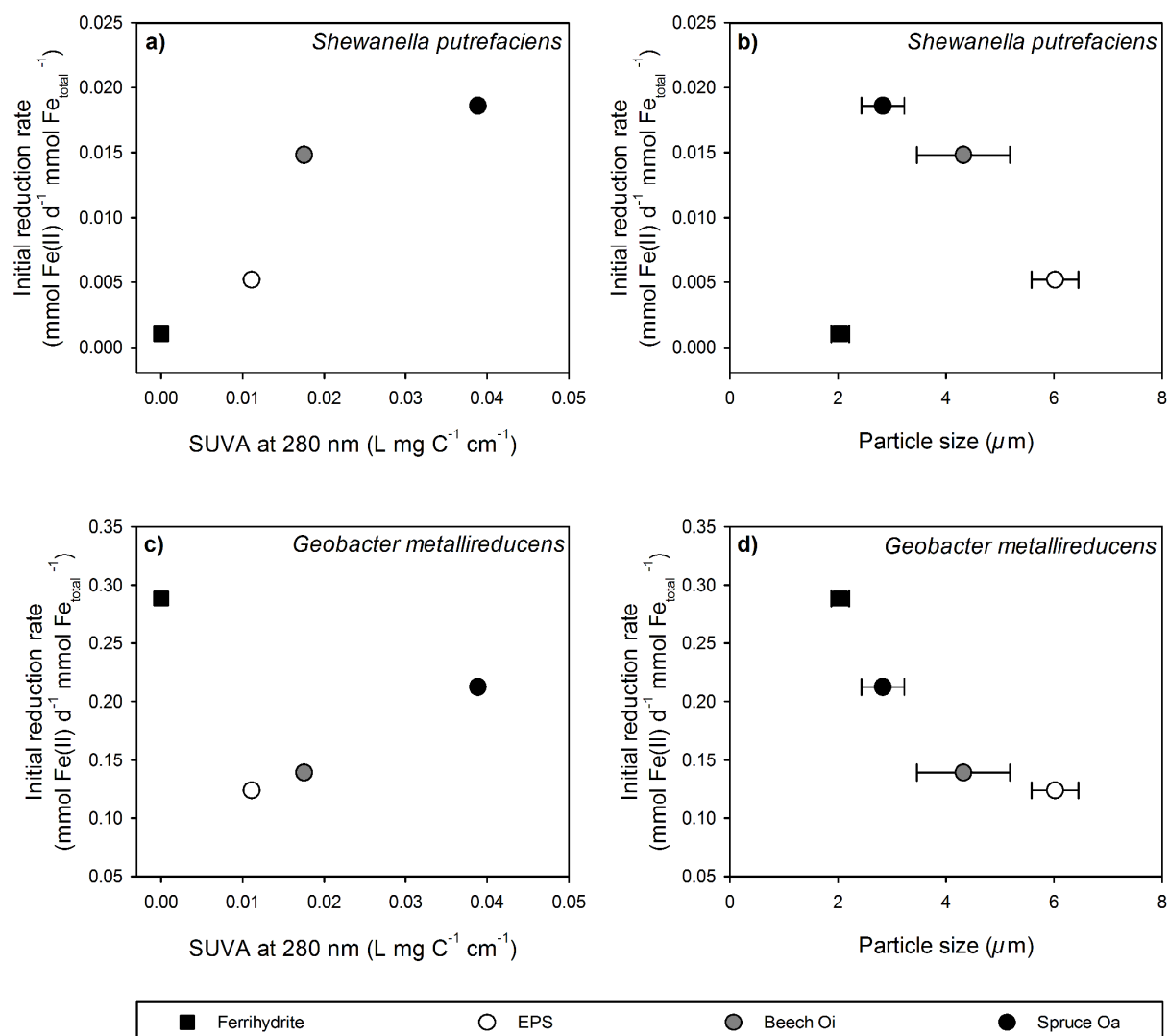


Fig. 6 Relationship between initial microbial reduction rates of ferrihydrite and coprecipitates and the SUVA (specific UV absorbance) at 280 nm of desorbed NOM and EPS in each respective microbial medium (a, c), relationship between initial microbial reduction rates and the initial particle size (in *Shewanella* or *Geobacter* medium, pH 7) of each sample (b, d). Error bars represent the standard deviation of triplicate experiments (Fe(II)_{total}) or measurements.

3.3 Microbial Reduction

3.3.1 Kinetics

The smallest Fe(III) reduction rates were found for Fh reduction by *Shewanella putrefaciens* (Fig. 5a). Initial reduction rates ranged from 0.001 mmol Fe(II) d⁻¹ mmol Fe_{total}⁻¹ for Fh to 0.019 mmol Fe(II) d⁻¹ mmol Fe_{total}⁻¹ for the spruce Oa coprecipitate. Both the initial reduction rates and the total amount of reduced Fe on day 16 increased in the order Fh < EPS

coprecipitate < beech Oi coprecipitate < spruce Oa coprecipitate. Enhanced reactivity therefore paralleled the rise in aromaticity of the coprecipitated NOM (i.e., with increasing UV absorbance at 280 nm; Fig. 6a). These findings generally agree with previous studies stating that humic acid-type molecules providing electron shuttling functionality for *Shewanella putrefaciens* enhanced microbial reduction if present at a sufficiently large concentration to overcome decelerating effects due to the passivation of mineral surface reduction sites by NOM sorption (Amstatter et al., 2012; Shimizu et al., 2013). As the pre-culture was grown aerobically, there were no electron shuttling molecules produced by the microorganism itself present in solution at the onset of the incubation experiments. The complete lack of electron shuttling compounds in the Fh suspensions may explain why it showed the smallest initial reduction rate. Conversely, the incubation flasks with coprecipitates likely contained electron shuttles that were associated with dissolved NOM or EPS. Despite the small aromaticity of the latter, Kang and Zhu (2013) found quinoid-like structures in EPS. Such quinone moieties have been suggested to act as electron shuttles and might have accounted for the slightly increased reduction rates of the EPS coprecipitate in comparison to Fh. Larger concentrations of electron shuttling quinones are expected for both beech Oi and spruce Oa NOMs, consistent with shuttling as an explanation for their larger initial reduction rates. However, Shimizu et al. (2013) reported increased reduction rates for humic acid-Fe coprecipitates only if the coprecipitates showed C/Fe ratios larger than 4.3. These ratios are considerably bigger than the ratios of the coprecipitates in our work. Furthermore, humic acids are expected to contain more electron shuttling moieties than the types of NOM used in this work. It is, however, possible that desorption of NOM from the coprecipitates was larger in our incubation systems due to larger phosphate contents of the nutrient solutions. Increased NOM desorption may have led to a greater absolute concentration of electron shuttling organic groups in solution and hence a larger enhancement in initial reduction rates than expected based on Shimizu et al. (2013). In addition, the method

of coprecipitate preparation used by Shimizu et al. (2013) probably resulted in more aggregated structures and thus decreased reduction rates in comparison to our coprecipitates. Noteworthy, the amount of C desorbed from the coprecipitates in the microbial medium ranged from 2.8 mg C L⁻¹ for the EPS coprecipitate to 5.3 mg C L⁻¹ for the Oi beech coprecipitate (Table E.1). These values only just approached the threshold value suggested by Jiang and Kappler (2008) required to initiate a noticeable increase in microbial reduction rates due to electron shuttling. Thus, the larger aromaticity derived from the SUVA of the NOM desorbed from the Oa spruce coprecipitate seemed to impact the Fe reduction to a greater extent than the larger amount of desorbed total C of the Oi beech coprecipitate.

Contrary to the abiotically mediated electrochemical reduction experiments, there was no straightforward correlation between particle or aggregate size and initial Fe(III) reduction rates by *Shewanella putrefaciens* (Fig. 6b) as previously suggested for Fh-humic acid adsorption complexes by Amstaetter et al. (2012). This apparent discrepancy might either be due to the smaller initial Fe(III) concentrations in our experiments resulting in smaller aggregates or due to the different degree of aggregation of coprecipitates in comparison to adsorption complexes studied by Amstaetter et al. (2012). Both effects would indeed leave electron shuttling to be the dominant rate-determining parameter for our experimental set-up. In contrast to *Shewanella putrefaciens*, initial Fe reduction rates by *Geobacter metallireducens* were largest for Fh (0.289 mmol Fe(II) d⁻¹ mmol Fe_{total}⁻¹; Figure 5b). This observation is in accordance with Eusterhues et al. (2014), who found decreased Fe reduction rates by *Geobacter bremensis* for Fh adsorption complexes and Fe-OM coprecipitates in comparison to pure Fh. Nevertheless, even though surface passivation by NOM may have decreased reduction rates in systems containing NOM or EPS, there was no relationship between reduction rates and C contents – and thus likely surface coverages – in our *Geobacter* incubations. However, unlike for the *Shewanella* culture and in line with the abiotic dissolution experiments, initial rates exponentially decreased with increasing particle

size (Fig. 6d), whereas there was no correlation with the BET-derived SSA (data not shown). It has to be noted that, in contrast to measurements in 10 mM KCl, measured particle size was smallest for Fh in the nutrient solution. This small particle size most likely originated from particle dispersion effects caused by Na and phosphate, once more highlighting the importance of considering background electrolyte solution and buffer systems.

Roden (2003) suggested that microbial reduction rates of Fe oxides are controlled by the available surface sites rather than by the thermodynamic properties of the underlying oxide crystals. In contrast, Eusterhues et al. (2014) attributed faster reaction rates of coprecipitates by *Geobacter bremensis* to a more defective crystal structure with increasing incorporation of NOM. While the results of Roden (2003) are applicable to pure Fe oxides with a uniform distribution of crystal properties, surface site access and crystal structure of coprecipitates may change throughout the microbial reduction even without considering microbial or secondary mineralization. Variations in the amount of NOM released, as different parts of the coprecipitate are dissolved, in addition to the preferential reduction of pure Fh, may change the aggregation state of coprecipitates during reduction to a larger extent than possible for pure Fe oxides. Due to the larger SSA, the decreased extent of reduction of the beech Oi coprecipitate could have reflected surface site passivation by readsorption of Fe(II) formed during the microbial reduction (Liu et al., 2001; Roden and Urrutia, 1999). As this assumption was not supported by the difference of total Fe(II) and concentrations of Fe(II) after filtration $<0.025 \mu\text{m}$, an influence of the less defective crystal structure due to smaller C contents in comparison to the other two coprecipitates seems to be a more reasonable explanation. Since Lovley et al. (1996) showed that *Geobacter metallireducens* can reduce humic acids and model quinones like AQDS, it cannot be ruled out that spruce Oa-derived redox-active molecules may have increased microbial Fe reduction via electron shuttling for *Geobacter metallireducens*, too. If electron shuttling had played a major role for this microorganism, however, the differences between the EPS and spruce Oa coprecipitate should have been more

pronounced, due to the smaller anticipated concentrations of shuttling moieties in the EPS. Moreover, differences between these two coprecipitates could also be explained by complexation of Fe(II) by spruce Oa-derived NOM.

For both *Shewanella putrefaciens* and *Geobacter metallireducens*, the reduction rates did not correlate with any of the XPS-identified carbon species (data not shown). In the case of *Shewanella*, this might be attributed to the inability of XPS to clearly distinguish between aliphatic and aromatic C, while the amount of easily desorbable electron shuttling molecules is likely to be more crucial than the total amount of potential electron shuttling molecules contained in the coprecipitates. Because coprecipitate reduction by *Geobacter* seems to be controlled by the impact of NOM on the aggregation state of the coprecipitates, the influential compounds may have been located predominantly at surfaces within aggregates and were therefore not entirely accessible to XPS analysis in the first place.

Even though the negative surface charge based on electrophoretic mobility (EM) measurements of the coprecipitate particles may have played a role by impeding the attachment of negatively charged microbial cells to the surface of the coprecipitates (van Loosdrecht et al., 1990), there was no correlation between the absolute values of the EM of coprecipitates and the Fe reduction rates (data not shown). The concentration of dissolved Fe(III) during the course of microbial reduction was negligible, suggesting that chelating and dispersion of Fe(III) by NOM did not exert a noticeable influence on coprecipitate reduction. A possible effect of the different initial cell concentrations for *Shewanella* and *Geobacter* on the electron transfer mechanisms during reduction has to be taken into consideration, as the relation between aromaticity and reduction rates coincided with the initially smaller cell concentrations for *Shewanella*, while the relation between particle size and reduction rate coincided with the initially larger cell concentration for *Geobacter*. However, if the reduction-governing parameter switched from aromaticity limiting at lower cell density to particle size limiting at higher cell density, the reduction rate by *Shewanella* should change accordingly

during the experiment. Especially the reduction rate of ferrihydrite, which clearly showed the smallest particle size and least aggregation of all samples, should have increased along with a growing cell density over time in comparison to the coprecipitates. Instead of this development, reduction of ferrihydrite by *Shewanella* remained constantly low in comparison to the coprecipitates during the course of the experiment. While the different initial cell densities can explain the larger reduction rate of *Geobacter metallireducens* in comparison to *Shewanella putrefaciens*, they seemed to have a minor impact on the reduction mechanism itself.

3.3.2 Transformation of minerals

Despite the attempt to minimize media-induced vivianite ($\text{Fe}_3(\text{PO}_4)_2 \cdot 8\text{H}_2\text{O}$) formation by using HEPES instead of phosphate buffer, this mineral was detectable after 16 days of incubation (Table 5, Fig. F.1). No other secondary minerals were detected. With *Shewanella putrefaciens* as the Fe-reducing microorganism, only the beech Oi coprecipitate showed neo-formation of vivianite. Incubations with *Geobacter metallireducens*, on the other hand, induced vivianite formation for Fh, the EPS and beech Oi coprecipitates but not the spruce Oa coprecipitate. While the Fe(II) concentrations were not sufficiently large to initiate vivianite precipitation during reduction of Fh and the EPS coprecipitate by *Shewanella putrefaciens*, modelling with Visual MINTEQ (Gustafsson, 2006) showed that vivianite should have formed in both set-ups containing the spruce Oa coprecipitate if dissolved OM had been absent from the solution. The transformation was therefore probably impeded by complexation of Fe(II) by spruce Oa-derived NOM desorbed from the coprecipitate.

Mineral transformation of Fh to goethite during faster reduction or magnetite during slower reduction has been reported in several studies (Cornell and Schwertmann, 2003). At the same time, decreasing formation or a complete lack of goethite and magnetite during Fe(III) reduction of Fh with increasing contents of humic acids or OM has been observed as

well (Amstaetter et al., 2012; Eusterhues et al., 2014; Henneberry et al., 2012; Shimizu et al., 2013). Sorbed NOM or EPS in our study probably impeded sorption of Fe(II) to the Fh surface, which is required for goethite formation (Hansel et al., 2003; Thompson et al., 2006) or magnetite formation at smaller Fe(II) concentrations (Yang et al., 2010). The lack of formation of both minerals during the reduction of pure Fh by *Geobacter metallireducens* might be due to the reduction rates being too fast for readsorption of Fe(II) to take place or due to site blockage by media-induced phosphate sorption (Piepenbrock et al., 2011; Porsch et al., 2010). In contrast to the studies by Amstaetter et al. (2012) and Shimizu et al. (2013), addition of NOM did not result in the formation of green rust phases during Fe reduction in our study. However, the microbial media in our experiments did not contain carbonate, which was the dominant interlayer anion in the green rust phases found by Amstaetter et al. (2012) and Shimizu et al. (2013). FTIR spectra of the solid phases after incubation did not differ significantly from the spectra taken before the reduction apart from a large additional peak between 920 and 1080 cm^{-1} . This new peak could be attributed to asymmetric ester O–P–O stretching modes from nucleic acids and P=O stretching of phosphodiester backbone of nucleic acid (Table 2), pointing towards bacterial cell remnants associated with the coprecipitates (Fig. F.2).

4 CONCLUSIONS

Our results suggest that physicochemical properties and the electrochemical stability of Fe-OM coprecipitates cannot easily be used to predict their durability under natural soil conditions, as different electron transfer mechanisms applied by different genera of microorganisms result in different parameters impacting the reactivity and therefore stability of coprecipitates. The composition of NOM directly influences the enhancement of Fe(III) reduction in coprecipitates by *Shewanella putrefaciens* via the amount of potentially usable electron shuttling molecules it provides. In our set-up for *Shewanella putrefaciens*, desorbable

OM thus affected Fe reduction to a larger extent than the varying aggregational properties evoked by sorbed NOM. In contrast, reductive dissolution of Fe-OM coprecipitates by *Geobacter metallireducens* was only indirectly controlled by NOM properties. The composition of NOM controlled the aggregation of the coprecipitates, which in turn influenced the Fe reduction by *Geobacter metallireducens* leading to the inhibition of reduction of the coprecipitates in comparison to pure Fh. The surface area inferred from BET-SSA measurements proved to be a poor predictor of Fe reduction rates of Fe-OM coprecipitates irrespective of the preferred electron transfer mechanism. This study highlights that naturally occurring coprecipitates are extremely complex and each experiment relying on pure bacterial cultures is only able to cover a narrow set of experimental parameters. Still, our experiments showed that both the composition of NOM and the type of microorganism involved considerably impact the dynamics of Fe-OM coprecipitate reduction and thus their long-term stability in soils.

Acknowledgements

This study was financially supported by the NTH-Graduate School “Geofluxes”. We are grateful to Anja Freund for providing the two additional coprecipitates used for the mediated electrochemical reduction experiments. We would also like to thank the reviewers and the editor for their helpful comments.

References

- Amstaetter, K., Borch, T., Kappler, A., 2012. Influence of humic acid imposed changes of ferrihydrite aggregation on microbial Fe(III) reduction. *Geochim. Cosmochim. Acta* 85, 326–341. doi:10.1016/j.gca.2012.02.003
- Angelico, R., Ceglie, A., He, J.Z., Liu, Y.R., Palumbo, G., Colombo, C., 2014. Particle size, charge and colloidal stability of humic acids coprecipitated with ferrihydrite. *Chemosphere* 99, 239–247. doi:10.1016/j.chemosphere.2013.10.092
- Bachand, P.A.M., Richardson, C.J., Vaithyanathan, P., 2000. Phase II low intensity chemical dosing (LICD): Development of management practices. Final report submitted to Florida Department of Environmental Protection in fulfillment of Contract No. WM720.

- Barrett, E.P., Joyner, L.G., Halenda, P.P., 1951. The Determination of Pore Volume and Area Distributions in Porous Substances. I. Computations from Nitrogen Isotherms. *J. Am. Chem. Soc.* 73, 373–380. doi:10.1021/ja01145a126
- Boesen, T., Nielsen, P., 2013. Molecular Dissection of Bacterial Nanowires. *MBio* 4, e00270–13. doi:10.1128/mBio.00270-13. Copyright
- Brümmer, G.W., Barrow, N.J., Fischer, L., 2013. Effect of porosity of goethite on the sorption of six heavy metal ions. *Eur. J. Soil Sci.* 64, 805–813. doi:10.1111/ejss.12091
- Brunauer, S., Emmett, P.H., Teller, E., 1938. Adsorption of Gases in Multimolecular Layers. *J. Am. Chem. Soc.* 60, 309–319.
- Chen, J., Gu, B., Royer, R. a, Burgos, W.D., 2003. The roles of natural organic matter in chemical and microbial reduction of ferric iron. *Sci. Total Environment* 307, 167–78. doi:10.1016/S0048-9697(02)00538-7
- Cheng, H., Hu, Y., Luo, J., Xu, B., Zhao, J., 2009. Geochemical processes controlling fate and transport of arsenic in acid mine drainage (AMD) and natural systems. *J. Hazard. Mater.* 165, 13–26. doi:10.1016/j.jhazmat.2008.10.070
- Chorover, J., Amistadi, M.K., 2001. Reaction of forest floor organic matter at goethite, birnessite and smectite surfaces. *Geochim. Cosmochim. Acta* 65, 95–109.
- Christoffersen, J., Christoffersen, M.R., 1976. The kinetics of dissolution of calcium sulphate dihydrate in water. *J. Cryst. Growth* 35, 79–88. doi:10.1016/0022-0248(76)90247-5
- Cismasu, A.C., Michel, F.M., Teaciu, A. P., Tyliczszak, T., Brown, Jr, G.E., 2011. Composition and structural aspects of naturally occurring ferrihydrite. *Comptes Rendus Geosci.* 343, 210–218. doi:10.1016/j.crte.2010.11.001
- Cornell, R.M., Schwertmann, U., 2003. *The iron oxides*, 2nd ed. Wiley-VCH. doi:10.1002/3527602097
- de Brouwer, J.F.C., Wolfstein, K., Stal, L.J., 2002. Physical characterization and diel dynamics of different fractions of extracellular polysaccharides in an axenic culture of a benthic diatom. *Eur. J. Phycol.* 37, 37–44.
- Dolfing, J., Chardon, W.J., Japenga, J., 1999. Association between colloidal iron, aluminum, phosphorus, and humic acids. *Soil Sci.* 164, 171–179. doi:10.1097/00010694-199903000-00003
- Downing, B.D., Bergamaschi, B.A., Evans, D.G., Boss, E., 2008. Assessing contribution of DOC from sediments to a drinking-water reservoir using optical profiling. *Lake Reserv. Manag.* 24, 381–391. doi:10.1080/07438140809354848
- El-Naggar, M.Y., Wanger, G., Leung, K.M., Yuzvinsky, T.D., Southam, G., Yang, J., Lau, W.M., Nealson, K.H., Gorby, Y.A., 2010. Electrical transport along bacterial nanowires from *Shewanella oneidensis* MR-1. *Proc. Natl. Acad. Sci. U. S. A.* 107, 18127–31. doi:10.1073/pnas.1004880107
- Eusterhues, K., Hädrich, A., Neidhardt, J., Küsel, K., Keller, T.F., Jandt, K.D., Totsche, K.U., 2014. Reduction of ferrihydrite with adsorbed and coprecipitated organic matter: microbial reduction by *Geobacter bremensis* vs. abiotic reduction by Na-dithionite. *Biogeosciences* 11, 4953–4966. doi:10.5194/bg-11-4953-2014
- Eusterhues, K., Wagner, F.E., Häusler, W., Hanzlik, M., Knicker, H., Totsche, K.U., Kögel-Knabner, I., Schwertmann, U., 2008. Characterization of Ferrihydrite-Soil Organic Matter Coprecipitates by X-ray Diffraction and Mössbauer Spectroscopy. *Environ. Sci. Technol.* 42, 7891–7.
- Gerin, P.A., Genet, M.J., Herbillon, A.J., Delvaux, B., 2003. Surface analysis of soil material by X-ray photoelectron spectroscopy. *Eur. J. Soil Sci.* 54, 589–603.
- Glasauer, S., Weidler, P.G., Langley, S., Beveridge, T.J., 2003. Controls on Fe reduction and mineral formation by a subsurface bacterium. *Geochim. Cosmochim. Acta* 67, 1277–1288. doi:10.1016/S0016-7037(00)01199-7
- Gorby, Y., Yanina, S., McLean, J.S., Rosso, K.M., Moyles, D., Dohnalkova, A., Beveridge,

- T.J., Chang, I.S., Kim, B.H., Kim, K.S., Culley, D.E., Reed, S.B., Romine, M.F., Saffarini, D.A., Hill, E.A., Shi, L., Elias, D.A., Kennedy, D.W., Pinchuk, G., Watanabe, K., Ishii, S., Logan, B., Nealson, K.H., Fredrickson, J.K., 2006. Correction for Lygeros et al., Stochastic hybrid modeling of DNA replication across a complete genome. *Proc. Natl. Acad. Sci. U.S.A.* 103, 11358–11363. doi:10.1073/pnas.0905246106
- Gorski, C.A., Klüpfel, L., Voegelin, A., Sander, M., Hofstetter, T.B., 2012. Redox properties of structural Fe in clay minerals. 2. Electrochemical and spectroscopic characterization of electron transfer irreversibility in ferruginous smectite, SWa-1. *Environ. Sci. Technol.* 46, 9369–9377. doi:10.1021/es302014u
- Gorski, C.A., Klüpfel, L.E., Voegelin, A., Sander, M., Hofstetter, T.B., 2013. Redox properties of structural Fe in clay minerals: 3. Relationships between smectite redox and structural properties. *Environ. Sci. Technol.* 47, 13477–13485. doi:10.1021/es403824x
- Gregg, S.H., Sing, K.S.W., 1982. Adsorption, Surface Area and Porosity, 2nd ed. Academic Press, New York.
- Gustafsson, J.P., 2006. Visual Minteq.
- Hanke, A., Cerli, C., Muhr, J., Borcken, W., Kalbitz, K., 2013. Redox control on carbon mineralization and dissolved organic matter along a chronosequence of paddy soils. *Eur. J. Soil Sci.* 64, 476–487. doi:10.1111/ejss.12042
- Hansel, C.M., Benner, S.G., Neiss, J., Dohnalkova, A., Kukkadapu, R.K., Fendorf, S., 2003. Secondary mineralization pathways induced by dissimilatory iron reduction of ferrihydrite under advective flow. *Geochim. Cosmochim. Acta* 67, 2977–2992. doi:10.1016/S0016-7037(03)00276-X
- Henneberry, Y.K., Kraus, T.E.C., Fleck, J.A., Krabbenhoft, D.P., Bachand, P.M., Horwath, W.R., 2011. Removal of inorganic mercury and methylmercury from surface waters following coagulation of dissolved organic matter with metal-based salts. *Sci. Total Environ.* 409, 631–637. doi:10.1016/j.scitotenv.2010.10.030
- Henneberry, Y.K., Kraus, T.E.C., Nico, P.S., Horwath, W.R., 2012. Structural stability of coprecipitated natural organic matter and ferric iron under reducing conditions. *Org. Geochem.* 48, 81–89. doi:10.1016/j.orggeochem.2012.04.005
- Ho, Y.S., McKay, G., 1998. A comparison of chemisorption kinetic models applied to pollutant removal on various sorbents. *Trans IChemE* 76, 332–340.
- Jiang, J., Kappler, A., 2008. Kinetics of Microbial and Chemical Reduction of Humic Substances: Implications for Electron Shuttling. *Environ. Sci. Technol.* 42, 3563–9.
- Jones, A.M., Collins, R.N., Rose, J., Waite, T.D., 2009. The effect of silica and natural organic matter on the Fe(II)-catalysed transformation and reactivity of Fe(III) minerals. *Geochim. Cosmochim. Acta* 73, 4409–4422. doi:10.1016/j.gca.2009.04.025
- Kaiser, K., Guggenberger, G., 2007. Sorptive stabilization of organic matter by microporous goethite: sorption into small pores vs. surface complexation. *Eur. J. Soil Sci.* 58, 45–59. doi:10.1111/j.1365-2389.2006.00799.x
- Kaiser, K., Guggenberger, G., 2003. Mineral surfaces and soil organic matter. *Eur. J. Soil Sci.* 54, 219–236.
- Kalbitz, K., Schwesig, D., Rethemeyer, J., Matzner, E., 2005. Stabilization of dissolved organic matter by sorption to the mineral soil. *Soil Biol. Biochem.* 37, 1319–1331. doi:10.1016/j.soilbio.2004.11.028
- Kang, F., Zhu, D., 2013. Abiotic reduction of 1,3-dinitrobenzene by aqueous dissolved extracellular polymeric substances produced by microorganisms. *J. Environ. Qual.* 42, 1441–8. doi:10.2134/jeq2012.0499
- Kleber, M., Eusterhues, K., Keiluweit, M., Mikutta, C., Mikutta, R., Nico, P.S., 2015. Mineral–organic associations: formation, properties, and relevance in soil environments. *Adv. Agron.* 130. doi:10.1016/bs.agron.2014.10.005
- Klüpfel, L., Keiluweit, M., Kleber, M., Sander, M., 2014. Redox properties of plant biomass-

- derived black carbon (biochar). *Environ. Sci. Technol.* 48, 5601–5611. doi:10.1021/es500906d
- Kögel-Knabner, I., 2000. Analytical approaches for characterizing soil organic matter. *Org. Geochem.* 31, 609–625.
- Kögel-Knabner, I., Amelung, W., Cao, Z., Fiedler, S., Frenzel, P., Jahn, R., Kalbitz, K., Kölbl, A., Schloter, M., 2010. Biogeochemistry of paddy soils. *Geoderma* 157, 1–14. doi:10.1016/j.geoderma.2010.03.009
- Kotloski, N.J., Gralnick, J.A., 2013. Flavin electron shuttles dominate extracellular electron transfer by *Shewanella oneidensis*. *MBio* 4, 10–13. doi:10.1128/mBio.00553-12
- Kraemer, S.M., 2004. Iron oxide dissolution and solubility in the presence of siderophores. *Aquat. Sci. - Res. Across Boundaries* 66, 3–18. doi:10.1007/s00027-003-0690-5
- Lagergren, S., 1898. About the Theory of So-Called Adsorption of Soluble Substance. *K. Sven. Vetenskapsakademiens Handl.* 24, 1–39.
- Larsen, O., Postma, D., 2001. Kinetics of reductive bulk dissolution of lepidocrocite, ferrihydrite, and goethite. *Geochim. Cosmochim. Acta* 65, 1367–1379. doi:10.1016/S0016-7037(00)00623-2
- Leone, L., Loring, J., Sj, S., Persson, P., Shchukarev, A., 2006. Surface characterization of the Gram-positive bacteria *Bacillus subtilis* - an XPS study. *Surf. Interface Anal.* 38, 202–205. doi:10.1002/sia
- Lies, D.P., Hernandez, M.E., Kappler, A., Mielke, R.E., Gralnick, J.A., Newman, D.K., 2005. *Shewanella oneidensis* MR-1 Uses Overlapping Pathways for Iron Reduction at a Distance and by Direct Contact under Conditions Relevant for Biofilms. *Appl. Environ. Microbiol.* 71, 4414–4426. doi:10.1128/AEM.71.8.4414
- Liu, C., Kota, S., Zachara, J.M., Fredrickson, J.K., Brinkman, C.K., 2001. Kinetic analysis of the bacterial reduction of goethite. *Environ. Sci. Technol.* 35, 2482–90.
- Liu, C., Zachara, J.M., Foster, N., Strickland, J., 2007. Kinetics of reductive dissolution of hematite by bioreduced anthraquinone-2,6-disulfonate 1–7.
- Lovley, D.R., Anderson, R.T., 2000. Influence of dissimilatory metal reduction on fate of organic and metal contaminants in the subsurface. *Hydrogeol. J.* 8, 77–88.
- Lovley, D.R., Blunt-Harris, E.L., 1999. Role of humic-bound iron as an electron transfer agent in dissimilatory Fe (III) reduction. *Appl. Environ. Microbiol.* 65, 4252–4254.
- Lovley, D.R., Coates, J.D., Blunt-Harris, E.L., Phillips, E.J.P., Woodward, J.C., 1996. Humic substances as electron acceptors for microbial respiration. *Nature* 382, 445–448.
- Lovley, D.R., Holmes, D.E., Nevin, K.P., 2004. Dissimilatory Fe(III) and Mn(IV) reduction. *Adv. Microb. Physiol.* 49, 219–86. doi:10.1016/S0065-2911(04)49005-5
- Lovley, D.R., Phillips, E.J., 1987. Rapid assay for microbially reducible ferric iron in aquatic sediments. *Appl. Environ. Microbiol.* 53, 1536–1540.
- Lovley, D.R., Phillips, E.J.P., 1988. Novel mode of microbial energy metabolism: organic carbon oxidation coupled to dissimilatory reduction of iron or manganese. *Appl. Environ. Microbiol.* 54, 1472–80.
- Lovley, D.R., Ueki, T., Zhang, T., Malvankar, N.S., Shrestha, P.M., Flanagan, K.A., Aklujkar, M., Butler, J.E., Giloteaux, L., Rotaru, A.-E., Holmes, D.E., Franks, A.E., Orellana, R., Risso, C., Nevin, K.P., 2011. *Geobacter*, in: Poole, R.K. (Ed.), *Advances in Microbial Physiology*. Elsevier, Amsterdam, pp. 1–100. doi:10.1016/B978-0-12-387661-4.00004-5
- Lovley, D.R., Woodward, J.C., Chapelle, F.H., 1994. Stimulated anoxic biodegradation of aromatic hydrocarbons using Fe(III) ligands. *Nature* 370, 128–131.
- Malvankar, N.S., Vargas, M., Nevin, K.P., Franks, A.E., Leang, C., Kim, B.-C., Inoue, K., Mester, T., Covalla, S.F., Johnson, J.P., Rotello, V.M., Tuominen, M.T., Lovley, D.R., 2011. Tunable metallic-like conductivity in microbial nanowire networks. *Nat. Nanotechnol.* 6, 573–579. doi:10.1038/nnano.2011.119

- Marschner, B., Brodowski, S., Dreves, A., Gleixner, G., Gude, A., Grootes, P.M., Hamer, U., Heim, A., Jandl, G., Ji, R., Kaiser, K., Kalbitz, K., Kramer, C., Leinweber, P., Rethemeyer, J., Schafer, A., Schmidt, M.W.I., Schwark, L., Wiesenberg, G.L.B., 2008. How relevant is recalcitrance for the stabilization of organic matter in soils? *J. Plant Nutr. Soil Sci.* 171, 91–110.
- Marsili, E., Baron, D.B., Shikhare, I.D., Coursolle, D., Gralnick, J. a, Bond, D.R., 2008. *Shewanella* secretes flavins that mediate extracellular electron transfer. *Proc. Natl. Acad. Sci. U. S. A.* 105, 3968–73. doi:10.1073/pnas.0710525105
- Mesuer, K., Fish, W., 1999. Chromate and oxalate adsorption on goethite. 2. Surface complexation modeling of competitive adsorption. *Environ. Sci. Technol.* 26, 2365–2370.
- Mikutta, C., 2011. X-ray absorption spectroscopy study on the effect of hydroxybenzoic acids on the formation and structure of ferrihydrite. *Geochim. Cosmochim. Acta* 75, 5122–5139. doi:10.1016/j.gca.2011.06.002
- Mikutta, C., Kretzschmar, R., 2008. Synthetic coprecipitates of exopolysaccharides and ferrihydrite. Part II: Siderophore-promoted dissolution. *Geochim. Cosmochim. Acta* 72, 1128–1142. doi:10.1016/j.gca.2007.11.034
- Mikutta, R., Baumgärtner, A., Schippers, A., Haumaier, L., Guggenberger, G., 2012. Extracellular polymeric substances from *Bacillus subtilis* associated with minerals modify the extent and rate of heavy metal sorption. *Environ. Sci. Technol.* 46, 3866–73. doi:10.1021/es204471x
- Mikutta, R., Kleber, M., Torn, M.S., Jahn, R., 2006. Stabilization of Soil Organic Matter: Association with Minerals or Chemical Recalcitrance? *Biogeochemistry* 77, 25–56. doi:10.1007/s10533-005-0712-6
- Mikutta, R., Lorenz, D., Guggenberger, G., Haumaier, L., Freund, A., 2014. Properties and reactivity of Fe-organic matter associations formed by coprecipitation versus adsorption: Clues from arsenate batch adsorption. *Geochim. Cosmochim. Acta* 144, 258–276. doi:10.1016/j.gca.2014.08.026
- Mikutta, R., Mikutta, C., Kalbitz, K., Scheel, T., Kaiser, K., Jahn, R., 2007. Biodegradation of forest floor organic matter bound to minerals via different binding mechanisms. *Geochim. Cosmochim. Acta* 71, 2569–2590. doi:10.1016/j.gca.2007.03.002
- Mikutta, R., Schaumann, G., Gildemeister, D., Bonneville, S., Kramer, M.G., Chorover, J., Chadwick, O.A., Guggenberger, G., 2009. Biogeochemistry of mineral–organic associations across a long-term mineralogical soil gradient (0.3–4100 kyr), Hawaiian Islands. *Geochim. Cosmochim. Acta* 73, 2034–2060.
- Mikutta, R., Zang, U., Chorover, J., Haumaier, L., Kalbitz, K., 2011. Stabilization of extracellular polymeric substances (*Bacillus subtilis*) by adsorption to and coprecipitation with Al forms. *Geochim. Cosmochim. Acta* 75, 3135–3154. doi:10.1016/j.gca.2011.03.006
- Myers, C.R., Nealson, K.H., 1988. Bacterial manganese reduction and growth with manganese oxide as the sole electron acceptor. *Science* 240, 1319–21. doi:10.1126/science.240.4857.1319
- Nevin, K.P., Lovley, D.R., 2002. Mechanisms for accessing insoluble Fe(III) oxide during dissimilatory Fe(III) reduction by *Geothrix fermentans*. *Appl. Environ. Microbiol.* 68, 2294–2299. doi:10.1128/AEM.68.5.2294
- Nevin, K.P., Lovley, D.R., 2000. Lack of production of electron-shuttling compounds or solubilization of Fe(III) during reduction of insoluble Fe(III) oxide by *Geobacter metallireducens*. *Appl. Environ. Microbiol.* 66, 2248–51.
- Newman, D.K., Kolter, R., 2000. A role for excreted quinones in extracellular electron transfer. *Nature* 405, 94–7. doi:10.1038/35011098
- Nierop, K.G.J., Jansen, B., Verstraten, J.M., 2002. Dissolved organic matter, aluminium and

- iron interactions: Precipitation induced by metal/carbon ratio, pH and competition. *Sci. Total Environ.* 300, 201–211. doi:10.1016/S0048-9697(02)00254-1
- Omoike, A., Chorover, J., 2006. Adsorption to goethite of extracellular polymeric substances from *Bacillus subtilis*. *Geochim. Cosmochim. Acta* 70, 827–838. doi:10.1016/j.gca.2005.10.012
- Omoike, A., Chorover, J., 2004. Spectroscopic study of extracellular polymeric substances from *Bacillus subtilis*: Aqueous chemistry and adsorption effects. *Biomacromolecules* 5, 1219–30. doi:10.1021/bm034461z
- Pédrot, M., Le Boudec, A., Davranche, M., Dia, A., Henin, O., 2011. How does organic matter constrain the nature, size and availability of Fe nanoparticles for biological reduction? *J. Colloid Interface Sci.* 359, 75–85. doi:10.1016/j.jcis.2011.03.067
- Perelomov, L. V., Pinskiy, D.L., Violante, A., 2011. Effect of organic acids on the adsorption of copper, lead, and zinc by goethite. *Eurasian Soil Sci.* 44, 22–28. doi:10.1134/S1064229311010091
- Piepenbrock, A., Dippon, U., Porsch, K., Appel, E., Kappler, A., 2011. Dependence of microbial magnetite formation on humic substance and ferrihydrite concentrations. *Geochim. Cosmochim. Acta* 75, 6844–6858. doi:10.1016/j.gca.2011.09.007
- Porsch, K., Dippon, U., Rijal, M.L., Appel, E., Kappler, A., 2010. In-situ magnetic susceptibility measurements as a tool to follow geomicrobiological transformation of Fe minerals. *Environ. Sci. Technol.* 44, 3846–52. doi:10.1021/es903954u
- R Development Core Team (Ed.), 2015. GNU R software, 3.1.1.
- Rancourt, D.G., Thibault, P.J., Mavrocordatos, D., Lamarche, G., 2005. Hydrous ferric oxide precipitation in the presence of nonmetabolizing bacteria: Constraints on the mechanism of a biotic effect. *Geochim. Cosmochim. Acta* 69, 553–577. doi:10.1016/j.gca.2004.07.018
- Reguera, G., McCarthy, K.D., Mehta, T., Nicoll, J.S., Tuominen, M.T., Lovley, D.R., 2005. Extracellular electron transfer via microbial nanowires. *Nature* 435, 1098–101. doi:10.1038/nature03661
- Roden, E.E., 2003. Fe(III) oxide reactivity toward biological versus chemical reduction. *Environ. Sci. Technol.* 37, 1319–1324. doi:10.1021/es026038o
- Roden, E.E., Urrutia, M.M., 1999. Ferrous iron removal promotes microbial reduction of crystalline iron(III) oxides. *Environ. Sci. Technol.* 33, 1847–1853. doi:10.1021/es9809859
- Royer, R.A., Burgos, W.D., Fisher, A.S., Jeon, B.-H., Unz, R.F., Dempsey, B. a, 2002. Enhancement of hematite bioreduction by natural organic matter. *Environ. Sci. Technol.* 36, 2897–904. doi:10.1021/es015735y
- Sander, M., Hofstetter, T.B., Gorski, C.A., 2015. Electrochemical analyses of redox-active iron minerals: A review of non-mediated and mediated approaches. *Environ. Sci. Technol.* 49, 5862–5878. doi:10.1021/acs.est.5b00006
- Sannino, F., De Martino, A., Pigna, M., Violante, A., Di Leo, P., Mesto, E., Capasso, R., 2009. Sorption of arsenate and dichromate on polymerin, Fe(OH)_x-polymerin complex and ferrihydrite. *J. Hazard. Mater.* 166, 1174–9. doi:10.1016/j.jhazmat.2008.12.015
- Scheel, T., Dörfel, C., Kalbitz, K., 2007. Precipitation of dissolved organic matter by aluminum stabilizes carbon in acidic forest soils. *Soil Sci. Soc. Am. J.* 71, 64–74. doi:10.2136/sssaj2006.0111
- Scheel, T., Haumaier, L., Ellerbrock, R.H., Rühlmann, J., Kalbitz, K., 2008. Properties of organic matter precipitated from acidic forest soil solutions. *Org. Geochem.* 39, 1439–1453. doi:10.1016/j.orggeochem.2008.06.007
- Schwertmann, U., Cornell, R.M., 2000. *Iron Oxides in the Laboratory: Preparation and Characterization*, 2nd ed. Wiley-VCH, Weinheim, Germany.
- Schwertmann, U., Wagner, F., Knicker, H., 2005. *Ferrihydrite–Humic Associations:*

- Magnetic Hyperfine Interactions. *Soil Sci. Soc. Am. J.* 69, 1009–1015. doi:10.2136/sssaj2004.0274
- Scott, D.T., McKnight, D.M., Blunt-Harris, E.L., Kolesar, S.E., Lovley, D.R., 1998. Quinone moieties act as electron acceptors in the reduction of humic substances by humics-reducing microorganisms. *Environ. Sci. Technol.* 32, 2984–2989. doi:10.1021/es980272q
- Shimizu, M., Zhou, J., Schröder, C., Obst, M., Kappler, A., Borch, T., 2013. Dissimilatory reduction and transformation of ferrihydrite-humic acid coprecipitates. *Environ. Sci. Technol.* 47, 13375–84. doi:10.1021/es402812j
- Stookey, L.L., 1970. Ferrozine---a new spectrophotometric reagent for iron. *Anal. Chem.* 42, 779–781. doi:10.1021/ac60289a016
- Stumm, W., 1997. Reactivity at the mineral-water interface: dissolution and inhibition. *Colloids and Surfaces* 120, 143–166.
- Thompson, A., Chadwick, O.A., Rancourt, D.G., Chorover, J., 2006. Iron-oxide crystallinity increases during soil redox oscillations. *Geochim. Cosmochim. Acta* 70, 1710–1727. doi:10.1016/j.gca.2005.12.005
- van Loosdrecht, M.C.M., Norde, W., Lyklema, J., Zehnder, A.J.B., 1990. Hydrophobic and electrostatic parameters in bacterial adhesion. *Aquat. Sci.* 52, 103–114. doi:10.1007/BF00878244
- Violante, A., Ricciardella, M., Pigna, M., 2003. Adsorption of heavy metals on mixed Fe-Al oxides in the absence or presence of organic ligands. *Water, Air, Soil Pollut.* 143, 289–306.
- von Canstein, H., Ogawa, J., Shimizu, S., Lloyd, J.R., 2008. Secretion of Flavins by *Shewanella* Species and their Role in Extracellular Electron Transfer. *Appl. Environ. Microbiol.* 74, 615–23. doi:10.1128/AEM.01387-07
- Wagai, R., Mayer, L.M., 2007. Sorptive stabilization of organic matter in soils by hydrous iron oxides. *Geochim. Cosmochim. Acta* 71, 25–35. doi:10.1016/j.gca.2006.08.047
- Waychunas, G., Rea, B., Fuller, C., Davis, J., 1993. Surface chemistry of ferrihydrite: Part 1. EXAFS studies of the geometry of coprecipitated and adsorbed arsenate. *Geochim. Cosmochim. Acta.* doi:10.1016/0016-7037(93)90567-G
- Weber, K.A., Achenbach, L.A., Coates, J.D., 2006. Microorganisms pumping iron: anaerobic microbial iron oxidation and reduction. *Nat. Rev. Microbiol.* 4, 752–64. doi:10.1038/nrmicro1490
- Weiss, J. V., Emerson, D., Megonigal, J.P., 2004. Geochemical control of microbial Fe(III) reduction potential in wetlands: Comparison of the rhizosphere to non-rhizosphere soil. *FEMS Microbiol. Ecol.* 48, 89–100. doi:10.1016/j.femsec.2003.12.014
- Wolf, M., Kappler, A., Jiang, J., Meckenstock, R.U., 2009. Effects of humic substances and quinones at low concentrations on ferrihydrite reduction by *Geobacter metallireducens* - Supporting Information. *Environ. Sci. Technol.* 43, 5679–85.
- Yang, L., Steefel, C.I., Marcus, M.A., Bargar, J.R., 2010. Kinetics of Fe(II)-catalyzed transformation of 6-line ferrihydrite under anaerobic flow conditions. *Environ. Sci. Technol.* 44, 5469–5475. doi:10.1021/es1007565
- Zachara, J.M., Kukkadapu, R.K., Peretyazhko, T., Bowden, M., Wang, C., Kennedy, D.W., Moore, D., Arey, B., 2011. The mineralogic transformation of ferrihydrite induced by heterogeneous reaction with bioreduced anthraquinone disulfonate (AQDS) and the role of phosphate. *Geochim. Cosmochim. Acta* 75, 6330–6349. doi:10.1016/j.gca.2011.06.030
- Zhu, W., Nan, Y., Huang, T., Wu, F., 2013. The mechanism, thermodynamic and kinetic characteristics of the microbial reduction of goethite mediated by anthraquinone-2-sulfonate. *Geomicrobiol. J.* 30, 928–940. doi:10.1080/01490451.2013.791356

SUPPORTING INFORMATION

**Microbial Reduction of Ferrihydrite-Organic Matter Coprecipitates by
Shewanella putrefaciens and *Geobacter metallireducens* in Comparison to
Mediated Electrochemical Reduction**

Christine Poggenburg^{1,2,*}, Robert Mikutta³, Michael Sander⁴, Axel Schippers⁵,
Alexander Marchanka^{6,7}, Reiner Dohrmann^{5,8}, Georg Guggenberger^{1,2}

¹ *Institute of Soil Science, Leibniz University Hannover,
Herrenhäuser Straße 2, 30419 Hannover, Germany*

² *Centre for Solid State Chemistry and New Materials, Leibniz University Hannover,
Callinstraße 3, 30167 Hannover, Germany*

³ *Soil Science and Soil Protection, Martin Luther University Halle-Wittenberg,
Von-Seckendorff-Platz 3, 06210 Halle (Saale), Germany*

⁴ *Institute of Biogeochemistry and Pollutant Dynamics, Swiss Federal Institute of Technology,
Universitätstrasse 16, 8029 Zurich, Switzerland*

⁵ *Bundesanstalt für Geowissenschaften und Rohstoffe (BGR),
Stilleweg 2, 30655 Hannover, Germany*

⁶ *Institute of Organic Chemistry, Leibniz University Hannover,
Schneiderberg 1B, 30167 Hannover, Germany*

⁷ *Centre of Biomolecular Drug Research (BMWZ), Leibniz University Hannover,
Schneiderberg 38, 30167 Hannover, Germany*

⁸ *Landesamt für Bergbau, Energie und Geologie (LBEG),
Stilleweg 2, 30655 Hannover, Germany*

*Corresponding author: poggenburg@ifbk.uni-hannover.de, +49 5117622625

Appendix A: Material and Methods - Characterization of Organic Matter, Ferrihydrite, and Coprecipitates

A.1 Nuclear magnetic resonance (NMR) spectroscopy

For characterization by NMR spectroscopy, ca. 35 mg of freeze-dried and homogenized material of each NOM was packed in a thin-wall 3.2-mm rotor. Solid-state NMR ^{13}C CP experiments were performed on a 600 MHz SB Bruker Avance III spectrometer (Bruker, Billerica, MA, USA) equipped with a 3.2 mm MAS $^1\text{H}/^{13}\text{C}/^{15}\text{N}$ probe head at 298 K. Magic angle spinning at 10 kHz was applied. The ^1H 90° pulse length was typically 2.6 μs with high power level proton decoupling at 96 kHz. The recycle delay time was 1.5 s. The Hartmann-Hahn condition was determined using a glycine standard and further optimized for each of the three NOM samples. Cross-polarization contact time for spruce Oa and EPS was 1 ms, while it was reduced to 200 μs for beech Oi in order to accommodate for a larger relaxation rate. The number of scans was 32768 for each sample. Spectra were acquired with 11.2 ms acquisition time and 1024 data points. Zero filling to 8192 points was performed and exponential window function with Lorentzian line broadening of 50 Hz was applied to all spectra. Chemical shift regions were assigned according to Kögel-Knabner (2000) and quantified by peak integration.

A.2 Elemental composition

The OC and total N contents of Fh and the coprecipitates were quantified with a CN analyzer (Vario EL III, Elementar GmbH, Hanau, Germany). Fe, P, and S contents of Fh and the coprecipitates were determined with inductively coupled plasma optical emission spectroscopy (ICP-OES, Varian 725-ES, Varian Inc., Palo Alto, CA, USA) after dissolution of approximately 5 mg of the freeze-dried solids in 2.5 mL of 10 M HCl and subsequent tenfold dilution with 0.1 M HCl. Fe contents were determined at the wavelengths of 259.940, 239.563, 238.204, and 234.350 nm, P contents at 214.914 and 213.618 nm, and S contents at 181.972 and 180.972 nm. Fe(II) contents of the Fe-OM coprecipitates were quantified using the ferrozine assay (Stookey, 1970) adapted according to Lovley and Phillips (1987). To quantify organically complexed Fe(III), approximately 30 mg of each coprecipitate was suspended in 30 mL 0.1 M $\text{Na}_4\text{P}_2\text{O}_7$ pre-adjusted to a pH of 9.5. After horizontally shaking at 100 rpm for 16 h and subsequent ultracentrifugation at 300,000 g for 6 h (Beckman Coulter Inc., Brea, CA, USA), Fe contents were determined with ICP-OES.

A.3 X-ray diffraction (XRD)

Powder samples of Fh and the coprecipitates were analyzed by XRD (Siemens D500, Siemens AG/Bruker AXS GmbH, Karlsruhe, Germany) using $\text{CuK}\alpha$ radiation and scanned from 2° to 80° 2Θ with a step size of 0.05° and a step time of 10 s.

A.4 X-ray photoelectron spectroscopy (XPS)

XPS spectra of the freeze-dried unreacted NOM, Fh, and the coprecipitates were acquired with a Kratos Axis Ultra DLD spectrometer (Kratos Analytical, Manchester, UK) using monochromatic Al $\text{K}\alpha$ -radiation with an excitation energy of 1486.7 eV. Survey spectra were

obtained applying a pass energy of 160 eV and a step size of 1 eV. In addition, C1s high resolution spectra were obtained applying a pass energy of 10 eV and a step size of 0.1 eV. The high resolution spectra were then charge corrected by setting the C1s peak to 285.0 eV, normalized and fitted to a Shirley-type background using the Unifit 2010 software package (Hesse et al., 2003). To quantify the relative contributions of different carbon oxidation states, the following subpeaks were assigned to the C1s peak according to Gerin et al. (2003), Omoike and Chorover (2004), and Leone et al. (2006): (i) aliphatic and aromatic carbon displaying bonds to carbon and hydrogen (C-C, C=C, C-H; at 285.0 ± 0.1 eV), (ii) carbon displaying a single bond to oxygen or nitrogen as in carbohydrates and amines (C-O, C-N; at 286.5 ± 0.2 eV), (iii) carbon displaying two bonds to oxygen as in aldehydes, ketones, and amides (C=O, O-C-O, O=C-N; at 288.0 ± 0.1 eV), (iv) carboxylic carbon displaying three bonds to oxygen (O-C=O; at 289.1 ± 0.2 eV).

A.5 Fourier transform infrared (FTIR) spectroscopy

FTIR spectra were recorded for the freeze-dried NOM, Fh, and coprecipitates using the attenuated total reflectance (ATR) mode (SENSOR 27, Bruker, Bremen, Germany). A total of 400 scans per sample were accumulated between 600 and 4,000 cm^{-1} at a resolution of 4 cm^{-1} . A polynomial background was fitted to the normalized spectra using the package *hyperSpec* (Beleites and Sergio, 2015) of the software GNU R 3.1.1 (R Development Core Team, 2015).

A.6 Specific surface area and pore analysis

The specific surface area (SSA) of Fh and the coprecipitates was determined in duplicate with an Autosorb-1 surface area analyzer (Quantachrome Instruments, Boynton Beach, FL, USA). After degassing under vacuum at 313 K for 24 h, N_2 was adsorbed to the minerals at 77 K. The Brunauer-Emmett-Teller (BET) equation was applied to the adsorption data in the relative pressure range of 0.05 to 0.3 P/P_0 (Brunauer et al., 1938). The total pore volume (TPV) was determined using the last data point of the adsorption branch of the isotherm at 0.995 P/P_0 . The micropore volume (<2 nm) was quantified by applying the Dubinin-Radushkevich (DR) method (Gregg and Sing, 1982) to adsorption points <0.01 P/P_0 . The mesopore volume (2-50 nm) was determined by applying the Barrett-Joyner-Halenda (BJH) method (Barrett et al., 1951). Differentiation between small (2-10 nm) and large (10-50 nm) mesopores was achieved by linear interpolation.

A.7 Electrophoretic mobility and particle size

The pH-dependent electrophoretic mobility (EM) of the Fh and coprecipitates was determined in 10 mM KCl background electrolyte and, in addition, for both types of microbial media used in the reduction experiments, as described in section 2.4 and 2.5. The EM was measured on a ZetaPALS Zeta Potential Analyzer (Brookhaven Instruments Corp., Holtsville, USA) with 10 runs comprising 10 cycles each. The size of particles and colloid-sized aggregates was quantified by applying a uniform sphere model to the measurements of a 532-nm laser, which were averaged over 8 runs lasting 60 s each. The particle size was calibrated with a 90-nm NanosphereTM size standard (Duke Scientific Corp.).

Appendix B: Material and Methods - Mediated Electrochemical Reduction

Electron transfer rates for each sample were calculated by assuming a pseudo-first-order rate law:

$$-k_{ET} \times t = \frac{\ln \left(1 - \frac{\int_0^t \frac{I_{Red}}{F} dt}{\int_0^{t_\infty} \frac{I_{Red}}{F} dt} \right)}{\int_0^{t_\infty} \frac{I_{Med}}{F} dt} \quad (B.1)$$

k_{ET} - electron transfer rate
 t - time
 I_{Red} - baseline corrected reductive current of the sample
 I_{Med} - baseline corrected reductive current of the electron transfer mediator

Fitting of k_{ET} analogous to eq. B.1 was conducted using the software GNU R 3.1.1 (R Development Core Team, 2015). To monitor the proper function of the cells as well as to determine the electron transfer rates of the mediators, 20 μL of each respective mediator solution were spiked and electrochemically quantified at the beginning, during, and at the end of the experiments.

Appendix C: Material and Methods – Microbial Reduction Experiments

Table C.1 Trace element solution of DSMZ Medium 141.

Trace element solution		
Nitrilotriacetic acid	1.50	g L ⁻¹
MgSO ₄ · 7H ₂ O	3.00	g L ⁻¹
MnSO ₄ · H ₂ O	0.50	g L ⁻¹
NaCl	1.00	g L ⁻¹
FeSO ₄ · 7H ₂ O	0.10	g L ⁻¹
CoSO ₄ · 7H ₂ O	0.18	g L ⁻¹
CaCl ₂ · 2H ₂ O	0.10	g L ⁻¹
ZnSO ₄ · 7H ₂ O	0.18	g L ⁻¹
CuSO ₄ · 5H ₂ O	0.01	g L ⁻¹
KAl(SO ₄) ₂ · 12H ₂ O	0.02	g L ⁻¹
H ₃ BO ₃	0.01	g L ⁻¹
Na ₂ MoO ₄ · 2H ₂ O	0.01	g L ⁻¹
NiCl ₂ · 6 H ₂ O	0.03	g L ⁻¹
Na ₂ SeO ₃ · 5H ₂ O	0.30	mg L ⁻¹

Table C.2 Vitamin solution of DSMZ Medium 141.

Vitamin solution		
Biotin	2.00	mg L ⁻¹
Folic acid	2.00	mg L ⁻¹
Pyridoxine-HCl	10.00	mg L ⁻¹
Thiamine-HCl · 2H ₂ O	5.00	mg L ⁻¹
Riboflavin	5.00	mg L ⁻¹
Nicotinic acid	5.00	mg L ⁻¹
D-Ca-pantothenate	5.00	mg L ⁻¹
Vitamin B12	0.10	mg L ⁻¹
p-aminobenzoic acid	5.00	mg L ⁻¹
Lipoic acid	5.00	mg L ⁻¹

C.1: Aqueous Fe(II) during Microbial Reduction

Despite the attempt to quantify both dissolved and total Fe(II) concentrations, reduction rates are discussed for the latter only. The quantified amount of dissolved Fe(II) after filtration through <0.2- μ m filters may have been artificially enlarged due to very small colloids with surface adsorbed Fe(II) also passing through the filter. Filtration through <0.025 μ m pore sized filters, on the other hand, may have withheld Fe(II) readsorbed to mineral phases and microbial cells, as well as partly preventing dissolved Fe(II) complexed by NOM from passing through the filter, thereby also causing artifacts.

Appendix D: X-Ray Diffraction after Microbial Reduction Experiments

XRD patterns of the solid post-incubation phase were recorded using a PANalytical X'Pert PRO MPD Θ - Θ (Kassel, Germany) diffractometer (CuK α radiation generated at 40 kV and 30 mA), equipped with a variable divergence slit (20 mm irradiated length), a primary and secondary soller slit, a proportional counter, a secondary monochromator, and a humidity chamber. The chamber CHC plus (Anton Paar, Austria) was purged with N₂ gas and relative humidity (RH) was monitored by a RH sensor in the chamber next to the sample. The oriented mounts were scanned from 2° to 80° 2 Θ with a step size of 0.03° 2 Θ . The measuring time varied between 10 and 60 s per step.

Appendix E: Properties of Ferrihydrite and Coprecipitates

E.1 Bulk and surface element contents

Preferential coprecipitation of more decomposed NOM in comparison to fresh litter-derived NOM has been reported before (Mikutta et al., 2014; Scheel et al., 2007). The larger content of phosphate in Oi-derived NOM solution (data not shown), which shows a high sorption affinity towards hydroxylated surfaces via complexation and thus competes with organic moieties for sorption sites during coprecipitation (Mikutta et al., 2007; Schneider et al., 2010), may have also contributed to the smaller OC contents of the beech Oi compared to the spruce Oa coprecipitate. Furthermore, a smaller accumulation of plant-derived polysaccharides in comparison to microbial-derived polysaccharides upon precipitation with Fe as reported by Eusterhues et al. (2011), might additionally account for the smaller OC content of the beech Oi coprecipitate in comparison to the EPS coprecipitate.

E.2 Additional Desorption Experiments

Table E.1 Desorbed organic carbon (OC_{desorbed}) after equilibrating with microbial nutrient solution for 24 h. Values in parentheses depict the standard deviation of triplicate measurements.

Sample	OC_{desorbed}	
	(mg L^{-1})	(mg g^{-1})
EPS	2.76 (0.38)	1.96 (0.29)
Beech Oi	5.30 (0.46)	4.09 (0.44)
Spruce Oa	4.52 (0.27)	2.98 (0.08)

Appendix F: Mineral Transformation during Microbial Reduction

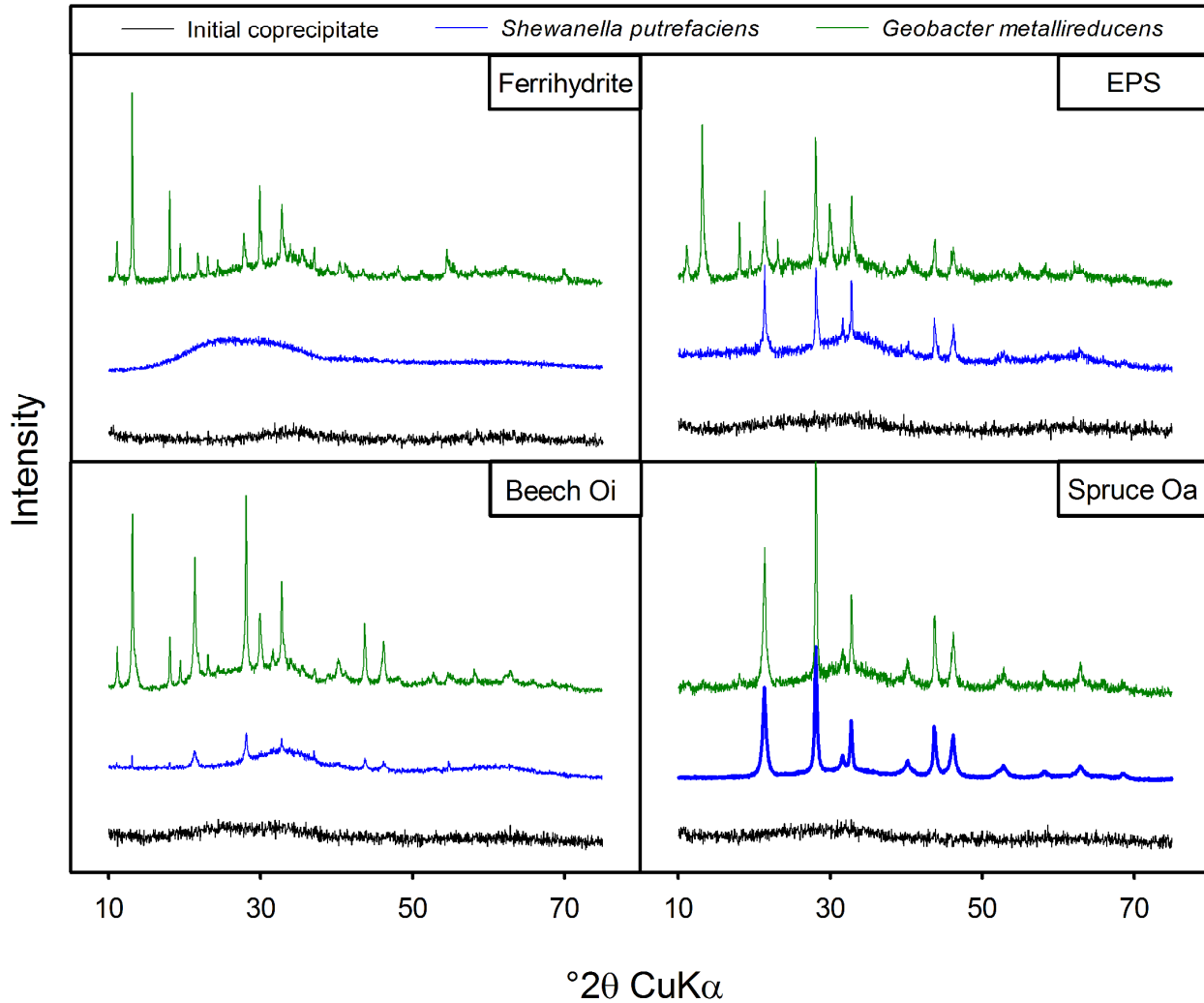


Fig. F.1 XRD diagrams of ferrihydrite and the coprecipitates before and after microbial reduction by *Shewanella putrefaciens* and *Geobacter metallireducens*.

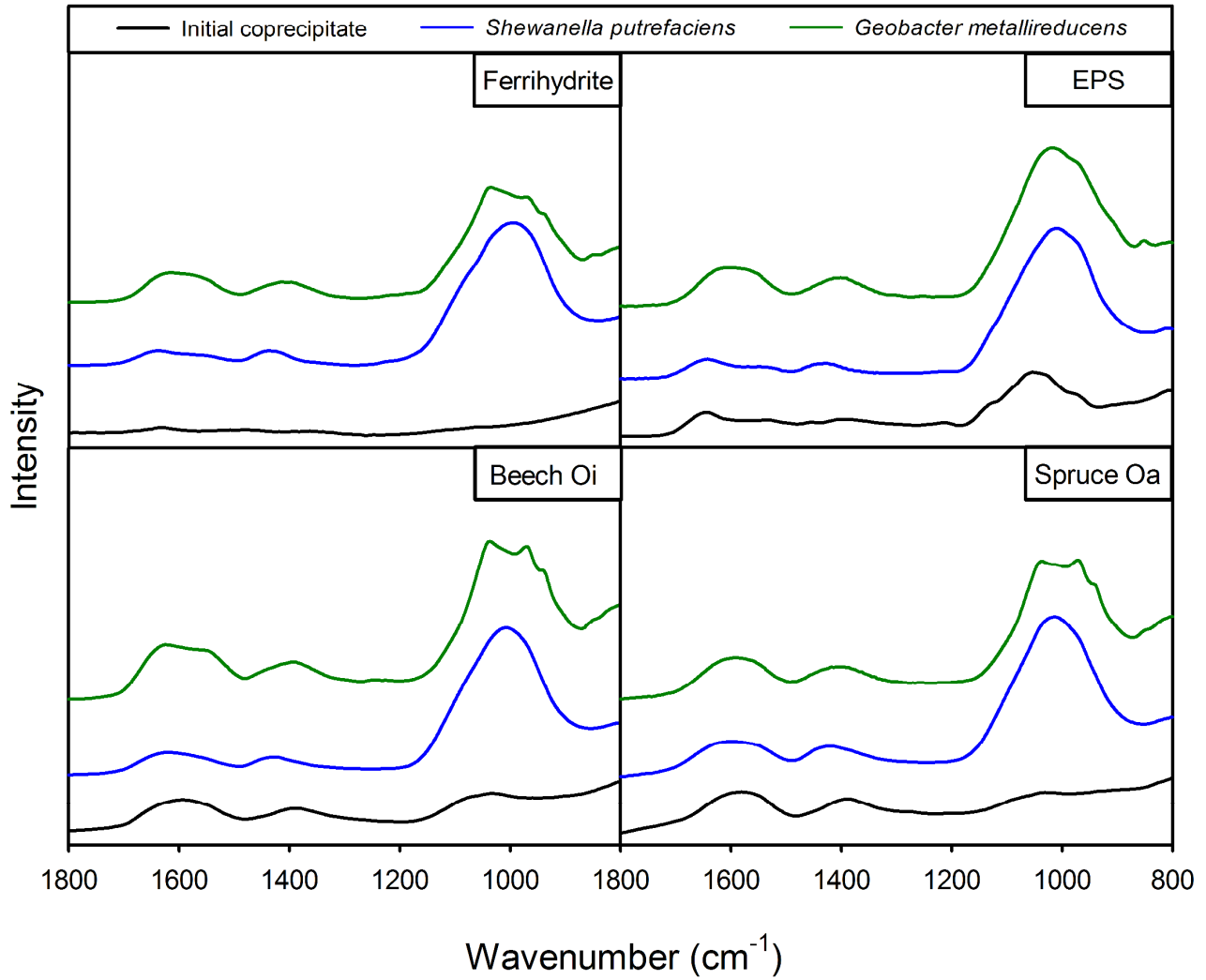


Fig. F.2 ATR-FTIR spectra of ferrihydrite and the coprecipitates before and after microbial reduction by *Shewanella putrefaciens* and *Geobacter metallireducens*.

References

- Barrett, E.P., Joyner, L.G., Halenda, P.P., 1951. The Determination of Pore Volume and Area Distributions in Porous Substances. I. Computations from Nitrogen Isotherms. *J. Am. Chem. Soc.* 73, 373–380. doi:10.1021/ja01145a126
- Beleites, C., Sergo, V., 2015. hyperSpec.
- Brunauer, S., Emmett, P.H., Teller, E., 1938. Adsorption of Gases in Multimolecular Layers. *J. Am. Chem. Soc.* 60, 309–319.
- Eusterhues, K., Rennert, T., Knicker, H., Kögel-Knabner, I., Totsche, K.U., Schwertmann, U., 2011. Fractionation of Organic Matter Due to Reaction with Ferrihydrite: Coprecipitation versus Adsorption. *Environ. Sci. Technol.* 45, 527–33. doi:10.1021/es1023898
- Gerin, P.A., Genet, M.J., Herbillon, A.J., Delvaux, B., 2003. Surface analysis of soil material by X-ray photoelectron spectroscopy. *Eur. J. Soil Sci.* 54, 589–603.
- Gregg, S.H., Sing, K.S.W., 1982. Adsorption, Surface Area and Porosity, 2nd ed. Academic Press, New York.
- Hesse, R., Chassé, T., Szargan, R., 2003. Unifit 2002-universal analysis software for photoelectron spectra. *Anal. Bioanal. Chem.* 375, 856–863. doi:10.1007/s00216-002-1705-0
- Kögel-Knabner, I., 2000. Analytical approaches for characterizing soil organic matter. *Org. Geochem.* 31, 609–625.
- Kögel-Knabner, I., 1997. ¹⁵N NMR spectroscopy as a tool in soil organic matter studies. *Geoderma* 80, 243–270.
- Leone, L., Loring, J., Sj, S., Persson, P., Shchukarev, A., 2006. Surface characterization of the Gram-positive bacteria *Bacillus subtilis* - an XPS study. *Surf. Interface Anal.* 38, 202–205. doi:10.1002/sia
- Lovley, D.R., Phillips, E.J., 1987. Rapid assay for microbially reducible ferric iron in aquatic sediments. *Appl. Environ. Microbiol.* 53, 1536–1540.
- Mikutta, R., Lorenz, D., Guggenberger, G., Haumaier, L., Freund, A., 2014. Properties and reactivity of Fe-organic matter associations formed by coprecipitation versus adsorption: Clues from arsenate batch adsorption. *Geochim. Cosmochim. Acta* 144, 258–276. doi:10.1016/j.gca.2014.08.026
- Mikutta, R., Mikutta, C., Kalbitz, K., Scheel, T., Kaiser, K., Jahn, R., 2007. Biodegradation of forest floor organic matter bound to minerals via different binding mechanisms. *Geochim. Cosmochim. Acta* 71, 2569–2590. doi:10.1016/j.gca.2007.03.002
- Omoike, A., Chorover, J., 2004. Spectroscopic study of extracellular polymeric substances from *Bacillus subtilis*: Aqueous chemistry and adsorption effects. *Biomacromolecules* 5, 1219–30. doi:10.1021/bm034461z
- R Development Core Team (Ed.), 2015. GNU R software, 3.1.1.
- Scheel, T., Dörfel, C., Kalbitz, K., 2007. Precipitation of dissolved organic matter by aluminum stabilizes carbon in acidic forest soils. *Soil Sci. Soc. Am. J.* 71, 64–74. doi:10.2136/sssaj2006.0111
- Schneider, M.P.W., Scheel, T., Mikutta, R., van Hees, P., Kaiser, K., Kalbitz, K., 2010. Sorptive stabilization of organic matter by amorphous Al hydroxide. *Geochim. Cosmochim. Acta* 74, 1606–1619. doi:10.1016/j.gca.2009.12.017
- Stookey, L.L., 1970. Ferrozine---a new spectrophotometric reagent for iron. *Anal. Chem.* 42, 779–781. doi:10.1021/ac60289a016

3 Study II

Impact of Natural Organic Matter Coatings on the Microbial Reduction of Iron Oxides

Contribution: I designed most of the experiments, prepared the Fe-organic associations, conducted the laboratory experiments and most of the analyses, collected and evaluated the data, compiled the tables and graphs, and wrote the manuscript.

Published in *Geochimica et Cosmochimica Acta* 224 (2018) 223-248.

DOI: 10.1016/j.gca.2018.01.004.

Impact of Natural Organic Matter Coatings on the Microbial Reduction of Iron Oxides

Christine Poggenburg^{1,2,}, Robert Mikutta³, Axel Schippers⁴,
Reiner Dohrmann^{4,5}, Georg Guggenberger^{1,2}*

¹ Institute of Soil Science, Leibniz University Hannover,
Herrenhäuser Straße 2, 30419 Hannover, Germany

² Centre for Solid State Chemistry and New Materials, Leibniz University Hannover,
Callinstraße 3, 30167 Hannover, Germany

³ Soil Science and Soil Protection, Martin Luther University Halle-Wittenberg,
Von-Seckendorff-Platz 3, 06210 Halle (Saale), Germany

⁴ Bundesanstalt für Geowissenschaften und Rohstoffe (BGR),
Stilleweg 2, 30655 Hannover, Germany

⁵ Landesamt für Bergbau, Energie und Geologie (LBEG),
Stilleweg 2, 30655 Hannover, Germany

*Corresponding author: poggenburg@ifbk.uni-hannover.de, +49 5117622625

Abstract

Iron (Fe) oxyhydroxides are important constituents of the soil mineral phase known to stabilize organic matter (OM) under oxic conditions. In an anoxic milieu, however, these Fe-organic associations are exposed to microbial reduction, releasing OM into soil solution. At present, only few studies have addressed the influence of adsorbed natural OM (NOM) on the reductive dissolution of Fe oxyhydroxides. This study therefore examined the impact of both the composition and concentration of adsorbed NOM on microbial Fe reduction with regard to (i) electron shuttling, (ii) complexation of Fe(II,III), (iii) surface site coverage and/or pore blockage, and (iv) aggregation. Adsorption complexes with varying carbon loadings were synthesized using different Fe oxyhydroxides (ferrihydrite, lepidocrocite, goethite, hematite, magnetite) and NOM of different origin (extracellular polymeric substances from *Bacillus subtilis*, OM extracted from soil Oi and Oa horizons). The adsorption complexes were characterized by X-ray diffraction (XRD), Fourier transform infrared spectroscopy (FTIR), X-ray photoelectron spectroscopy (XPS), N₂ gas adsorption, electrophoretic mobility and particle size measurements, and OM desorption. Incubation experiments under anaerobic conditions were conducted for 16 days comparing two different strains of dissimilatory Fe(III)-reducing bacteria (*Shewanella putrefaciens*, *Geobacter metallireducens*). Mineral transformation during reduction was assessed via XRD and FTIR. Microbial reduction of the pure Fe oxyhydroxides was controlled by the specific surface area (SSA) and solubility of the minerals. For *Shewanella putrefaciens*, the Fe reduction of adsorption complexes strongly correlated with the concentration of potentially usable electron-shuttling molecules for NOM concentrations <2 mg C L⁻¹, whereas for *Geobacter metallireducens*, Fe reduction depended on the particle size and thus aggregation of the adsorption complexes. These diverging results suggest that the influence of NOM on the stability of Fe-organic associations in soils cannot easily be assessed without considering the composition of the microbial soil community.

1 INTRODUCTION

Under oxic conditions, oxides, hydroxides and oxyhydroxides of iron (henceforth summarized as 'Fe oxides') are known to effectively stabilize soil organic matter (OM) against microbial decomposition via sorption (Mikutta et al., 2006; Kaiser and Guggenberger, 2007). However, in an anoxic environment, these iron (Fe)-organic associations may be subject to microbial reduction and thus mobilization (Hagedorn et al., 2000; Glasauer et al., 2003; Weiss et al., 2004; Lovley et al., 2004), which counteract the stabilizing effect of Fe oxides. Under these conditions, formerly bound OM can be exposed to microbial oxidation and decomposition (Canfield et al., 1993), causing the emission of greenhouse gases (CO₂, CH₄, N₂O). The dissimilatory dissolution of Fe oxides can furthermore pose severe environmental threats due to the accompanied release of associated organic contaminants (Lovley and Anderson, 2000), heavy metals (Violante et al., 2003; Perelomov et al., 2011; Brümmer et al., 2013), or oxyanions (Mesuere and Fish, 1999; Sannino et al., 2009) into the soil solution and groundwater. Furthermore, at large Fe(II) concentrations, a possible toxic effect for various bacteria by Fe(II) uptake at the expense of magnesium should also be taken into consideration (Hantke, 1997). Despite numerous publications studying the effect of different organic compounds (quinones, humic acids) on the reactivity and stability of Fe oxides in soils (Liu et al., 2007; Zachara et al., 2011; Amstaetter et al., 2012; Zhu et al., 2013), studies analyzing the effect of either adsorbed (Royer et al., 2002a; O'Loughlin, 2008; Eusterhues et al., 2014a) or coprecipitated (Pédrot et al., 2011; Henneberry et al., 2012; Shimizu et al., 2013) natural OM (NOM) on the microbial reduction of Fe-organic associations are still rare.

Most of the NOM in soils is present in the form of dissolved OM or as compounds associated with mineral surfaces (Kleber et al., 2015) with both fractions existing in a continuum of mutual exchange reactions. Dissolved NOM can potentially influence microbial reduction and solubility of Fe oxides by (i) complexation of Fe(II) thus increasing

thermodynamically favorable conditions for Fe(III) reduction (Roden and Urrutia, 1999; Royer et al., 2002b), (ii) acting as a ligand towards Fe(III) thereby promoting solubilisation (Nevin and Lovley, 2002a, 2002b; Jones et al., 2009), and (iii) providing redox active electron-shuttling compounds for Fe-reducing microorganisms (Lovley et al., 1996; Jiang and Kappler, 2008; Amstaetter et al., 2012; Poggenburg et al., 2016). Following adsorption of dissolved OM to Fe oxides these components can (iv) block surface sites (Kaiser and Guggenberger, 2003) and induce aggregation (Amstaetter et al., 2012). Structurally heterogeneous NOM of different origin and therefore different composition will likely influence each of these processes to differing degrees. Yet many previous studies examining the influence of NOM on microbially mediated Fe reduction preferred the utilization of either NOM fractions like purified humic acid (Amstaetter et al., 2012; Shimizu et al., 2013) or defined model compounds (e.g. Liu et al., 2007; Zachara et al., 2011; Zhu et al., 2013), particularly anthraquinone-2,6-disulfonic acid (AQDS). This molecule serves as an excellent electron shuttle and quinones or quinone-type molecules exhibiting a similar redox potential have been suggested to play a major part in providing electron-shuttling compounds in soils (Lovley and Blunt-Harris, 1999). This process may, nevertheless, not be conclusively restricted to these types of compounds. Chen et al. (2003) attributed electron shuttling-mediated accelerated Fe reduction rates to humic acid-derived high-molecular-weight aromatic structures and to a lesser but still considerable extent to NOM-derived low-molecular-weight polyphenolic compounds. Moreover, Wolf et al. (2009) demonstrated the sorption affinity of AQDS towards ferrihydrite not only to be one of the lowest amongst several tested quinones of various composition but also to be 10-fold exceeded by fulvic and humic acids. Experiments using AQDS, therefore, offer always easily available electron-shuttling compounds and neglect the preferential sorption of many complex aromatic compounds naturally occurring in soils (Chorover and Amistadi, 2001; Kalbitz et al., 2005; Scheel et al., 2007). Sorptive fractionation varies with NOM composition and concentration,

as more aromatic and complex compounds are sorbed and stabilized preferentially (Kalbitz et al., 2005), which highly impacts aggregation, bioavailable surface area, and thus the reactivity of Fe-organic associations. Nevertheless, the systematic influence exerted by different carbon loadings of Fe oxide adsorption complexes in combination with the varying aromaticity of different NOM sources has been neglected so far.

Since pure Fe oxides as well as mineral-organic associations are not able to pass the bacterial outer cell membrane in order to be reduced, Fe-reducing microorganisms developed different electron transfer mechanisms (Weber et al., 2006). These include (i) directly transferring electrons via either outer-membrane redox-enzymes (Myers and Nealson, 1988; Nevin and Lovley, 2000) or conductive cellular nanowires (Reguera et al., 2005; Gorby et al., 2006; El-Naggar et al., 2010) and (ii) mediating the electron transfer to the mineral by using either Fe-chelating compounds (Lovley et al., 1994; Nevin and Lovley, 2002a; Kraemer, 2004) or electron-shuttling molecules like endogenously produced flavins (Newman and Kolter, 2000; Nevin and Lovley, 2002a, 2002b; von Canstein et al., 2008; Marsili et al., 2008) or exogenous compounds as provided by NOM (Lovley et al., 1996).

Apart from the properties of adsorbed NOM, microbial reduction rates of Fe oxide adsorption complexes may be controlled by the type of Fe-reducing bacteria, since the reduction of the same Fe-OM coprecipitates by both *Shewanella putrefaciens* and *Geobacter metallireducens* were influenced by different NOM-derived parameters (Poggenburg et al., 2016). Even though the exact mechanisms behind species-specific extracellular electron transfer are still a field of intensive research, Shewanellaceae exhibit the ability to excrete flavins acting as electron-shuttling molecules instead of relying on electron transfer via direct contact to the mineral (von Canstein et al., 2008; Kotloski and Gralnick, 2013). Moreover, the microbial reduction of Fe oxides by *Shewanella* species was shown to be stimulated by model quinones (Newman and Kolter, 2000) and humic acids (Amstaetter et al., 2012; Shimizu et al., 2013), given that the concentration of dissolved organic carbon (OC) reached a threshold

of 5-10 mg C L⁻¹ (Jiang and Kappler, 2008) and the amount of Fe oxide was small enough for the induced aggregation to not outweigh the Fe reduction accelerating processes. In contrast, the reduction of Fe-OM coprecipitates by *Shewanella putrefaciens* containing different types of NOM seemed to depend on the aromaticity of the coprecipitated NOM and thus the amount of potentially usable electron-shuttling molecules rather than the aggregate size of the coprecipitates (Poggenburg et al., 2016).

Unlike *Shewanella* species, Geobacteraceae do not release endogenous electron-shuttling molecules or chelators (Nevin and Lovley, 2000) but rather seem to facilitate electron transfer to solid Fe minerals via direct contact or conducting nanowires (Malvankar et al., 2011; Boesen and Nielsen, 2013). Although *Geobacter* species have been shown to reduce dissolved extracellular quinone moieties (Scott et al., 1998) and humic acid (Lovley et al., 1996; Jiang and Kappler, 2008) in solutions free of Fe, *Geobacter bremensis* exhibited decelerated Fe reduction rates for Fe-NOM coprecipitates and adsorption complexes (Eusterhues et al., 2014), while *Geobacter metallireducens* showed smaller Fe reduction rates for Fe-NOM coprecipitates than for pure ferrihydrite (Poggenburg et al., 2016). Both studies thus suggest external electron shuttling to exert a minor influence on the reduction of Fe-NOM associations by *Geobacter* species.

Taking these different aspects into consideration, this study aims to elucidate the impact of both the composition and concentration of adsorbed and easily desorbable NOM on the microbial reduction of Fe oxides in terms of both *reduction-enhancing factors* (i.e., electron shuttling, complexation of Fe(II,III)) and *reduction-decelerating factors* (i.e., surface site coverage and/or pore blockage by OM, aggregation). Furthermore, the influence of these different NOM-derived factors was examined in relation to the influence of the bacteria species involved in the Fe reduction. To assess these relations, Fe-organic adsorption complexes with varying OC contents were synthesized using five different Fe oxides (ferrihydrite, lepidocrocite, goethite, hematite, magnetite) and NOM of different origin

(microbially-derived extracellular polymeric substances extracted from *Bacillus subtilis* and two types of plant-derived NOM extracted from the Oi horizon of a Cambisol and the Oa horizon of a Podzol). The initial Fe oxides and adsorption complexes were characterized by N₂ gas adsorption, FTIR (Fourier transform infrared spectroscopy), XRD (X-ray diffraction), XPS (X-ray photoelectron spectroscopy), zeta potential and desorption experiments. Microbial reduction experiments under anoxic conditions were conducted for 16 days using two different strains of dissimilatory Fe(III)-reducing bacteria (*Shewanella putrefaciens*, *Geobacter metallireducens*) favoring different cell-to-mineral electron transfer pathways. The mineral transformation was determined by XRD and FTIR analysis of the post-incubation phase.

2 MATERIAL AND METHODS

2.1 Preparation of Iron Oxides

Two-line ferrihydrite was synthesized by titrating a solution of 0.2 M FeCl₃ · 6H₂O to a pH of 7.0 using 1 M NaOH (Schwertmann and Cornell, 2000). The suspension was dialyzed against doubly deionized water (Spectra/Por 7, 1,000 MWCO) until the electric conductivity was <10 μS cm⁻¹. Lepidocrocite (γ-FeOOH) was synthesized analogous to Schwertmann and Cornell (2000) via aerobic oxidation by slowly adjusting a solution of 0.2 M FeCl₂ · 4H₂O to a pH of 6.8 under constant flow of synthetic air using 1 M NaOH. The suspension was washed with doubly deionized water to decrease the electric conductivity <10 μS cm⁻¹. Goethite (α-FeOOH) was synthesized by adding 10 M NaOH to 0.5 M FeCl₃ · 6H₂O to obtain a pH of 12 (modified according to Atkinson et al. (1967)). After aging at 328 K for 48 h, the suspension was also washed with doubly deionized water. Hematite (α-Fe₂O₃, Bayferrox 512 Z) and magnetite (Fe₃O₄, Bayferrox 360 Z) were provided by LANXESS Deutschland GmbH, Leverkusen. Both Fe oxides were washed with doubly deionized water three times. All minerals were frozen in liquid nitrogen at 77 K, freeze-dried and sieved to a size <200 μm.

2.2 Extraction of Extracellular Polymeric Substances and Natural Organic Matter

Extracellular polymeric substances (EPS) were extracted from a culture of *Bacillus subtilis* (ATCC 7003; BCCMTM/LMG Bacteria Collection) in LB-Lennox medium at early stationary growth phase, separated by centrifugation, precipitated with 277 K cold ethanol, purified by dialyzing against sterile water for 72 h and freeze-dried. Residual cells in the purified EPS were quantified with fluorescence microscopy (Zeiss Axiophat Fluorescence Microscope, Carl Zeiss AG, Jena, Germany) after embedding an EPS aliquot in Moviol-Mounting medium and staining it with SYBR-Green. The freeze-dried EPS contained approximately 7.85×10^6 cells mg^{-1} EPS.

Plant-derived NOM was extracted from the Oi horizon of a Eutric Cambisol under European beech and from the Oa horizon of a Haplic Podzol under Norway spruce. After equilibrating with doubly deionized water for 16 hours, the solutions were filtrated through $0.7\text{-}\mu\text{m}$ glass fiber filters (GF 92, Whatman GmbH, Dassel, Germany) and $0.45\text{-}\mu\text{m}$ cellulose nitrate membrane filters (G, Sartorius AG, Göttingen, Germany). Please refer to Appendix A.1 and Poggenburg et al. (2016) for a more detailed description of both extraction procedures.

2.3 Preparation of Adsorption Complexes

To prepare adsorption complexes with varying NOM loadings, 1-5 g of each Fe oxide were weighed into 1-L polyethylene bottles and suspended in 200 mL doubly deionized water. The suspension was adjusted to a pH of 4 using 0.1 M HCl, readjusted after 30 min, and once more readjusted after an equilibration time of 16 h. Prior to sorption, the EPS-, beech Oi- and spruce Oa-solutions were also titrated to a pH of 4.0 by adding 1 M HCl in order to achieve a maximum load of sorbed EPS and NOM. Both the freshly extracted beech Oi- and spruce Oa-derived dissolved OM solutions already displayed a pH of ~ 4 — a pH value regularly found

in temperate and tropical soils (Wagai and Mayer, 2007). The initial OC concentrations ranged from 50 to 500 mg C L⁻¹. Differences in the ionic strength of each solution were compensated by the addition of KCl, corresponding to a final ionic strength of 0.005 mol L⁻¹. After adding 500 mL of the NOM solution to each mineral suspension, the mixture was shaken manually, left undisturbed for 30 min before readjusting the pH, and equilibrated by shaking for 24 h in the dark at 298 K and 15 rpm in an end-over-end shaker. The suspension was then centrifuged for 1 h at 6,000 g. Before decanting, the pH of the suspension was measured. The pH of the post-sorption equilibrium solutions increased between 0.2 and 1.8 units. To remove non-sorbed components, the adsorption complexes were washed with doubly deionized water 2-3 times until the electric conductivity of the supernatant was <10 $\mu\text{S cm}^{-1}$ and the pH reached a value of 7. The adsorption complexes were then frozen in liquid nitrogen at 77 K, freeze-dried, and sieved to a size <200 μm . The OC and total N contents were quantified with a CNS analyzer (Vario EL III, Elementar GmbH, Hanau, Germany). The total Fe content was determined with inductively coupled plasma optical emission spectroscopy (ICP-OES, Varian 725-ES, Varian Inc., Palo Alto, CA, USA) after complete digestion in 6 M HCl. Iron concentrations were averaged over the values obtained at the wavelengths 259.940, 239.563, 238.204, and 234.350 nm.

Covering the span of tightly bound NOM at smaller C loadings to more loosely bound NOM at sorption maximum, the approximate OC loadings for ferrihydrite, lepidocrocite, and goethite were 5, 10, and 20 mg C g⁻¹ Fe oxide for all three OM types with an additional adsorption complex of 40 mg C g⁻¹ for beech Oi-derived NOM. For hematite and magnetite, OC loadings covered approximate C concentrations of 2, 4, and 8 mg C g⁻¹ for all three OM types with an additional adsorption complex of 15 mg C g⁻¹ for beech Oi-derived NOM. The largest OC loadings approximate the sorption capacity for each type of Fe oxide and OM, which was determined by fitting the Langmuir model to the sorption isotherm. The exact OC

and Fe contents are provided in Table B.1. For the purpose of easier readability, these will be referred to as small, medium and large C loading throughout the text.

2.4 Characterization of Organic Matter, Iron Oxides, and Adsorption Complexes

2.4.1 X-ray diffraction (XRD)

The pure Fe oxides were characterized by XRD (Siemens D500, Siemens AG/Bruker AXS GmbH, Karlsruhe, Germany) applying CuK α radiation and a 2Θ range from 2° to 80° 2Θ using a step size of 0.05° and a step time of 10 s. The XRD pattern of ferrihydrite revealed two characteristically broad peaks at 0.25 and 0.15 nm (Fig. B.1, Schwertmann et al., 2005). The other XRD diagrams confirmed the purity of lepidocrocite, goethite, hematite, and magnetite.

2.4.2 Fourier transform infrared (FTIR) spectroscopy

The freeze-dried NOM, pure Fe oxides, and adsorption complexes were characterized by FTIR applying the attenuated total reflectance (ATR) mode (TENSOR 27, Bruker, Bremen, Germany). From 600 to 4,000 cm^{-1} , a total of 400 scans were recorded per sample at a resolution of 4 cm^{-1} . After normalization, difference spectra were calculated for each adsorption complex in relation to its corresponding pure Fe oxide.

2.4.3 X-ray photoelectron spectroscopy (XPS)

XPS spectra of the freeze-dried unreacted NOM, pure Fe oxides, and adsorption complexes were recorded using a Kratos Axis Ultra DLD spectrometer (Kratos Analytical, Manchester, UK) applying monochromatic Al K α -radiation with an excitation energy of 1486.7 eV. Survey spectra were acquired using a pass energy of 160 eV and a step size of 1 eV. Furthermore, C1s high resolution spectra were acquired using a pass energy of 10 eV and a step size of 0.1 eV. Before normalizing and fitting the high resolution spectra to a Shirley-

type background, the charge-induced shift was accounted for by assigning the C1s peak to 285.0 eV using the Unifit 2010 software package (Hesse et al., 2003). In order to determine the relative amount of each C oxidation state, the C1s peak was divided into subpeaks suggested by Gerin et al. (2003), Omoike and Chorover (2004), and Leone et al. (2006): (i) aliphatic and aromatic carbon displaying bonds to carbon and hydrogen (C-C, C=C, C-H; at 285.0 ± 0.1 eV), (ii) carbon displaying a single bond to oxygen or nitrogen as in carbohydrates and amines (C-O, C-N; at 286.5 ± 0.2 eV), (iii) carbon displaying two bonds to oxygen as in aldehydes, ketones, and amides (C=O, O-C-O, O=C-N; at 288.0 ± 0.1 eV), (iv) carboxylic carbon displaying three bonds to oxygen (O-C=O; at 289.1 ± 0.2 eV).

2.4.4 Specific surface area and pore analysis

The specific surface area (SSA) of the pure Fe oxides and adsorption complexes was analyzed in duplicate with an Autosorb-1 surface area analyzer (Quantachrome Instruments, Boynton Beach, FL, USA). The samples were degassed under vacuum at 313 K for 24 h before adsorbing N₂ to the minerals at 77 K. The SSA was determined by applying the Brunauer-Emmett-Teller (BET) equation to the adsorption branch of the N₂ sorption isotherm in the relative pressure range of 0.05-0.3 P/P₀ (Brunauer et al., 1938). The total pore volume (TPV) was derived from the last data point of the adsorption branch at 0.995 P/P₀. The micropore volume (<2 nm) was determined via the Dubinin-Radushkevich (DR) method (Gregg and Sing, 1982) restricted to adsorption points <0.01 P/P₀. The mesopore volume (2-50 nm) was determined via the Barrett-Joyner-Halenda (BJH) method (Barrett et al., 1951). Furthermore, the mesopores were divided into small (2-10 nm) and large (10-50 nm) mesopores via linear interpolation.

2.4.5 Electrophoretic mobility and particle size

The electrophoretic mobility (EM) of the pure Fe oxides and adsorption complexes was measured in the microbial media used in the reduction experiments (section 2.5). The EM was determined with a ZetaPALS Zeta Potential Analyzer (Brookhaven Instruments Corp., Holtsville, NY, USA) and averaged over 10 runs consisting of 10 cycles each. The particle size (including mineral particles as well as colloid-sized aggregates) in suspension was determined via static light scattering using a 532-nm laser. The uniform sphere model was applied after measuring 8 runs lasting 60 s each. Calibration was carried out using a 90-nm NanosphereTM size standard (Duke Scientific Corp., Palo Alto, CA, USA).

2.4.6 Sorptive fractionation

The chemical fractionation of EPS and NOM during adsorption was examined by analyzing the initial and post-sorption solutions for various chemical properties: OC and total N were analyzed with a TOC/TN_b-Analyzer (liqui TOC II, Elementar Analysensysteme GmbH, Hanau, Germany); Na, K, Mg, Ca, Fe, Mn, Al, Si, P, and S were determined with ICP-OES, and NH₄⁺, NO₃⁻, SO₄²⁻, and PO₄³⁻ with ion chromatography (Dionex ICS-90 Ion Chromatography System, Dionex Corporation, Sunnyvale, CA, United States). Furthermore, the UV absorbance at 280 nm was measured with a UV-Visible Spectrophotometer (Cary 50 Scan, Varian Inc., Mulgrave, Victoria, Australia) using a 1-cm quartz cuvette. The specific UV absorbance (SUVA) at 280 nm of a solution normalized to its OC content was used as proxy for the preferential sorption of aromatic OM moieties (Chorover and Amistadi, 2001; Scheel et al., 2007).

2.4.7 Desorption experiments

Easily desorbable NOM and EPS of the adsorption complexes were determined in desorption experiments with the same solid-to-solution ratios and microbial nutrient solutions

as in the reduction experiments but without HEPES and lactate or acetate (see section 2.5). After adjustment to a pH of 7.0 with 1 M NaOH, the suspensions were equilibrated on an end-over-end shaker for 24 h at 298 K. The samples were centrifuged for 1 h at 6,000 g, before the supernatants were filtered <math><0.45 \mu\text{m}</math> and analyzed for OC with a TOC/TN_b-Analyzer. The P and S contents of the supernatants were determined with ICP-OES. Each treatment was examined in triplicates.

2.5 Microbial Reduction Experiments

Liquid cultures of both *Shewanella putrefaciens* (DSM-6067) and *Geobacter metallireducens* (DSM-7210) were obtained from the Leibniz Institute DSMZ-German Collection of Microorganisms and Cell Cultures. For *Shewanella putrefaciens*, 50 mL of altered medium DSM 948 (meat extract, 1.0 g L⁻¹; yeast extract, 2.0 g L⁻¹; casein peptone, 5.0 g L⁻¹; NaCl 5.0 g L⁻¹) were filled into a sterile 100-mL flask with an air-conductive aluminum cap, inoculated with 500 μL of the *Shewanella putrefaciens* culture and incubated on a horizontal shaker at 303 K and 120 rpm for 72 h. For the Fe reduction experiments, an inoculum was prepared by transferring 1 mL of the aerobic culture to 100 mL of initially oxic DSM 948 medium contained in a sterile flask. After incubation on a horizontal shaker at 303 K and 120 rpm for 16 h, the culture had reached the late exponential growth phase and therefore cells had switched to anaerobic metabolism (Lies et al., 2005). The inorganic nutrient solution for the Fe reduction experiments with *Shewanella putrefaciens* contained CaCl₂ · 2H₂O, 0.1 g L⁻¹; KCl, 0.1 g L⁻¹; NH₄Cl, 1.5 g L⁻¹; NaH₂PO₄ · H₂O, 0.6 g L⁻¹; NaCl, 0.1 g L⁻¹; MgCl₂ · 6H₂O, 0.1 g L⁻¹; MgSO₄ · 7H₂O, 0.1 g L⁻¹; MnCl₂ · 4H₂O, 0.005 g L⁻¹; NaMoO₄ · 2H₂O, 0.001 g L⁻¹ (Lovley and Phillips, 1988) and 5 mmol Na-lactate as electron donor.

For *Geobacter metallireducens*, 10 mL of the culture were transferred with a syringe to a sterile, crimp sealed 150-mL serum flask holding 100 mL anoxic *Geobacter* medium DSM

579 (Fe(III)-citrate, 13.70 g L⁻¹; NaHCO₃, 2.50 g L⁻¹; NH₄Cl, 1.50 g L⁻¹; NaH₂PO₄, 0.60 g L⁻¹; KCl, 0.10 g L⁻¹; Na-acetate, 2.50 g L⁻¹; trace element solution (DSMZ medium 141, Table A.1), 10.00 mL L⁻¹; vitamin solution (DSMZ medium 141, Table A.2), 10.00 mL L⁻¹; Na₂WO₄ · 2H₂O, 0.25 mg L⁻¹). The inoculated solution was incubated on a horizontal shaker at 303 K and 120 rpm for 5 days, until the Fe(III)-citrate had been visibly reduced. The procedure was repeated with fresh medium to obtain an inoculum for the Fe reduction experiments with *Geobacter metallireducens*. Fe(III)-citrate and NaHCO₃ were omitted from the medium described above for the Fe reduction experiments, while Na-acetate serving as electron donor was adjusted to a concentration of 5 mM.

HEPES was utilized to buffer the solutions in the reduction experiments to a pH of 7 in order to minimize media-induced precipitation of siderite and vivianite and phosphate-induced desorption of NOM and EPS from the adsorption complexes. HEPES was chosen as a buffer because it exhibited the smallest sorption affinity to Fe oxides of all tested common buffers (BisTris, HEPES, MOPS, PIPES, bicarbonate, phosphate; data not shown). Further pre-tests with lactate and acetate showed no detectable adsorption to the Fe oxides used in our experiments. Every solution was sterilized either in an autoclave or by filtration (Supor R-200, Pall Corporation, Ann Arbor, MI, USA) and turned anoxic by bubbling with N₂ for 1 h during the cooling down after autoclaving.

Approximately 30-40 mg of Fe oxide or adsorption complex equivalent to 10 mM Fe(III) were weighed into sterile 50-mL serum flasks and suspended in 30 mL of nutrient solution. To assess the ability of the bacteria to use NOM-derived organic moieties desorbed from the adsorption complexes as electron donors, the adsorption complexes containing the largest EPS- and spruce Oa-derived C loading were additionally suspended in nutrient solution devoid of lactate or acetate. A further experimental variant was established by adding 15 mL of an EPS-, beech Oi-, or spruce Oa-derived NOM solution to 15 mL of a two-fold concentrated nutrient solution resulting in a final concentration of 50 mg C L⁻¹ for each

respective NOM. Prior to the experiments, the NOM solutions had been sterilized by filtration. For each Fe oxide, the solutions were added to the largest C loading and thus saturated adsorption complex of each corresponding NOM.

The flasks were crimp sealed with butyl rubber stoppers, before flushing the suspensions with N₂ (containing 20 % CO₂ for set-ups with *Geobacter metallireducens*) for 30 min once more and leaving the suspension to equilibrate for 24 h. Experiments with *Shewanella putrefaciens* were inoculated with the pre-culture to obtain a final cell concentration of 2×10^5 cells mL⁻¹, while experiments with *Geobacter metallireducens* were inoculated with the pre-culture to obtain a final cell concentration of 1×10^7 cells mL⁻¹. Cell numbers were quantified as described in section 2.2. The different initial cell concentrations were derived from pre-tests revealing that *Geobacter* grew slower than *Shewanella* when each of the cultures were inoculated into medium containing the same nutrients and dissolved Fe(III). Moreover, *Geobacter* did not show any reduction of Fe oxides at initial cell concentrations below 1×10^7 cells mL⁻¹. Furthermore, our study aimed to keep up the comparability to previous studies by other authors, which usually used smaller initial cell densities for *Shewanella* (e.g., Amstatter et al., 2012) and larger initial cell densities for *Geobacter* (e.g. Wolf et al., 2009). At the same time, we aimed to keep the initial cell concentrations as small as possible to minimize the impact of dead cells as a C source (O'Loughlin et al., 2010). In an attempt to compromise between these issues, we decided to apply different initial cell concentrations.

The suspensions were incubated at 303 K in the dark for a period of 16 days, during which samples were taken after 1, 3, 6, 10, and 16 days. In order to determine Fe(II) and Fe_{total} contents, 1 mL of the suspension was taken with a syringe and instantly acidified with 20 μL of 5 M H₂SO₄. For quantification of dissolved Fe(II) and Fe(III), samples were filtered through 0.2-μm polyethersulfone membrane filters. For the quantification of total Fe(II) contents, samples were dissolved in 0.5 M H₂SO₄ for 1 h before applying the ferrozine assay

(Stookey, 1970) adapted according to Lovley and Phillips (1987). The concentration of total dissolved Fe was quantified by adding 2 % (v/v) of a 10 % (w/w) ascorbic acid solution (food grade, AppliChem GmbH, Darmstadt, Germany) before applying the ferrozine assay once more. The concentration of Fe(III) was determined from the difference between total Fe and Fe(II). Despite the attempt to quantify both dissolved and total Fe(II) concentrations, Fe(III) reduction rates are discussed for the latter only. The quantified amount of dissolved Fe(II) after filtration through $<0.2\text{-}\mu\text{m}$ filters may have been artificially enlarged due to very small colloids with surface adsorbed Fe(II) also passing the filter. Filtration through $<0.025\ \mu\text{m}$ pore sized filters, on the other hand, would have withheld Fe(II) re-adsorbed to mineral phases, as well as partly preventing dissolved Fe(II) complexed by NOM from passing the filter, thereby also causing artifacts. Control experiments conducted without bacteria exhibited no production of Fe(II). Pretests conducted with FeCl_3 had not revealed any Fe(III) reduction by desorbed NOM, lactate, or acetate during the acidic dissolution process of the samples.

The solid post-incubation phases were separated after 16 days by centrifugation for 1 h at 6,000 g, dried and stored under N_2 atmosphere. For FTIR analysis, the same parameters were applied as listed in section 2.4. For XRD analysis, microbial reduction was stopped by resuspending approximately 10 mg of the solid phase in 1 mL of anoxic $4\ \mu\text{M}$ HgCl_2 . After drying the suspension on glass slides of 25 mm, the samples were transferred to bottles flushed with N_2 , transported to the XRD chamber and analyzed in the absence of oxygen. (A more detailed description is provided in Appendix A.3)

To estimate the ability of *Shewanella putrefaciens* and *Geobacter metallireducens* to reduce NOM-derived organic moieties which might provide electron shuttling capacities, EPS-, beech Oi-, and spruce Oa-derived NOM solutions sterilized by filtration through $<0.1\text{-}\mu\text{m}$ filters were incubated applying the same nutrient solutions, cell concentrations, and experimental parameters as described above. Furthermore, each variant was also prepared without the addition of lactate or acetate acting as electron donor. After 1, 3, 6, 10, and 16

days, the headspace was sampled with a sterile syringe and analyzed for CO₂ via gas chromatography (Perkin Elmer, Waltham, MA, USA). After each sampling, the headspace was flushed with N₂ once more.

2.6 Statistics

The initial rates of the microbial reduction of the pure Fe oxides and the adsorption complexes were determined via linear regression of the linear part of the Fe(II) concentrations plotted versus time. To compare the means of the parameters characterizing the adsorption complexes and the microbial reduction rates of the different experimental treatments, two-sided t-tests for unpaired samples with a significance level of $\alpha = 0.05$ were carried out using the software GNU R 3.3.2 (R Development Core Team, 2016). In case of different variances, which were determined by a preceding F-test, Welch's variation of the t-test was performed instead. In order to test the influence of the different characteristics of the adsorption complexes on microbial Fe reduction, partial least-squares regression (PLSR) analysis was conducted using the package *ggm 2.3* (Marchetti et al., 2015) of the software GNU R 3.3.2 (R Development Core Team, 2016), as this method has been shown to be unaffected by the multicollinearity found among the parameters that were used to characterize the adsorption complexes (Carrascal et al., 2009).

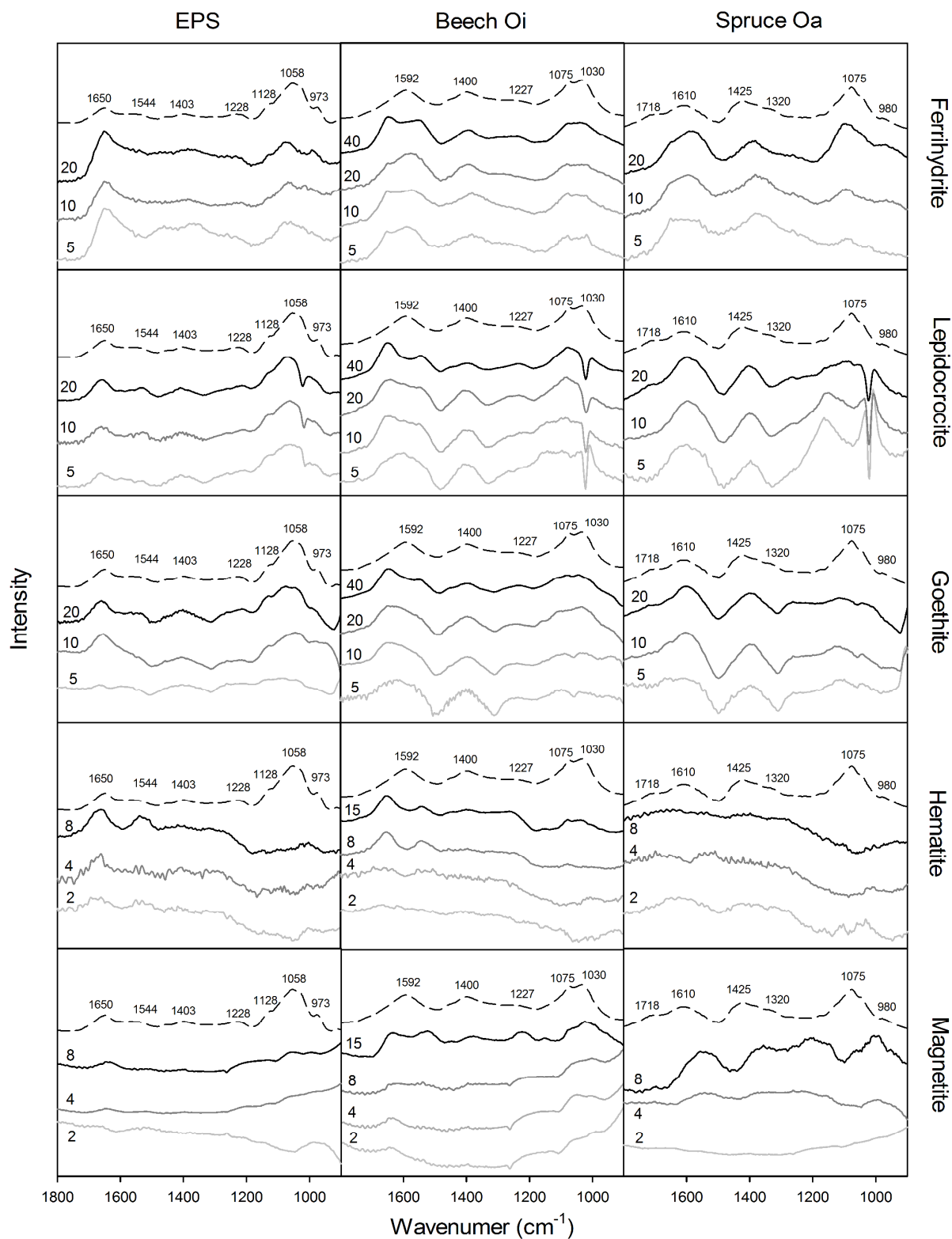


Fig. 1 ATR-FTIR spectra of freeze-dried NOM (dashed line) and adsorption complexes (solid lines). Numbers next to solid lines represent carbon loadings (mg C g⁻¹ Fe oxide) of adsorption complexes.

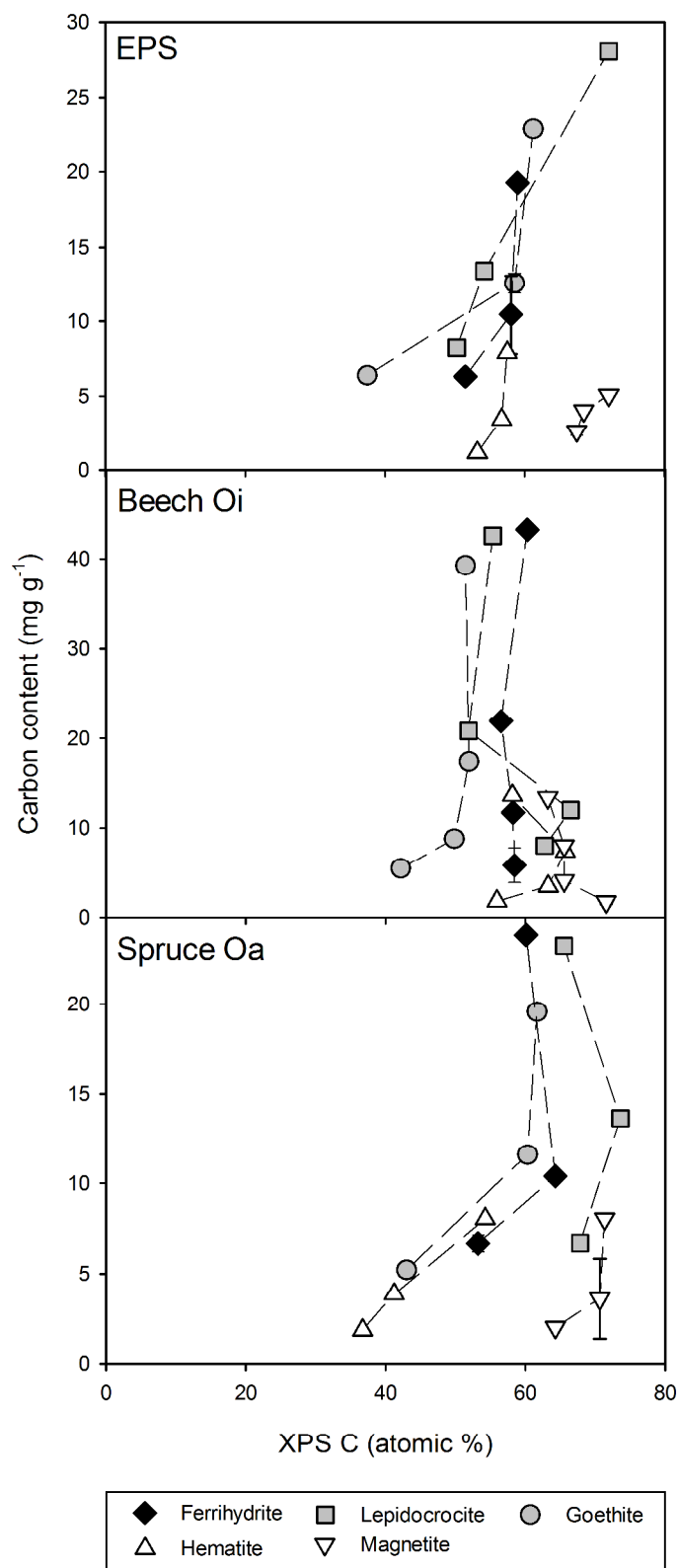


Fig. 2 XPS-derived carbon surface concentration in relation to the carbon content of the adsorption complexes. Error bars depict the standard deviation of at least triplicate measurements.

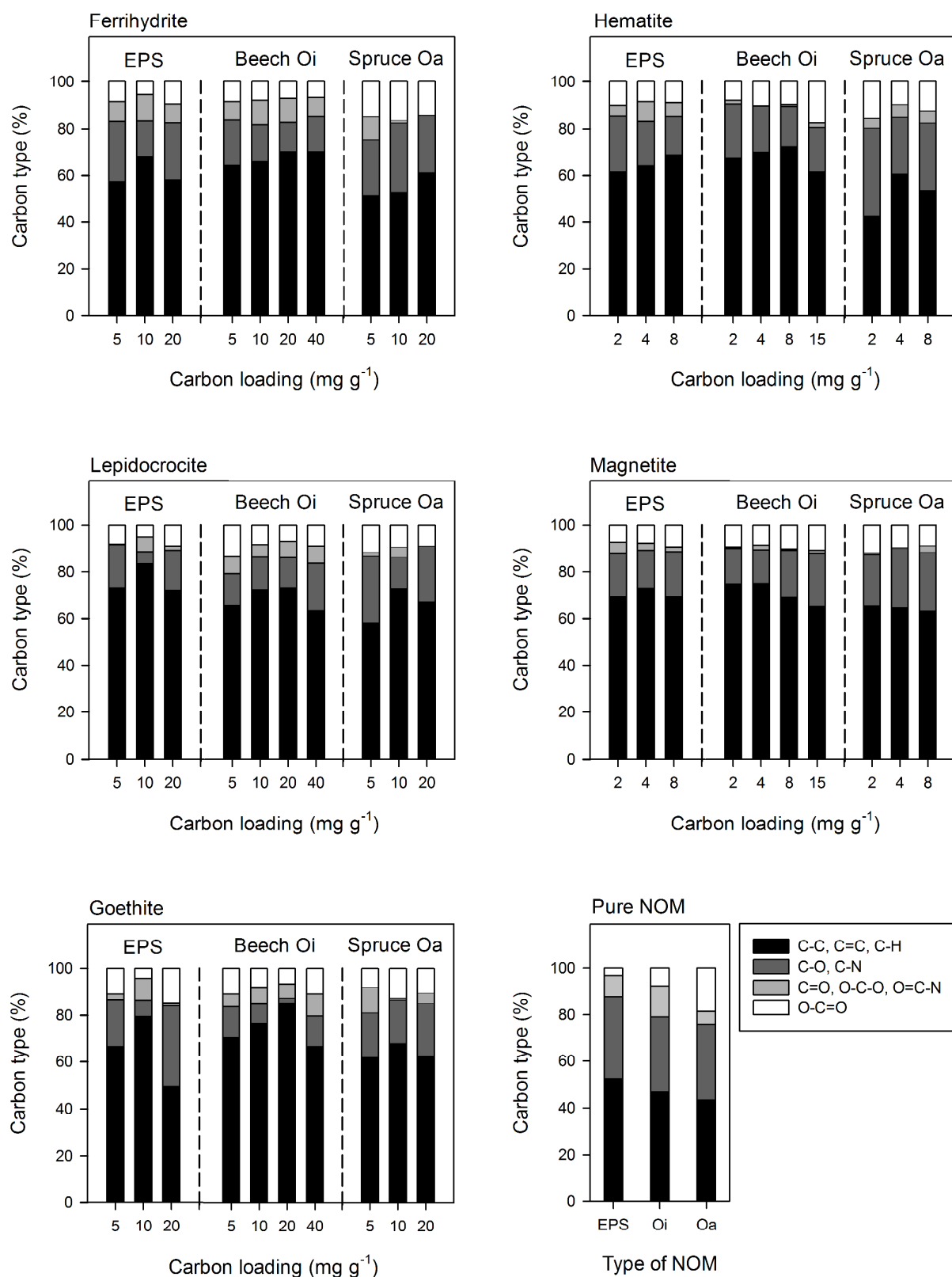


Fig. 3 Distribution of different carbon species of freeze-dried NOM and adsorption complexes derived from detail XPS C1s measurements.

3 RESULTS

3.1 Characterization of the NOM, Iron Oxides and Adsorption Complexes

3.1.1 Bulk carbon speciation of original and adsorbed NOM

In line with Omoike and Chorover (2006), the FTIR spectrum of pure EPS (Fig. 1) indicated proteins (amide I, 1650 cm^{-1} and amide II, 1544 cm^{-1}), complexed carboxylic groups (1403 cm^{-1}), polysaccharides (1128 cm^{-1} , 1058 cm^{-1}), and nucleic acids (1228 cm^{-1} , 1058 cm^{-1} , 973 cm^{-1}). Analogous to the adsorption of *Bacillus subtilis*-derived EPS to goethite (Omoike and Chorover, 2006; Liu et al., 2012), the FTIR difference spectra of the EPS adsorption complexes revealed preferential sorption of protein structures to the Fe oxides in comparison to polysaccharides. The extent of the sorptive fractionation decreased in the order ferrihydrite > lepidocrocite > goethite > hematite > magnetite, as evident from the intensity of the bands at 1650 cm^{-1} (amide I) and 1544 cm^{-1} (amide II) in relation to the bands indicating polysaccharides and nucleic acids. A partial contribution of nucleic acids to the band at 1058 cm^{-1} is supported by the complete depletion of P in the post-sorption solution (see also Table B.2). The SUVA at 280 nm of the EPS solution both before and after adsorption revealed very small contents of aromatic moieties rendering their adsorption and sorptive fractionation to be negligible (Table B.3). These results are consistent with the solid-state ^{13}C -NMR spectrum indicating less than 5 % of aromatic C for pure EPS, while O alkyl C was the most abundant functional group with 77 % (Poggenburg et al., 2016).

Similar to (Scheel et al., 2008), the FTIR spectra of pure beech Oi- and spruce Oa-derived NOM were governed by deprotonated carboxylic groups (1610 , 1592 and 1320 cm^{-1}), complexed carboxylic groups (1425 and 1400 cm^{-1}), and polysaccharides (1075 - 1030 cm^{-1} , Fig. 1) with minor contributions of protonated carboxylic groups (1720 cm^{-1}). The band at 1078 cm^{-1} may either reflect polysaccharides or phosphate (Omoike and Chorover, 2006). The latter is supported by the large phosphate content of the beech Oi- (51.4 mg L^{-1}) and spruce Oa-derived NOM solution (7.9 mg L^{-1}). In accordance with the results of the FTIR analysis,

solid-state ^{13}C -NMR spectroscopy showed that spruce Oa-derived NOM exhibited the largest relative amount of carboxylic and aryl C (15 % and 18 %, respectively), followed by beech Oi-derived NOM (7 and 11 %). Mirroring the trend seen for EPS, O-alkyl C made up the largest part of OC for both types of plant-derived NOM (42 % for spruce Oa, 61 % for beech Oi) (Poggenburg et al., 2016).

Adsorption complexes of beech Oi- and spruce Oa-derived NOM were generally depleted in polysaccharides in comparison to deprotonated carboxylic groups and complexed carboxylic groups as reported for ferrihydrite (Eusterhues et al., 2011; Chen et al., 2014), goethite (Kaiser and Guggenberger, 2007), and hematite (Kaiser and Guggenberger, 2003) before. The band intensity of complexed carboxylic groups decreased with increasing C loading and shifted towards smaller wavenumbers along with the band position of deprotonated carboxylic groups. The band representing protonated carboxylic groups (1720 cm^{-1}) disappeared at smaller C loadings but reappeared at larger C loadings. These observations indicate the abundance of carboxylate-Fe complexes formed via ligand exchange particularly at smaller C loadings (Kaiser and Guggenberger, 2007; Chen et al., 2014), whereas weaker outer-sphere complexes (Kaiser and Guggenberger, 2007; Eusterhues et al., 2011) formed at larger C loadings (Kaiser et al., 1997; Kaiser, 2003). For large C loadings of beech Oi adsorption complexes, the band at 1592 cm^{-1} shifted to 1547 cm^{-1} with an additional band appearing at 1648 cm^{-1} . While this may point towards outer-sphere carboxylate complexes (Eusterhues et al., 2011), the adsorption of amide components cannot entirely be excluded (Omoike and Chorover, 2006). Since phosphate was always completely adsorbed, parts of the polysaccharide band can also be attributed to adsorbed phosphorous compounds (Omoike and Chorover, 2006, see also Table B.2). In agreement with the larger content of aromatic compounds suggested by ^{13}C -NMR spectroscopy, the SUVA of spruce Oa-derived NOM ($0.055\text{ L mg C}^{-1}\text{ cm}^{-1}$) was larger than that of beech Oi-derived NOM ($0.018\text{ L mg C}^{-1}\text{ cm}^{-1}$). Upon adsorption to the Fe oxides, the SUVA of beech Oi- and spruce Oa-

derived NOM remaining in solution decreased by up to 87 % and 79 %, respectively (Table B.3). Although the uptake of aromatic moieties thus appeared more pronounced for beech Oi-derived NOM, the adsorption of spruce Oa-derived NOM resulted in comparatively larger absolute contents of aromatic compounds. However, this effect diminished along with growing C loadings as reported previously (Kaiser and Guggenberger, 2007; Chen et al., 2014). Sorptive fractionation of aromatic compounds was distinct and comparable for ferrihydrite, lepidocrocite and goethite at similar C loadings, whereas it was less pronounced for hematite and magnetite. (Please refer to Appendix B.1 for a more in depth discussion of the FTIR spectroscopy.)

3.1.2 Surface carbon contents and carbon speciation

The XPS-derived surface C content of the adsorption complexes ranged between 38 and 74 atomic % (Fig. 2) and was thus significantly larger than the C content of the bulk adsorption complexes. The surface C content of the EPS adsorption complexes increased along with the bulk C content for each Fe oxide, whereas the beech Oi and spruce Oa adsorption complexes did not show this straightforward relationship. For both plant-derived NOM types this can most likely be attributed to the formation of patches with organic multilayers upon adsorption to Fe oxides at larger surface loadings rather than sorbing in a spread-out conformation (Kaiser and Guggenberger, 2003) as discussed in section 3.1.3.

The XPS carbon detail spectra of all OM types revealed aliphatic and aromatic C displaying bonds to carbon and hydrogen (C-C, C=C, C-H) as the largest fraction followed by C displaying a single bond to oxygen or nitrogen as in carbohydrates and amines (C-O, C-N) (Fig. 3). The SUVA at 280 nm and the NMR-derived data (Poggenburg et al., 2016) showed very small contents of aromatic C in the EPS, implying a negligible contribution of aromatic C to the subpeak at 285 eV. Spruce Oa exhibited the largest fraction of carboxylic C, followed by beech Oi and EPS.

Irrespective of the OM source and type of mineral, adsorption to the Fe oxides left the aliphatic and aromatic C to be the largest fraction of surface C species (Fig. 3), supporting the larger affinity of aromatic compounds towards Fe oxides (Chorover and Amistadi, 2001; Kalbitz et al., 2005; Scheel et al., 2007). Analogously, the relative amount of carboxylic C increased during adsorption to all Fe oxides whereas the carbohydrate-derived C decreased significantly in comparison to the source NOM.

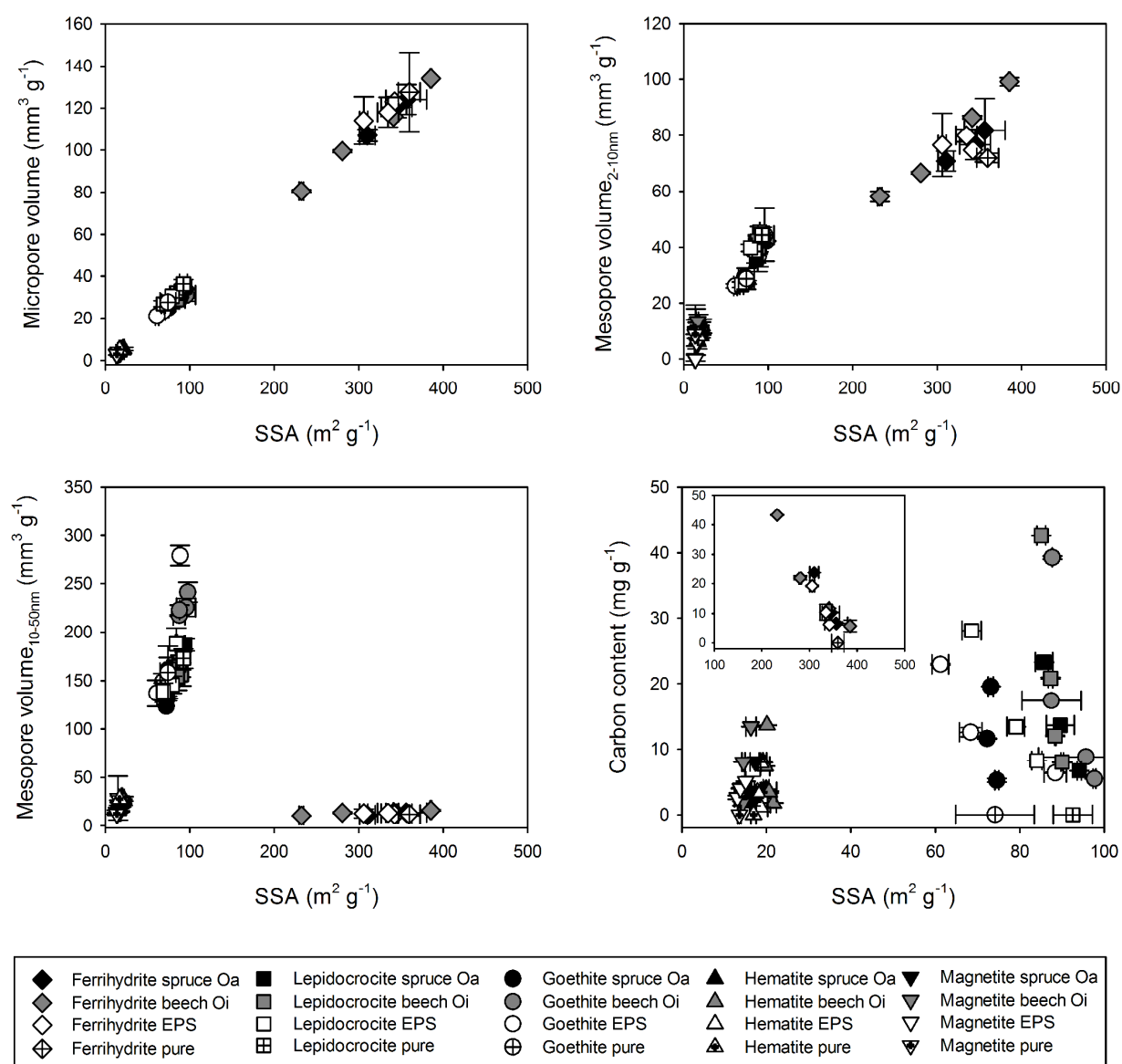


Fig. 4 Relationship between the BET-derived specific surface area (SSA) and the micropore volume, the small and large mesopore volume, and the carbon content of pure Fe oxides and adsorption complexes. Error bars depict the standard deviation of at least duplicate measurements.

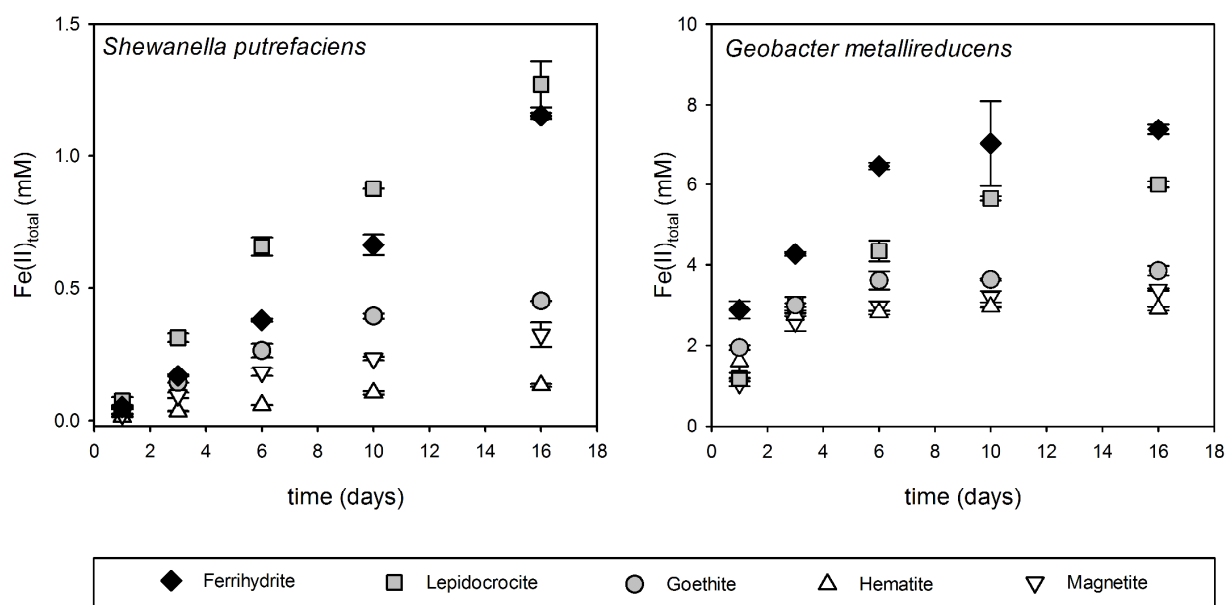


Fig. 5 Microbial reduction of the pure Fe oxides by *Shewanella putrefaciens* and *Geobacter metallireducens*. Fe(II)_{total} contents were determined after acidic digestion of the adsorption complexes. Error bars represent the standard deviation of triplicate experiments.

3.1.3 Surface area and porosity

The BET-derived SSA of the pure Fe oxides decreased in the order ferrihydrite > lepidocrocite > goethite > hematite > magnetite (359.7, 92.5, 74.1, 16.9, and 13.6 m² g⁻¹; Fig. 4).

Adsorption of EPS and NOM generally lead to a decrease of the SSA, although not in a uniformly constant manner. To some extent, the decrease in SSA could be attributed to the small N₂ sorption capacity of OM, which usually yields SSA values <1 m² g⁻¹ (Kaiser and Guggenberger, 2003). At similar C loadings, EPS caused a more pronounced decrease of the SSA of each respective Fe oxide than the beech Oi- and spruce Oa-derived NOM. Kaiser and Guggenberger (2003) attributed this irregular decrease of the SSA with increasing adsorption of NOM to (i) the sorption of organic molecules in an uncoiled spread-out conformation at smaller surface C loadings and thus a larger available surface area, (ii) the formation of organic multilayers via hydrophobic interactions and bridging by polyvalent cations at larger surface loadings, and (iii) the preferential sorption of organic molecules to small pores via

clogging. Both beech Oi- and spruce Oa-derived NOM contained Mg^{2+} (11 and 10 mg g C^{-1}) and Ca^{2+} (32 and 20 mg g C^{-1}), which decreased significantly in the post-sorption solution with increasing C loadings, whereas the amount of polyvalent cations in the pure EPS solution was already negligible. Both types of plant-derived NOM thus seem to build multilayer-like patches upon adsorption by formation of cation bridges instead of a continuous coating, thus causing less reduction of the SSA. Furthermore, the EPS adsorption complexes did not show a systematically larger decrease in micro- or mesopores, which could therefore not account for the more pronounced decrease of SSA for the EPS adsorption complexes.

Ferrihydrite exhibited the largest micropore volume of all Fe oxides, with 50 % of the total pore volume (TPV) located within micropores. Irrespective of the Fe oxide and type of OM, the micropore volume and the SSA showed the same linear relationship for all adsorption complexes (Fig. 4). Analogous to the micropores, the volume of the small mesopores was largest for the ferrihydrite-OM adsorption complexes. In comparison to the other adsorption complexes, however, the slope of the linear small mesopore-SSA correlation was significantly smaller. Conversely, the volume of large mesopores was negligible for the ferrihydrite-OM adsorption complexes, while lepidocrocite, goethite, hematite, and magnetite still exhibited a linear decrease of the large mesopore volume with decreasing SSA.

3.2 Microbial Reduction of the Iron Oxides, Adsorption Complexes and NOM

3.2.1 Microbial Fe reduction by *Shewanella putrefaciens*

Initial reduction rates of the pure Fe oxides by *Shewanella putrefaciens* ranged from 0.0073 mmol Fe(II) d^{-1} mmol Fe_{total}^{-1} to 0.0015 mmol Fe(II) d^{-1} mmol Fe_{total}^{-1} decreasing in the order ferrihydrite > lepidocrocite > goethite > hematite > magnetite (Fig. 5) thus reflecting the decreasing SSA of the minerals (Fig. 10).

For ferrihydrite, lepidocrocite and goethite, between 4 and 50 % of the initial Fe contents of the adsorption complexes had been reduced after 16 days (Fig. 6a). The reduction rates of adsorption complexes containing EPS hardly differed from the reduction rates of the pure minerals, irrespective of the EPS concentration (Fig. 6a). In contrast, the microbial reduction rates significantly increased for the adsorption complexes containing beech Oi- and spruce Oa-derived NOM. For both types of plant-derived NOM, the initial reduction rates increased linearly with the amount of C desorbed from each respective adsorption complex upon suspension in the microbial medium as described in section 2.4.7 (Fig. 9). The addition of dissolved EPS to the adsorption complexes containing the largest EPS loading did not influence the reduction rates. In contrast, adding dissolved beech Oi-derived NOM to the largest C loading of beech Oi adsorption complexes resulted in reduction rates significantly larger than the reduction rates for the pure Fe oxides but did not exceed the reduction rate of each respective adsorption complex. Additional dissolved spruce Oa-derived NOM, however, lead to significantly increased reduction rates in comparison to the largest spruce Oa-derived loadings without added NOM.

In the case of hematite and magnetite, the adsorption complexes with EPS, beech Oi, and spruce Oa did not show significantly different reduction rates compared to the pure Fe oxides with approximately 2 and 4 % of the Fe contents having been reduced after 16 days for hematite and magnetite, respectively (Fig. 6b). Unlike the addition of dissolved EPS to the largest EPS loading, however, both the introduction of additional beech Oi- and spruce Oa-derived NOM to the largest C loading resulted in significantly increased reduction rates in comparison to the other experimental variants.

Omitting lactate as additional electron donor caused reduction rates close to zero for all adsorption complexes containing EPS (Fig. 6a and b). For spruce Oa adsorption complexes, leaving out the additional electron donor resulted in reduction rates only slightly exceeding the rates without microorganisms. Overall, the PLSR analysis revealed that 32 % of the

variance of the initial reduction rates by *Shewanella putrefaciens* could be explained by the amount of desorbed OC (see also Table D.1).

3.2.2 Microbial Fe reduction by *Geobacter metallireducens*

The reduction rates by *Geobacter metallireducens* were overall larger than the reduction rates by *Shewanella putrefaciens* owing to the larger initial cell concentrations (see also section 4.1.5). Similar to the Fe reduction by *Shewanella putrefaciens*, reduction rates for the pure Fe oxides increased with increasing SSA for the *Geobacter metallireducens* incubations ranging from 0.105 mmol Fe(II) d⁻¹ mmol Fe_{total}⁻¹ (magnetite) to 0.289 mmol Fe(II) d⁻¹ mmol Fe_{total}⁻¹ (ferrihydrite) with up to 80 % of the initial Fe having been reduced after 16 days (Fig. 5, 10). Irrespective of OM source and C loading, the reduction rates were largest for pure ferrihydrite, lepidocrocite, and goethite, with the exception of the lepidocrocite-beech Oi adsorption complex containing the largest C loading with additional dissolved OM (Fig. 7a). The reduction rates for the largest C loading of the ferrihydrite, lepidocrocite, and goethite adsorption complexes with additional dissolved beech Oi- and spruce Oa-derived NOM were significantly larger than the corresponding pure adsorption complexes, even though these reduction rates were still smaller than the reduction rates of the pure Fe oxides. Thus, the adsorption of NOM in different variants usually resulted in decreased reduction rates in comparison to the pure Fe oxide. There was no correlation between reduction rates and SSA, whereas the reduction rates increased with decreasing particle size (Fig. 9).

For hematite and magnetite, the EPS- and beech Oi-derived adsorption complexes hardly showed different reduction rates among each other and in comparison to the pure Fe oxide (Fig. 7b). The reduction rates for adsorption complexes containing spruce Oa-derived NOM, however, were significantly smaller than the reduction rates for pure hematite and magnetite. The reduction rates for the largest C loading of the hematite and magnetite spruce Oa adsorption complexes significantly increased with additional dissolved NOM in comparison

to adsorption complexes without additional dissolved NOM but were still smaller than the reduction rates of the pure Fe oxides. According to the PLSR analysis, the particle size accounted for 21 % of the variance of the initial reduction rates by *Geobacter metallireducens* (see also Table D.1).

Omitting acetate as additional electron donor resulted in reduction rates close to zero for both the EPS and spruce Oa containing adsorption complexes of all Fe oxides (Fig. 7a and b). Potentially additional electron donating compounds in the EPS or NOM can therefore not account for increased reduction rates in any of the experimental variants.

3.2.3 Microbial reduction of EPS and NOM

Incubations of pure OM types in presence of an electron donor (lactate, acetate) caused significantly higher CO₂ emissions in comparison to the experiments without additional electron donor for the experiments with *Shewanella putrefaciens*. Control samples containing no bacteria showed no release of CO₂. The production of CO₂ during the incubation of the OM solutions for both *Shewanella putrefaciens* and *Geobacter metallireducens* increased in the order EPS < beech Oi < spruce Oa (Fig. 8) with the CO₂ production by *Shewanella putrefaciens* significantly exceeding the production by *Geobacter metallireducens*. Hence, donor-derived electrons could be transferred to all OM types, though at different extent.

STUDY II

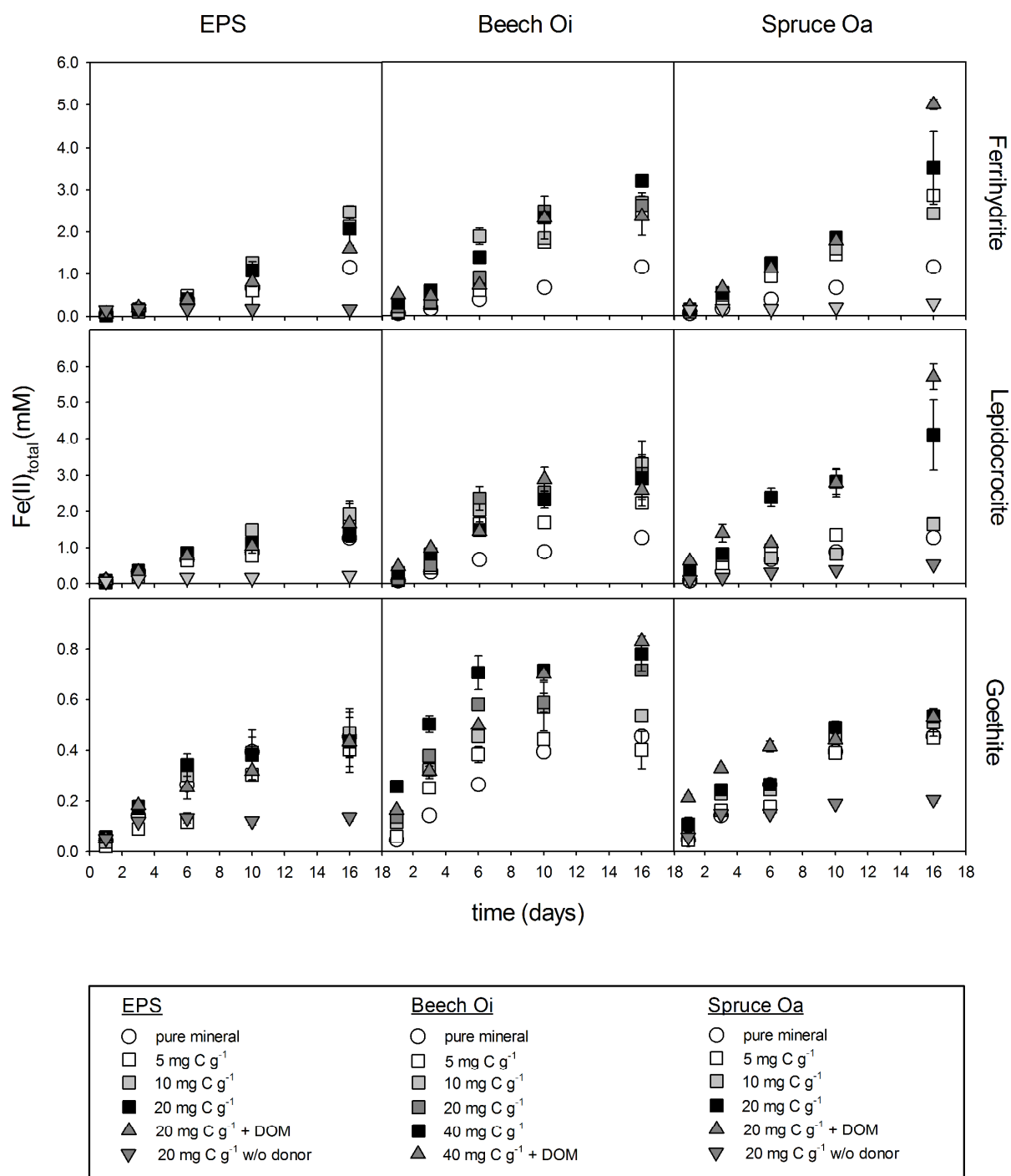


Fig. 6a Microbial reduction of the ferrhydrite, lepidocrocite, and goethite adsorption complexes by *Shewanella putrefaciens*. $Fe(II)_{total}$ contents were determined after acidic digestion of the adsorption complexes. Error bars represent the standard deviation of triplicate experiments.

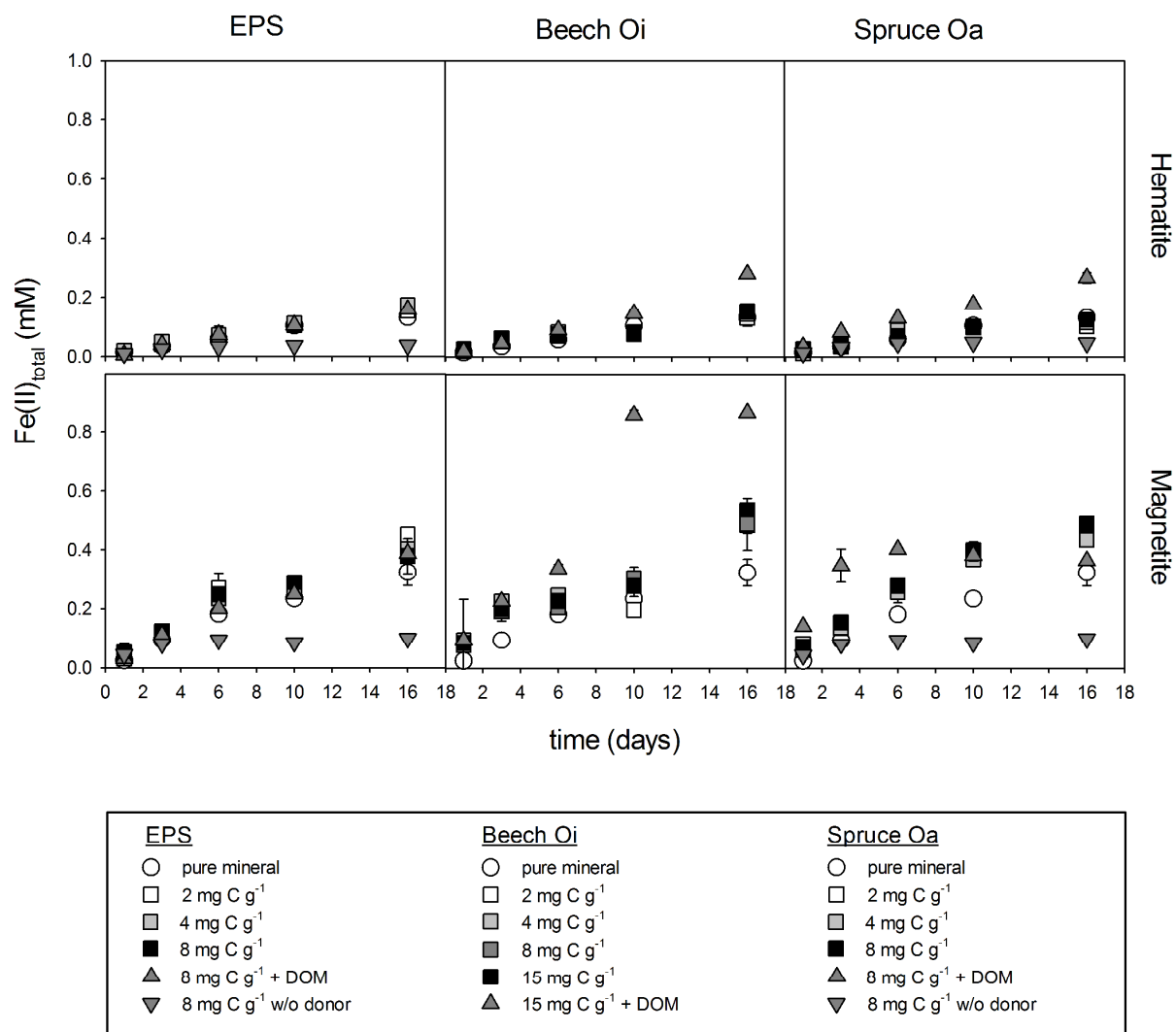


Fig. 6b Microbial reduction of the hematite and magnetite adsorption complexes by *Shewanella putrefaciens*. $\text{Fe(II)}_{\text{total}}$ contents were determined after acidic digestion of the adsorption complexes. Error bars represent the standard deviation of triplicate experiments.

STUDY II

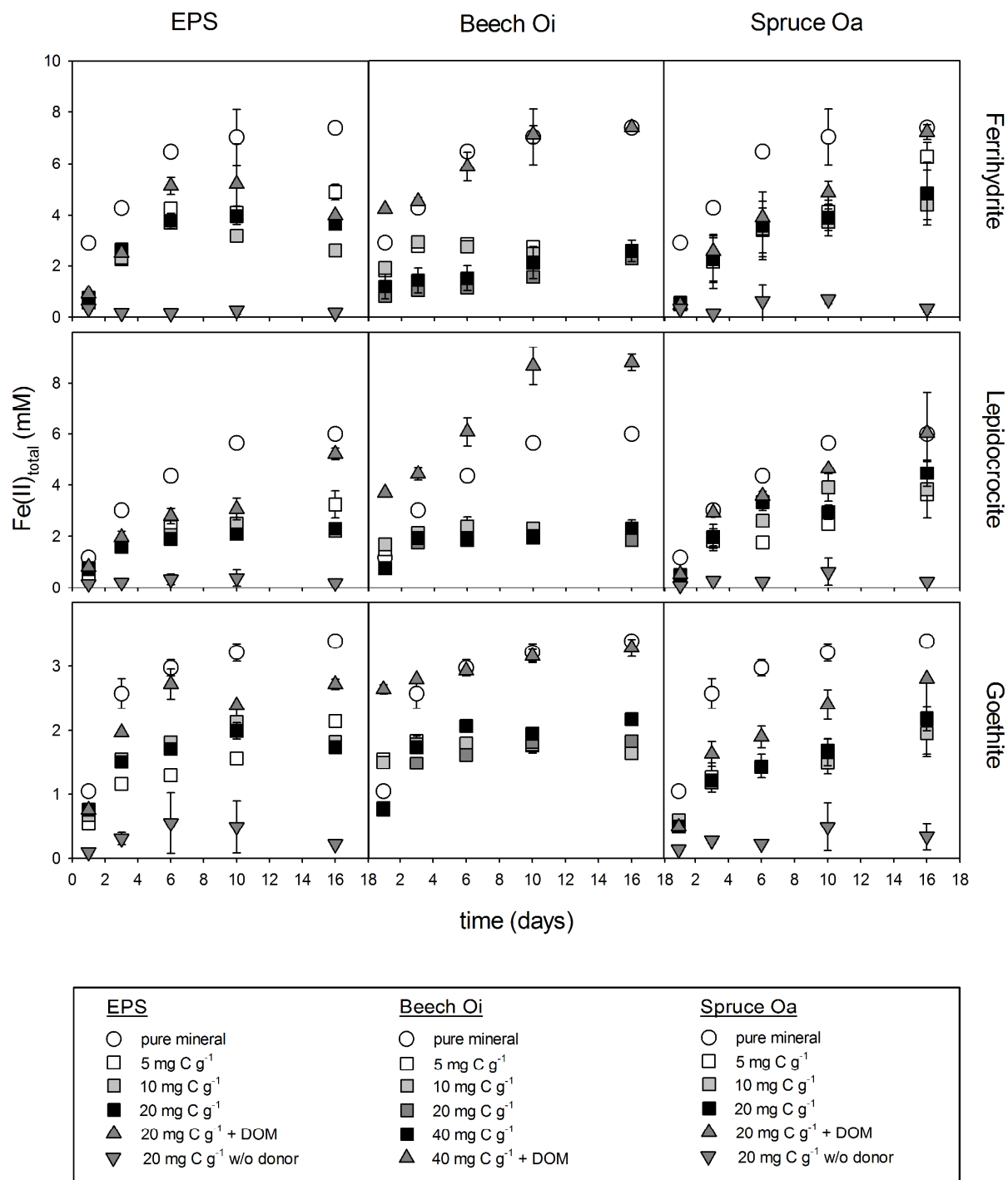


Fig. 7a Microbial reduction of the ferrhydrite, lepidocrocite, and goethite adsorption complexes by *Geobacter metallireducens*. Fe(II)_{total} contents were determined after acidic digestion of the adsorption complexes. Error bars represent the standard deviation of triplicate experiments.

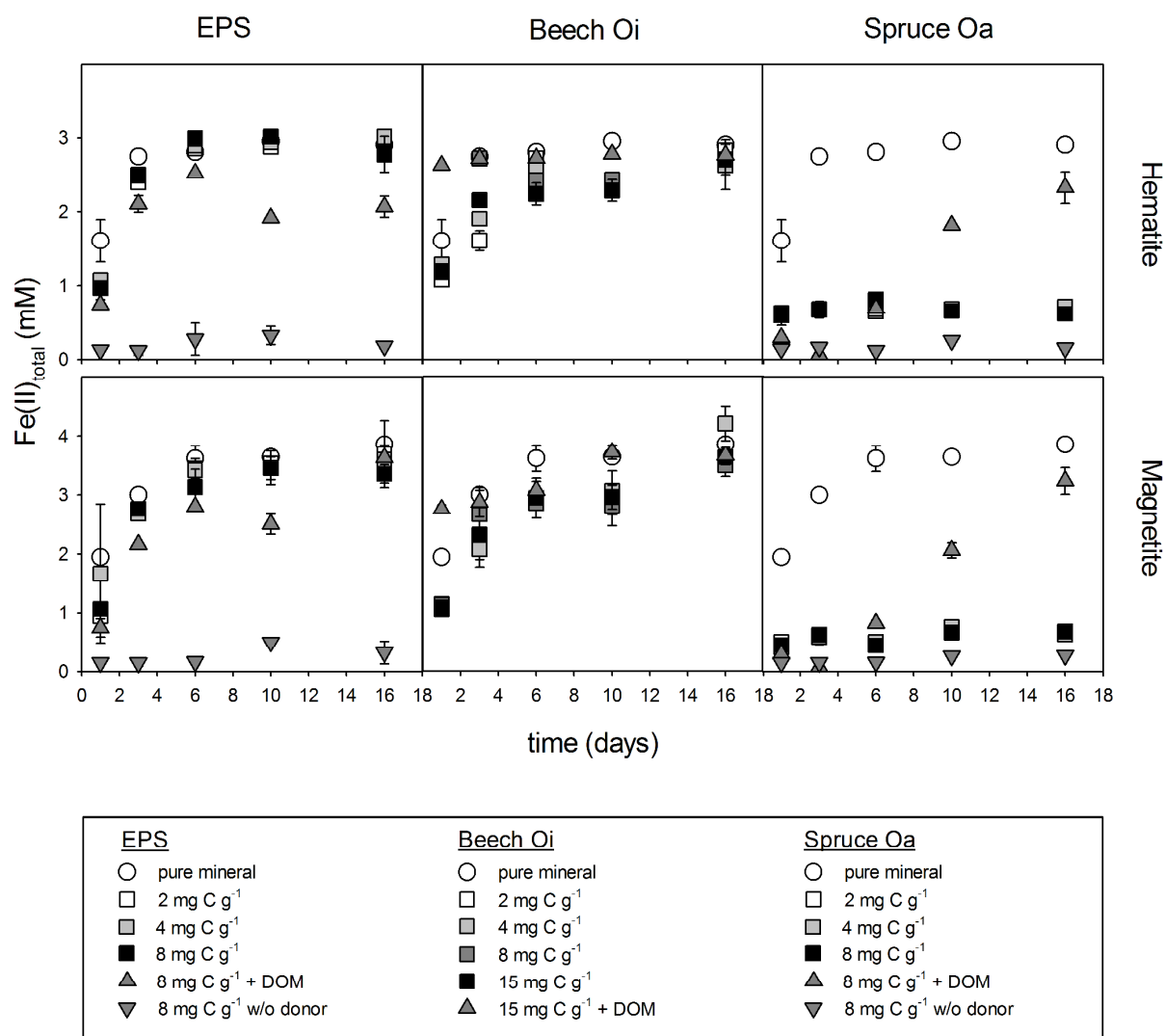


Fig. 7b Microbial reduction of the hematite and magnetite adsorption complexes by *Geobacter metallireducens*. $\text{Fe(II)}_{\text{total}}$ contents were determined after acidic digestion of the adsorption complexes. Error bars represent the standard deviation of triplicate experiments.

3.3 Transformation of Iron Oxides during Microbial Reduction

The XRD analysis of the solid post-incubation phase of the hematite and magnetite spruce Oa adsorption complexes after reduction by *Geobacter metallireducens* revealed additional peaks (Fig. C.1 and C.2) corresponding to d-spacings of 6.24, 5.94, and 3.54 Å. According to Bernal et al. (1959), these patterns can most likely be attributed to green rust phases containing SO_4^{2-} as dominant interlayer anion. Whenever additional dissolved EPS or NOM was added to the largest C loading of each adsorption complex, the XRD diagrams of the solid post incubation phase exhibited broad signals around 0.25 nm characteristically

displayed in XRD patterns of Fe-OM coprecipitates (Waychunas et al., 1993; Eusterhues et al., 2008), apart for the hematite and magnetite adsorption complexes reduced by *Shewanella putrefaciens*. The media-derived phosphate-induced formation of vivianite ($\text{Fe}_3(\text{PO}_4)_2 \cdot 8\text{H}_2\text{O}$) was found after the reduction of the pure Fe oxides by both *Shewanella putrefaciens* and *Geobacter metallireducens* with the exception of hematite and magnetite reduced by *Shewanella putrefaciens* (see also Appendix C). The FTIR spectra taken of the solid phases after microbial reduction were not significantly different from the spectra acquired of the initial adsorption complexes apart from a large additional peak between 920 and 1080 cm^{-1} (data not shown). This peak could be assigned to asymmetric ester O–P–O stretching modes from nucleic acids and P=O stretching of phosphodiester backbone of nucleic acid, which can be attributed to bacterial cell remnants associated with the adsorption complexes.

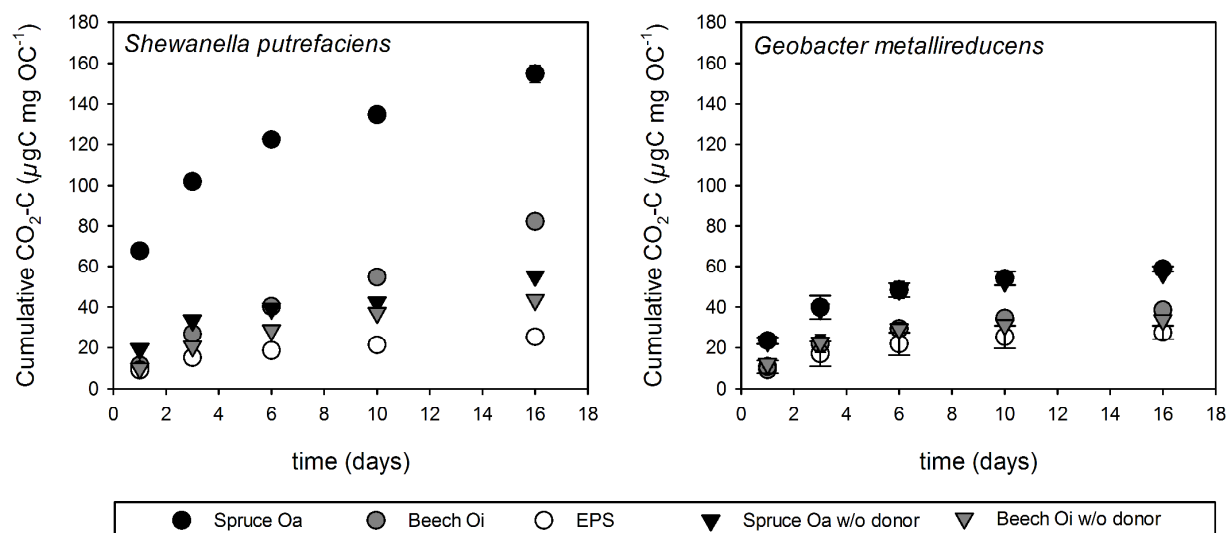


Fig. 8 Microbial reduction of dissolved EPS, Beech Oi, and Spruce Oa by *Shewanella putrefaciens* and *Geobacter metallireducens*. Error bars represent the standard deviation of triplicate experiments.

4 DISCUSSION

In the discussion below, the reduction of the adsorption complexes by both *Shewanella putrefaciens* and *Geobacter metallireducens* will be discussed in relation to the significance of each of the following NOM-derived factors: (i) electron shuttling, (ii) complexation of Fe(III) and Fe(II) by desorbed NOM, (iii) specific surface area and surface coverage, and (iv) surface charge, particle size and aggregation.

4.1 Microbial Reduction Kinetics

4.1.1 Impact of electron shuttling

The initial reduction rates of the ferrihydrite, lepidocrocite, and goethite adsorption complexes by *Shewanella putrefaciens* increased linearly with the amount of desorbed OC for both beech Oi and spruce Oa-derived NOM (Fig. 9). In addition, PLSR analysis attributed 32 % of the variance of the initial reduction rates by *Shewanella putrefaciens* to the amount of desorbed OC. These findings were generally in accordance with previous studies linking enhanced reduction rates of Fe-organic associations by *Shewanella putrefaciens* to electron-shuttling molecules provided by humic acid-type compounds (O'Loughlin 2008; Amstatter et al., 2012; Shimizu et al., 2013). These experiments usually required a threshold concentration of 5-10 mg C L⁻¹ to detect increased reduction rates mediated by electron shuttling (Jiang and Kappler, 2008; O'Loughlin et al., 2010; Piepenbrock et al., 2011; Amstatter et al., 2012; Shimizu et al., 2013), whereas we found enhanced initial reduction rates in comparison to the pure Fe oxide at concentrations of desorbed OC exceeding 2 mg C L⁻¹ for spruce Oa-derived NOM and 3 mg C L⁻¹ for beech Oi-derived NOM, respectively. These results illustrate the problem of defining threshold concentrations independent from the composition of electron-shuttling compounds and the range of parameters usually varying between different studies. The bigger threshold concentrations of electron-shuttling molecules in former studies may thus be attributed to several factors: (i) Larger concentrations of phosphate possibly

constraining microbial Fe reduction due to its strong sorption affinity and surface site blockage (Borch et al., 2007; O'Loughlin et al., 2010), (ii) increased Fe concentrations most likely decreasing reduction rates due to enhanced particle aggregation (Amstaetter et al., 2012), (iii) different initial cell numbers, (iv) larger amounts of electron donors, or (v) purified humic acids initiating passivation of surface reduction sites and particle aggregation to a greater degree than the conditions applied in our study.

The initial reduction rates of EPS adsorption complexes by *Shewanella putrefaciens* increased only slightly with the amount of desorbed OC for ferrihydrite, lepidocrocite, and goethite. Although the amount of aromatic-derived compounds of the EPS in our experiments was very small (Poggenburg et al., 2016), Kang and Zhu (2013) found quinoid-like structures suggested to act as electron-shuttling molecules in EPS, which might explain the minor increase of the reduction rates of EPS adsorption complexes in comparison to the pure Fe oxides. Since the pre-culture of *Shewanella putrefaciens* had been grown aerobically, there were no microorganism-bound electron-shuttling molecules present at the onset of the experiments, which is why all electron shuttling found for the initial reduction rates has to be attributed to dissolved NOM.

Despite its larger SUVA and NMR-derived aromaticity, larger electron acceptor capacity (Poggenburg et al., 2016), and larger concentration of compounds prone to be reduced by *Shewanella putrefaciens* (Fig. 8), the spruce Oa adsorption complexes did not show significantly greater reduction rates in comparison to the beech Oi adsorption complexes at similar C loadings. As the beech Oi adsorption complexes showed neither significantly smaller particle sizes nor larger SSAs compared to the spruce Oa adsorption complexes, the similar reduction rates can most likely be attributed to the larger media-induced desorption of beech Oi-derived NOM in comparison to spruce Oa-derived NOM. Increased desorption, in turn, points towards more loosely bound NOM moieties, as the original dissolved beech Oi-

derived NOM contained greater amounts of phosphate competing for high-affinity binding sites with other organic moieties.

The lack of difference of reduction rates by *Shewanella putrefaciens* between the hematite and magnetite adsorption complexes can most likely be explained by the small amounts of desorbed C, which ranged from 0.7 to 2.2 mg C g⁻¹ (Table B.4) and thus lay in the same range of desorbed NOM as observed for the ferrihydrite, lepidocrocite and goethite adsorption complexes that did not show significantly different initial reduction rates compared to the pure Fe oxides, either. Despite surface saturation for the largest C loading, hematite and magnetite, the two Fe oxides with the smallest SSAs, did thus not provide a sufficiently large amount of desorbable OC to initiate a noticeable increase in reduction rate mediated by electron shuttling. Adding additional dissolved OM to the largest C loading of each respective type of NOM to the different hematite and magnetite adsorption complexes resulted in considerably increased initial reduction rates for the beech Oi and spruce Oa adsorption complexes, which is in line with the studies observing a required threshold concentration as mentioned above. Due to their highly crystalline nature, thermodynamic constraints might not only account for the overall smaller reduction rates for hematite and magnetite (Kappler and Straub, 2005) but also for their reluctant response towards stimulation via external electron-shuttling compounds. Since the threshold concentration for increased microbial Fe reduction was found for all Fe oxides, regardless of their crystallinity, however, thermodynamic constraints do not seem to exert a major influence on the extent of Fe reduction controlled by NOM-derived electron shuttling.

In spite of several studies reporting *Geobacter* species to be able to reduce extracellular quinone moieties (Scott et al., 1998) and humic acid (Lovley et al., 1996; Jiang and Kappler, 2008) when no Fe was present in solution, the addition of NOM resulted in decreased microbial reduction in comparison to each respective pure Fe oxide for nearly all our experimental variants (Fig. 7a and b). These findings are in line with *Geobacter bremensis*

exhibiting decreased Fe reduction rates for ferrihydrite adsorption complexes and Fe-OM coprecipitates in comparison to pure ferrihydrite (Eusterhues et al., 2014) and are not indicative of electron shuttling playing a major role for microbial Fe reduction by *Geobacter metallireducens* in our experimental set-up. The discrepancy between these different studies might either be attributed to (i) the missing influence of surface coverage and aggregation (see section 4.1.3 and 4.1.4) in studies with pure dissolved organic compounds, (ii) potential electron-shuttling compounds not lying in the required range of redox potential (Wolf et al., 2009), or (iii) electron-shuttling moieties in the NOM used in this study not being present in a concentration large enough to stimulate Fe reduction in comparison to the humic acids used in previous studies. The last consideration is supported by several fulvic and humic acids exhibiting electron acceptor capacities between 800 and 2,000 $\mu\text{mol}_e\text{-g}^{-1}$ (Aeschbacher et al., 2010), whereas the spruce Oa-derived NOM, the beech Oi-derived NOM and the EPS exhibited electron acceptor capacities of only 600, 210 and 30 $\mu\text{mol}_e\text{-g}^{-1}$, respectively (Poggenburg et al., 2016).

To assess the ability of both *Shewanella putrefaciens* and *Geobacter metallireducens* to reduce NOM-derived organic moieties which might act as electron-shuttling compounds, all types of NOM were incubated with each respective microorganism while monitoring the production of CO_2 (Fig. 8). While this method is not suitable for quantifying the exact electron shuttling capacity for each respective NOM, it still displayed the different capabilities of both types of microorganisms to transfer electrons to the different types of NOM used in our experiments. Even though the production of CO_2 during the incubation of dissolved OM was generally significantly smaller for *Geobacter metallireducens* in comparison to *Shewanella putrefaciens*, the reduction of spruce Oa-derived NOM by *Geobacter metallireducens* was still noticeably larger than the reduction of beech Oi-derived NOM and EPS (Fig. 8). If electron shuttling had been the only factor responsible for the increased reduction rates by *Geobacter metallireducens* for the largest C loading in presence

of an additional dissolved OM concentration of 50 mg C L⁻¹ in comparison to the largest C loading without additional dissolved OM, the increase in reduction rates should have been more pronounced for spruce Oa than for beech Oi. Instead, the addition of 50 mg C L⁻¹ dissolved beech Oi-derived NOM to the largest C loading of beech Oi adsorption complexes resulted in significantly greater reduction rates than for the corresponding spruce Oa counterparts. Unlike for the spruce Oa complexes, however, the addition of dissolved beech Oi NOM caused a further decrease of the particle size of the adsorption complexes, which might be a more suitable explanation for the increased reduction rates as discussed in section 4.1.4.

Overall, a considerably larger concentration of electron-shuttling compounds in plant-derived water-extractable NOM seemed to be required to noticeably stimulate Fe reduction by *Geobacter metallireducens* than by *Shewanella putrefaciens*.

4.1.2 Impact of complexation of Fe(III) and Fe(II) by desorbed organic matter

The adsorption complexes contained significant quantities of weakly bound OM being detached during the Fe reduction experiments. Since rising amounts of desorbed beech Oi- and spruce Oa-derived NOM paralleled the increasing initial reduction rates by *Shewanella putrefaciens* for the ferrihydrite, lepidocrocite, and goethite adsorption complexes (Fig. 9), a reduction-accelerating effect via complexation of Fe(III) or Fe(II) by OM moieties has to be considered as well. Natural OM has been reported to provide chelating agents facilitating the solubilization of Fe(III) bound in Fe oxides (Nevin and Lovley, 2002b; Jones et al., 2009), while the complexation of already reduced Fe(II) might accelerate microbial reduction due to the advanced thermodynamic driving force (Roden and Urrutia, 1999; Royer et al., 2002a, 2002b). The concentration of dissolved Fe(II) and Fe(III) after equilibration of the adsorption complexes with each respective microbial medium was below detection limit in all our experimental variants. Furthermore, no Fe(III) was detected in the 0.2- μ m (ferrihydrite 0.025-

μm) filtrates after 16 days of the experiment, suggesting that the release of Fe(III) via chelating by EPS or NOM was negligible during the microbial reduction of the adsorption complexes.

The capacity of NOM to complex Fe can be estimated from its acidity (Royer et al., 2002b). According to Ritchie and Michael Perdue (2003) and the International Humic Substance Society IHSS, the largest acidity determined for several tested fulvic acids, humic acids and aquatic NOM was $12 \text{ mmol}_c \text{ g C}^{-1}$ at pH 7. Since one mol of acidity can be assumed to bind 0.5 mol of Fe(II) (Royer et al., 2002b), the corresponding Fe(II) complexation capacity would equal $6 \text{ mmol Fe(II) g C}^{-1}$. Taking into account the amount of OC which is desorbed from the adsorption complexes (Table B.4) with regard to the concentration of Fe(II) produced within 24 hours of microbial reduction, the fraction of reduced Fe(II) that might be complexed by dissolved OM never exceeded 10 % for the *Shewanella putrefaciens* incubations with even smaller fractions for *Geobacter metallireducens*. Given that these calculations provide an upper limit of average complexation capacity without considering sorptive fractionation, which favors the preferential binding of acidic carboxyl groups to Fe oxides (Kalbitz et al., 2003; Kalbitz et al., 2005), the amount of Fe(II) complexed by dissolved OM was most likely even smaller. While we cannot exclude that microbial reduction was influenced by the complexation of Fe(II) to some extent, it did not seem to exert a noticeable influence on Fe reduction of the adsorption complexes in our experiments, supporting the lack of impact of Fe(II) complexation by humic acids on ferrihydrite reduction observed by Amstaetter et al. (2012).

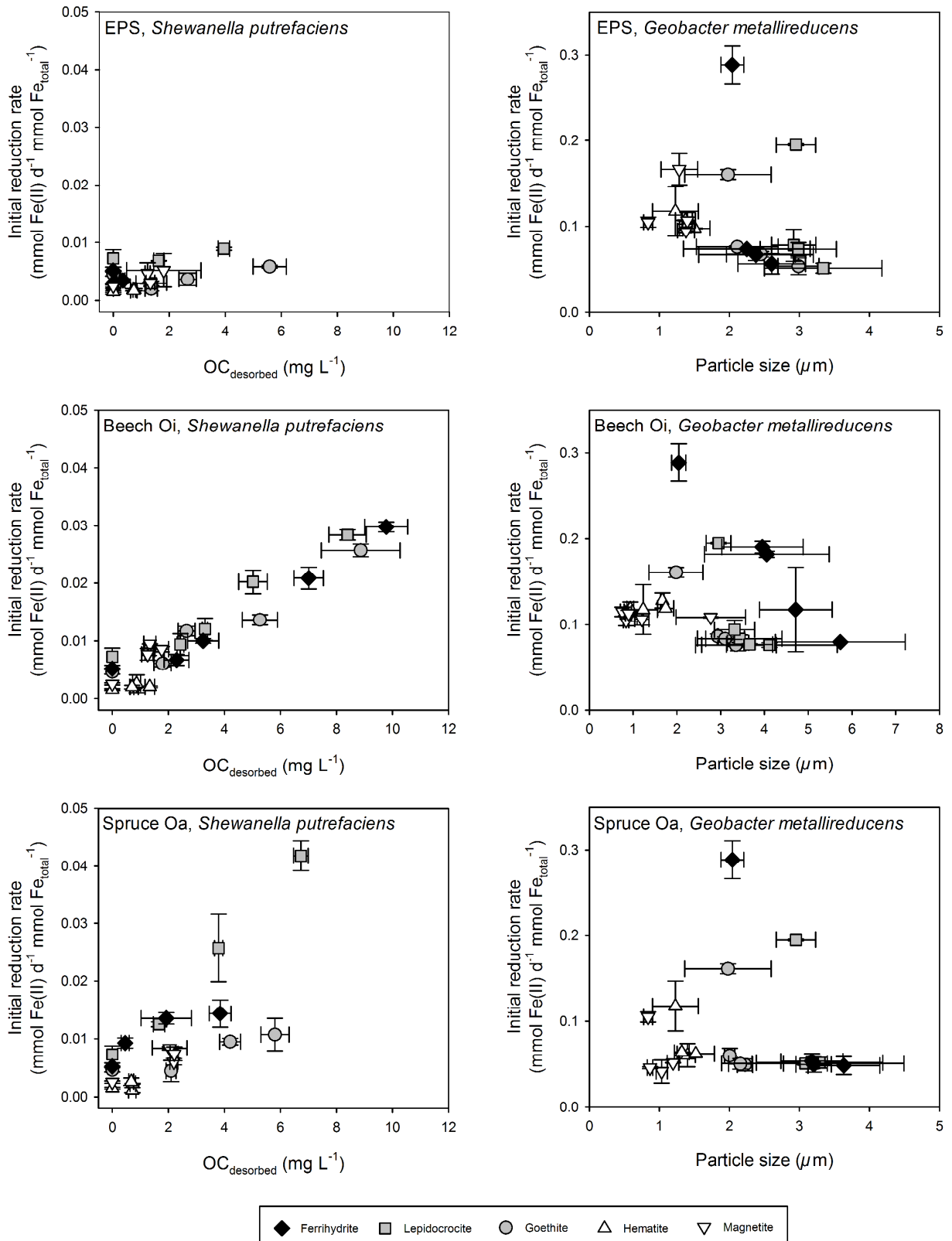


Fig. 9 Relationship between the initial microbial reduction rates of the adsorption complexes and the desorbed organic carbon (OC) of NOM and EPS for *Shewanella putrefaciens* and the relationship between the initial microbial reduction rates and the initial particle size for *Geobacter metallireducens*. Error bars represent the standard deviation of triplicate experiments or measurements.

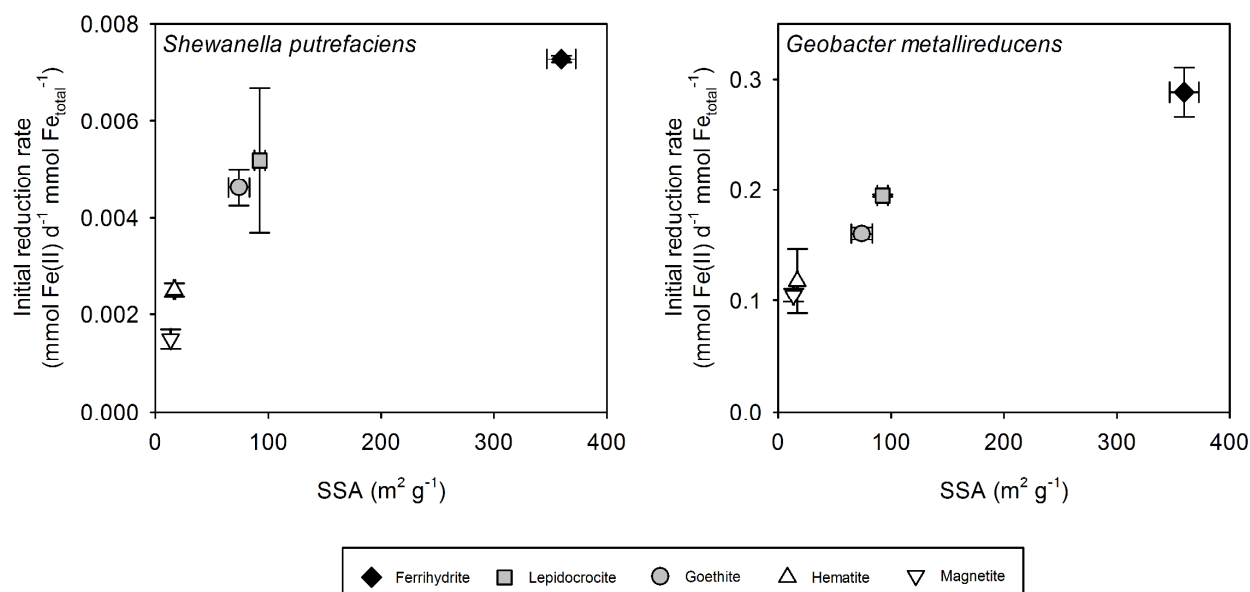


Fig. 10 Relationship between the initial microbial reduction rates of the adsorption complexes and the BET-derived specific surface area (SSA) for *Shewanella putrefaciens* and *Geobacter metallireducens*. Error bars represent the standard deviation of triplicate experiments or measurements.

4.1.3 Impact of specific surface area and surface coverage

Even though the initial reduction rates by both *Shewanella putrefaciens* and *Geobacter metallireducens* increased with rising SSA of the pure minerals, we did not find the same linear correlation between those two parameters as Roden (2003), who suggested that microbial reduction rates depend on the SSA of Fe oxides rather than on the underlying crystal order. However, Larsen and Postma (2001) reported the straightforward relation between SSA and abiotic reduction rates to be applicable only to Fe oxides with a similar crystal structure, while Bonneville et al. (2009) found the reduction of different Fe oxides by *Shewanella putrefaciens* to strongly depend on the mineral solubility and thus the thermodynamic stability. Since the Fe oxides in our study were similar to the ones used by Bonneville et al. (2009), a similar relation seems very likely. On the other hand, the SSA of Fe oxides is supposed to exert a larger influence on Fe reduction when particles of Fe oxides

directly adsorb to the cells of *Shewanella* (Bonneville et al., 2006). The nanoparticles used in the cited study, however, displayed particle sizes <10 nm, whereas the particle sizes of the Fe oxides or adsorption complexes in our study were above 1 μm (Fig. 9) and are thus expected to behave differently.

However, the relationship between SSA and Fe reduction rates was no longer valid for the *Shewanella putrefaciens* incubations when NOM was introduced into our experiments. On the contrary, reduction rates increased with increasing surface C coverage and thus decreasing SSAs, suggesting other parameters to control the Fe reduction of the adsorption complexes.

As nearly all *Geobacter* incubations exhibited decreased reduction rates for the adsorption complexes in comparison to the pure Fe oxides, the reduction could have been impaired by surface passivation due to adsorbed EPS or NOM. However, if the accessible SSA had been the crucial factor, reduction rates should have decreased with increasing C loadings of the adsorption complexes — but no such relationship was found. The SSA thus does not seem to be a suitable parameter to predict Fe reduction rates of adsorption complexes. Several reasons may account for this finding: First of all, the BET-derived SSA includes micro- and mesopores (<50 nm), which are not necessarily accessible for electron transfer via direct contact of the cell membrane to the mineral. As dissolved OM at lower concentrations preferentially sorbs to Fe oxides via clogging of small pores (Kaiser and Guggenberger, 2003; see also section 3.1.3), a large portion of the SSA, which is subjected to passivation via OM sorption, would not have been accessible for microbial reduction in the first place. This is corroborated by the initial Fe reduction rates normalized to the SSA, which increased in the order ferrihydrite < lepidocrocite < goethite < hematite < magnetite for both *Shewanella putrefaciens* ($0.020 < 0.056 < 0.062 < 0.110 < 0.148 \mu\text{mol Fe(II) d}^{-1} \text{mmol Fe}_{\text{total}}^{-1} \text{m}^{-3}$) and *Geobacter metallireducens* ($0.802 < 2.105 < 2.167 < 6.940 < 7.705 \mu\text{mol Fe(II) d}^{-1} \text{mmol Fe}_{\text{total}}^{-1} \text{m}^{-3}$). The initial Fe reduction rates normalized to the SSA thus decreased along with increasing micro- and mesopore volumes. Second, at smaller C loadings, patches of

negatively charged adsorbed OM and areas of positively charged uncovered mineral surface attract each other, thus enhancing particle aggregation. At larger C loadings aggregation is impaired by charge repulsion between the more abundant areas with negatively charged OM (Kaiser and Guggenberger, 2003; Illés and Tombácz, 2006). Adsorption complexes with smaller C loading and thus larger SSA are therefore more prone to aggregation than adsorption complexes with larger C loadings and smaller SSA. Aggregation, in turn, may restrict the bioavailable surface area of Fe oxides and diminish Fe reduction rates (see section 4.1.4).

Analogous to Bonneville et al. (2006), Yan et al. (2008) found the reduction of hematite by *Geobacter sulfurreducens* to depend on the adsorption of the mineral to the cell surface. Again, the mineral particles in that study were small enough to display colloidal and thus entirely different behavior compared to the mineral particles in our study.

In summary, the BET-derived SSA turned out to be a poor predictor of microbial Fe reduction rates for both *Shewanella putrefaciens* and *Geobacter metallireducens* when comparing adsorption complexes derived from different types of OM and Fe oxides.

4.1.4 Impact of surface charge, particle size and aggregation

In spite of the negative surface charge of all adsorption complexes being expected to repulse the negatively charged cells of both *Shewanella putrefaciens* and *Geobacter metallireducens*, none of the adsorption complexes exhibited a straightforward relationship between Fe reduction rates and the electrophoretic mobility (data not shown), which is in accordance with previous studies for *Shewanella putrefaciens* (Roberts et al., 2006).

The initial reduction rates of the ferrihydrite, lepidocrocite, and goethite adsorption complexes by *Shewanella putrefaciens* for both beech Oi- and spruce Oa-derived NOM seemed to accelerate due to decreasing particle sizes (data not shown). It has to be noted, however, that decreasing particle sizes coincided with increasing C loadings and thus

increasing concentrations of potential electron-shuttling compounds as discussed in section 4.1.1. The pure Fe oxides displaying the smallest particle sizes coinciding with the smallest initial reduction rates (Fig. 6) also suggests that particle size and aggregation were no rate-determining factors for the Fe reduction. Moreover, if the initial reduction rates by *Shewanella putrefaciens* had been dictated by aggregation rather than by electron shuttling, the reduction of the EPS adsorption complexes should have shown the same pattern as the beech Oi and spruce Oa adsorption complexes, independent from potential electron-shuttling compounds. For the reduction of adsorption complexes with small C loadings (and larger particle sizes) by *Shewanella putrefaciens*, it was not possible to differentiate whether aggregation outweighed the stimulation of reduction via electron shuttling or whether the concentration of electron-shuttling molecules was *per se* not large enough. In any case, the NOM-induced aggregation of adsorption complexes did not result in smaller reduction rates in comparison to the pure Fe oxides in our experiments with *Shewanella putrefaciens* to the same degree as previously found for ferrihydrite-humic acid adsorption complexes (Amstatter et al., 2012). The OM-to-mineral ratio of the adsorption complexes showing aggregation-induced decreased Fe reduction rates in the cited study was similar to our adsorption complexes with small and medium C loadings, which did not show decreased Fe reduction rates. The aggregation by larger Fe concentrations as applied in the cited study thus seemed to exert a larger influence on reduction by *Shewanella putrefaciens* than the adsorbed NOM-induced aggregation.

In contrast to *Shewanella putrefaciens*, the initial reduction rates by *Geobacter metallireducens* showed a decreasing trend with increasing particle size when considering each type of NOM and Fe oxide separately (Fig. 9). Noteworthy, the pure Fe oxides exhibited the smallest particle size in microbial nutrient solution in comparison to the adsorption complexes, which can be attributed to dispersion effects by Na^+ and the repulsive negative charge imposed on the surfaces by media-derived phosphate (Gálvez et al., 1999). When all

adsorption complexes were combined, however, the trend of smaller reduction rates and larger particle sizes was not as clear as for the individual Fe oxides (Fig. 9), with the PLSR analysis attributing only 21 % of the variance of the initial reduction rates to the particle size of the adsorption complexes. This result suggests that particle size and aggregation was not the only important factor controlling reduction by *Geobacter metallireducens* either. Since the largest differences in reduction rates still relate to the solubility of the pure minerals, the rate-controlling variable seems to be a combination of both solubility and particle aggregation.

Despite the larger expected amount of electron-shuttling moieties contained in the spruce Oa-derived NOM (see section 4.1.1), the addition of 50 mg C L⁻¹ dissolved beech Oi-derived NOM to the largest C loading of beech Oi adsorption complexes caused a considerably greater increase in reduction rates compared to the corresponding spruce Oa adsorption complexes (Fig. 7). Since the addition of beech Oi-derived NOM to the largest loading resulted in a further decrease of the particle size of the adsorption complexes, whereas the addition of spruce Oa-derived NOM had no impact on the particle size, the increased reduction rates can more likely be attributed to the decreased particle size than to electron shuttling. Unlike spruce Oa, the beech Oi-derived NOM contained significantly larger amounts of phosphate, which opposes aggregation as mentioned above.

Overall, microbial Fe reduction rates by *Geobacter metallireducens* were mainly controlled by the particle size of the adsorption complexes, whereas no such relation emerged for the Fe reduction rates by *Shewanella putrefaciens*.

4.1.5 Cell concentrations

Since the correlation between desorbed C concentrations and reduction rates coincided with the initially smaller cell numbers for *Shewanella putrefaciens*, whereas the correlation between particle size and reduction rates coincided with the initially larger cell numbers for *Geobacter metallireducens*, a potential effect of the different initial cell concentration on the

prevailing electron transfer path during microbial Fe reduction has to be considered. The reduction rates of beech Oi and spruce Oa adsorption complexes of ferrihydrite, lepidocrocite, and goethite remained larger than the reduction rates of the corresponding pure minerals throughout the whole experiment. If the reduction-governing parameter had changed from limitation by external electron-shuttling compounds at lower cell density to limitation by particle size at higher cell density, the reduction rates should have changed along with the growing cell numbers of *Shewanella putrefaciens* during the course of the experiment. No such development was observed for any of the experiments involving *Shewanella putrefaciens*. To estimate the cell number to surface area ratio, we calculated the surface coverage density using the cell dimensions suggested by Lee et al. (2016) for *Shewanella putrefaciens* and the cell dimensions suggested by Lebedev et al. (2014) for *Geobacter metallireducens* assuming an optimal coverage of the iron oxide surface by the cells. None of the Fe oxides and adsorption complexes exhibited an initial cell surface coverage of more than 0.005 %. Even at cell concentrations of 10^8 mL^{-1} , which was the largest cell concentration found for *Shewanella putrefaciens* in preliminary experiments, the cell coverage did not exceed 1 % for any of the adsorption complexes.

When relating the initial Fe reduction rates of ferrihydrite, lepidocrocite, goethite, hematite, and magnetite to initial cell concentrations, *Shewanella putrefaciens* exhibited reduction rates of 3.64, 2.59, 2.31, 1.25, and $0.75 \times 10^8 \text{ mmol Fe(II) d}^{-1} \text{ mmol Fe}_{\text{total}}^{-1} \text{ cells}_{\text{initial}}^{-1}$. The cell normalized reduction rates of *Geobacter metallireducens* were only slightly smaller with initial reduction rates of 2.89, 1.95, 1.61, 1.18, and $1.05 \times 10^8 \text{ mmol Fe(II) d}^{-1} \text{ mmol Fe}_{\text{total}}^{-1} \text{ cells}_{\text{initial}}^{-1}$. While the different initial cell densities thus seemed to have a minor influence on the electron transfer mechanism in our experimental set-up, they can still account for the larger initial reduction rates by *Geobacter metallireducens* in comparison to *Shewanella putrefaciens*.

4.2 Microbial Transformation of the Iron Oxides

Fe oxides commonly formed during microbial reductive transformation include magnetite, goethite, and lepidocrocite (Hansel et al., 2005), neither of which was found in our experiments. The inhibition of the formation of these Fe oxides during microbial Fe reduction by adsorbed phosphate has been reported in several studies (Kukkadapu et al., 2004; Borch et al., 2007; O'Loughlin et al., 2010; Zachara et al., 2011). Despite using HEPES to buffer the solution during microbial reduction, phosphate had to be added as a nutrient in our experiments, which might account for the absence of these Fe oxides during microbial mineral transformation to some extent and particular for the reduction of the pure minerals. In addition to phosphate, adsorbed or coprecipitated humic acids and NOM have been reported to decrease or impede the formation of magnetite and goethite during Fe(III) reduction of ferrihydrite (Amstaetter et al., 2012; Henneberry et al., 2012; Shimizu et al., 2013; Eusterhues et al., 2014). Recrystallization of goethite and lepidocrocite requires readsorption of Fe(II) to the mineral surface (Hansel et al., 2003; Thompson et al., 2006), while the conversion of ferrihydrite to magnetite even requires surface loadings of more than 1.0 mmol Fe(II) g⁻¹ ferrihydrite (Hansel et al., 2005), which were most likely blocked by adsorbed NOM or EPS in our study. Furthermore, the recrystallization of goethite is promoted by the presence CO₃²⁻ (Hansel et al., 2005; Zachara et al., 2011), which was omitted from the media in our experiments. Moreover, Dippon et al. (2015) found that reductive transformation to magnetite is more likely to occur in reaction vessels causing minerals to form a thick pellet instead of a more evenly distributed thin layer of sediment on the bottom of the serum bottle as in our experiments.

Both phosphate and NOM can stimulate the formation of green rust during the microbial reduction of ferrihydrite (Kukkadapu et al., 2004; Amstaetter et al., 2012) and lepidocrocite (Ona-Nguema et al., 2009; O'Loughlin et al., 2010). However, the mineral phases found in the cited studies were identified as carbonate green rust with CO₃²⁻ as the dominant interlayer

anion, whereas our microbial media did not contain carbonate. Moreover, Ona-Nguema et al. (2009) and O’Loughlin et al. (2010) found the formation of green rust to be promoted by initial cell numbers between 2×10^9 and 2×10^{10} cells mL⁻¹, which are several magnitudes larger than the initial cell numbers in our study and thus might further account for the absence of green rust for most of our experiments. At the same time, O’Loughlin et al. (2010) suggested the precipitation of green rust to be more pronounced during slower Fe reduction, which would explain, why it was only found for the hematite and magnetite adsorption complexes in our experiments.

To our knowledge, no neo-formation of Fe-OM coprecipitates during microbial reduction of Fe oxides — as observed in our treatments containing additionally added dissolved NOM — has been reported so far, in spite of previous studies working with even larger concentrations of organic C. This might either be explained by the routine of only considering crystalline phases when monitoring the mineral transformation during microbial reduction or by the Fe-OM coprecipitates being reduced again prior to analysis. Although Fe-OM coprecipitates are prone to further microbial reduction (Shimizu et al., 2013; Eusterhues et al., 2014), they might thus still prolong the microbial reduction or mineral transformation to some extent.

5 CONCLUSIONS

Despite the ongoing scientific dispute over the significance of different electron transfer mechanisms applied by different types of Fe-reducing bacteria, our experiments showed different responses of *Shewanella putrefaciens* and *Geobacter metallireducens* to the impact of adsorbed OM on the Fe reduction of Fe oxides. The reduction of different pure Fe oxides was controlled by the SSA and solubility of the minerals, the influence of which diminished with the introduction of NOM as organic coatings. For *Shewanella putrefaciens*, accelerated Fe reduction was strongly related to the concentration of potentially usable electron-shuttling

molecules of easily desorbable NOM. Stimulating effects were only absent for NOM concentrations $<2 \text{ mg C L}^{-1}$, while the influence of the particle size and thus the inhibition by NOM-induced aggregation was negligible. Fe reduction by *Geobacter metallireducens*, on the other hand, strongly correlated with the particle size of the adsorption complexes, which overall pointed towards an inhibitory effect of adsorbed NOM. Despite a slight accelerating influence of electron shuttling, not even a NOM concentration of 50 mg C L^{-1} was large enough to outweigh the aggregation-induced inhibition of Fe reduction in comparison to pure Fe oxides, which is an uncharacteristically large concentration of free dissolved OM in many Fe-reducing soil environments.

The importance of the role of organic coatings on mobilizing Fe-organic associations grows with the increasing challenge of environmental threats like the emission of greenhouse gases and the leaching of Fe oxide-associated organic contaminants, heavy metals, and oxyanions into the groundwater. However, our experiments showed that conclusions about the enhancing or decelerating nature of NOM with respect to the long-term stability of Fe-organic associations in soils cannot easily be drawn without assessing the composition of the microbial soil community.

Acknowledgements

This study was financially supported by the NTH-Graduate School “Geofluxes” of the federal state of Lower Saxony, Germany. We would like to thank Patrick Liebmann and Britta Osterkamp for their assistance with the electrophoretic mobility and particle size measurements, Fabian Kalks and Marie Rinne for their help with the FTIR measurements, and Markus Koch for his contribution to the adsorption experiments. Furthermore, we are grateful to 4 anonymous reviewers and the editor for their very constructive comments.

References

- Aeschbacher M., Sander M. and Schwarzenbach R. P. (2010) Novel electrochemical approach to assess the redox properties of humic substances. *Environ. Sci. Technol.* **44**, 87–93. Available at: <http://www.ncbi.nlm.nih.gov/pubmed/19950897>.
- Amstaetter K., Borch T. and Kappler A. (2012) Influence of humic acid imposed changes of ferrihydrite aggregation on microbial Fe(III) reduction. *Geochim. Cosmochim. Acta* **85**, 326–341. Available at: <http://linkinghub.elsevier.com/retrieve/pii/S0016703712000816>.
- Atkinson R. J., Posner A. M. and Quirk J. P. (1967) Adsorption of potential-determining ions at the ferric oxide-aqueous electrolyte interface. *J. Phys. Chem.* **71**, 550–558.
- Barrett E. P., Joyner L. G. and Halenda P. P. (1951) The determination of pore volume and area distributions in porous substances. I. Computations from nitrogen isotherms. *J. Am. Chem. Soc.* **73**, 373–380.
- Bernal J. D., Dasgupta D. R. and Mackay A. L. (1959) The oxides and hydroxides of iron and their structural inter-relationships. *Clay Miner.* **21**, 15–30.
- Boesen T. and Nielsen P. (2013) Molecular dissection of bacterial nanowires. *MBio* **4**, e00270-13.
- Bonneville S., Behrends T. and Van Cappellen P. (2009) Solubility and dissimilatory reduction kinetics of iron(III) oxyhydroxides: A linear free energy relationship. *Geochim. Cosmochim. Acta* **73**, 5273–5282. Available at: <http://linkinghub.elsevier.com/retrieve/pii/S0016703709003913>.
- Bonneville S., Behrends T., Cappellen P. Van, Hyacinthe C. and Röling W. F. M. (2006) Reduction of Fe(III) colloids by *Shewanella putrefaciens*: A kinetic model. *Geochim. Cosmochim. Acta* **70**, 5842–5854. Available at: <http://linkinghub.elsevier.com/retrieve/pii/S0016703706002286>.
- Borch T., Masue Y., Kukkadapu R. K. and Fendorf S. (2007) Phosphate imposed limitations on biological reduction and alteration of ferrihydrite. *Environ. Sci. Technol.* **41**, 166–172.
- Brümmer G. W., Barrow N. J. and Fischer L. (2013) Effect of porosity of goethite on the sorption of six heavy metal ions. *Eur. J. Soil Sci.* **64**, 805–813. Available at: <http://doi.wiley.com/10.1111/ejss.12091>.
- Brunauer S., Emmett P. H. and Teller E. (1938) Adsorption of gases in multimolecular layers. *J. Am. Chem. Soc.* **60**, 309–319.
- Canfield D. E., Jorgensen B. B., Fossing H., Glud R., Gundersen J., Ramsing N. B., Thamdrup B., Hansen J. W., Nielsen L. P. and Hall P. O. (1993) Pathways of organic carbon oxidation in three continental margin sediments. *Mar. Geol.* **113**, 27–40.
- von Canstein H., Ogawa J., Shimizu S. and Lloyd J. R. (2008) Secretion of flavins by *Shewanella* species and their role in extracellular electron transfer. *Appl. Environ. Microbiol.* **74**, 615–23. Available at: <http://www.pubmedcentral.nih.gov/articlerender.fcgi?artid=2227709&tool=pmcentrez&endertype=abstract>.
- Carrascal L. M., Galván I. and Gordo O. (2009) Partial least squares regression as an alternative to current regression methods used in ecology. *Oikos* **118**, 681–690. Available at: <http://doi.wiley.com/10.1111/j.1600-0706.2008.16881.x>.
- Chen C., Dynes J. J., Wang J. and Sparks D. L. (2014) Properties of Fe-organic matter associations via coprecipitation versus adsorption. *Environ. Sci. Technol.* **48**, 13751–13759.
- Chen J., Gu B., Royer R. A. and Burgos W. D. (2003) The roles of natural organic matter in chemical and microbial reduction of ferric iron. *Sci. Total Environment* **307**, 167–78. Available at: <http://www.ncbi.nlm.nih.gov/pubmed/12711432>.
- Chorover J. and Amistadi M. K. (2001) Reaction of forest floor organic matter at goethite ,

- birnessite and smectite surfaces. *Geochim. Cosmochim. Acta* **65**, 95–109.
- Dippon U., Schmidt C., Behrens S. and Kappler A. (2015) Secondary mineral formation during ferrihydrite reduction by *Shewanella oneidensis* MR-1 depends on incubation vessel orientation and resulting gradients of cells, Fe²⁺ and Fe minerals. *Geomicrobiol. J.* **451**, 00–00. Available at: <http://www.tandfonline.com/doi/full/10.1080/01490451.2015.1017623>.
- El-Naggar M. Y., Wanger G., Leung K. M., Yuzvinsky T. D., Southam G., Yang J., Lau W. M., Nealson K. H. and Gorby Y. A. (2010) Electrical transport along bacterial nanowires from *Shewanella oneidensis* MR-1. *Proc. Natl. Acad. Sci. U. S. A.* **107**, 18127–31. Available at: <http://www.pubmedcentral.nih.gov/articlerender.fcgi?artid=2964190&tool=pmcentrez&rendertype=abstract>.
- Eusterhues K., Hädrich A., Neidhardt J., Küsel K., Keller T. F., Jandt K. D. and Totsche K. U. (2014) Reduction of ferrihydrite with adsorbed and coprecipitated organic matter: microbial reduction by *Geobacter bremerensis* vs. abiotic reduction by Na-dithionite. *Biogeosciences* **11**, 4953–4966. Available at: <http://www.biogeosciences.net/11/4953/2014/>.
- Eusterhues K., Rennert T., Knicker H., Kögel-Knabner I., Totsche K. U. and Schwertmann U. (2011) Fractionation of organic matter due to reaction with ferrihydrite: coprecipitation versus adsorption. *Environ. Sci. Technol.* **45**, 527–33. Available at: <http://www.ncbi.nlm.nih.gov/pubmed/21126068>.
- Eusterhues K., Wagner F. E., Häusler W., Hanzlik M., Knicker H., Totsche K. U., Kögel-Knabner I. and Schwertmann U. (2008) Characterization of ferrihydrite-soil organic matter coprecipitates by X-ray diffraction and Mössbauer spectroscopy. *Environ. Sci. Technol.* **42**, 7891–7. Available at: <http://www.ncbi.nlm.nih.gov/pubmed/19031877>.
- Galvez N., Barron V. and Torrent J. (1999) Effect of Phosphate on the Crystallization of Hematite, Goethite, and Lepidocrocite from Ferrihydrite. *Clays Clay Miner.* **47**, 304–311.
- Gerin P. A., Genet M. J., Herbillon A. J. and Delvaux B. (2003) Surface analysis of soil material by X-ray photoelectron spectroscopy. *Eur. J. Soil Sci.* **54**, 589–603.
- Glasauer S., Weidler P. G., Langley S. and Beveridge T. J. (2003) Controls on Fe reduction and mineral formation by a subsurface bacterium. *Geochim. Cosmochim. Acta* **67**, 1277–1288.
- Gorby Y., Yanina S., McLean J. S., Rosso K. M., Moyles D., Dohnalkova A., Beveridge T. J., Chang I. S., Kim B. H., Kim K. S., Culley D. E., Reed S. B., Romine M. F., Saffarini D. A., Hill E. A., Shi L., Elias D. A., Kennedy D. W., Pinchuk G., Watanabe K., Ishii S., Logan B., Nealson K. H. and Fredrickson J. K. (2006) Correction for Lygeros et al., Stochastic hybrid modeling of DNA replication across a complete genome. *Proc. ...* **103**, 11358–11363. Available at: <http://www.pnas.org/cgi/doi/10.1073/pnas.0905246106%5Cnhttp://www.pnas.org/content/103/30/11358.short>.
- Gregg S. H. and Sing K. S. W. (1982) *Adsorption, Surface Area and Porosity*. 2nd ed., Academic Press, New York.
- Hagedorn F., Schleppe P., Waldner P. and Fluehler H. (2000) Export of dissolved organic carbon and nitrogen from Gleysol dominated catchments - the significance of water flow paths. *Biogeochemistry* **50**, 137–161.
- Hansel C. M., Benner S. G. and Fendorf S. (2005) Competing Fe (II)-induced mineralization pathways of ferrihydrite. *Environ. Sci. Technol.* **39**, 7147–53. Available at: <http://www.ncbi.nlm.nih.gov/pubmed/16201641>.
- Hansel C. M., Benner S. G., Neiss J., Dohnalkova A., Kukkadapu R. K. and Fendorf S. (2003) Secondary mineralization pathways induced by dissimilatory iron reduction of

- ferrihydrite under advective flow. *Geochim. Cosmochim. Acta* **67**, 2977–2992. Available at: <http://linkinghub.elsevier.com/retrieve/pii/S001670370300276X>.
- Hantke K. (1997) Ferrous iron uptake by a magnesium transport system is toxic for *Escherichia coli* and *Salmonella typhimurium*. *J. Bacteriol.* **179**, 6201–4. Available at: <http://www.pubmedcentral.nih.gov/articlerender.fcgi?artid=179529&tool=pmcentrez&rendertype=abstract>.
- Henneberry Y. K., Kraus T. E. C., Nico P. S. and Horwath W. R. (2012) Structural stability of coprecipitated natural organic matter and ferric iron under reducing conditions. *Org. Geochem.* **48**, 81–89. Available at: <http://linkinghub.elsevier.com/retrieve/pii/S0146638012000782>.
- Hesse R., Chassé T. and Szargan R. (2003) Unifit 2002-universal analysis software for photoelectron spectra. *Anal. Bioanal. Chem.* **375**, 856–863.
- Illés E. and Tombácz E. (2006) The effect of humic acid adsorption on pH-dependent surface charging and aggregation of magnetite nanoparticles. *J. Colloid Interface Sci.* **295**, 115–123.
- Jiang J. and Kappler A. (2008) Kinetics of microbial and chemical reduction of humic substances: implications for electron shuttling. *Environ. Sci. Technol.* **42**, 3563–9. Available at: <http://www.ncbi.nlm.nih.gov/pubmed/18546690>.
- Jones A. M., Collins R. N., Rose J. and Waite T. D. (2009) The effect of silica and natural organic matter on the Fe(II)-catalysed transformation and reactivity of Fe(III) minerals. *Geochim. Cosmochim. Acta* **73**, 4409–4422. Available at: <http://www.sciencedirect.com/science/article/pii/S0016703709002464>.
- Kaiser K. (2003) Sorption of natural organic matter fractions to goethite (α -FeOOH): effect of chemical composition as revealed by liquid-state ^{13}C NMR and wet-chemical analysis. *Org. Geochem.* **34**, 1569–1579. Available at: <http://linkinghub.elsevier.com/retrieve/pii/S0146638003001207>.
- Kaiser K. and Guggenberger G. (2003) Mineral surfaces and soil organic matter. *Eur. J. Soil Sci.* **54**, 219–236.
- Kaiser K. and Guggenberger G. (2007) Sorptive stabilization of organic matter by microporous goethite: sorption into small pores vs. surface complexation. *Eur. J. Soil Sci.* **58**, 45–59. Available at: <http://doi.wiley.com/10.1111/j.1365-2389.2006.00799.x>.
- Kaiser K., Guggenberger G., Haumaier L. and Zech W. (1997) Dissolved organic matter sorption on subsoils and minerals studied by ^{13}C -NMR and DRIFT spectroscopy. *Eur. J. Soil Sci.* **48**, 301–310.
- Kalbitz K., Schwesig D., Rethemeyer J. and Matzner E. (2005) Stabilization of dissolved organic matter by sorption to the mineral soil. *Soil Biol. Biochem.* **37**, 1319–1331. Available at: <http://linkinghub.elsevier.com/retrieve/pii/S0038071705000027>.
- Kalbitz K., Schwesig D., Schmerwitz J., Kaiser K., Haumaier L., Glaser B., Ellerbrock R. and Leinweber P. (2003) Changes in properties of soil-derived dissolved organic matter induced by biodegradation. *Soil Biol. Biochem.* **35**, 1129–1142. Available at: <http://linkinghub.elsevier.com/retrieve/pii/S0038071703001652>.
- Kang F. and Zhu D. (2013) Abiotic reduction of 1,3-dinitrobenzene by aqueous dissolved extracellular polymeric substances produced by microorganisms. *J. Environ. Qual.* **42**, 1441–8. Available at: <http://www.ncbi.nlm.nih.gov/pubmed/24216421>.
- Kappler A. and Straub K. (2005) Geomicrobiological cycling of iron. *Rev. Mineral. Geochem.* **59**, 85–108.
- Kleber M., Eusterhues K., Keiluweit M., Mikutta C., Mikutta R. and Nico P. S. (2015) Mineral–organic associations: formation, properties, and relevance in soil environments. *Adv. Agron.* **130**. Available at: <http://dx.doi.org/10.1016/bs.agron.2014.10.005>.
- Kotloski N. J. and Gralnick J. A. (2013) Flavin electron shuttles dominate extracellular

- electron transfer by *Shewanella oneidensis*. *MBio* **4**, 10–13. Available at: <http://www.ncbi.nlm.nih.gov/pmc/articles/PMC3551548/pdf/mBio.00553-12.pdf>.
- Kraemer S. M. (2004) Iron oxide dissolution and solubility in the presence of siderophores. *Aquat. Sci. - Res. Across Boundaries* **66**, 3–18. Available at: <http://link.springer.com/10.1007/s00027-003-0690-5>.
- Kukkadapu R. K., Zachara J. M., Fredrickson J. K. and Kennedy D. W. (2004) Biotransformation of two-line silica-ferrihydrite by a dissimilatory Fe(III)-reducing bacterium: formation of carbonate green rust in the presence of phosphate. *Geochim. Cosmochim. Acta* **68**, 2799–2814. Available at: <http://linkinghub.elsevier.com/retrieve/pii/S0016703704000808>.
- Larsen O. and Postma D. (2001) Kinetics of reductive bulk dissolution of lepidocrocite, ferrihydrite, and goethite. *Geochim. Cosmochim. Acta* **65**, 1367–1379. Available at: <http://linkinghub.elsevier.com/retrieve/pii/S0016703700006232>.
- Lebedev N., Strycharz-Glaven S. M. and Tender L. M. (2014) High resolution AFM and single-cell resonance Raman spectroscopy of *Geobacter sulfurreducens* biofilms early in growth. *Front. Energy Res.* **2**, 1–8. Available at: <http://journal.frontiersin.org/article/10.3389/fenrg.2014.00034/abstract>.
- Lee C. K., Kim A. J., Santos G. S., Lai P. Y., Lee S. Y., Qiao D. F., Anda J. De, Young T. D., Chen Y., Rowe A. R., Nealon K. H., Weiss P. S. and Wong G. C. L. (2016) Evolution of cell size homeostasis and growth rate diversity during initial surface colonization of *Shewanella oneidensis*. *ACS Nano* **10**, 9183–9192.
- Leone L., Loring J., Sj S., Persson P. and Shchukarev A. (2006) Surface characterization of the gram-positive bacteria *Bacillus subtilis* - an XPS study. *Surf. Interface Anal.* **38**, 202–205.
- Lies D. P., Hernandez M. E., Kappler A., Mielke R. E., Gralnick J. A. and Newman D. K. (2005) *Shewanella oneidensis* MR-1 Uses overlapping pathways for iron reduction at a distance and by direct contact under conditions relevant for biofilms. *Appl. Environ. Microbiol.* **71**, 4414–4426.
- Liu C., Zachara J. M., Foster N. and Strickland J. (2007) Kinetics of reductive dissolution of hematite by bioreduced anthraquinone-2,6-disulfonate. , 1–7.
- Liu X., Eusterhues K., Thiema J., Höschen C., Müller C. W., Kögel-Knabner I. and U T. K. (2012) Characterization of EPS fractions before and after adsorption to goethite.
- Lovley D. R. and Anderson R. T. (2000) Influence of dissimilatory metal reduction on fate of organic and metal contaminants in the subsurface. *Hydrogeol. J.* **8**, 77–88.
- Lovley D. R. and Blunt-Harris E. L. (1999) Role of humic-bound iron as an electron transfer agent in dissimilatory Fe (III) reduction. *Appl. Environ. Microbiol.* **65**, 4252–4254.
- Lovley D. R., Coates J. D., Blunt-Harris E. L., Phillips E. J. P. and Woodward J. C. (1996) Humic substances as electron acceptors for microbial respiration. *Nature* **382**, 445–448.
- Lovley D. R., Holmes D. E. and Nevin K. P. (2004) Dissimilatory Fe(III) and Mn(IV) reduction. *Adv. Microb. Physiol.* **49**, 219–86. Available at: <http://www.ncbi.nlm.nih.gov/pubmed/18497157>.
- Lovley D. R. and Phillips E. J. (1987) Rapid assay for microbially reducible ferric iron in aquatic sediments. *Appl. Environ. Microbiol.* **53**, 1536–1540.
- Lovley D. R. and Phillips E. J. P. (1988) Novel mode of microbial energy metabolism: organic carbon oxidation coupled to dissimilatory reduction of iron or manganese. *Appl. Environ. Microbiol.* **54**, 1472–80. Available at: <http://www.pubmedcentral.nih.gov/articlerender.fcgi?artid=202682&tool=pmcentrez&rendertype=abstract>.
- Lovley D. R., Woodward J. C. and Chapelle F. H. (1994) Stimulated anoxic biodegradation of aromatic hydrocarbons using Fe(III) ligands. *Nature* **370**, 128–131.
- Malvankar N. S., Vargas M., Nevin K. P., Franks A. E., Leang C., Kim B.-C., Inoue K.,

- Mester T., Covalla S. F., Johnson J. P., Rotello V. M., Tuominen M. T. and Lovley D. R. (2011) Tunable metallic-like conductivity in microbial nanowire networks. *Nat. Nanotechnol.* **6**, 573–579.
- Marchetti G. M., Drton M. and Sadeghi K. (2015) ggm 2.3.
- Marsili E., Baron D. B., Shikhare I. D., Coursolle D., Gralnick J. A. and Bond D. R. (2008) *Shewanella* secretes flavins that mediate extracellular electron transfer. *Proc. Natl. Acad. Sci. U. S. A.* **105**, 3968–73. Available at: <http://www.pubmedcentral.nih.gov/articlerender.fcgi?artid=2268775&tool=pmcentrez&rendertype=abstract>.
- Mesuere K. and Fish W. (1999) Chromate and oxalate adsorption on goethite. 2. Surface complexation modeling of competitive adsorption. *Environ. Sci. Technol.* **26**, 2365–2370.
- Mikutta R., Kleber M., Torn M. S. and Jahn R. (2006) Stabilization of soil organic matter: association with minerals or chemical recalcitrance? *Biogeochemistry* **77**, 25–56. Available at: <http://link.springer.com/10.1007/s10533-005-0712-6>.
- Myers C. R. and Nealson K. H. (1988) Bacterial manganese reduction and growth with manganese oxide as the sole electron acceptor. *Science* **240**, 1319–21. Available at: <http://www.ncbi.nlm.nih.gov/pubmed/17815852>.
- Nevin K. P. and Lovley D. R. (2000) Lack of production of electron-shuttling compounds or solubilization of Fe(III) during reduction of insoluble Fe(III) oxide by *Geobacter metallireducens*. *Appl. Environ. Microbiol.* **66**, 2248–51. Available at: <http://www.pubmedcentral.nih.gov/articlerender.fcgi?artid=101484&tool=pmcentrez&rendertype=abstract>.
- Nevin K. P. and Lovley D. R. (2002a) Mechanisms for accessing insoluble Fe(III) oxide during dissimilatory Fe(III) reduction by *Geothrix fermentans*. *Appl. Environ. Microbiol.* **68**, 2294–2299. Available at: <http://www.pubmedcentral.nih.gov/articlerender.fcgi?artid=127553&tool=pmcentrez&rendertype=abstract>.
- Nevin K. P. and Lovley D. R. (2002b) Mechanisms for Fe(III) oxide reduction in sedimentary environments. *Geomicrobiol. J.* **19**, 141–159.
- Newman D. K. and Kolter R. (2000) A role for excreted quinones in extracellular electron transfer. *Nature* **405**, 94–7. Available at: <http://www.ncbi.nlm.nih.gov/pubmed/10811225>.
- O’Loughlin E. J. (2008) Effects of electron transfer mediators on the bioreduction of lepidocrocite (γ -FeOOH) by *Shewanella putrefaciens* CN32. *Environ. Sci. Technol.* **42**, 6876–82. Available at: <http://www.ncbi.nlm.nih.gov/pubmed/18853803>.
- O’Loughlin E. J., Gorski C. A., Cook R. E., Kemner K. M., Boyanov M. I. and Scherer M. M. (2010) Effects of oxyanions and natural organic matter on the bioreduction of lepidocrocite (γ -FeOOH) and the formation of secondary mineralization products. *Environ. Sci. Technol.* **44**, 4570–4576.
- Omoike A. and Chorover J. (2006) Adsorption to goethite of extracellular polymeric substances from *Bacillus subtilis*. *Geochim. Cosmochim. Acta* **70**, 827–838. Available at: <http://linkinghub.elsevier.com/retrieve/pii/S0016703705008331>.
- Omoike A. and Chorover J. (2004) Spectroscopic study of extracellular polymeric substances from *Bacillus subtilis*: Aqueous chemistry and adsorption effects. *Biomacromolecules* **5**, 1219–30. Available at: <http://www.ncbi.nlm.nih.gov/pubmed/15244434>.
- Ona-Nguema G., Morin G., Wang Y., Menguy N., Juillot F., Olivi L., Aquilanti G., Abdelmoula M., Ruby C., Bargar J. R., Guyot F., Calas G. and Brown G. E. (2009) Arsenite sequestration at the surface of nano-Fe(OH)₂, ferrous-carbonate hydroxide, and green-rust after bioreduction of arsenic-sorbed lepidocrocite by *Shewanella putrefaciens*. *Geochim. Cosmochim. Acta* **73**, 1359–1381. Available at:

- <http://linkinghub.elsevier.com/retrieve/pii/S0016703708007370>.
- Pédrot M., Le Boudec A., Davranche M., Dia A. and Henin O. (2011) How does organic matter constrain the nature, size and availability of Fe nanoparticles for biological reduction? *J. Colloid Interface Sci.* **359**, 75–85. Available at: <http://www.ncbi.nlm.nih.gov/pubmed/21482426>.
- Perelomov L. V., Pinskiy D. L. and Violante A. (2011) Effect of organic acids on the adsorption of copper, lead, and zinc by goethite. *Eurasian Soil Sci.* **44**, 22–28. Available at: <http://link.springer.com/10.1134/S1064229311010091>.
- Piepenbrock A., Dippon U., Porsch K., Appel E. and Kappler A. (2011) Dependence of microbial magnetite formation on humic substance and ferrihydrite concentrations. *Geochim. Cosmochim. Acta* **75**, 6844–6858. Available at: <http://linkinghub.elsevier.com/retrieve/pii/S001670371100528X>.
- Poggenburg C., Mikutta R., Sander M., Schippers A., Marchanka A., Dohrmann R. and Guggenberger G. (2016) Microbial reduction of ferrihydrite-organic matter coprecipitates by *Shewanella putrefaciens* and *Geobacter metallireducens* in comparison to mediated electrochemical reduction. *Chem. Geol.* **447**, 133–147. Available at: <http://dx.doi.org/10.1016/j.chemgeo.2016.09.031>.
- R Development Core Team (Ed.), 2016. GNU R software, 3.3.2.
- Reguera G., McCarthy K. D., Mehta T., Nicoll J. S., Tuominen M. T. and Lovley D. R. (2005) Extracellular electron transfer via microbial nanowires. *Nature* **435**, 1098–101. Available at: <http://www.ncbi.nlm.nih.gov/pubmed/15973408>.
- Ritchie J. D. and Perdue E. M. (2003) Proton-binding study of standard and reference fulvic acids, humic acids, and natural organic matter. *Geochim. Cosmochim. Acta* **67**, 85–93.
- Roberts J. A., Fowle D. A., Hughes B. T. and Kulczycki E. (2006) Attachment behavior of *Shewanella putrefaciens* onto magnetite under aerobic and anaerobic conditions. *Geomicrobiol. J.* **23**, 631–640. Available at: <http://www.tandfonline.com/doi/abs/10.1080/01490450600964441>.
- Roden E. E. (2003) Fe(III) oxide reactivity toward biological versus chemical reduction. *Environ. Sci. Technol.* **37**, 1319–1324. Available at: <http://pubs.acs.org/doi/abs/10.1021/es026038o>.
- Roden E. E. and Urrutia M. M. (1999) Ferrous iron removal promotes microbial reduction of crystalline iron(III) oxides. *Environ. Sci. Technol.* **33**, 1847–1853. Available at: <http://pubs.acs.org/doi/abs/10.1021/es9809859>.
- Royer R. A., Burgos W. D., Fisher A. S., Jeon B.-H., Unz R. F. and Dempsey B. A. (2002a) Enhancement of hematite bioreduction by natural organic matter. *Environ. Sci. Technol.* **36**, 2897–904. Available at: <http://www.ncbi.nlm.nih.gov/pubmed/12144265>.
- Royer R. A., Burgos W. D., Fisher A. S., Unz R. F. and Dempsey B. A. (2002b) Enhancement of biological reduction of hematite by electron shuttling and Fe(II) complexation. *Environ. Sci. Technol.* **36**, 1939–1946.
- Sannino F., De Martino A., Pigna M., Violante A., Di Leo P., Mesto E. and Capasso R. (2009) Sorption of arsenate and dichromate on polymerin, Fe(OH)_x-polymerin complex and ferrihydrite. *J. Hazard. Mater.* **166**, 1174–9. Available at: <http://www.ncbi.nlm.nih.gov/pubmed/19153008>.
- Scheel T., Dörfel C. and Kalbitz K. (2007) Precipitation of dissolved organic matter by aluminum stabilizes carbon in acidic forest soils. *Soil Sci. Soc. Am. J.* **71**, 64–74.
- Scheel T., Haumaier L., Ellerbrock R. H., Rühlmann J. and Kalbitz K. (2008) Properties of organic matter precipitated from acidic forest soil solutions. *Org. Geochem.* **39**, 1439–1453. Available at: <http://linkinghub.elsevier.com/retrieve/pii/S0146638008001733>.
- Schwertmann U. and Cornell R. M. (2000) *Iron Oxides in the Laboratory: Preparation and Characterization*. 2nd ed., Wiley-VCH, Weinheim, Germany.
- Schwertmann U., Wagner F. and Knicker H. (2005) Ferrihydrite–Humic Associations:

- Magnetic Hyperfine Interactions. *Soil Sci. Soc. Am. J.* **69**, 1009–1015.
- Scott D. T., McKnight D. M., Blunt-Harris E. L., Kolesar S. E. and Lovley D. R. (1998) Quinone moieties act as electron acceptors in the reduction of humic substances by humics-reducing microorganisms. *Environ. Sci. Technol.* **32**, 2984–2989. Available at: <http://pubs.acs.org/doi/abs/10.1021/es980272q>.
- Shimizu M., Zhou J., Schröder C., Obst M., Kappler A. and Borch T. (2013) Dissimilatory reduction and transformation of ferrihydrite-humic acid coprecipitates. *Environ. Sci. Technol.* **47**, 13375–84. Available at: <http://www.ncbi.nlm.nih.gov/pubmed/24219167>.
- Stookey L. L. (1970) Ferrozine - a new spectrophotometric reagent for iron. *Anal. Chem.* **42**, 779–781. Available at: <http://pubs.acs.org/doi/abs/10.1021/ac60289a016>.
- Thompson A., Chadwick O. A., Rancourt D. G. and Chorover J. (2006) Iron-oxide crystallinity increases during soil redox oscillations. *Geochim. Cosmochim. Acta* **70**, 1710–1727. Available at: <http://linkinghub.elsevier.com/retrieve/pii/S0016703705009427>.
- Violante A., Ricciardella M. and Pigna M. (2003) Adsorption of heavy metals on mixed Fe-Al oxides in the absence or presence of organic ligands. *Water. Air. Soil Pollut.* **143**, 289–306.
- Wagai R. and Mayer L. M. (2007) Sorptive stabilization of organic matter in soils by hydrous iron oxides. *Geochim. Cosmochim. Acta* **71**, 25–35.
- Waychunas G. ., Rea B. ., Fuller C. . and Davis J. . (1993) Surface chemistry of ferrihydrite: Part 1. EXAFS studies of the geometry of coprecipitated and adsorbed arsenate. *Geochim. Cosmochim. Acta* **57**, 2251–2269.
- Weber K. A., Achenbach L. A. and Coates J. D. (2006) Microorganisms pumping iron: anaerobic microbial iron oxidation and reduction. *Nat. Rev. Microbiol.* **4**, 752–64. Available at: <http://www.ncbi.nlm.nih.gov/pubmed/16980937>.
- Weiss J. V., Emerson D. and Magonigal J. P. (2004) Geochemical control of microbial Fe(III) reduction potential in wetlands: comparison of the rhizosphere to non-rhizosphere soil. *FEMS Microbiol. Ecol.* **48**, 89–100.
- Wolf M., Kappler A., Jiang J. and Meckenstock R. U. (2009) Effects of humic substances and quinones at low concentrations on ferrihydrite reduction by *Geobacter metallireducens*. *Environ. Sci. Technol.* **43**, 5679–85. Available at: <http://www.ncbi.nlm.nih.gov/pubmed/19731662>.
- Yan B., Wrenn B. a, Basak S., Biswas P. and Giammar D. E. (2008) Microbial reduction of Fe(III) in hematite nanoparticles by *Geobacter sulfurreducens*. *Environ. Sci. Technol.* **42**, 6526–31. Available at: <http://www.ncbi.nlm.nih.gov/pubmed/18800525>.
- Zachara J. M., Kukkadapu R. K., Peretyazhko T., Bowden M., Wang C., Kennedy D. W., Moore D. and Arey B. (2011) The mineralogic transformation of ferrihydrite induced by heterogeneous reaction with bioreduced anthraquinone disulfonate (AQDS) and the role of phosphate. *Geochim. Cosmochim. Acta* **75**, 6330–6349. Available at: <http://linkinghub.elsevier.com/retrieve/pii/S0016703711003681>.
- Zhu W., Nan Y., Huang T. and Wu F. (2013) The mechanism, thermodynamic and kinetic characteristics of the microbial reduction of goethite mediated by anthraquinone-2-sulfonate. *Geomicrobiol. J.* **30**, 928–940. Available at: <http://www.tandfonline.com/doi/abs/10.1080/01490451.2013.791356>.

SUPPORTING INFORMATION

Impact of Natural Organic Matter Coatings on the Microbial Reduction of Iron Oxides

Christine Poggenburg^{1,2,}, Robert Mikutta³, Axel Schippers⁴,
Reiner Dohrmann^{4,5}, Georg Guggenberger^{1,2}*

¹ Institute of Soil Science, Leibniz University Hannover,
Herrenhäuser Straße 2, 30419 Hannover, Germany

² Centre for Solid State Chemistry and New Materials, Leibniz University Hannover,
Callinstraße 3, 30167 Hannover, Germany

³ Soil Science and Soil Protection, Martin Luther University Halle-Wittenberg,
Von-Seckendorff-Platz 3, 06210 Halle (Saale), Germany

⁴ Bundesanstalt für Geowissenschaften und Rohstoffe (BGR),
Stilleweg 2, 30655 Hannover, Germany

⁵ Landesamt für Bergbau, Energie und Geologie (LBEG),
Stilleweg 2, 30655 Hannover, Germany

*Corresponding author: poggenburg@ifbk.uni-hannover.de, +49 5117622625

Contents**Material and Methods**

<i>Extraction of extracellular polymeric substances and natural organic matter</i>	3
<i>Microbial reduction experiment nutrient solutions</i>	4
<i>X-Ray diffraction after microbial reduction experiments</i>	5

Characterization of Fe Oxides and Adsorption Complexes

<i>XRD diagrams of the pure Fe oxides</i>	6
<i>Fe, C and N contents of the adsorption complexes</i>	7
<i>P and S contents of the adsorption complexes</i>	9
<i>SUVA of the pre- and post-sorption solution of the adsorption complexes</i>	11
<i>Desorption of OC and complexation capacity of Fe(II)</i>	13
<i>Bulk carbon speciation of original and adsorbed NOM</i>	15

Mineral Transformation **17****Partial Regression** **22****References** **23**

Appendix A: Material and Methods

A.1 Extraction of extracellular polymeric substances and natural organic matter

Extraction of extracellular polymeric substances (EPS) was conducted in line with de Brouwer et al. (2002) and Omoike and Chorover (2006). First, a freeze-dried culture of *Bacillus subtilis* (ATCC 7003; BCCMTM/LMG Bacteria Collection) was activated aerobically in LB-Lennox medium (yeast extract, 5 g L⁻¹; trypton, 10 g L⁻¹; NaCl, 5 g L⁻¹) at 303 K for 24 h. One milliliter of the culture was then inoculated into 500 mL of the same medium in a 1-L flask with air-conductive aluminum caps and incubated at 303 K and 120 rpm on a horizontal shaker. When reaching the early stationary growth phase, bacterial cells were removed by centrifuging the suspension at 5,000 g and 277 K for 15 min, before removing residual cell components by centrifuging the decanted supernatant at 10,000 g for 50 min once more. For precipitation of EPS, the collected supernatant was mixed with 277 K cold ethanol at a ratio of 1:3 (v/v supernatant/ethanol) and stored at 248 K for 18 h, before centrifuging the mixture at 10,000 g for 50 min. Residual medium and ethanol were removed by re-suspending the obtained EPS pellet in sterile water (filtered <100 nm) and dialyzing for 72 h (Spectra/Por 7, 1,000 MWCO) with two changes of sterile water per day. After this purification step, the EPS solution was freeze-dried. Residual cells in the purified EPS were quantified with fluorescence microscopy (Zeiss Axiophat Fluorescence Microscope, Carl Zeiss AG, Jena, Germany) after embedding an EPS aliquot in Moviol-Mounting medium and staining it with SYBR-Green (Lunau et al., 2005). The freeze-dried EPS contained approximately 7.85×10^6 cells mg⁻¹ EPS.

Material for natural organic matter (NOM) extraction was sampled from the Oi horizon of a Eutric Cambisol under European beech (*Fagus sylvatica* L.) in the Deister Mountains (Germany) and from the Oa horizon of a Haplic Podzol under Norway spruce (*Picea abies* (L.) Karst.) in the Fichtelgebirge Mountains (Germany). After tearing the air-dried beech litter manually, mixing with doubly deionized water (1/10 w/v), and stirring for 15 min, the suspension was equilibrated at 298 K for 16 h. NOM from the Oa horizon was extracted with doubly deionized water (1/5 w/v) and equilibrated on a horizontal shaker at 1,000 rpm at 298 K for 16 h. Both types of NOM solutions were pre-filtrated through 0.7- μ m glass fiber filters (GF 92, Whatman GmbH, Dassel, Germany) before filtration through 0.45- μ m cellulose nitrate membrane filters (G, Sartorius AG, Göttingen, Germany). Dissolved total organic carbon (TOC) and total nitrogen (TN) were determined with a TOC/TN_b-Analyzer (liqui TOC II, Elementar Analysensysteme GmbH, Hanau, Germany).

*A.2 Microbial reduction experiments***Table A.1** Trace element solution of DSMZ Medium 141.

Trace element solution		
Nitrilotriacetic acid	1.50	g L ⁻¹
MgSO ₄ · 7H ₂ O	3.00	g L ⁻¹
MnSO ₄ · H ₂ O	0.50	g L ⁻¹
NaCl	1.00	g L ⁻¹
FeSO ₄ · 7H ₂ O	0.10	g L ⁻¹
CoSO ₄ · 7H ₂ O	0.18	g L ⁻¹
CaCl ₂ · 2H ₂ O	0.10	g L ⁻¹
ZnSO ₄ · 7H ₂ O	0.18	g L ⁻¹
CuSO ₄ · 5H ₂ O	0.01	g L ⁻¹
KAl(SO ₄) ₂ · 12H ₂ O	0.02	g L ⁻¹
H ₃ BO ₃	0.01	g L ⁻¹
Na ₂ MoO ₄ · 2H ₂ O	0.01	g L ⁻¹
NiCl ₂ · 6 H ₂ O	0.03	g L ⁻¹
Na ₂ SeO ₃ · 5H ₂ O	0.30	mg L ⁻¹

Table A.2 Vitamin solution of DSMZ Medium 141.

Vitamin solution		
Biotin	2.00	mg L ⁻¹
Folic acid	2.00	mg L ⁻¹
Pyridoxine-HCl	10.00	mg L ⁻¹
Thiamine-HCl · 2H ₂ O	5.00	mg L ⁻¹
Riboflavin	5.00	mg L ⁻¹
Nicotinic acid	5.00	mg L ⁻¹
D-Ca-pantothenate	5.00	mg L ⁻¹
Vitamin B12	0.10	mg L ⁻¹
p-aminobenzoic acid	5.00	mg L ⁻¹
Lipoic acid	5.00	mg L ⁻¹

A.3 X-Ray diffraction after microbial reduction experiments

For XRD analysis, microbial reduction was stopped by resuspending approximately 10 mg of the solid phase in 1 mL of anoxic 4 μM HgCl_2 . After drying the suspension under N_2 -atmosphere on glass slides of 25 mm, the samples were transferred to bottles flushed with N_2 , transported to the XRD chamber and analyzed in the absence of oxygen. XRD patterns of the solid post-incubation phase were recorded using a PANalytical X'Pert PRO MPD Θ - Θ (Kassel, Germany) diffractometer (CuK α radiation generated at 40 kV and 30 mA), equipped with a variable divergence slit (20 mm irradiated length), a primary and secondary soller slit, a proportional counter, a secondary monochromator, and a humidity chamber. The chamber CHC plus (Anton Paar, Austria) was purged with N_2 gas and relative humidity (RH) was monitored by a RH sensor in the chamber next to the sample. The oriented mounts were scanned from 2° to 80° 2Θ with a step size of 0.03° 2Θ . The measuring time varied between 10 and 60 s per step.

Appendix B: Characterization of Fe Oxides and Adsorption Complexes

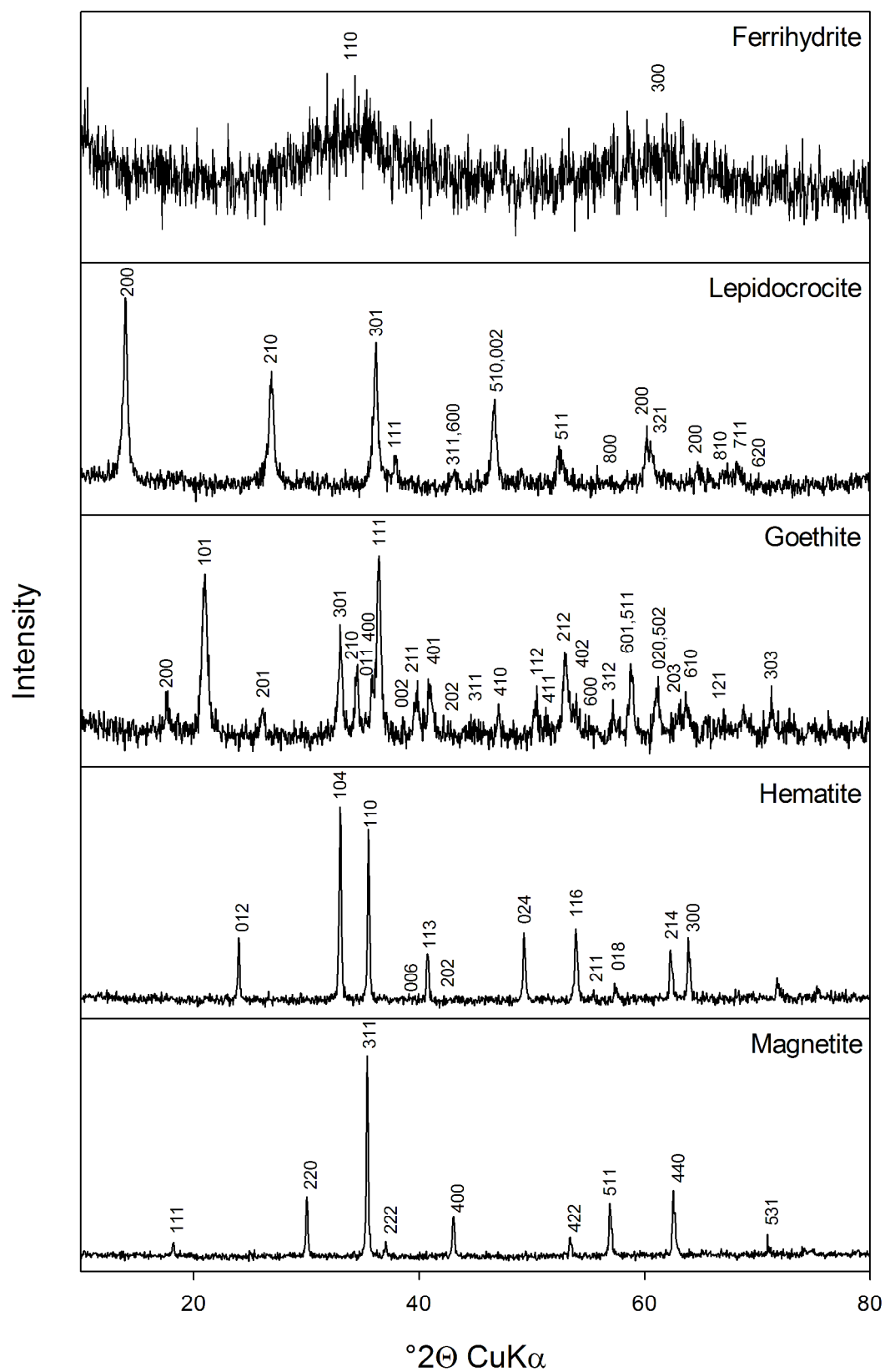


Fig. B.3 XRD diagrams of the pure Fe oxides. Numbers above peaks represent Miller indices.

STUDY II

Table B.2 Fe, C and N contents of the adsorption complexes. Values in parentheses depict the standard deviation of triplicate measurements.

Fe oxide	Type of NOM	Approximate C loading	Fe content (mg g ⁻¹)	C content (mg g ⁻¹)	N content (mg g ⁻¹)	
Ferrihydrite	EPS	5	757.0	6.3 (0.0)	1.1 (0.1)	
		10	750.9	10.5 (2.6)	1.5 (0.0)	
		20	738.1	19.3 (0.2)	2.6 (0.1)	
	Beech Oi	5	751.5	5.8 (2.0)	0.4 (0.2)	
		10	749.0	11.7 (0.1)	0.9 (0.0)	
		20	734.3	21.9 (0.7)	1.5 (0.3)	
		40	705.5	43.3 (0.0)	5.2 (0.1)	
	Spruce Oa	5	756.5	6.7 (0.4)	0.3 (0.2)	
		10	750.9	10.4 (0.1)	0.8 (0.0)	
		20	745.9	23.8 (0.1)	0.8 (0.0)	
	Lepidocrocite	EPS	5	618.3	8.2 (0.0)	1.3 (0.1)
			10	612.1	13.4 (0.0)	1.7 (0.1)
20			595.1	28.1 (0.0)	4.4 (0.2)	
Beech Oi		5	618.6	8.0 (0.1)	0.6 (0.2)	
		10	613.8	12.0 (0.1)	2.1 (0.0)	
		20	603.4	20.8 (0.1)	2.8 (0.1)	
		40	579.2	42.6 (0.0)	7.1 (0.2)	
Spruce Oa		5	620.2	6.7 (0.0)	0.6 (0.1)	
		10	611.8	13.6 (0.0)	1.0 (0.1)	
		20	600.6	23.3 (0.0)	1.3 (0.3)	
Goethite		EPS	5	620.6	6.4 (0.1)	1.3 (0.1)
			10	613.1	12.6 (0.7)	1.5 (0.2)
	20		601.0	22.9 (0.1)	4.3 (0.1)	
	Beech Oi	5	621.7	5.4 (0.0)	0.8 (0.0)	
		10	617.7	8.8 (0.0)	1.0 (0.1)	
		20	607.4	17.4 (0.0)	1.9 (0.1)	
		40	582.8	39.3 (0.2)	6.1 (0.3)	
	Spruce Oa	5	622.0	5.2 (0.3)	0.2 (0.4)	
		10	614.3	11.6 (0.1)	0.6 (0.1)	
		20	604.9	19.6 (0.0)	1.1 (0.1)	
	Hematite	EPS	2	697.8	1.2 (0.0)	0.5 (0.0)
			4	694.7	3.4 (0.1)	0.3 (0.2)
8			688.6	7.9 (0.1)	0.6 (0.0)	
Beech Oi		2	696.9	1.8 (0.0)	0.3 (0.0)	
		4	694.6	3.5 (0.1)	0.9 (0.0)	
		8	689.2	7.4 (0.0)	0.4 (0.0)	
		15	680.9	13.6 (0.0)	2.8 (0.0)	
Spruce Oa		2	696.9	1.8 (0.0)	0.4 (0.0)	
		4	694.1	3.9 (0.0)	0.4 (0.1)	
		8	688.4	8.0 (0.1)	0.4 (0.0)	

STUDY II

Magnetite	EPS	2	719.8	2.6 (0.3)	0.5 (0.0)
		4	717.8	4.0 (0.0)	0.8 (0.1)
		8	716.3	5.1 (0.0)	1.0 (0.0)
	Beech Oi	2	721.1	1.7 (0.3)	0.2 (0.0)
		4	717.8	4.1 (0.0)	0.6 (0.0)
		8	712.2	8.0 (0.0)	0.3 (0.0)
	Spruce Oa	15	704.7	13.4 (0.0)	2.3 (0.0)
		2	720.7	2.0 (0.1)	0.3 (0.0)
		4	718.4	3.6 (2.2)	0.3 (0.0)
		8	712.1	8.0 (0.0)	0.2 (0.1)

STUDY II

Table B.2 P and S contents of the adsorption complexes. Values in parentheses depict the standard deviation of triplicate measurements.

Fe oxide	Type of NOM	Approximate C loading	P content (mg g ⁻¹)	S content (mg g ⁻¹)	
Ferrihydrite	EPS	5	0.35 (0.00)	0.03 (0.00)	
		10	0.66 (0.00)	0.06 (0.00)	
		20	1.22 (0.12)	0.10 (0.01)	
	Beech Oi	5	0.15 (0.00)	0.06 (0.00)	
		10	0.31 (0.00)	0.13 (0.00)	
		20	0.92 (0.00)	0.24 (0.00)	
		40	7.54 (0.00)	4.17 (0.00)	
	Spruce Oa	5	0.11 (0.00)	0.31 (0.00)	
		10	0.31 (0.00)	0.86 (0.01)	
		20	1.33 (0.01)	3.51 (0.08)	
	Lepidocrocite	EPS	5	0.36 (0.00)	0.03 (0.00)
			10	0.72 (0.00)	0.07 (0.00)
20			1.91 (0.00)	0.17 (0.00)	
Beech Oi		5	0.15 (0.00)	0.05 (0.00)	
		10	0.31 (0.00)	0.14 (0.00)	
		20	0.92 (0.00)	0.15 (0.00)	
		40	6.60 (0.07)	4.17 (0.00)	
Spruce Oa		5	0.11 (0.00)	0.31 (0.00)	
		10	0.31 (0.00)	0.30 (0.18)	
		20	1.24 (0.04)	0.72 (1.18)	
Goethite		EPS	5	0.36 (0.00)	0.03 (0.00)
			10	0.72 (0.00)	0.07 (0.00)
	20		1.89 (0.00)	0.16 (0.00)	
	Beech Oi	5	0.15 (0.00)	0.05 (0.00)	
		10	0.31 (0.00)	0.12 (0.00)	
		20	0.92 (0.00)	0.16 (0.00)	
		40	7.41 (0.10)	4.17 (0.00)	
	Spruce Oa	5	0.11 (0.00)	0.28 (0.00)	
		10	0.16 (0.10)	0.30 (0.04)	
		20	1.27 (0.01)	0.31 (0.35)	
	Hematite	EPS	2	0.10 (0.00)	0.00 (0.00)
			4	0.12 (0.00)	0.00 (0.00)
8			0.20 (0.01)	0.01 (0.00)	
2			0.00 (0.00)	0.00 (0.00)	
4			0.00 (0.00)	0.00 (0.00)	
Beech Oi		8	0.06 (0.01)	0.00 (0.00)	
		15	0.09 (0.37)	0.02 (0.20)	
		2	0.16 (0.00)	0.34 (0.00)	
Spruce Oa		4	0.17 (0.00)	0.99 (0.00)	
		8	0.91 (0.00)	1.98 (0.00)	

STUDY II

Magnetite	EPS	2	0.24 (0.00)	0.00 (0.00)
		4	0.41 (0.00)	0.00 (0.00)
		8	0.58 (0.00)	0.00 (0.00)
Beech Oi		2	0.00 (0.00)	0.00 (0.00)
		4	0.10 (0.00)	0.00 (0.00)
		8	0.15 (0.00)	0.00 (0.00)
Spruce Oa		15	0.22 (0.32)	0.03 (0.13)
		2	0.01 (0.00)	0.00 (0.00)
		4	0.02 (0.00)	0.00 (0.00)
		8	0.49 (0.01)	0.00 (0.37)

Table B.3 Specific ultra violet absorption (SUVA) characterizing the pre- and post-sorption solution of the adsorption complexes.

Fe oxide	Type of NOM	Approximate C loading	SUVA _{post-sorption} at 280 nm (L mg C ⁻¹ cm ⁻¹)	SUVA _{post-sorption} /SUVA _{pre-sorption}
Ferrihydrite	EPS	5	0.0008	0.10
		10	0.0004	0.04
		20	0.0039	0.46
	Beech Oi	5	0.0027	0.15
		10	0.0018	0.14
		20	0.0064	0.66
		40	0.0238	1.10
	Spruce Oa	5	0.0138	0.36
		10	0.0418	0.77
20		0.0471	1.24	
Lepidocrocite	EPS	5	0.0058	0.67
		10	0.0001	0.01
		20	0.0040	0.47
	Beech Oi	5	0.0047	0.26
		10	0.0035	0.26
		20	0.0045	0.46
		40	0.0208	1.03
	Spruce Oa	5	0.0125	0.33
		10	0.0162	0.30
20		0.0387	1.02	
Goethite	EPS	5	0.0053	0.62
		10	0.0030	0.35
		20	0.0018	0.21
	Beech Oi	5	0.0036	0.20
		10	0.0038	0.29
		20	0.0047	0.49
		40	0.0214	1.08
	Spruce Oa	5	0.0138	0.36
		10	0.0114	0.21
20		0.0384	1.01	
Hematite	EPS	2	0.0076	0.90
		4	0.0087	1.02
		8	0.0088	1.03
	Beech Oi	2	0.0103	0.90
		4	0.0266	1.07
		8	0.0224	1.00
		15	0.0160	1.34
	Spruce Oa	2	0.0348	0.67
		4	0.0737	0.89
8		0.0657	0.88	

STUDY II

Magnetite	EPS	2	0.0076	0.89
		4	0.0036	0.43
		8	0.0085	1.00
Beech Oi		2	0.0067	0.59
		4	0.0228	1.01
		8	0.0131	1.15
Spruce Oa		15	0.0149	1.31
		2	0.0376	0.64
		4	0.0645	0.70
		8	0.0667	0.96

STUDY II

Table B.4 Desorbed organic carbon (OC_{desorbed}) after equilibration of the adsorption complexes with microbial nutrient solution for 24 h and derived complexation capacity of Fe(II). Values in parentheses depict the standard deviation of triplicate measurements.

Fe oxide	Type of NOM	Approximate C loading	OC_{desorbed} (mg g^{-1})	Complexation capacity (mMol Fe(II))	
Ferrihydrite	EPS	5	0.00 (0.00)	0.000	
		10	0.04 (0.09)	0.000	
		20	0.34 (0.07)	0.002	
	Beech Oi	5	2.29 (0.44)	0.014	
		10	3.24 (0.55)	0.019	
		20	7.01 (0.53)	0.042	
		40	9.78 (0.77)	0.059	
	Spruce Oa	5	0.46 (0.14)	0.003	
		10	1.93 (0.90)	0.012	
		20	3.85 (0.39)	0.023	
	Lepidocrocite	EPS	5	1.36 (0.55)	0.008
			10	1.63 (0.18)	0.010
20			3.95 (2.06)	0.024	
Beech Oi		5	2.43 (0.12)	0.015	
		10	3.31 (0.10)	0.020	
		20	5.02 (0.51)	0.030	
		40	8.40 (0.67)	0.050	
Spruce Oa		5	1.67 (0.21)	0.010	
		10	3.80 (0.15)	0.023	
		20	6.73 (0.26)	0.040	
Goethite		EPS	5	1.36 (0.22)	0.008
			10	2.66 (0.31)	0.016
	20		5.58 (0.59)	0.034	
	Beech Oi	5	1.80 (0.30)	0.011	
		10	2.65 (0.30)	0.016	
		20	5.27 (0.63)	0.032	
		40	8.87 (1.41)	0.053	
	Spruce Oa	5	2.10 (0.18)	0.013	
		10	4.21 (0.37)	0.025	
		20	5.81 (0.50)	0.035	
	Hematite	EPS	2	0.71 (0.06)	0.004
			4	0.73 (0.08)	0.004
8			0.76 (0.12)	0.005	
Beech Oi		2	0.70 (0.16)	0.004	
		4	0.78 (0.14)	0.005	
		8	0.87 (0.07)	0.005	
		15	1.34 (0.17)	0.008	
Spruce Oa		2	0.68 (0.13)	0.004	
		4	0.71 (0.10)	0.004	
		8	0.73 (0.09)	0.004	

STUDY II

Magnetite	EPS	2	1.23 (0.09)	0.007
		4	1.33 (0.15)	0.008
		8	1.80 (1.32)	0.011
	Beech Oi	2	1.26 (0.15)	0.008
		4	1.31 (0.22)	0.008
		8	1.34 (0.21)	0.008
		15	1.77 (0.24)	0.011
	Spruce Oa	2	2.05 (0.62)	0.012
		4	2.19 (1.44)	0.013
		8	2.21 (1.44)	0.013

B.1 Bulk carbon speciation of original and adsorbed NOM

Analogous to Omoike and Chorover (2006), the main broad signals of the FTIR spectrum of pure EPS (Fig. 1) could be assigned to vibrations of amide bonds in proteins (amide I, 1650 cm^{-1}), deformation vibrations of N-H and valence vibrations of C-N in -CO-NH- of proteins (amide II, 1544 cm^{-1}), symmetric C-O vibrations of carboxylic groups in complexes (1403 cm^{-1}), and C-O stretching vibrations of polysaccharides overlapping with symmetric stretching vibrations of P=O in the phosphodiester backbone of nucleic acids (1058 cm^{-1}) with less pronounced bands for asymmetric stretching vibrations of P=O in the phosphodiester backbone of nucleic acids (1228 cm^{-1}), O-H deformation and ring vibrations of polysaccharides (1128 cm^{-1}), and asymmetric ester O-P-O stretching (973 cm^{-1}). In line with previous studies on adsorption of *Bacillus subtilis*-derived EPS to goethite (Liu et al., 2013; Omoike and Chorover, 2006), the FTIR difference spectra of the EPS adsorption complexes indicated preferential sorption of protein structures to the Fe oxides in comparison to polysaccharides. Increased bands of amides were most pronounced for EPS ferrihydrite adsorption complexes and decreased in the order lepidocrocite > goethite > hematite > magnetite. The at least partial contribution of nucleic acids to the band at 1058 cm^{-1} for the adsorption complexes is supported by the complete depletion of P in the post-sorption solution (see also Table B.2).

The SUVA at 280 nm of the EPS solution both before and after adsorption revealed very small contents of aromatic moieties rendering their adsorption and sorptive fractionation to be negligible (Table B.3). These results are consistent with the solid-state ^{13}C -NMR spectrum indicating less than 5 % of aromatic C for pure EPS, while O alkyl C was the most abundant functional group with 77 % (Poggenburg et al., 2016).

The FTIR spectra of pure beech Oi- and spruce Oa-derived NOM (Fig. 1) were governed by C=O stretching of deprotonated carboxylic groups (1592 and 1610 cm^{-1}), carboxylic groups in complexes (1400 and 1425 cm^{-1}), and C-O stretching of polysaccharides (1030-1075 cm^{-1}) with minor contributions of protonated carboxylic groups and C-O stretching of deprotonated carboxylic groups indicated by the additional shoulders in the spruce Oa spectrum at 1720 cm^{-1} and 1320 cm^{-1} , respectively (Scheel et al., 2008). The band at 1078 cm^{-1} can either be assigned to polysaccharides or, most likely to a larger part for the beech Oi-derived NOM, to symmetric P=O stretching (Omoike and Chorover, 2006). This observation is supported by the large phosphate content in the dissolved beech Oi-derived NOM (51.4 mg L^{-1}) in comparison to the spruce Oa-derived NOM (7.9 mg L^{-1}) before freeze-drying.

In accordance with the results of the FTIR analysis, solid-state ^{13}C -NMR spectroscopy showed that spruce Oa-derived NOM exhibited the largest relative amount of carboxylic and aryl C (15 % and 18 %, respectively), followed by beech Oi-derived NOM (7 and 11 %). Mirroring the trend seen for EPS, O-alkyl C made up the largest part of OC for both types of plant-derived NOM (42 % for spruce Oa, 61 % for beech Oi; Poggenburg et al., 2016).

Adsorption of beech Oi- and spruce Oa-derived NOM to the Fe oxides generally resulted in a depletion of polysaccharides in comparison to deprotonated carboxylic groups (1592/1610 cm^{-1}) and carboxylic groups in complexes (1400/1425 cm^{-1}) as reported for ferrihydrite (Chen et al., 2014; Eusterhues et al., 2011), goethite (Kaiser and Guggenberger,

2007), and hematite (Kaiser and Guggenberger, 2003) before. Furthermore, the band indicative of carboxylic groups in complexes exhibited an increased intensity shifting towards smaller wavenumbers along with decreasing C loading of the adsorption complexes, whereas the band pointing towards deprotonated carboxylic groups shifted towards smaller wavenumbers along with increasing C loading. The band representing protonated carboxylic groups (1720 cm^{-1}) disappeared for smaller C loadings but reappeared for larger C loadings. Since the decrease of the protonated carboxylic band in combination with the shift of the complexed carboxylic band reflects carboxylate-Fe complex formation via ligand exchange (Chen et al., 2014; Kaiser and Guggenberger, 2007), while the shift of the deprotonated carboxylic band designates weaker outer-sphere complex formation (Eusterhues et al., 2011; Kaiser and Guggenberger, 2007), these findings suggest the dominance of NOM being tightly bound via multiple strong carboxylate complex bonds at smaller C loadings and more loosely bound compounds at larger C loadings of the adsorption complexes (Kaiser, 2003; Kaiser et al., 1997). For large C loadings of beech Oi adsorption complexes, the band at 1592 cm^{-1} shifted to 1547 cm^{-1} with an additional band appearing at 1648 cm^{-1} . While Eusterhues et al. (2011) explained a similar observation for forest floor extract adsorption to ferrihydrite with the formation of outer-sphere complexes by carboxylate, the possibility of a pronounced amide adsorption cannot entirely be excluded (Omoike and Chorover, 2006). Since the post-adsorption solution was for all adsorption complexes completely depleted of phosphate, parts of the C-O stretching polysaccharide band increasing analogous to increasing C loadings, can be attributed to adsorbed phosphorous compounds (Omoike and Chorover, 2006, see also Table B.2). Moreover, the shift of the band at 1075 cm^{-1} , which was more pronounced for the spruce Oa than the beech Oi-derived NOM, indicates the preferential sorption of specific polysaccharide compounds to the Fe oxides (Eusterhues et al., 2011).

In agreement with the larger content of aromatic compounds suggested by ^{13}C -NMR spectroscopy, the SUVA of spruce Oa-derived NOM ($0.055\text{ L mg C}^{-1}\text{ cm}^{-1}$) was larger than the SUVA of the beech Oi-derived NOM ($0.018\text{ L mg C}^{-1}\text{ cm}^{-1}$). Upon adsorption to the Fe oxides, the SUVA of beech Oi- and spruce Oa-derived NOM remaining in solution decreased by up to 87 % and 79 %, respectively (Table B.3). Although the relative sorptive fractionation of aromatic moieties was thus more pronounced for beech Oi-derived NOM, the adsorption of spruce Oa-derived NOM resulted in comparatively larger absolute contents of aromatic compounds. However, this effect diminished along with growing C loadings as reported previously (Chen et al., 2014; Kaiser and Guggenberger, 2007). Sorptive fractionation of aromatic compounds was comparable for ferrihydrite, lepidocrocite and goethite at similar C loadings, whereas the sorptive fractionation was less pronounced for the sorption of beech Oi- and spruce Oa-derived NOM to hematite and magnetite. The sharp decline in peak intensity around 1020 cm^{-1} for the lepidocrocite adsorption complex spectra can be attributed to Si-O-Si groups (Ellerbrock et al., 2016) and are a remnant of the difference spectra calculation process.

Appendix C: Mineral Transformation**Table C.1** Mineral transformation during reduction of adsorption complexes by *Shewanella putrefaciens* derived from XRD (an “x” depicts the formation of each respective mineral after 16 days of incubation)

Fe oxide	Type of NOM	Approximate C loading	w/o donor	extra DOM	Vivianite	Coprecipitate	Green rust
Ferrihydrite	EPS	5					
		10					
		20					
		20	√				
		20		√			x
	Beech Oi	5					
		10					
		20					
		40					
		40			√		x
	Spruce Oa	5					
		10					
		20					
		20	√				
		20			√		x
pure Fe oxide	-				x		
Lepidocrocite	EPS	5					
		10					
		20					
		20	√				
		20			√		x
	Beech Oi	5					
		10					
		20					
		40					
		40			√		x
	Spruce Oa	5					
		10					
		20					
		20	√				
		20			√		x
pure Fe oxide	-				x		
Goethite	EPS	5					
		10					
		20					
		20	√				
		20			√		x
	Beech Oi	5					
		10					
		20					
		40					
		40			√		x
	Spruce Oa	5					
		10					
		20					

STUDY II

		20	√				
		20		√			
	pure Fe oxide	-			x	x	
Hematite	EPS	2					
		4					
		8					
			8	√			
			8		√		
	Beech Oi	2					
		4					
		8					
			15				
			15		√		
	Spruce Oa	2					
		4					
8							
		8	√				
		8		√			
	pure Fe oxide	-					
Magnetite	EPS	2					
		4					
		8					
			8	√			
			8		√		
	Beech Oi	2					
		4					
		8					
			15				
			15		√		
	Spruce Oa	2					
		4					
8							
		8	√				
		8		√			
	pure Fe oxide	-					

STUDY II

Table C.3 Mineral transformation during reduction of adsorption complexes by *Geobacter metallireducens* derived from XRD (an “x” depicts the formation of each respective mineral after 16 days of incubation)

Fe oxide	Type of NOM	Approximate C loading	w/o donor	extra DOM	Vivianite	Coprecipitate	Green rust	
Ferrihydrite	EPS	5						
		10						
		20						
		20	√					
		20		√			x	
	Beech Oi	5						
		10						
		20						
		40						
		40			√			x
	Spruce Oa	5						
		10						
		20						
		20	√					
20			√				x	
pure Fe oxide	-				x			
Lepidocrocite	EPS	5						
		10						
		20						
		20	√					
		20		√			x	
	Beech Oi	5						
		10						
		20						
		40						
		40			√			x
	Spruce Oa	5						
		10						
		20						
		20	√					
20			√				x	
pure Fe oxide	-				x			
Goethite	EPS	5						
		10						
		20						
		20	√					
		20		√			x	
	Beech Oi	5						
		10						
		20						
		40						
		40			√			x
	Spruce Oa	5						
		10						
		20						
		20	√					
20			√				x	

STUDY II

	pure Fe oxide	-			x		
Hematite	EPS	2					
		4					
		8					
		8	√				
		8		√		x	
	Beech Oi	2					
		4					
		8					
		15					
		15		√		x	
	Spruce Oa	2					x
		4					x
		8					x
		8	√				
		8		√		x	
	pure Fe oxide	-			x		
Magnetite	EPS	2					
		4					
		8					
		8	√				
		8		√		x	
	Beech Oi	2					
		4					
		8					
		15					
		15		√		x	
	Spruce Oa	2					x
		4					x
		8					x
		8	√				
		8		√		x	
	pure Fe oxide	-			x		

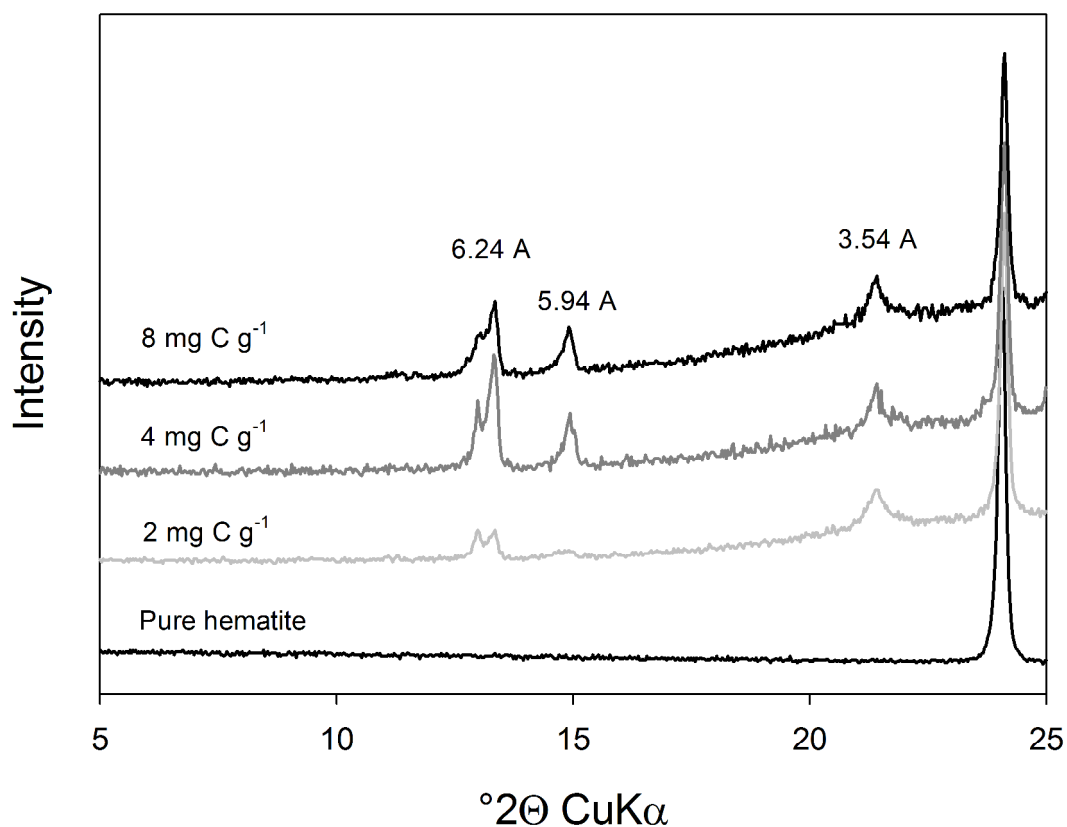


Fig. C.1 XRD diagrams of the hematite spruce Oa adsorption complexes after incubation with *Geobacter metallireducens* for 16 days.

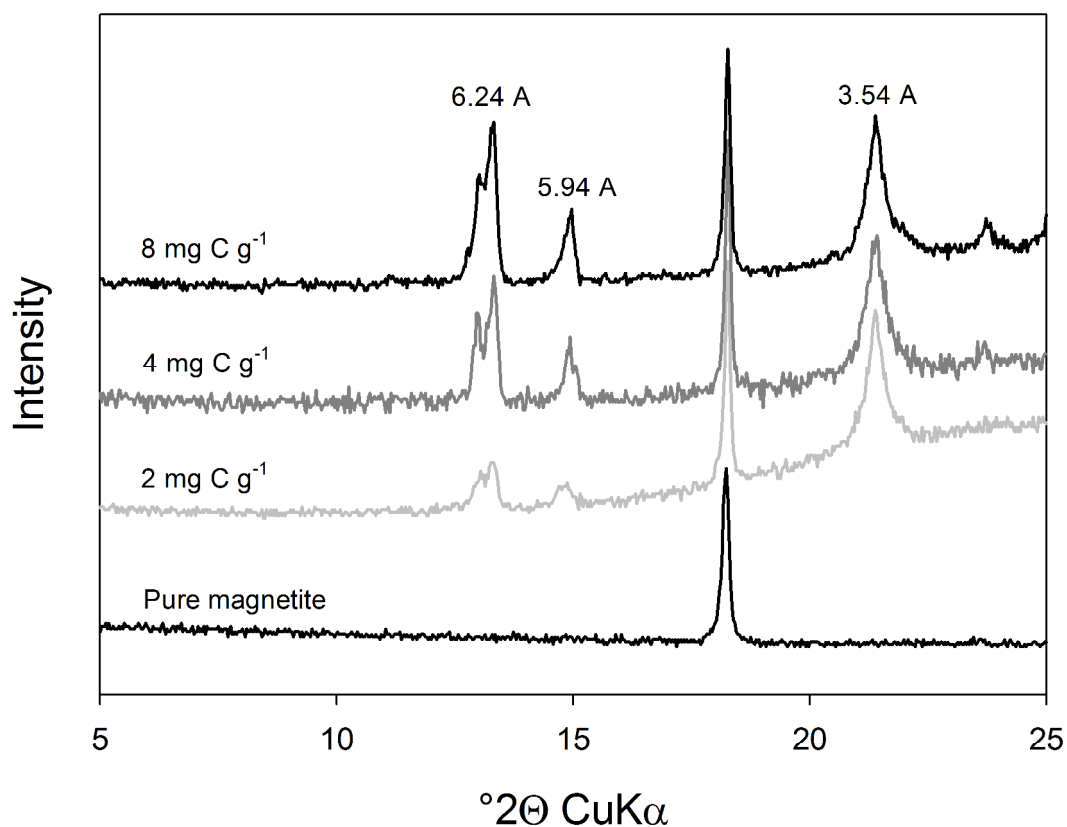


Fig. C.2 XRD diagrams of the magnetite spruce Oa adsorption complexes after incubation with *Geobacter metallireducens* for 16 days.

Appendix D: Partial Regression

Table D.1 Partial least-squares regression (PLSR) analyzing the partial correlation of different adsorption complexes-derived characteristics with the initial microbial Fe reduction rates

Factor	<i>Shewanella putrefaciens</i>		<i>Geobacter metallireducens</i>	
	R ²	p-value	R ²	p-value
Particle size	0.02	0.11	0.21	9.18×10^{-7}
SSA	0.01	0.35	0.03	0.07
EM	0.01	0.45	0.04	0.05
C loading	0.00	0.52	0.02	0.19
C _{desorbed}	0.32	5.56×10^{-10}	0.00	0.61
SUVA	0.00	0.57	0.01	0.28
XPS-C	0.01	0.10	0.00	0.76

References

- Chen, C., Dynes, J.J., Wang, J., Sparks, D.L., 2014. Properties of Fe-organic matter associations via coprecipitation versus adsorption. *Environ. Sci. Technol.* 48, 13751–13759. doi:10.1021/es503669u
- de Brouwer, J.F.C., Wolfstein, K., Stal, L.J., 2002. Physical characterization and diel dynamics of different fractions of extracellular polysaccharides in an axenic culture of a benthic diatom. *Eur. J. Phycol.* 37, 37–44.
- Ellerbrock, R.H., Leue, M., Gerke, H.H., 2016. Interpretation of infrared spectra for OM characterization of soil structural surfaces of Bt-horizons. *J. Plant Nutr. Soil Sci.* 179, 29–38. doi:10.1002/jpln.201400619
- Eusterhues, K., Rennert, T., Knicker, H., Kögel-Knabner, I., Totsche, K.U., Schwertmann, U., 2011. Fractionation of organic matter due to reaction with ferrihydrite: coprecipitation versus adsorption. *Environ. Sci. Technol.* 45, 527–33. doi:10.1021/es1023898
- Kaiser, K., 2003. Sorption of natural organic matter fractions to goethite (α -FeOOH): effect of chemical composition as revealed by liquid-state ^{13}C NMR and wet-chemical analysis. *Org. Geochem.* 34, 1569–1579. doi:10.1016/S0146-6380(03)00120-7
- Kaiser, K., Guggenberger, G., 2007. Sorptive stabilization of organic matter by microporous goethite: sorption into small pores vs. surface complexation. *Eur. J. Soil Sci.* 58, 45–59. doi:10.1111/j.1365-2389.2006.00799.x
- Kaiser, K., Guggenberger, G., 2003. Mineral surfaces and soil organic matter. *Eur. J. Soil Sci.* 54, 219–236.
- Kaiser, K., Guggenberger, G., Haumaier, L., Zech, W., 1997. Dissolved organic matter sorption on subsoils and minerals studied by ^{13}C -NMR and DRIFT spectroscopy. *Eur. J. Soil Sci.* 48, 301–310.
- Liu, X., Eusterhues, K., Thiema, J., Ciobota, V., Höschen, C., Mueller, C.W., Küsel, K., Kögel-Knabner, I., Rösch, P., Popp, J., Totsche, K.U., 2013. STXM and NanoSIMS investigations on EPS fractions before and after adsorption to goethite. *Environ. Sci. Pollut. Res. Int.* 47, 3158–3166. doi:10.1021/es3039505
- Lunau, M., Lemke, A., Walther, K., Martens-Habbena, W., Simon, M., 2005. An improved method for counting bacteria from sediments and turbid environments by epifluorescence microscopy. *Environ. Microbiol.* 7, 961–968. doi:10.1111/j.1462-2920.2005.00767.x
- Omoike, A., Chorover, J., 2006. Adsorption to goethite of extracellular polymeric substances from *Bacillus subtilis*. *Geochim. Cosmochim. Acta* 70, 827–838. doi:10.1016/j.gca.2005.10.012
- Poggenburg, C., Mikutta, R., Sander, M., Schippers, A., Marchanka, A., Dohrmann, R., Guggenberger, G., 2016. Microbial reduction of ferrihydrite-organic matter coprecipitates by *Shewanella putrefaciens* and *Geobacter metallireducens* in comparison to mediated electrochemical reduction. *Chem. Geol.* 447, 133–147. doi:10.1016/j.chemgeo.2016.09.031
- Scheel, T., Haumaier, L., Ellerbrock, R.H., Rühlmann, J., Kalbitz, K., 2008. Properties of organic matter precipitated from acidic forest soil solutions. *Org. Geochem.* 39, 1439–1453. doi:10.1016/j.orggeochem.2008.06.007

4 Study III

Siderophore-promoted dissolution of ferrihydrite associated with adsorbed and coprecipitated natural organic matter

Contribution: I designed the experiments, prepared the Fe-organic associations, conducted most of the laboratory experiments and analyses, collected and evaluated the data, compiled the tables and graphs, and wrote the manuscript.

Submitted for publication in Organic Geochemistry

**Siderophore-promoted dissolution of ferrihydrite associated with
adsorbed and coprecipitated natural organic matter**

Christine Poggenburg^{1,}, Robert Mikutta², Patrick Liebmann¹,
Markus Koch¹, Georg Guggenberger¹*

¹ Institute of Soil Science and Centre for Solid State Chemistry and New Materials (ZFM),
Leibniz Universität Hannover, Herrenhäuser Straße 2, 30419 Hannover, Germany

² Soil Science and Soil Protection, Martin Luther University Halle-Wittenberg,
Von-Seckendorff-Platz 3, 06210 Halle (Saale), Germany

*Corresponding author: poggenburg@ifbk.uni-hannover.de, +49 5117622625

Abstract

Acquisition of Fe(III) from hardly soluble Fe oxyhydroxides by bacteria, fungi, and plants in the soil is often facilitated by Fe(III)-chelating siderophores. While the siderophore-promoted dissolution of pure Fe oxyhydroxides and the influence of defined low molecular weight organic acids has been investigated meticulously, studies examining Fe oxyhydroxides coated with more complex adsorbed organic matter (OM) or Fe-OM coprecipitates have been sparse. This study therefore explored the impact of the composition of both adsorbed and coprecipitated OM on the siderophore-promoted dissolution of ferrihydrite (Fh) in relation to (i) surface site coverage and pore blockage, (ii) aggregation state, (iii) charge characteristics, and (iv) crystallinity. Fh-OM adsorption complexes and Fe-OM coprecipitates were synthesized in addition to pure Fh using OM of different origin (extracellular polymeric substances of *Bacillus subtilis*, natural OM (NOM) extracted from soil Oi and Oa horizons). The Fe-organic associations were characterized by N₂ gas adsorption, X-ray photoelectron spectroscopy (XPS), electrophoretic mobility, particle size measurements and desorption experiments. Siderophore-mediated dissolution experiments with desferrioxamine-B (DFOB) were conducted at pH 4 and pH 7. At pH 4, adsorbed OM provided a more effective protection against DFOB due to its larger sorption affinity. At pH 7, the surface site blockage by adsorbed OM at comparable C loadings was less effective, while less aggregated particles were more prone to dissolution. The accelerating and inhibiting influence of OM coprecipitated with Fe on DFOB-promoted dissolution largely varied with its composition. Our results corroborate the importance of considering the heterogeneous composition of soil OM when investigating the mobilization of Fe-organic associations.

Key Words: coprecipitation; desferrioxamine-B; ferrihydrite; extracellular polymeric substances; mineral-organic associations; natural organic matter; siderophores

1 INTRODUCTION

In well aerated soil, associations of iron (Fe) oxyhydroxides with soil organic matter (OM) are regarded as fairly long-term stable phases (Kaiser and Guggenberger, 2007; Mikutta et al., 2006). Under these conditions, the associated OM is thus protected against microbial decomposition (Canfield et al., 1993) with the accompanying decreased emission of greenhouse gases (CO₂, CH₄, N₂O), while the leaching of associated organic contaminants (Lovley and Anderson, 2000), complexed, adsorbed and incorporated heavy metals (Brümmer et al., 2013; Perelomov et al., 2011; Violante et al., 2003) or adsorbed oxyanions (Mesuere and Fish, 1999; Sannino et al., 2009) into the soil solution and groundwater is kept at a minimum. Their stability is further increased by the very low solubility of Fe oxyhydroxides under circumneutral conditions (Schwertmann, 1991). Since Fe is an essential micronutrient for many organisms, several bacteria, fungi and graminaceous plants meet this constraint by exuding Fe-chelating siderophores (Neilands, 1957; Roemheld, 1991; Takagi, 1976; Winkelmann, 1992). Exhibiting a large specificity and selectivity for Fe(III), siderophores act as a ligand towards Fe(III) thereby promoting solubilization of otherwise poorly soluble Fe oxyhydroxides.

While the siderophore-promoted dissolution of pure Fe oxyhydroxides has been investigated meticulously (Kraemer, 2004; Kraemer et al., 2006), studies under more realistic conditions examining Fe oxyhydroxides coated with adsorbed OM or Fe-OM coprecipitates have been sparse (Goebel et al., 2017; Mikutta and Kretzschmar, 2008). The process of Fe-organic coprecipitation comprises several parallel occurring and therefore interacting mechanisms, including the complexation of hydrolyzed Fe(II) and Fe(III) by OM, precipitation of insoluble Fe-organic complexes, adsorption of OM to ferrihydrite (Fh), and occlusion of pure OM precipitates into newly formed Fh aggregates (Kleber et al., 2015). In contrast to mineral-organic associations that are exclusively formed by adsorption of OM to already existing pure Fh surfaces, Fe-OM coprecipitates exhibit smaller crystal sizes, a more

defective crystallographic structure (Cismasu et al., 2011; Eusterhues et al., 2008; Schwertmann et al., 2005), and different aggregation properties (Mikutta et al., 2012). Fe-OM coprecipitation occurs under a range of different soil environmental conditions, like, e.g., well drained soils (Dolfing et al., 1999), temporarily waterlogged paddy soils (Kögel-Knabner et al., 2010), acidic mineral soils (Nierop et al., 2002) like Spodosols (Wagai and Mayer, 2007), acid mine drainages (Cheng et al., 2009), or industrial coagulation water treatment landfills (Bachand et al., 2000; Downing et al., 2008; Henneberry et al., 2011). Not restricted to plant-derived natural OM (NOM), coprecipitated organic compounds can also be of microbial origin such as extracellular polymeric substances (EPS) (Rancourt et al., 2005; Marschner et al., 2008; Mikutta et al., 2009), which are found in biofilms originating from both living and dead microbial cells (Beveridge et al., 1997).

Combining low molecular weight organic acids (LMWO) like oxalate, citrate, malonate and ascorbate with the siderophore desferrioxamine-B (DFOB) has been reported to increase dissolution rates of Fe oxyhydroxides due to synergistic effects (Cheah et al., 2003; Reichard et al., 2007; Wang et al., 2015). However, the effect of more complex, heterogeneous natural organic matter adsorbed to Fe oxyhydroxide has not been addressed systematically so far.

The abiotic reduction of Fe oxyhydroxides has repeatedly been reported to depend on their specific surface area (SSA) and the underlying crystal order (Larsen and Postma, 2001; Roden, 2003). Since both adsorbed and coprecipitated OM decrease the SSA by blocking surface sites on the Fh surfaces and initiating aggregation (Eusterhues et al., 2011; Kaiser and Guggenberger, 2007, 2003), sorbed OM is expected to decelerate the abiotic dissolution of both adsorption complexes and coprecipitates. While Eusterhues et al. (2014) found decreased dithionite-induced Fe dissolution rates for both adsorbed and coprecipitated NOM extracted from a forest floor, Mikutta and Kretzschmar (2008) reported increased siderophore-induced Fe dissolution rates of polygalacturonic acid-derived Fe coprecipitates in comparison to pure Fh. Latter was also observed for abiotic electrochemical reduction of both microbial- and

plant-derived OM (Poggenburg et al., 2016). Furthermore, Mikutta and Kretzschmar (2008) attributed the increased dissolution of the same coprecipitates to smaller and less aggregated particles induced by greater charged-derived repulsive forces, with only a minor influence of their crystallinity. Poggenburg et al. (2016), on the other hand, found increasing electrochemical dissolution rates with decreasing crystallinity for coprecipitates of similar particle size. These discrepancies mirror the difficulty of assessing the reactivity of Fe-OM coprecipitates due to their wide variability in physicochemical properties. Special attention should therefore be paid to the composition of the coprecipitated OM.

The studies of Fe-organic associations mentioned previously were conducted at circumneutral pH. Particularly the rhizosphere, however, usually exhibits lower pH values, as organic acids and protons are released into the soil via plant roots (April and Keller, 1990; Bonneville et al., 2011; Brantley et al., 2011). The pH affects the charge and therefore particle size and aggregation of Fe-organic associations (Alvarez-Puebla and Garrido, 2005; Angelico et al., 2014; Siéliéchi et al., 2008) and ultimately the sorption and desorption behaviour of OM (Kaiser and Zech, 1999). Thus, it should be considered as well.

Combining the factors discussed above, the purpose of this study was, therefore, to investigate the impact of the composition of both adsorbed and coprecipitated OM on the ligand-promoted dissolution of Fe-organic associations with regard to (i) surface site coverage and/or pore blockage, (ii) aggregation state, (iii) charge characteristics, and (iv) crystallinity. In order to explore these relations, both Fh-OM adsorption complexes and Fe-OM coprecipitates were synthesized in addition to pure Fh using OM of microbial origin (extracellular polymeric substance derived from *Bacillus subtilis*) and two types of NOM of plant origin differing in their composition (derived from the Oi horizon of a Cambisol and the Oa horizon of a Podzol). The properties of initial Fh, adsorption complexes and coprecipitates were determined by N₂ gas adsorption, X-ray photoelectron spectroscopy (XPS), electrophoretic mobility, particle size measurements and desorption experiments.

Siderophore-mediated dissolution experiments with DFOB were conducted at both pH 4 and pH 7. DFOB was chosen as a trihydroxamate siderophore, which has been reported to evenly promote the dissolution of Fe oxyhydroxides over a pH range of 3 to 9 (Yoshida et al., 2002), thus facilitating to specifically assess the influence of adsorbed and coprecipitated OM.

2 MATERIAL AND METHODS

2.1 Extraction of Extracellular Polymeric Substances and Natural Organic Matter

Microbial-derived EPS and plant-derived NOM were prepared as described by Poggenburg et al. (2016). Briefly, EPS were separated from a culture of *Bacillus subtilis* (ATCC 7003; BCCMTM/LMG Bacteria Collection) grown on LB-Lennox medium by centrifugation at early stationary growth phase, precipitated with 277 K cold ethanol, purified via dialysis against sterile H₂O for 72 h, and freeze-dried. Fluorescence microscopy revealed approximately 7.85×10^6 cells mg⁻¹ of residual cells in the purified EPS.

Plant-derived NOM was extracted from the Oi horizon of a Eutric Cambisol under European beech and from the Oa horizon of a Haplic Podzol under Norway spruce via equilibration with doubly deionized H₂O for 16 h. The extracts were filtrated through 0.7- μ m glass fiber filters (GF 92, Whatman GmbH, Dassel, Germany) and 0.45- μ m cellulose nitrate membrane filters (G, Sartorius AG, Göttingen, Germany).

2.2 Preparation of Ferrihydrite and Coprecipitates

Two-line Fh was prepared by titrating 0.2 M FeCl₃ solution to a pH of 7.0 with 1 M NaOH (Schwertmann and Cornell, 2000). Coprecipitates were synthesized by rapidly mixing a solution of FeCl₃ and each respective OM to obtain initial Fe(III) and OC concentrations of 4.17 mM and thus a molar Fe(III)/C ratio of 1.0. The solutions were instantly titrated to a pH of 7.0 to avoid aggregation of OM induced by the initially acidic conditions (Angelico et al., 2014; Mikutta et al., 2014). The suspensions were dialyzed against doubly deionized H₂O

(Spectra/Por 7, 1,000 MWCO) until the electric conductivity was $<10 \mu\text{S cm}^{-1}$, to minimize structural change and aggregation due to centrifugation. After freeze-drying, the precipitates were homogenized by sieving to a size of $<200 \mu\text{m}$.

2.3 Preparation of Adsorption Complexes

Adsorption complexes with differing OM loadings were prepared by weighing 1 to 5 g of Fh into 1-L polyethylene bottles and adding 200 mL of doubly deionized H_2O . Both the Fh suspension and the EPS-, beech Oi- and spruce Oa-derived solutions were adjusted to a pH of 4 using 0.1 M HCl and readjusted after equilibration for 16 h. The initial OC concentrations of the solutions ranged from 50 to 500 mg C L^{-1} with the ionic strength being balanced by KCl. Following the addition of 500 mL OM solution, the suspension was shaken manually and equilibrated for 30 min before readjusting the pH. After shaking for 24 h in the dark at 298 K and 15 rpm in an end-over-end shaker, the suspension was centrifuged for 1 h at 6000 g. The pH of the suspensions increased between 0.2 and 1.8 units upon adsorption, indicating sorption via ligand exchange. The adsorption complexes were washed with doubly deionized H_2O 2 to 3 times removing non-sorbed components, until the electric conductivity of the supernatant decreased to $<10 \mu\text{S cm}^{-1}$. Following freeze-drying, the adsorption complexes were sieved to a size $<200 \mu\text{m}$.

To examine both tightly bound OM at smaller loadings and more loosely bound OM at sorption maximum, the adsorption complexes covered approximate OC loadings of 5, 10, and 20 mg C g^{-1} for all three types of OM with a further adsorption complex of 40 mg C L^{-1} for beech Oi-derived NOM. The precise OC contents are provided in Table 1. For clarity, these will henceforth be referred to as small, medium and large C loading. The OC and total N contents of the adsorption complexes and the coprecipitates were determined with a CNS analyzer (Vario EL III, Elementar GmbH, Hanau, Germany). Total Fe contents were

quantified by inductively coupled plasma optical emission spectroscopy (ICP-OES, Varian 725-ES, Varian Inc., Palo Alto, CA, USA) following complete acidic digestion by 6 M HCl.

2.4 Characterization of Organic Matter, Ferrihydrite, Adsorption Complexes and Coprecipitates

2.4.1 X-ray photoelectron spectroscopy

X-ray photoelectron spectroscopy (XPS) spectra of the freeze-dried unreacted OM, Fh, the adsorption complexes, and the coprecipitates were obtained using a Kratos Axis Ultra DLD spectrometer (Kratos Analytical, Manchester, UK) providing monochromatic Al K α -radiation and an excitation energy of 1486.7 eV. For survey spectra, the pass energy was set to 160 eV with a step size of 1 eV. For C1s high resolution spectra, the pass energy was 10 eV with a step size of 0.1 eV. To specify different C oxidation states, the high resolution spectra were corrected for charge by shifting the C1s peak to 285.0 eV, normalized and fitted to a Shirley-type background with the Unifit 2010 software package (Hesse et al., 2003). In accordance with Gerin et al. (2003), Omoike and Chorover (2004), and Leone et al. (2006), the C1s peak was split into four subpeaks: (i) aliphatic and aromatic carbon exhibiting bonds to carbon and hydrogen (C-C, C=C, C-H; at 285.0 ± 0.1 eV), (ii) carbon exhibiting a single bond to oxygen or nitrogen as in carbohydrates and amines (C-O, C-N; at 286.5 ± 0.2 eV), (iii) carbon exhibiting two bonds to oxygen as in aldehydes, ketones, and amides (C=O, O-C-O, O=C-N; at 288.0 ± 0.1 eV), (iv) carboxylic carbon exhibiting three bonds to oxygen (O-C=O; at 289.1 ± 0.2 eV).

2.4.2 Specific surface area and pore analysis

The SSA of Fh, the adsorption complexes, and the coprecipitates was acquired in duplicate using an Autosorb-1 surface area analyzer (Quantachrome Instruments, Boynton Beach, FL, USA). Following degassing under vacuum at 313 K for 24 h, N₂ adsorption

isotherms were recorded at 77 K. The SSA was derived from adsorption data in the relative pressure range of 0.05 to 0.3 P/P_0 applying the Brunauer-Emmett-Teller (BET) equation (Brunauer et al., 1938). The total pore volume (TPV) was obtained from the last point of the adsorption isotherm at 0.995 P/P_0 . The micropore volume (<2 nm) was derived from the adsorption points <0.01 P/P_0 using the Dubinin-Radushkevich (DR) method (Gregg and Sing, 1982). The mesopore volume (2-50 nm) was quantified via the Barrett-Joyner-Halenda (BJH) method (Barrett et al., 1951). The small (2-10 nm) and large (10-50 nm) mesopores were determined by linear interpolation.

2.4.3 Electrophoretic mobility and particle size

The electrophoretic mobility (EM) of Fh, the adsorption complexes and the coprecipitates was determined in a 10 mM KCl solution using a ZetaPALS Zeta Potential Analyzer (Brookhaven Instruments Corp., Holtsville, USA) and averaged over 10 runs comprising 10 cycles each. The size of particles and colloid-sized aggregates in 10 mM KCl was quantified using a 532-nm laser with measurements being averaged over 8 runs lasting 60 s each. The validity of the particle size measurements was tested with a 90-nm NanosphereTM size standard (Duke Scientific Corp.).

2.4.4 Desorption

The amount of easily desorbable EPS and NOM of the adsorption complexes and coprecipitates was analyzed in a solution of 10 mM KCl adjusted to a pH of 7.0 with 1 M NaOH, using the same solid-to-solution ratios as in the dissolution experiments (see section 2.5). The suspensions were left on a magnetic stirrer for 10 h at 298 K before centrifugation for 1 h at 6,000 g . After filtration <0.45 μm , the OC concentration of the supernatant was determined with a TOC/TN_b-Analyzer (liqui TOC II, Elementar Analysensysteme GmbH, Hanau, Germany). Furthermore, Na, K, Mg, Ca, Fe, Mn, Al, Si, P, and S in the supernatant

were determined with ICP-OES. The Fe contents of both the post-sorption solution (section 2.3) and the desorbed OM were below detection limit. A significant complexation of Fe(III) by LMWOs and the different types of OM can therefore be ruled out.

2.5 DFOB-induced Abiotic Dissolution Experiments

Prior to the experiments, all solutions were purged with N₂ for 1 h. Circa 40-80 mg of Fh, adsorption complex, or coprecipitate were weighed into 250-mL beakers wrapped with aluminum foil before adding 150 mL of 10 mM KCl solution, thus providing a constant Fe(III) concentration of 3.6 mM. Both the suspensions and the DFOB (EMD Chemicals Inc. San Diego, USA) solution were adjusted to a pH of either 7.0 or 4.0 using HCl (0.1, 0.01 M) and NaOH (0.1, 0.01 M). After equilibration on a magnetic stirrer for 1 h, the reductive dissolution was started by spiking the suspensions with 1 mL of a 7.5 mM DFOB solution obtaining a final DFOB concentration of 50 μM. This concentration represents the upper part of the concentration range of hydroxamate siderophores usually found in soil solutions (Crowley et al., 1991). The pH was monitored and readjusted manually if necessary. Samples were taken after 10, 20, 30, 40, 50, 60, 90, 120, 180, 240, 360, 480, and 600 min. For quantification of dissolved Fe(II) and Fe_{total} contents, 5 mL of the suspension were sampled with a syringe, filtered through 0.025-μm polyethersulfone membrane filters (Anotop 25, Whatman GmbH, Dassel, Germany), and immediately acidified with 200 μL of 5 M H₂SO₄. The concentration of Fe(II) was determined with the ferrozine assay (Stookey, 1970) adapted according to Lovley and Phillips (1987). The concentration of total dissolved Fe was quantified by adding ascorbic acid (food grade, AppliChem GmbH, Darmstadt, Germany) before applying the ferrozine assay once more. None of the experimental treatments exhibited dissolved Fe (III) contents of more than 5 % of the total dissolved Fe contents. Control experiments conducted without DFOB exhibited neither production of Fe(II) nor of Fe(III).

2.6 Statistics

The initial dissolution rates of the ligand-promoted dissolution of Fh, the adsorption complexes and the coprecipitates were determined via linear regression of the linear part of the dissolution curves, which usually resembled a time period of 1 h. Differences between the means of the initial dissolution rates and the different methods of characterization were tested for significance ($\alpha = 0.05$) by applying Welch's variation of the t-test using the software GNU R 3.1.1 (R Development Core Team, 2015). In order to test the impact of the different characteristics of the Fh, adsorption complexes, and coprecipitates on the variance of the dissolution kinetics, partial least-squares regression (PLSR) analysis was carried out with the package *ggm* 2.3 (Marchetti et al., 2015) of the software GNU R 3.3.2 (R Development Core Team, 2016). This method was chosen because of its proven insensitivity towards the multicollinearity revealed by the parameters characterizing the adsorption complexes and coprecipitates (Carrascal et al., 2009).

Table 1 Carbon (C) content, organic carbon (OC) desorbed in 10 mM KCl, and XPS-derived surface carbon content of adsorption complexes and coprecipitates derived from extracellular polymeric substances (EPS) and two types of plant-derived natural organic matter (NOM) extracted from an Oi horizon under beech and an Oa horizon under spruce. Values in parentheses depict the standard deviation of at least triplicate measurements.

Iron oxyhydroxide	Type of NOM	Approximate C loading (mg g ⁻¹)	C content (mg g ⁻¹)	OC _{desorbed} (mg L ⁻¹) pH 7, KCl 10 mM	XPS - C 1s (atom %)
Ferrihydrite	EPS	5	6.3 (0.0)	0.093 (0.0)	47.66 (3.9)
		10	10.5 (2.6)	0.362 (0.0)	53.23 (5.9)
		20	19.3 (0.2)	1.014 (0.3)	64.28 (5.5)
	Beech Oi	5	5.8 (2.0)	0.402 (0.2)	60.11 (1.7)
		10	11.7 (0.1)	0.657 (0.0)	58.45 (2.4)
		20	21.9 (0.7)	1.367 (0.1)	58.24 (2.9)
		40	43.3 (0.0)	2.340 (0.3)	56.53 (4.1)
	Spruce Oa	5	6.7 (0.4)	0.003 (0.0)	60.29 (2.6)
		10	10.4 (0.1)	0.008 (0.0)	58.01 (3.3)
		20	23.8 (0.1)	0.082 (0.0)	51.49 (3.0)
Coprecipitate	EPS	-	138.7 (0.0)	0.453 (0.0)	68.2 (0.6)
	Beech Oi	-	83.8 (0.0)	0.990 (0.1)	63.1 (2.1)
	Spruce Oa	-	151.0 (0.4)	0.778 (0.2)	69.4 (1.6)

3 RESULTS AND DISCUSSION

3.1 Characterization of Fh, Adsorption Complexes, and Coprecipitates

3.1.1 Bulk and surface carbon contents

The C loading of the Fh adsorption complexes ranged from 5.8 to 43.3 mg C g⁻¹ (Table 1). The coprecipitates exhibited significantly larger C contents with the EPS and spruce Oa coprecipitates (138.8 and 151.0 mg C g⁻¹, respectively) displaying considerably larger C contents than the beech Oi coprecipitate (83.8 mg C g⁻¹). The remarkably differing C contents of the coprecipitates may be attributed to several factors. First, the beech Oi-derived NOM solution contained significantly more phosphate (51.3 mg g C⁻¹ L⁻¹) than the other two OM solutions. Phosphate exhibits a high sorption affinity towards hydroxylated mineral surfaces via ligand exchange reactions and therefore competes with organic compounds for sorption sites (Mikutta et al., 2007; Schneider et al., 2010), which would result in smaller C contents of the beech Oi coprecipitate in comparison to the EPS and spruce Oa coprecipitates. Second, microbial-derived polysaccharides accumulate to a larger extent than plant-derived polysaccharides during coprecipitation (Eusterhues et al., 2011), which would explain the larger C content of the EPS coprecipitate in comparison to the beech Oi coprecipitate. Finally, spruce Oa-derived NOM contains further decomposed, more aromatic components, which are precipitated preferentially compared to freshly beech litter-derived NOM (Mikutta et al., 2014; Scheel et al., 2007) and thus additionally accounts for the larger C content of the spruce Oa coprecipitate.

The surface C contents of the adsorption complexes as revealed by XPS ranged between 48 and 64 atomic % (Table 1), which equaled a 75- to 100-fold surface enrichment for the small C loadings and a 20- to 30-fold surface enrichment for the large C loadings in comparison to the bulk C contents. While surface C contents of the EPS adsorption complexes increased along with rising bulk C contents, both the beech Oi and spruce Oa adsorption complexes did not exhibit the same correlation. However, instead of adsorbing

to Fh as homogeneous coating, both types of plant-derived NOM tend to rather adsorb as patches of organic multilayers to Fe hydroxides with growing surface C loadings (Kaiser and Guggenberger, 2003), which might account for this finding (see also section 3.1.3). The coprecipitates showed similar XPS-derived surface C contents ranging from 63 to 69 % (Table 1) corresponding to an 40 to 80-fold increase of the C/Fe weight ratios in relation to the bulk C contents. This finding also suggests that OM accumulated on the surfaces of precipitated Fe oxyhydroxide aggregates, rather than being homogeneously distributed within the mineral matrix.

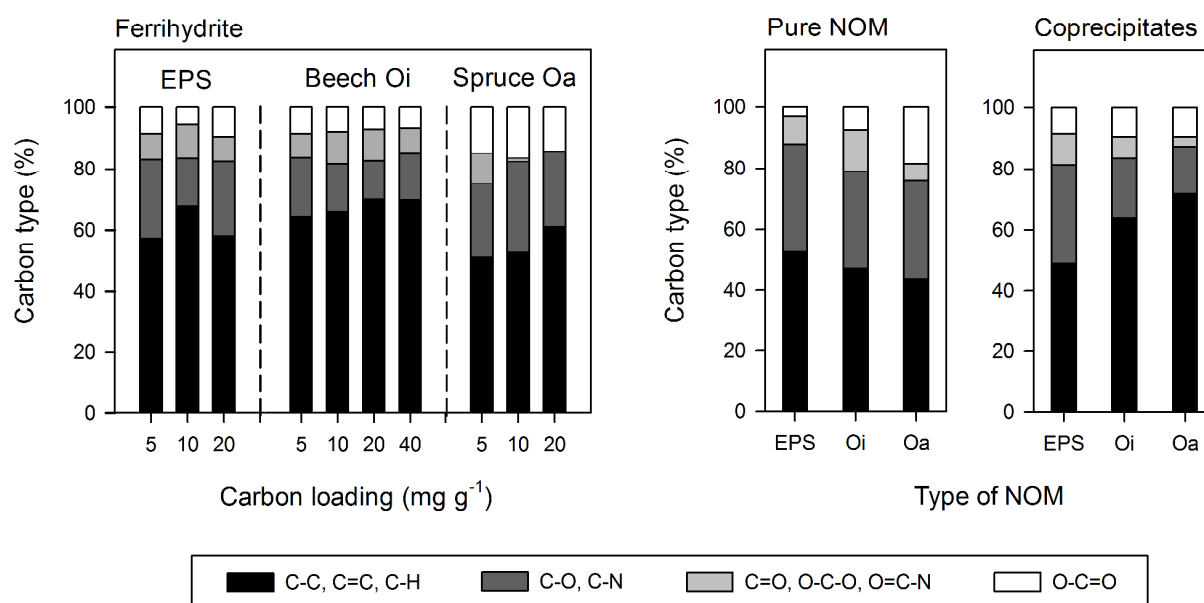


Figure 1 Different carbon species of freeze-dried EPS (extracellular polymeric substances), NOM (natural organic matter extracted from an Oi horizon under beech and an Oa horizon under spruce), adsorption complexes, and coprecipitates derived from detail XPS C1s spectra. Different types of carbon were assigned as follows: (i) aliphatic and aromatic carbon displaying bonds to carbon and hydrogen (C-C, C=C, C-H; at 285.0 ± 0.1 eV), (ii) carbon displaying a single bond to oxygen or nitrogen as in carbohydrates and amines (C-O, C-N; at 286.5 ± 0.2 eV), (iii) carbon displaying two bonds to oxygen as in aldehydes, ketones, and amides (C=O, O-C-O, O=C-N; at 288.0 ± 0.1 eV), and (iv) carboxylic carbon displaying three bonds to oxygen (O-C=O; at 289.1 ± 0.2 eV).

3.1.2 Surface carbon speciation

The two main fractions of C species in the original EPS, beech Oi-, and spruce Oa-derived OM were identified by XPS as aliphatic and aromatic C exhibiting bonds to carbon and hydrogen (C-C, C=C, C-H) and C exhibiting a single bond to oxygen or nitrogen as in carbohydrates and amines (C-O, C-N) (Fig. 1). Since both the specific UV absorbance (SUVA) at 280 nm and NMR revealed very small contents of aromatic C in the EPS (Poggenburg et al., 2016), the amount of aromatic C contributing to the subpeak at 285 eV was most likely negligible. For both the beech Oi- and spruce Oa-derived NOM, significant fractions of this peak were most likely ascribable to aromatic C as suggested by ^{13}C -NMR spectroscopy (Poggenburg et al., 2016). Spruce Oa-derived NOM revealed the largest amount of carboxylic C with concentrations decreasing in the order spruce Oa > beech Oi > EPS.

Upon adsorption, the C species comprising aliphatic and aromatic C was preferentially sorbed to the surface of Fh for all three types of OM (Fig. 1), thus making it the dominant fraction of surface C species, which is in line with the pronounced affinity of aromatic compounds towards Fe oxyhydroxides (Chorover and Amistadi, 2001; Kalbitz et al., 2005; Scheel et al., 2007). Despite sorptive fractionation causing a significant decrease in carbohydrate C for all three types of adsorbed OM in comparison to the original OM, adsorbed EPS still exhibited greater amounts of carbohydrate C than both beech Oi- and spruce Oa-derived NOM. While EPS-derived carboxylic C revealed the largest relative fractionation during adsorption, the largest absolute amounts of carboxylic C were still found for adsorbed spruce Oa-derived NOM.

Coprecipitation of EPS, spruce Oi- and spruce Oa-derived OM with Fe generally had a similar effect on the C species as adsorption to Fh (Fig. 1). According to the C1s XPS spectra, aliphatic and aromatic C was preferentially coprecipitated, whereas the surface content of carbohydrate C diminished in comparison to the corresponding OM. Preferential coprecipitation of aromatic moieties tended to increase in the order EPS < beech Oi < spruce

Oa, which was confirmed in a previous study showing the post-coprecipitation SUVA of beech Oi- and spruce Oa-derived NOM in comparison to the initial NOM solution to decrease by 67 and 83 %, respectively (Poggenburg et al., 2016). Contrary to both types of plant-derived NOM, the EPS coprecipitate exhibited a significant amount of amide C. This observation points towards preferential incorporation of protein structures into the EPS coprecipitate and is in agreement with FTIR measurements on the same sample (Poggenburg et al., 2016) and previous findings on EPS adsorption to goethite (Omoike and Chorover, 2006). The contents of XPS-derived carboxylic C did not differ significantly among the different coprecipitates.

3.1.3 Surface area and porosity

Pure Fh exhibited the largest SSA with 359.7 m² g⁻¹ (Fig. 2), which is in accordance with previous studies of Fh (e.g., Eusterhues et al., 2008; Mikutta et al., 2014; Schwertmann and Cornell, 2000). Upon adsorption of EPS and NOM, the SSA decreased along with growing C loadings but not uniformly. When comparing similar C loadings, the SSA of the EPS adsorption complexes declined to a greater extent than those of the beech Oi and spruce Oa adsorption complexes at smaller loadings, whereas the SSA of the beech Oi adsorption complexes declined to a greater extent at larger loadings. An irregularly decreasing SSA along with increasing adsorption of NOM may originate from the sorption of organic molecules in a more uncoiled spread-out conformation at smaller surface C loadings than at larger surface C loadings, the formation of organic multilayers patches by either hydrophobic interactions or polyvalent cations bridging at larger surface loadings, or the clogging of small pores by preferential sorption of organic molecules to their openings (Kaiser and Guggenberger, 2003).

Unlike the original EPS solution, both beech Oi- and spruce Oa-derived NOM contained Mg²⁺ (11 and 10 mg g C⁻¹) and Ca²⁺ (32 and 20 mg g C⁻¹). As the concentration of both

cations decreased significantly in the post-sorption solution along with increasing C loadings, both types of plant-derived NOM most likely adsorbed to the Fh surface in the form of multilayer patches rather than as a continuous coating, which would reduce the SSA to a lesser extent. Moreover, there was no systematically larger decrease in micro- or mesopore volumes for the EPS adsorption complexes, which indicates a continuously coated Fh surface by adsorbed EPS rather than a preferential sorption to the opening of small pores.

All coprecipitates exhibited a remarkably larger decrease of the SSA than any of the adsorption complexes (Fig. 2) with the SSA of the EPS and spruce Oa coprecipitate being reduced by 93 % and the SSA of the beech Oi coprecipitate being reduced by 60 % in comparison to pure Fh. These values are in line with previous studies of Fe-OM coprecipitates displaying comparable initial molar Fe/C ratios (Eusterhues et al., 2008; Mikutta et al., 2014; Shimizu et al., 2013).

Analogously to the SSA, pure Fh showed the largest total pore volume (TPV), 50 % of which was located within micropores. The volume of both the micropores and small mesopores correlated linearly with the SSA of the adsorption complexes and thus decreased along with increasing C loadings regardless of the source of OM (Fig. 2). By comparison, the volume of the large mesopores was negligible for all adsorption complexes.

In contrast to the adsorption complexes, the micropore volumes decreased by 95 % for both the EPS and spruce Oa coprecipitate and by 60 % for the beech Oi coprecipitate (Fig. 2). The small mesopores decreased accordingly, whereas the large mesopores hardly differed among the coprecipitates. Furthermore, the ratio of $SSA_{\text{coprecipitate}}/SSA_{\text{pureFh}}$ was 0.07 for both the EPS and spruce Oa coprecipitate, and 0.4 for the beech Oi-coprecipitate, which pointed towards significant particle aggregation and shielding of the Fh surface by the precipitated OM.

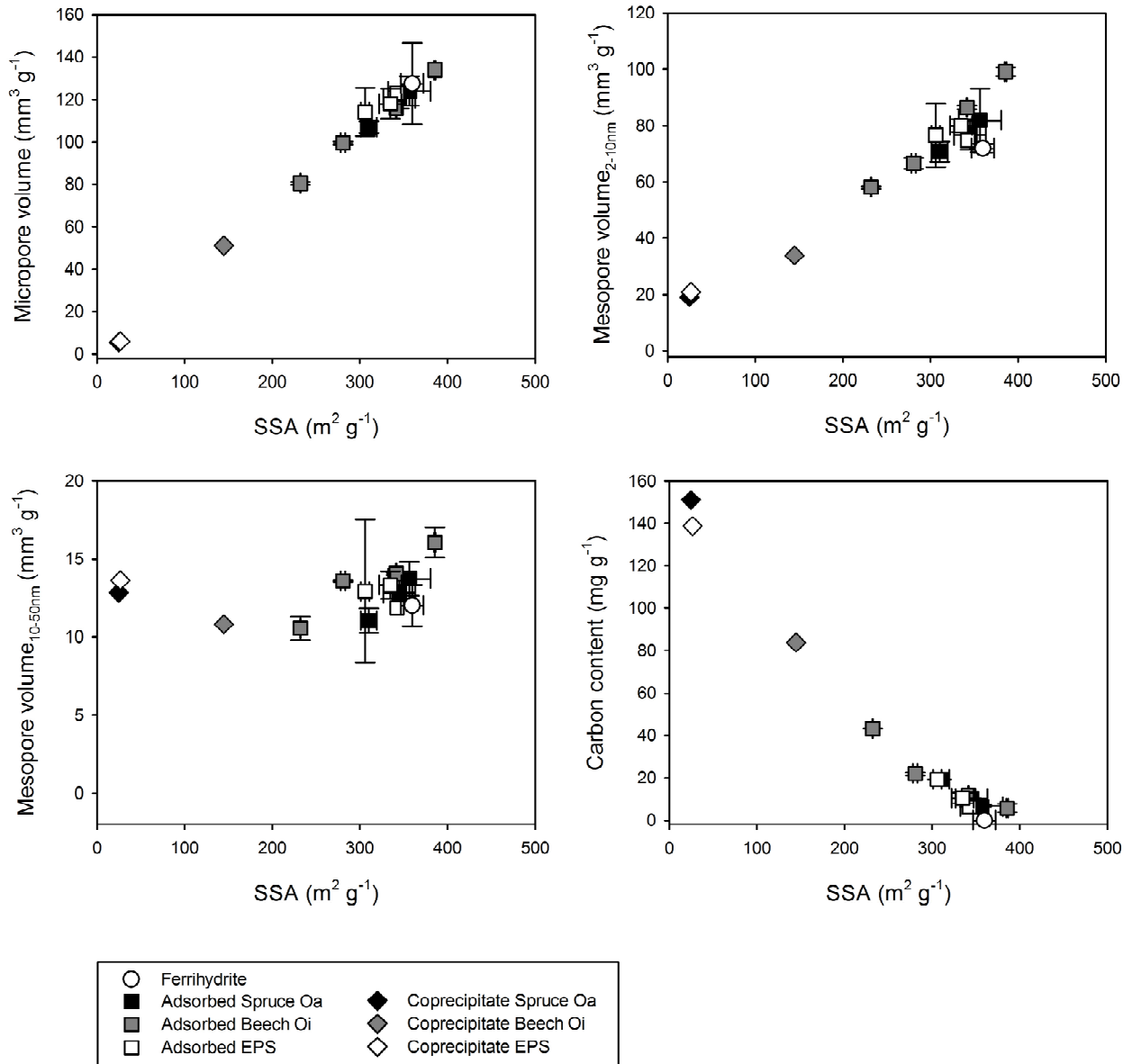


Figure 2 Relationship between the BET-derived specific surface area (SSA) and the micropore volume, the small and large mesopore volume, and the carbon content of pure ferrihydrate, adsorption complexes, and coprecipitates derived from extracellular polymeric substances (EPS) and two types of plant-derived natural organic matter (NOM) extracted from an Oi horizon under beech and an Oa horizon under spruce. Error bars depict the standard deviation of at least duplicate measurements.

3.1.4 Surface Charge, Particle Size and Aggregation

Electrophoretic mobility (EM) measurements for pure Fh revealed values between $2.0 \cdot 10^{-8} \text{ m}^2 \text{ V}^{-1} \text{ s}^{-1}$ at pH 3 and $-2.2 \cdot 10^{-8} \text{ m}^2 \text{ V}^{-1} \text{ s}^{-1}$ at pH 9 (Fig. 3) with the point of zero charge (PZC) located at pH 7.4, which lies within the range of PZC reported for Fh before (Antelo et al., 2010; Cornell and Schwertmann, 2003; Hanna, 2007). In contrast, the adsorption complexes and coprecipitates showed negative EM values over the whole range of pH decreasing along

with the C loading of the adsorption complexes. The PZC of the adsorption complexes and coprecipitates therefore was smaller than pH 3 or near pH 3 for the smallest C loading.

The particle size was largest for pure Fh at pH 7 (Table 2) and decreased with growing C loadings for the adsorption complexes most likely due to increasing repulsive forces with increasing negative surface charge. The particle size of the coprecipitate increased in the order Oa spruce < beech Oi < EPS. In contrast, the particle size of pure Fh at pH 4 was smaller than the smallest loading of the adsorption complexes, while the particle size of both adsorption complexes and coprecipitates at pH 4 was generally larger than the particle size of each respective sample at pH 7. Both observations can be ascribed to the adsorption complexes and coprecipitates approaching the PZC at pH 4 and therefore to smaller surface charge-derived repulsive forces, which are not large enough to prevent flocculation (Angelico et al., 2014).

Table 2 Particle size (determined in 10 mM KCl at pH 4 and pH 7) and specific surface area (SSA)-based initial dissolution rates of ferrihydrite, adsorption complexes, and coprecipitates derived from extracellular polymeric substances (EPS) and two types of plant-derived natural organic matter (NOM) extracted from an Oi horizon under beech and an Oa horizon under spruce. Values in parentheses depict the standard deviation of at least 10 measurements.

Iron oxyhydroxide	Type of NOM	Approximate C loading (mg g ⁻¹)	Particle size (μm)		SSA-based dissolution rates $\mu\text{mol Fe}_{\text{aq}} \text{ h}^{-1} \text{ mM Fe}_{\text{total}}^{-1} \text{ m}^{-2} \times 10^{-3}$	
			pH 4, KCl 10 mM	pH 7, KCl 10 mM	pH 4	pH 7
Ferrihydrite	Pure	-	4.856 (0.376)	6.154 (0.163)	0.98	0.62
		5	6.721 (0.297)	1.529 (0.272)	0.52	2.56
		10	6.019 (0.294)	1.589 (0.360)	0.33	2.15
		20	2.586 (0.293)	1.078 (0.235)	0.15	0.73
	Beech Oi	5	4.179 (0.507)	2.389 (0.402)	0.73	0.94
		10	3.553 (0.678)	1.700 (0.543)	0.69	1.02
		20	3.123 (0.509)	1.768 (0.370)	0.60	1.11
		40	3.140 (0.576)	1.627 (0.386)	0.50	0.96
	Spruce Oa	5	3.214 (0.223)	1.458 (0.456)	0.68	1.68
		10	2.416 (0.288)	1.158 (0.305)	0.57	1.61
		20	1.837 (0.242)	0.838 (0.311)	0.53	0.76
Coprecipitate	EPS	-	3.586 (0.403)	2.664 (0.434)	9.93	21.42
	Beech Oi	-	2.936 (0.392)	2.321 (0.860)	1.90	5.29
	Spruce Oa	-	2.118 (0.293)	1.831 (0.397)	25.61	37.87

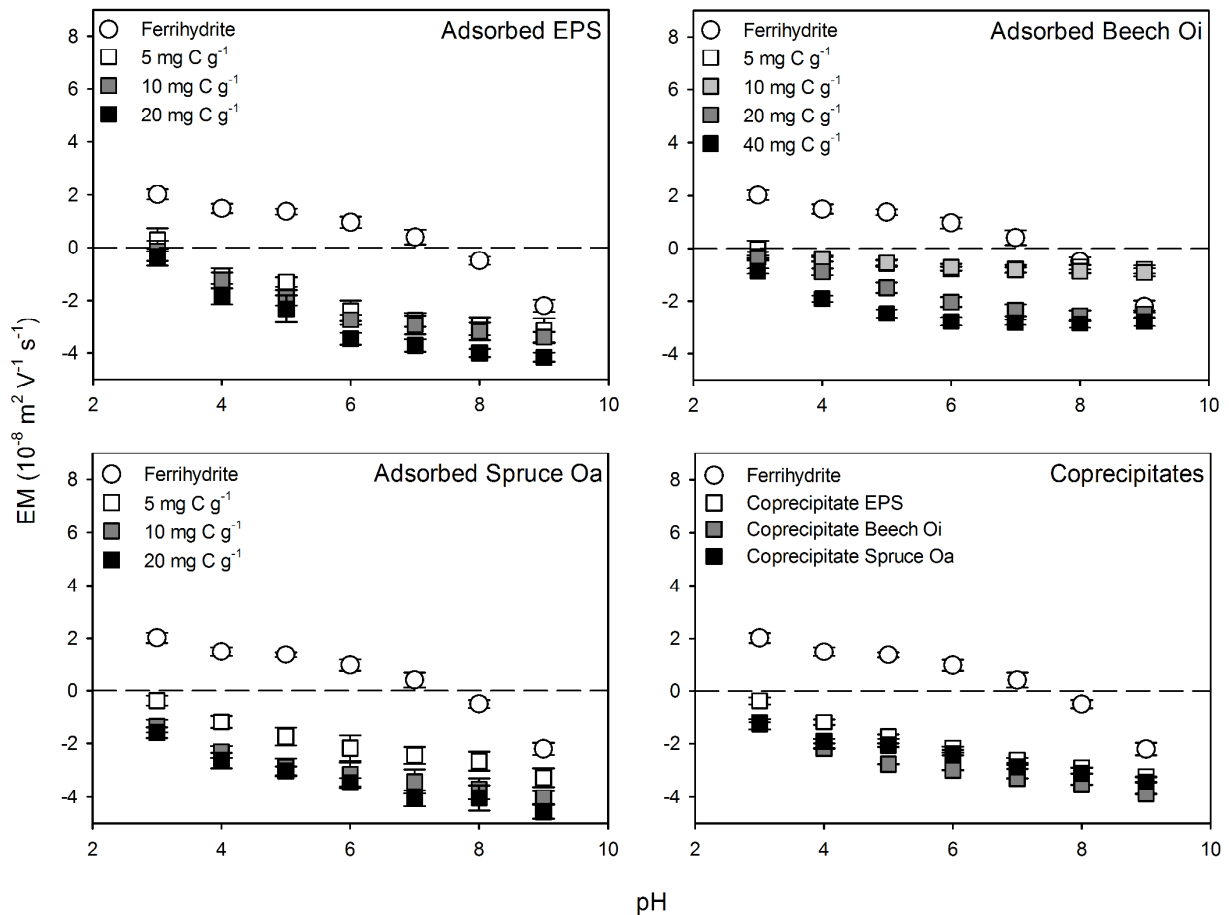


Figure 3 Electrophoretic mobility (EM) in 10 mM KCl in relation to pH for ferrihydrate, adsorption complexes, and coprecipitates derived from extracellular polymeric substances (EPS) and two types of plant-derived natural organic matter (NOM) extracted from an Oi horizon under beech and an Oa horizon under spruce. Error bars depict the standard deviation of 10 circles of measurement.

3.2 Siderophore-promoted dissolution

3.2.1 Dissolution of *Fh* and adsorption complexes

The initial dissolution rate of *Fh* at pH 7 was $0.22 \mu\text{mol Fe}_{\text{aq}} \text{ h}^{-1} \text{ mM Fe}_{\text{total}}^{-1}$ (Figure 4) and therefore in line with experiments conducted under similar conditions (Mikutta and Kretzschmar, 2008). Irrespective of the type of OM, at pH 7, the largest C loading of the adsorption complexes exhibited slightly decreased initial dissolution rates in comparison to pure *Fh*, whereas the initial dissolution rates at low and medium C loadings were larger than

the one of pure Fh. In general, the initial Fe dissolution rates decreased along with increasing C loadings and thus decreasing SSA, which agrees with abiotic dissimilatory reduction experiments conducted with similar samples before (Eusterhues et al., 2014). If the available SSA or surface coverage had been the only rate determining parameter, however, Fh should have displayed the largest initial dissolution rate of all samples. To some extent, this observation might be attributed to 50 % of the TPV of Fh being located within micropores < 2 nm. The preferential sorption of OM to the opening of small pores (see also section 3.1.3) would have restricted access of DFOB to a fraction of the SSA, which would not have been accessible to the ligand before OM sorption, either. This consideration is supported by the findings of Yoshida et al. (2002), who found larger siderophore-promoted, surface area based dissolution rates for goethite than for Fh, with the former featuring considerably less micropores than the latter. Furthermore, at pH 7, up to 20 % of the OM was desorbed upon suspension of the adsorption complexes in background electrolyte (Table 1) thus diminishing the influence of the BET-derived SSA even more. Since the SSA-based initial dissolution rates of the adsorption complexes were larger than the one of pure Fh (Table 2), the smaller particle size, which largely coincided with larger C loadings, seemed to outweigh the surface coverage to some extent. As neither the SSA nor the particle size were solely able to account for the initial dissolution rates, a combined influence of both seems likely. This line of reasoning was supported by PLSR analysis of the adsorption complexes at pH 7, which attributed 14 % of the variability of the results to the SSA ($p = 0.006$) and 10 % to the particle size ($p = 0.005$), while no other parameter exhibited a significant partial correlation with the initial Fe dissolution rates. Even though DFOB is a cationic species below pH 8 (Borgias et al., 1989), the initial dissolution rates decreased with increasingly negative charge characteristics, implying a negligible influence of electrostatic attraction between the siderophore and the negatively charged surface. It is possible, that DFOB might have been increasingly immobilized with increasing amounts of negatively charged OM, since cationic

DFOB is subject to complexation by negatively charged humic acids (Higashi et al., 1998). However, since the major complexing functional groups of OM are mostly involved in the formation of bonds towards Fe oxyhydroxide surfaces in adsorption complexes (Mikutta et al., 2007), the influence is most likely a minor one, too.

When comparing the different types of OM at similar C loadings, initial dissolution rates decreased in the order spruce Oa > EPS > beech Oi. Since the EPS adsorption complexes exhibited the largest particle size (Table 2) and the smallest SSA due to the tendency of EPS to adsorb in a more spread out manner (see also section 3.1.3), smaller initial dissolution rates in comparison to the spruce Oa adsorption complexes are to be expected. The decreased initial dissolution rates of the beech Oi adsorption complexes in comparison to the EPS adsorption complexes can additionally be attributed to their larger phosphate contents described by Poggenburg et al. (2016). While the DFOB-derived hydroxamate groups building mononuclear bidentate innersphere complexes serve as excellent precursor for Fe dissolution (Furrer and Stumm, 1986), phosphate tends to coordinate several surface sites per molecule, thus preventing detachment of the Fe atom due to thermodynamically unfavourable conditions (Bondietti et al., 1993).

At pH 4, the initial dissolution rate of pure Fh was elevated by 50 % in comparison to pH 7 (Figure 5), which seems to contrast the previously reported evenly DFOB-accelerated dissolution of Fe oxyhydroxides over a large pH range (Kraemer, 2004). Possible explanations for this observation include (i) additional proton-promoted dissolution due to the lower pH (Cornell et al., 1976), (ii) enhanced dissolution due to the formation of HCl-derived Fe-Cl surface complexes (Sidhu, 1981), (iii) less readsorption of reduced Fe(II) or DFOB(Fe) complexes due to a more positive surface charge at lower pH (Figure 3), (iv) a smaller particle size of Fh derived from larger surface charge-derived repulsive forces at pH 4 (Figure 3, Table 2), and (v) a faster recovery of the surface site after detachment of the Fe atom due to a

faster protonation at lower pH (Wieland, 1988). Since the concentration of dissolved Fe(III) was below 5 % of the concentration of Fe(II) during the whole experiment (data not shown), a significant contribution of proton-promoted dissolution seems unlikely. Taking into consideration that dissolved Fe(III) might have been immediately reduced by DFOB (Holmén and Casey, 1996), dissolution stimulated by a larger proton concentration should still have been detectable in the experiments conducted without addition of DFOB. As mentioned in section 2.5, release of both Fe(II) and Fe(III) in those experiments was negligible, indicating a minor influence of proton-promoted dissolution at pH 4. While Schwertmann (1991) attributed increased goethite dissolution rates at lower pH to Fe-Cl surface complexes, the formation of Fe(DFOB)(Cl) surface complexes has been suggested to decelerate dissolution at larger concentrations of Cl⁻ (Kraemer, 2004). Since pretests of Fh dissolution conducted in both KCl with added HCl and NaClO₄ with added HClO₄ did not exhibit significantly differently dissolution rates, the influence of Cl⁻ ions at pH 4 seems to be a minor one, too. Furthermore, Schwertmann (1991) reported the adsorption of Fe(II) to enhance dissolution rather than blocking it by the exchange of electrons between adsorbed Fe(II) and Fe(III) still bound in the crystal lattice. As decreased Fe(II) readsorption cannot account for the increased reduction of Fh at pH 4, both the faster surface site recovery and the smaller particle size remain as the most likely explanation.

In contrast to dissolution at pH 7, adsorption of OM resulted in decreased initial dissolution rates in comparison to Fh for all types of OM (Figure 5) with a similar pattern of decreasing initial dissolution rates with increasing C loading. In comparison to pH 7, desorption of OM at pH 4 was negligible (Table 1), which suggests a larger influence of OM-induced surface site blockage. This is supported by PLSR attributing 18 % of the variability of the initial dissolution rates to the SSA ($p = 0.007$) with 21 % of the variability being explained by the particle size ($p = 0.048$). Furthermore, 20 % could be assigned to the XPS-derived C ($p = 0.044$) and 28 % to the BET-derived C constant ($p = 0.009$), which both serve

as proxy for the surface coverage and sorption affinity of OM. Overall, a smaller available mineral surface area in combination with larger particle sizes thus seemed to account for the smaller dissolution rates of the adsorption complexes at pH 4.

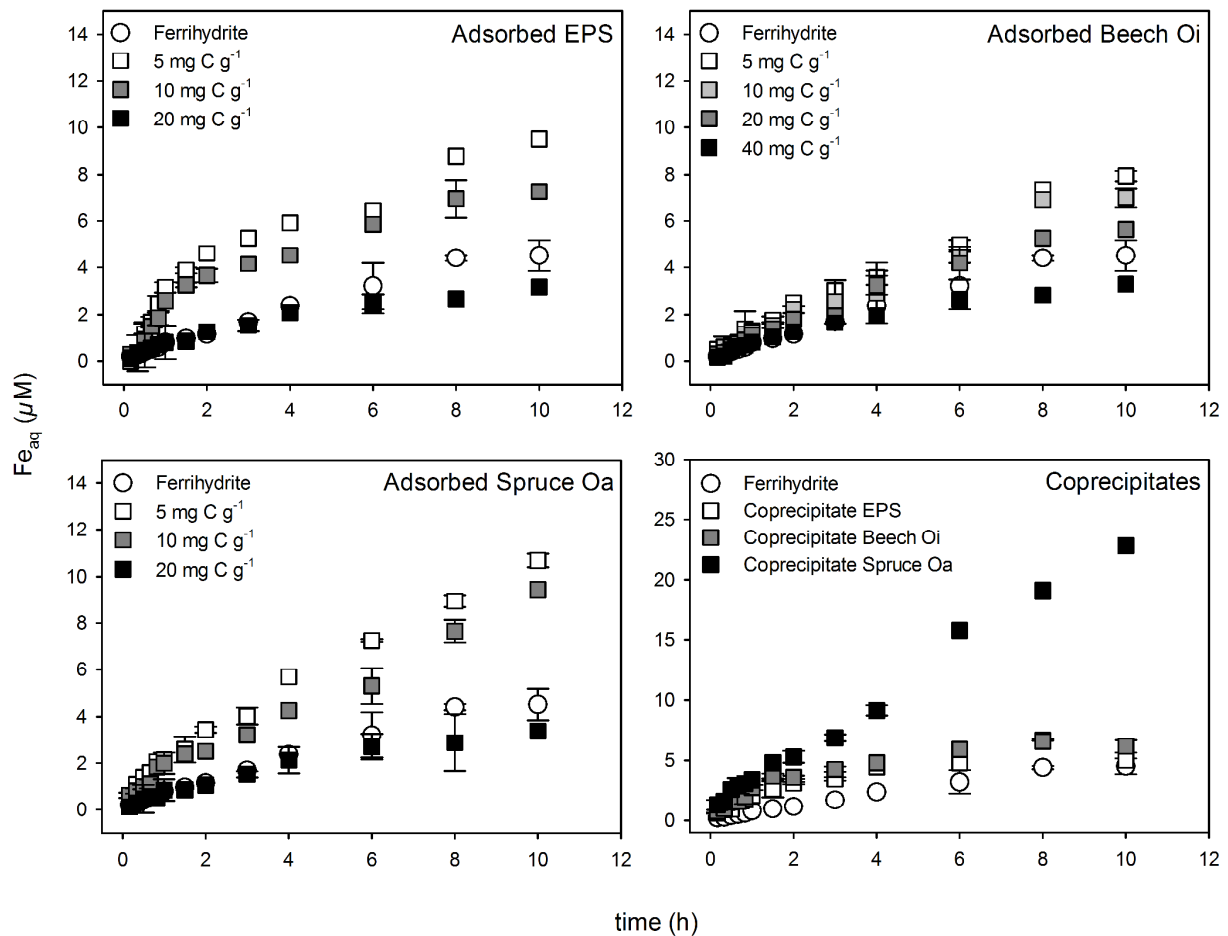


Figure 4 Dissolution of ferrihydrite, adsorption complexes, and cocipitates by 50 μM DFOB (desferrioxamine-B) in 10 mM KCl at pH 7. Organic matter (OM) was extracted from extracellular polymeric substances (EPS) and two types of plant-derived natural OM (NOM) derived from an Oi horizon under beech and an Oa horizon under spruce. Error bars depict the standard deviation of triplicate measurements. Please note the different scale of the y-axis for the cocipitates.

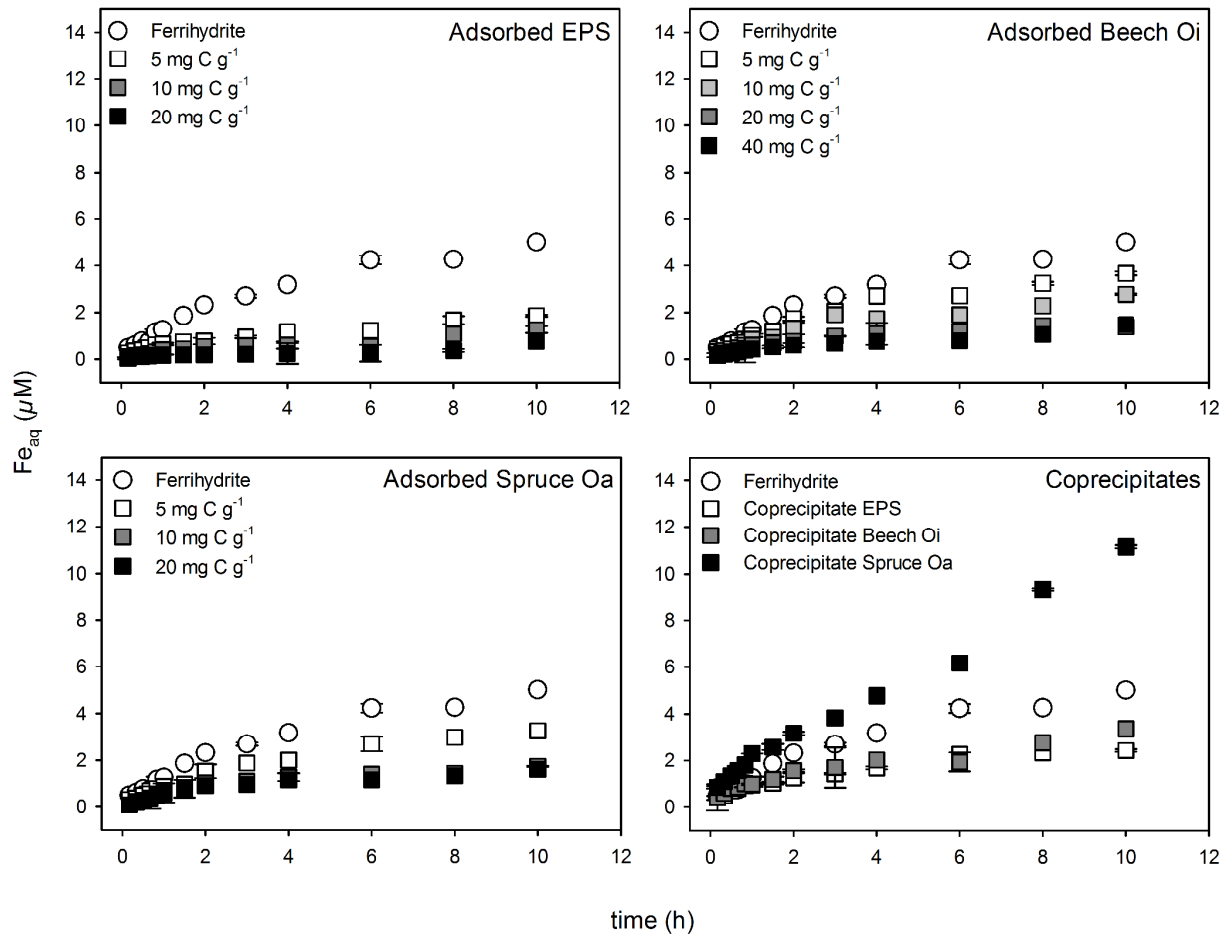


Figure 5 Dissolution of ferrihydrite, adsorption complexes, and coprecipitates by 50 μM DFOB (desferrioxamine-B) in 10 mM KCl at pH 4. Organic matter (OM) was extracted from extracellular polymeric substances (EPS) and two types of plant-derived natural OM (NOM) derived from an Oi horizon under beech and an Oa horizon under spruce. Error bars depict the standard deviation of triplicate measurements.

3.2.2 Dissolution of coprecipitates

At pH 7, the EPS and beech Oi coprecipitate exhibited initial dissolution rates twice as large as Fh, whereas the dissolution rate of the spruce Oa coprecipitate became even larger during the course of the experiment (Figure 4). At pH 4, the initial dissolution rates of the coprecipitates were only half as large, while the dissolution of the EPS and beech Oi coprecipitate was smaller than the one of Fh (Figure 5). Mikutta and Kretzschmar (2008) ascribed the enhanced dissolution of polygalacturonate-Fe coprecipitates by DFOB in comparison to Fh at pH 7 to electrostatic particle stabilization caused by a larger EM of the

coprecipitates, which would outweigh the smaller SSA. This may account for the change in the initial dissolution rates of the coprecipitates with respect to Fh at different pH, since the particle size of the coprecipitates increased at lower pH, whereas the particle size of Fh decreased at lower pH (Table 2). Smaller particle sizes indicate less aggregation and therefore larger initial dissolution rates. However, neither the SSA nor the particle size could sufficiently explain the different dissolution rates among the coprecipitates. Despite its larger SSA (Figure 2) and smaller particle size indicating less aggregation, the beech Oi coprecipitate exhibited initial dissolution rates hardly differing from the EPS coprecipitate. This finding can most likely be attributed to site blockage by phosphate as discussed in section 3.2.1, since the beech Oi coprecipitate contained even more phosphate than the adsorption complexes (Poggenburg et al., 2016).

For the spruce Oa coprecipitate, XRD analysis of the same coprecipitate had revealed diminished Fh-derived peaks at 0.25 and 0.15 nm and a shift towards smaller 2θ values in comparison to Fh (Poggenburg et al., 2016), which indicate less crystalline structures due to disruption of the cross-linking of $\text{Fe}(\text{O},\text{OH})_6$ octahedra chains by OM compounds during coprecipitation (Eusterhues et al., 2008; Waychunas et al., 1993). Since the disturbance of the structure was most pronounced for the spruce Oa coprecipitate and less crystalline and generally irregular structures are preferentially dissolved (Schwertmann, 1984), the considerably larger dissolution rates for the spruce Oa coprecipitate can most likely be attributed to its more defective structure. Furthermore, the Oa coprecipitate contained 2 % Fe(II) owing to marginal reduction of Fe(III) during coprecipitation with NOM compounds (Mikutta, 2011), which further destabilizes the structure and might thus account for increased dissolution rates (Schwertmann, 1991).

4 CONCLUSIONS

Our results suggest that the pH-dependent impact of both adsorbed and coprecipitated OM on the siderophore-promoted dissolution of Fe-organic associations exerts a larger influence on their stability than the proton-promoted dissolution of the uncoated pure Fe oxyhydroxide phases. At lower pH, OM provides a more effective protection against siderophores due to its larger sorption affinity. At circumneutral pH, the surface site blockage by OM at comparable C loadings is less effective, while electrostatic repulsion leads to less aggregated particles even more prone to dissolution. Depending on the origin of the OM, coprecipitation with Fe can both accelerate and inhibit siderophore-promoted dissolution. This finding stresses the importance of considering the heterogeneous and complex composition of soil OM when investigating the mobilization of Fe-organic associations instead of relying on model compounds.

Acknowledgements

This study was financially supported by the NTH-Graduate School “Geofluxes” of the federal state of Lower Saxony, Germany.

References

- Alvarez-Puebla, R.A., Garrido, J.J., 2005. Effect of pH on the aggregation of a gray humic acid in colloidal and solid states. *Chemosphere* 59, 659–667. doi:10.1016/j.chemosphere.2004.10.021
- Angelico, R., Ceglie, A., He, J.Z., Liu, Y.R., Palumbo, G., Colombo, C., 2014. Particle size, charge and colloidal stability of humic acids coprecipitated with ferrihydrite. *Chemosphere* 99, 239–247. doi:10.1016/j.chemosphere.2013.10.092
- Antelo, J., Fiol, S., Pérez, C., Mariño, S., Arce, F., Gondar, D., López, R., 2010. Analysis of phosphate adsorption onto ferrihydrite using the CD-MUSIC model. *J. Colloid Interface Sci.* 347, 112–119. doi:10.1016/j.jcis.2010.03.020
- April, R., Keller, D., 1990. Mineralogy of the rhizosphere in forest soils of the eastern United States. *Biogeochemistry*. doi:10.1007/BF00002714
- Bachand, P.A.M., Richardson, C.J., Vaithyanathan, P., 2000. Phase II low intensity chemical dosing (LICD): Development of management practices. Final report submitted to Florida Department of Environmental Protection in fulfillment of Contract No. WM720.
- Barrett, E.P., Joyner, L.G., Halenda, P.P., 1951. The determination of pore volume and area distributions in porous substances. I. Computations from nitrogen isotherms. *J. Am.*

- Chem. Soc. 73, 373–380. doi:10.1021/ja01145a126
- Beveridge, T.J., Makin, S.A., Kadurugamuwa, J.L., Li, Z., 1997. Interactions between biofilms and the environment. *FEMS Microbiol. Rev.* 20, 291–303. doi:10.1016/S0168-6445(97)00012-0
- Bondietti, G., Sinniger, J., Stumm, W., 1993. The reactivity of Fe(III) (hydr)oxides - Effects of ligands in inhibiting the dissolution. *Colloids Surfaces A Physicochem. Eng. Asp.* 79, 157–167.
- Bonneville, S., Morgan, D.J., Schmalenberger, A., Bray, A., Brown, A., Banwart, S.A., Benning, L.G., 2011. Tree-mycorrhiza symbiosis accelerate mineral weathering: Evidences from nanometer-scale elemental fluxes at the hypha-mineral interface. *Geochim. Cosmochim. Acta* 75, 6988–7005. doi:10.1016/j.gca.2011.08.041
- Borgias, B., Hugi, A.D., Raymond Kenneth N., 1989. Isomerization and Solution Structures of Desferrioxamine B Complexes of Al^{3+} and Ga^{3+} . *Inorg. Chem.* 28, 3538–3545. doi:10.1021/ic00317a029
- Brantley, S.L., Megonigal, J.P., Scatena, F.N., Balogh-Brunstad, Z., Barnes, R.T., Bruns, M.A., Van Cappellen, P., Dontsova, K., Hartnett, H.E., Hartshorn, A.S., Heimsath, A., Herndon, E., Jin, L., Keller, C.K., Leake, J.R., Mcdowell, W.H., Meinzer, F.C., Mozdzer, T.J., Petsch, S., Pett-Ridge, J., Pregitzer, K.S., Raymond, P.A., Riebe, C.S., Shumaker, K., Sutton-Grier, A., Walter, R., Yoo, K., 2011. Twelve testable hypotheses on the geobiology of weathering. *Geobiology* 9, 140–165. doi:10.1111/j.1472-4669.2010.00264.x
- Brümmer, G.W., Barrow, N.J., Fischer, L., 2013. Effect of porosity of goethite on the sorption of six heavy metal ions. *Eur. J. Soil Sci.* 64, 805–813. doi:10.1111/ejss.12091
- Brunauer, S., Emmett, P.H., Teller, E., 1938. Adsorption of gases in multimolecular layers. *J. Am. Chem. Soc.* 60, 309–319.
- Canfield, D.E., Jorgensen, B.B., Fossing, H., Glud, R., Gundersen, J., Ramsing, N.B., Thamdrup, B., Hansen, J.W., Nielsen, L.P., Hall, P.O., 1993. Pathways of organic carbon oxidation in three continental margin sediments. *Mar. Geol.* 113, 27–40. doi:10.1016/0025-3227(93)90147-N
- Carrascal, L.M., Galván, I., Gordo, O., 2009. Partial least squares regression as an alternative to current regression methods used in ecology. *Oikos* 118, 681–690. doi:10.1111/j.1600-0706.2008.16881.x
- Cheah, S.-F., Kraemer, S.M., Cervini-Silva, J., Sposito, G., 2003. Steady-state dissolution kinetics of goethite in the presence of desferrioxamine B and oxalate ligands: implications for the microbial acquisition of iron. *Chem. Geol.* 198, 63–75. doi:10.1016/S0009-2541(02)00421-7
- Cheng, H., Hu, Y., Luo, J., Xu, B., Zhao, J., 2009. Geochemical processes controlling fate and transport of arsenic in acid mine drainage (AMD) and natural systems. *J. Hazard. Mater.* 165, 13–26. doi:10.1016/j.jhazmat.2008.10.070
- Chorover, J., Amistadi, M.K., 2001. Reaction of forest floor organic matter at goethite, birnessite and smectite surfaces. *Geochim. Cosmochim. Acta* 65, 95–109.
- Cismasu, A.C., Michel, F.M., Tcaciuc, A. P., Tylliszczak, T., Brown, Jr, G.E., 2011. Composition and structural aspects of naturally occurring ferrihydrite. *Comptes Rendus Geosci.* 343, 210–218. doi:10.1016/j.crte.2010.11.001
- Cornell, R.M., Posner, A.M., Quirk, J.P., 1976. Kinetics and mechanisms of the acid dissolution of goethite (α -FeOOH). *J. Inorg. Nucl. Chem.* 38, 563–567. doi:10.1016/0022-1902(76)80305-3
- Cornell, R.M., Schwertmann, U., 2003. *The iron oxides*, 2nd ed. Wiley-VCH. doi:10.1002/3527602097
- Crowley, D.E., Wang, Y.C., Reid, C.P.P., Szaniszlo, P.J., 1991. Mechanisms of iron acquisition from siderophores by microorganismes and plants. *Plant Soil* 130, 179–198.

- Dolfing, J., Chardon, W.J., Japenga, J., 1999. Association between colloidal iron, aluminum, phosphorus, and humic acids. *Soil Sci.* 164, 171–179. doi:10.1097/00010694-199903000-00003
- Downing, B.D., Bergamaschi, B.A., Evans, D.G., Boss, E., 2008. Assessing contribution of DOC from sediments to a drinking-water reservoir using optical profiling. *Lake Reserv. Manag.* 24, 381–391. doi:10.1080/07438140809354848
- Eusterhues, K., Hädrich, A., Neidhardt, J., Küsel, K., Keller, T.F., Jandt, K.D., Totsche, K.U., 2014. Reduction of ferrihydrite with adsorbed and coprecipitated organic matter: microbial reduction by *Geobacter bremerensis* vs. abiotic reduction by Na-dithionite. *Biogeosciences* 11, 4953–4966. doi:10.5194/bg-11-4953-2014
- Eusterhues, K., Rennert, T., Knicker, H., Kögel-Knabner, I., Totsche, K.U., Schwertmann, U., 2011. Fractionation of organic matter due to reaction with ferrihydrite: coprecipitation versus adsorption. *Environ. Sci. Technol.* 45, 527–33. doi:10.1021/es1023898
- Eusterhues, K., Wagner, F.E., Häusler, W., Hanzlik, M., Knicker, H., Totsche, K.U., Kögel-Knabner, I., Schwertmann, U., 2008. Characterization of ferrihydrite-soil organic matter coprecipitates by X-ray diffraction and Mössbauer spectroscopy. *Environ. Sci. Technol.* 42, 7891–7.
- Furrer, G., Stumm, W., 1986. The coordination chemistry of weathering: I. Dissolution kinetics of δ -Al₂O₃ and BeO. *Geochim. Cosmochim. Acta* 50, 1847–1860. doi:10.1016/0016-7037(86)90243-7
- Gerin, P.A., Genet, M.J., Herbillon, A.J., Delvaux, B., 2003. Surface analysis of soil material by X-ray photoelectron spectroscopy. *Eur. J. Soil Sci.* 54, 589–603.
- Goebel, M.-O., Adams, F., Boy, J., Guggenberger, G., Mikutta, R., 2017. Mobilization of glucose-6-phosphate from ferrihydrite by ligand-promoted dissolution is higher than of orthophosphate. *J. Plant Nutr. Soil Sci.* 180, 279–282. doi:10.1002/jpln.201600479
- Gregg, S.H., Sing, K.S.W., 1982. Adsorption, Surface Area and Porosity, 2nd ed. Academic Press, New York.
- Hanna, K., 2007. Adsorption of aromatic carboxylate compounds on the surface of synthesized iron oxide-coated sands. *Appl. Geochemistry* 22, 2045–2053. doi:10.1016/j.apgeochem.2007.05.005
- Henneberry, Y.K., Kraus, T.E.C., Fleck, J.A., Krabbenhoft, D.P., Bachand, P.M., Horwath, W.R., 2011. Removal of inorganic mercury and methylmercury from surface waters following coagulation of dissolved organic matter with metal-based salts. *Sci. Total Environ.* 409, 631–637. doi:10.1016/j.scitotenv.2010.10.030
- Hesse, R., Chassé, T., Szargan, R., 2003. Unifit 2002-universal analysis software for photoelectron spectra. *Anal. Bioanal. Chem.* 375, 856–863. doi:10.1007/s00216-002-1705-0
- Higashi, R.M., Fan, T.W.-M., Lane, A.N., 1998. Association of desferrioxamine with humic substances and their interaction with cadmium(II) as studied by pyrolysis–gas chromatography–mass spectrometry and nuclear magnetic resonance spectroscopy†. *Analyst* 123, 911–918. doi:10.1039/a708177d
- Holmén, B.A., Casey, W.H., 1996. Hydroxamate ligands, surface chemistry, and the mechanism of ligand-promoted dissolution of goethite [α -FeOOH(s)]. *Geochim. Cosmochim. Acta* 60, 4403–4416. doi:10.1016/S0016-7037(96)00278-5
- Kaiser, K., Guggenberger, G., 2007. Sorptive stabilization of organic matter by microporous goethite: sorption into small pores vs. surface complexation. *Eur. J. Soil Sci.* 58, 45–59. doi:10.1111/j.1365-2389.2006.00799.x
- Kaiser, K., Guggenberger, G., 2003. Mineral surfaces and soil organic matter. *Eur. J. Soil Sci.* 54, 219–236.
- Kaiser, K., Zech, W., 1999. Release of natural organic matter sorbed to oxides and a subsoil. *Soil Sci. Soc. Am. J.* 63, 1157–1166.

- Kalbitz, K., Schwesig, D., Rethemeyer, J., Matzner, E., 2005. Stabilization of dissolved organic matter by sorption to the mineral soil. *Soil Biol. Biochem.* 37, 1319–1331. doi:10.1016/j.soilbio.2004.11.028
- Kleber, M., Eusterhues, K., Keiluweit, M., Mikutta, C., Mikutta, R., Nico, P.S., 2015. Mineral–organic associations: formation, properties, and relevance in soil environments. *Adv. Agron.* 130. doi:10.1016/bs.agron.2014.10.005
- Kögel-Knabner, I., Amelung, W., Cao, Z., Fiedler, S., Frenzel, P., Jahn, R., Kalbitz, K., Kölbl, A., Schloter, M., 2010. Biogeochemistry of paddy soils. *Geoderma* 157, 1–14. doi:10.1016/j.geoderma.2010.03.009
- Kraemer, S.M., 2004. Iron oxide dissolution and solubility in the presence of siderophores. *Aquat. Sci. - Res. Across Boundaries* 66, 3–18. doi:10.1007/s00027-003-0690-5
- Kraemer, S.M., Crowley, D.E., Kretzschmar, R., 2006. Geochemical aspects of phytosiderophore-promoted iron acquisition by plants. *Adv. Agron.* 91, 1–46. doi:10.1016/S0065-2113(06)91001-3
- Larsen, O., Postma, D., 2001. Kinetics of reductive bulk dissolution of lepidocrocite, ferrihydrite, and goethite. *Geochim. Cosmochim. Acta* 65, 1367–1379. doi:10.1016/S0016-7037(00)00623-2
- Leone, L., Loring, J., Sj, S., Persson, P., Shchukarev, A., 2006. Surface characterization of the gram-positive bacteria *Bacillus subtilis* - an XPS study. *Surf. Interface Anal.* 38, 202–205. doi:10.1002/sia
- Lovley, D.R., Anderson, R.T., 2000. Influence of dissimilatory metal reduction on fate of organic and metal contaminants in the subsurface. *Hydrogeol. J.* 8, 77–88.
- Lovley, D.R., Phillips, E.J., 1987. Rapid assay for microbially reducible ferric iron in aquatic sediments. *Appl. Environ. Microbiol.* 53, 1536–1540.
- Marchetti, G.M., Drton, M., Sadeghi, K., 2015. ggm 2.3.
- Mesuer, K., Fish, W., 1999. Chromate and oxalate adsorption on goethite. 2. Surface complexation modeling of competitive adsorption. *Environ. Sci. Technol.* 26, 2365–2370.
- Mikutta, C., 2011. X-ray absorption spectroscopy study on the effect of hydroxybenzoic acids on the formation and structure of ferrihydrite. *Geochim. Cosmochim. Acta* 75, 5122–5139. doi:10.1016/j.gca.2011.06.002
- Mikutta, C., Kretzschmar, R., 2008. Synthetic coprecipitates of exopolysaccharides and ferrihydrite. Part II: Siderophore-promoted dissolution. *Geochim. Cosmochim. Acta* 72, 1128–1142. doi:10.1016/j.gca.2007.11.034
- Mikutta, R., Baumgärtner, A., Schippers, A., Haumaier, L., Guggenberger, G., 2012. Extracellular polymeric substances from *Bacillus subtilis* associated with minerals modify the extent and rate of heavy metal sorption. *Environ. Sci. Technol.* 46, 3866–73. doi:10.1021/es204471x
- Mikutta, R., Kleber, M., Torn, M.S., Jahn, R., 2006. Stabilization of soil organic matter: association with minerals or chemical recalcitrance? *Biogeochemistry* 77, 25–56. doi:10.1007/s10533-005-0712-6
- Mikutta, R., Lorenz, D., Guggenberger, G., Haumaier, L., Freund, A., 2014. Properties and reactivity of Fe-organic matter associations formed by coprecipitation versus adsorption: Clues from arsenate batch adsorption. *Geochim. Cosmochim. Acta* 144, 258–276. doi:10.1016/j.gca.2014.08.026
- Mikutta, R., Mikutta, C., Kalbitz, K., Scheel, T., Kaiser, K., Jahn, R., 2007. Biodegradation of forest floor organic matter bound to minerals via different binding mechanisms. *Geochim. Cosmochim. Acta* 71, 2569–2590. doi:10.1016/j.gca.2007.03.002
- Neilands, J.B., 1957. Some aspects of microbial iron metabolism. *Anal. Biochem.* 21, 220–230.
- Nierop, K.G.J., Jansen, B., Verstraten, J.M., 2002. Dissolved organic matter, aluminium and

- iron interactions: Precipitation induced by metal/carbon ratio, pH and competition. *Sci. Total Environ.* 300, 201–211. doi:10.1016/S0048-9697(02)00254-1
- Omoike, A., Chorover, J., 2006. Adsorption to goethite of extracellular polymeric substances from *Bacillus subtilis*. *Geochim. Cosmochim. Acta* 70, 827–838. doi:10.1016/j.gca.2005.10.012
- Omoike, A., Chorover, J., 2004. Spectroscopic study of extracellular polymeric substances from *Bacillus subtilis*: Aqueous chemistry and adsorption effects. *Biomacromolecules* 5, 1219–30. doi:10.1021/bm034461z
- Perelomov, L. V., Pinskiy, D.L., Violante, A., 2011. Effect of organic acids on the adsorption of copper, lead, and zinc by goethite. *Eurasian Soil Sci.* 44, 22–28. doi:10.1134/S1064229311010091
- Poggenburg, C., Mikutta, R., Sander, M., Schippers, A., Marchanka, A., Dohrmann, R., Guggenberger, G., 2016. Microbial reduction of ferrihydrite-organic matter coprecipitates by *Shewanella putrefaciens* and *Geobacter metallireducens* in comparison to mediated electrochemical reduction. *Chem. Geol.* 447, 133–147. doi:10.1016/j.chemgeo.2016.09.031
- Rancourt, D.G., Thibault, P.J., Mavrocordatos, D., Lamarche, G., 2005. Hydrous ferric oxide precipitation in the presence of nonmetabolizing bacteria: Constraints on the mechanism of a biotic effect. *Geochim. Cosmochim. Acta* 69, 553–577. doi:10.1016/j.gca.2004.07.018
- Reichard, P.U., Kretzschmar, R., Kraemer, S.M., 2007. Dissolution mechanisms of goethite in the presence of siderophores and organic acids. *Geochim. Cosmochim. Acta* 71, 5635–5650. doi:10.1016/j.gca.2006.12.022
- Roden, E.E., 2003. Fe(III) oxide reactivity toward biological versus chemical reduction. *Environ. Sci. Technol.* 37, 1319–1324. doi:10.1021/es026038o
- Roemheld, V., 1991. The Role of phytosiderophores in acquisition of iron and other micronutrients in graminaceous species: an ecological approach. *Plant Soil* 130, 127–134.
- Sannino, F., De Martino, A., Pigna, M., Violante, A., Di Leo, P., Mesto, E., Capasso, R., 2009. Sorption of arsenate and dichromate on polymerin, Fe(OH)_x-polymerin complex and ferrihydrite. *J. Hazard. Mater.* 166, 1174–9. doi:10.1016/j.jhazmat.2008.12.015
- Scheel, T., Dörfel, C., Kalbitz, K., 2007. Precipitation of dissolved organic matter by aluminum stabilizes carbon in acidic forest soils. *Soil Sci. Soc. Am. J.* 71, 64–74. doi:10.2136/sssaj2006.0111
- Schneider, M.P.W., Scheel, T., Mikutta, R., van Hees, P., Kaiser, K., Kalbitz, K., 2010. Sorptive stabilization of organic matter by amorphous Al hydroxide. *Geochim. Cosmochim. Acta* 74, 1606–1619. doi:10.1016/j.gca.2009.12.017
- Schwertmann, U., 1991. Solubility and dissolution of iron oxides. *Plant Soil* 130, 1–25.
- Schwertmann, U., 1984. The influence of aluminium on iron oxides: IX. Dissolution of Al-goethites in 6 M HCl. *Clay Miner.* 19, 9–19. doi:10.1180/claymin.1984.019.1.02
- Schwertmann, U., Cornell, R.M., 2000. *Iron Oxides in the Laboratory: Preparation and Characterization*, 2nd ed. Wiley-VCH, Weinheim, Germany.
- Schwertmann, U., Wagner, F., Knicker, H., 2005. Ferrihydrite–Humic Associations: Magnetic Hyperfine Interactions. *Soil Sci. Soc. Am. J.* 69, 1009–1015. doi:10.2136/sssaj2004.0274
- Shimizu, M., Zhou, J., Schröder, C., Obst, M., Kappler, A., Borch, T., 2013. Dissimilatory reduction and transformation of ferrihydrite-humic acid coprecipitates. *Environ. Sci. Technol.* 47, 13375–84. doi:10.1021/es402812j
- Sidhu, P.S., 1981. Dissolution of Iron Oxides and Oxyhydroxides in Hydrochloric and Perchloric Acids. *Clays Clay Miner.* 29, 269–276. doi:10.1346/CCMN.1981.0290404
- Siéliéchi, J.M., Lartiges, B.S., Kayem, G.J., Hupont, S., Frochot, C., Thieme, J., Ghanbaja, J.,

- d'Espinose de la Caillerie, J.B., Barrès, O., Kamga, R., Levitz, P., Michot, L.J., 2008. Changes in humic acid conformation during coagulation with ferric chloride: Implications for drinking water treatment. *Water Res.* 42, 2111–2123. doi:10.1016/j.watres.2007.11.017
- Stookey, L.L., 1970. Ferrozine - a new spectrophotometric reagent for iron. *Anal. Chem.* 42, 779–781. doi:10.1021/ac60289a016
- Takagi, S., 1976. Naturally occurring iron-chelating compounds in oat- and rice-root washings. *Soil Sci. Plant Nutr.* 22, 423–433. doi:10.1080/00380768.1976.10433004
- Team, R.D.C., 2015. GNU R.
- Violante, A., Ricciardella, M., Pigna, M., 2003. Adsorption of heavy metals on mixed Fe-Al oxides in the absence or presence of organic ligands. *Water. Air. Soil Pollut.* 143, 289–306.
- Wagai, R., Mayer, L.M., 2007. Sorptive stabilization of organic matter in soils by hydrous iron oxides. *Geochim. Cosmochim. Acta* 71, 25–35. doi:10.1016/j.gca.2006.08.047
- Wang, Z., Schenkeveld, W.D.C., Kraemer, S.M., Giammar, D.E., 2015. Synergistic Effect of Reductive and Ligand-Promoted Dissolution of Goethite. *Environ. Sci. Technol.* 49, 7236–7244. doi:10.1021/acs.est.5b01191
- Waychunas, G., Rea, B., Fuller, C., Davis, J., 1993. Surface chemistry of ferrihydrite: Part 1. EXAFS studies of the geometry of coprecipitated and adsorbed arsenate. *Geochim. Cosmochim. Acta.* doi:10.1016/0016-7037(93)90567-G
- Winkelmann, G., 1992. Structures and functions of fungal siderophores containing hydroxamate and complexone type iron binding ligands. *Mycol. Res.* 96, 529–534. doi:10.1016/S0953-7562(09)80976-3
- Yoshida, T., Hayashi, K.I., Ohmoto, H., 2002. Dissolution of iron hydroxides by marine bacterial siderophore. *Chem. Geol.* 184, 1–9. doi:10.1016/S0009-2541(01)00297-2

5 SYNTHESIS

5.1 Variability of characteristics of Fe-organic associations

In order to link microbial reduction kinetics of Fe-organic associations to their physiochemical properties, both adsorption complexes and coprecipitates were synthesized combining the most important Fe oxyhydroxides found in soils (ferrihydrite, lepidocrocite, goethite, hematite, magnetite) with organic matter (OM) of different origin. Latter comprised both microbially derived OM (extracellular polymeric substances (EPS) extracted from *Bacillus subtilis*) and two different types of plant-derived natural OM (NOM) (extracted from the Oi horizon of a Eutric Cambisol under European beech and the Oa horizon of a Haplic Podzol under Norway spruce). The pure OM, pure Fe oxyhydroxides, adsorption complexes, and Fe-OM coprecipitates were characterized by nuclear magnetic resonance spectroscopy (NMR), X-ray diffraction (XRD), Fourier transform infrared spectroscopy (FTIR), X-ray photoelectron spectroscopy (XPS), N₂ gas adsorption, electrophoretic mobility and particle size measurements, and OM desorption experiments.

The specific surface area (SSA) of the pure Fe oxyhydroxides decreased in the order ferrihydrite > lepidocrocite > goethite > hematite > magnetite (359.7, 92.5, 74.1, 16.9, and 13.6 m² g⁻¹; study II, Fig. 4) mirroring the transition of the poorly crystalline characteristics of ferrihydrite to the distinctive crystallinity of hematite and magnetite, with the adsorption of EPS and NOM generally resulting in a decrease of the SSA. Analogously, coprecipitation of Fe with OM revealed significantly decreased SSA in comparison to pure ferrihydrite (study I), with XRD indicating slightly less crystalline structures.

The carbon contents of the ferrihydrite, lepidocrocite, and goethite adsorption complexes ranged from 5 to 40 mg C g⁻¹, while the carbon contents of the hematite and magnetite adsorption complexes ranged from 2 to 15 mg C g⁻¹ (study II). The coprecipitates exhibited C contents between 84 mg C g⁻¹ and 151.0 mg C g⁻¹ (study I). Our samples thus covered both

contents of topsoil horizons exceeding OC contents of 100 mg C g⁻¹ as well as subsoil horizons often displaying OC contents < 10 mg C g⁻¹ (Kaiser and Guggenberger, 2003; Tipping et al., 1999).

¹³C-NMR spectroscopy and specific UV absorption (SUVA) revealed the aromaticity of the original OM to increase in the order EPS < beech Oi < spruce Oa. The amount of FTIR- and XPS-derived carboxylic C increased in the same order (study I). The main constituents of all types of OM were carbohydrates. Unlike both types of plant-derived NOM, EPS contained significant amounts of protein structures confirmed by both FTIR and XPS. Irrespective of the OM source and type of mineral, both aromatic and carboxylic C were adsorbed and coprecipitated preferentially, supporting the larger affinity of aromatic compounds towards Fe oxides (Chorover and Amistadi, 2001; Kalbitz et al., 2005; Scheel et al., 2007). Accordingly, sorbed OM was depleted in carbohydrates in comparison to the source OM.

5.2 Enhancement of microbial Fe reduction by organic matter

Dissolved OM has been suggested to enhance microbial reduction and thereby solubility of Fe oxyhydroxides by (i) complexation of Fe(II) thus increasing thermodynamically favorable conditions for Fe(III) reduction (Roden and Urrutia, 1999; Royer et al., 2002), (ii) acting as a ligand towards Fe(III) thereby promoting solubilisation (Nevin and Lovley, 2002; Jones et al., 2009), and (iii) providing redox active electron-shuttling compounds for Fe-reducing microorganisms (Lovley et al., 1996; Jiang and Kappler, 2008; Amstatter et al., 2012; Poggenburg et al., 2016). To examine these enhancing factors, the adsorption complexes described in section 5.1 were exposed to microbial Fe(III) reduction by *Shewanella putrefaciens* and *Geobacter metallireducens* (study II).

The concentration of dissolved Fe(II) and Fe(III) after equilibration of the adsorption complexes with each respective microbial medium was below detection limit for each sample.

Moreover, the capacity of desorbed OM to complex Fe(II) estimated from its acidity (Ritchie and Perdue, 2003; Royer et al., 2002) was not large enough to account for increased Fe reduction rates by *Shewanella putrefaciens*, while no Fe(III) was detected in the 0.2- μ m filtrates after 16 days of microbial reduction, suggesting a negligible release of Fe(III) via chelating by EPS or NOM. While we cannot exclude that microbial reduction was influenced by the complexation of Fe(II) to some extent, it did not seem to exert a noticeable influence on Fe reduction of the adsorption complexes in our experiments, supporting the lack of impact of Fe(II) complexation by humic acids on ferrihydrite reduction observed by Amstaetter et al. (2012).

When examining the stimulating effect of organic compounds like humic acids on microbial Fe reduction, it is common practice to add them to a suspension of a certain Fe oxyhydroxide and review the compound concentration of the whole system without differentiating between adsorbed and dissolved C (Jiang and Kappler, 2008). Attempts to quantify the concentration of humic acids in suspensions of Fe-organic associations via specific wavelengths using UV-Vis spectrometry without determining the C concentration (Amstaetter et al., 2012), are rather unreliable as they are sensitive towards the changing density of suspensions and do not take sorptive fractionation into consideration (Kalbitz et al., 2003; Scheel et al., 2007; Schneider et al., 2010). Our approach of freeze-drying and subsequent exposure of the adsorption complexes to nutrient media-induced desorption allowed for a separate evaluation of both adsorbed and dissolved OM.

In comparison to the pure Fe oxyhydroxides, initial microbial reduction rates by *Shewanella putrefaciens* increased linearly with the amount of desorbed OC at concentrations exceeding 2 mg C L⁻¹ for spruce Oa-derived NOM and 3 mg C L⁻¹ for beech Oi-derived NOM, whereas the initial reduction rates of EPS adsorption complexes by *Shewanella putrefaciens* increased only slightly with the amount of desorbed OC (study II, Fig. 6 and 9).

In contrast, no strong correlation of adsorbed OM and initial microbial reduction rates was found.

The SUVA and NMR-derived aromaticity (study I, Table 3), the FTIR-derived phenolic compounds (study I, Fig. 1), the electron acceptor capacity (study I, Fig. 4), and the concentration of compounds prone to be reduced by *Shewanella putrefaciens* (study II, Fig. 8) each increased in the order EPS < beech Oi < spruce Oa, while the threshold concentration of observable increased microbial reduction rates decreased in the same order. Since the pre-culture of *Shewanella putrefaciens* had been grown aerobically, there were no microorganism-bound electron-shuttling molecules present at the onset of the experiments, which is why increasing microbial reduction rates can be attributed to OM-derived electron shuttling.

In contrast to *Shewanella putrefaciens*, however, no such relationship was found for *Geobacter metallireducens*, suggesting other parameters to control microbial reduction by *Geobacter metallireducens*, as discussed in section 5.3.

5.3 Inhibition of microbial Fe reduction by organic matter

Microbial reduction rates of Fe oxyhydroxides are well established to depend on their SSA (Roden, 2003). Accordingly, the initial reduction rates of pure Fe oxyhydroxides by both *Shewanella putrefaciens* and *Geobacter metallireducens* increased with rising SSA of the pure minerals (study II, Fig. 5 and 10). Following adsorption of dissolved OM to Fe oxides, however, these OM moieties might (i) block surface sites (Kaiser and Guggenberger, 2003) and (ii) induce aggregation (Amstaetter et al., 2012). Despite the potential to inhibit microbial Fe reduction, the relationship between both the SSA and particle size of adsorption complexes and microbial reduction rates had not been examined systematically so far.

Unlike for the pure Fe oxyhydroxides, the BET-derived SSA of the adsorption complexes and Fe reduction rates by *Shewanella putrefaciens* no longer correlated with each other (study II, Fig. 6). On the contrary, reduction rates even increased with increasing surface C coverage and thus decreasing SSAs. Even though *Geobacter metallireducens* incubations exhibited decreased reduction rates for the adsorption complexes in comparison to the pure Fe oxyhydroxides, suggesting surface passivation by adsorbed OM, reduction rates did not decrease with increasing C loadings of the adsorption complexes (study II, Fig. 7). The BET-derived SSA thus turned out to be a poor predictor of microbial Fe reduction rates for both species of microorganism when comparing adsorption complexes derived from different types of OM and Fe oxyhydroxides.

On the one hand, this may be attributed to the BET-derived SSA including micro- and mesopores (<50 nm), which are not entirely accessible for electron transfer via enzymes located in the cell membrane, pili, or electron-shuttling compounds (study II, Fig. 4). Preferential sorption of dissolved OM to Fe oxyhydroxides via clogging of small pores (Kaiser and Guggenberger, 2003) would therefore decrease the SSA, but not necessarily the bioavailable surface area. On the other hand, at smaller C loadings, patches of negatively charged adsorbed OM and areas of positively charged uncovered mineral surface attract each other, thus enhancing particle aggregation. At larger C loadings, aggregation is impaired by charge repulsion between the more abundant areas with negatively charged OM (Illés and Tombácz, 2006; Kaiser and Guggenberger, 2003). Adsorption complexes with smaller C loading and thus larger SSA are therefore more prone to reduction-inhibiting aggregation than adsorption complexes with larger C loadings and smaller SSA.

Unlike *Shewanella putrefaciens*, the initial reduction rates by *Geobacter metallireducens* showed an exponentially decreasing trend with increasing particle size when considering each type of OM and Fe oxyhydroxide separately (study II, Fig. 9). Noteworthy, the pure Fe oxides exhibited the smallest particle size in microbial nutrient solution in comparison to the

adsorption complexes, which can be attributed to dispersion effects by Na^+ and the repulsive negative charge imposed on the surfaces by media-derived phosphate (Gálvez et al., 1999).

Even though the reduction rates were partly dictated by the solubility of the pure Fe oxyhydroxides (study II, Fig. 7), microbial Fe reduction by *Geobacter metallireducens* was mainly controlled by the particle size of the adsorption complexes. Instead of initiating surface passivation with increasing C loading, adsorption of OM thus rather enhanced microbial Fe reduction by stabilizing smaller aggregates in suspension.

5.4 Impact of organic matter on Fe oxyhydroxide transformation

Organic matter may not only inhibit Fe reduction but also influence the transformation of Fe oxyhydroxides during microbial Fe reduction.

Fe oxyhydroxides commonly formed during microbial reductive transformation include magnetite, goethite, and lepidocrocite (Hansel et al., 2005), neither of which was detected by XRD after 16 days of incubation with *Shewanella putrefaciens* and *Geobacter metallireducens* (study I and II). Apart from media-induced phosphate, adsorbed or coprecipitated humic acids and litter extracts have been reported to decrease or impede the formation of magnetite and goethite during Fe(III) reduction of ferrihydrite (Amstaetter et al., 2012; Eusterhues et al., 2014; Henneberry et al., 2012; Shimizu et al., 2013). Both the readsorption of Fe(II) to the mineral surface required for recrystallization of goethite and lepidocrocite (Hansel et al., 2003; Thompson et al., 2006) and the even larger surface loadings required for conversion to magnetite (Hansel et al., 2005) were most likely blocked by adsorbed NOM or EPS (study I and II).

Despite the ability of OM to stimulate the formation of green rust during the microbial reduction of ferrihydrite (Amstaetter et al., 2012; Kukkadapu et al., 2004) and lepidocrocite (O'Loughlin et al., 2010; Ona-Nguema et al., 2009), green rust phases were only found for the solid post-incubation phase of hematite and magnetite spruce Oa adsorption complexes after

reduction by both *Shewanella putrefaciens* and *Geobacter metallireducens*. This observation might be attributed to the lack of CO_3^{2-} as potential interlayer anion in our microbial media, smaller initial cell numbers in comparison to the cited studies above (Ona-Nguema et al., 2009); O'Loughlin et al., 2010), or the comparably larger Fe reduction rates of the other samples (O'Loughlin et al., 2010).

Adding additional dissolved EPS or NOM to the largest C loading of each adsorption complex resulted in the solid post incubation phase exhibiting broad signals around 0.25 nm characteristically displayed in XRD patterns of Fe-OM coprecipitates (Eusterhues et al., 2008; Waychunas et al., 1993). So far, no neo-formation of Fe-OM coprecipitates during microbial reduction of Fe oxyhydroxides has been reported in other studies, in spite of previous studies working with even larger concentrations of organic C. This might either be explained by the routine of only considering crystalline phases when monitoring the mineral transformation during microbial reduction or by the Fe-OM coprecipitates being reduced again prior to analysis. Although Fe-OM coprecipitates are prone to further microbial reduction (Eusterhues et al., 2014; Shimizu et al., 2013), they might thus still prolong the mineral transformation to some extent.

The inhibition of mineral transformation was even more pronounced for the microbial reduction of Fe-OM coprecipitates (study I), since the only mineral detectable after 16 days of incubation was media-induced vivianite ($\text{Fe}_3(\text{PO}_4)_2 \cdot 8\text{H}_2\text{O}$).

5.5 Impact of adsorption vs. coprecipitation

The microbial reduction of ferrihydrite-OM coprecipitates by *Shewanella putrefaciens* generally followed the same trend as the ferrihydrite-OM adsorption complexes, as initial reduction rates increased in the order ferrihydrite < EPS coprecipitate < beech Oi coprecipitate < spruce Oa coprecipitate (study I, Fig. 5 and 6). Enhanced reactivity therefore paralleled the rise in potential electron-shuttling compounds in the OM as discussed in section

5.1. Shimizu et al. (2013) only reported increased reduction rates for humic acid-Fe coprecipitates showing C/Fe ratios larger than 4.3, thus considerably exceeding the C/Fe ratios of our study. This discrepancy might either be attributed to a larger nutrient solution-promoted desorption of OM and thus a greater absolute concentration of electron-shuttling organic groups in solution or to the method of coprecipitate preparation used by Shimizu et al. (2013), which most likely caused more aggregated structures and thus decreased reduction rates in comparison to our coprecipitates. In contrast to *Shewanella putrefaciens* and in line with the microbial reduction of ferrihydrite-OM adsorption complexes, initial Fe reduction rates by *Geobacter metallireducens* exponentially decreased with increasing particle size (Study I, Fig. 5 and 6), whereas there was no correlation with the BET-derived SSA. Since ferrihydrite exhibited the smallest particle size, this observation is in accordance with Eusterhues et al. (2014), who found decreased Fe reduction rates by *Geobacter bremensis* for Fe-OM coprecipitates in comparison to pure ferrihydrite.

Despite a smaller concentration of desorbed OM, a smaller SSA, and comparable particle sizes, the reduction rates of the Fe-OM coprecipitates by *Shewanella putrefaciens* were larger than the ones of the ferrihydrite-OM adsorption complexes exhibiting the largest C content (study II, Fig. 6a and 9). Similarly, the reduction rates of the Fe-OM coprecipitates by *Geobacter metallireducens* were larger than the ones of the ferrihydrite-OM adsorption complexes exhibiting the largest C content, although the particle sizes of the coprecipitates were not significantly larger than their adsorption complexes counterparts (study II, Fig. 7a and 9). As the major difference between coprecipitates and adsorption complexes lies with the decreased crystallinity of the former in comparison to the latter, the increased microbial reduction rates can most likely be explained by the more defective crystal structure. Roden (2003) suggested that microbial reduction rates of Fe oxides are controlled by the available surface sites rather than by the thermodynamic properties of the underlying oxide crystals. In contrast, Eusterhues et al. (2014) attributed faster reaction rates of coprecipitates by

Geobacter bremensis to a more defective crystal structure with increasing incorporation of OM. While the results of Roden (2003) may be applicable to pure Fe oxyhydroxides with a uniform distribution of crystal properties, surface site access and crystal structure of coprecipitates may change throughout the microbial reduction even without considering microbial or secondary mineral transformation. Variations in the amount of OM released, as different parts of the coprecipitate are dissolved, in addition to the preferential reduction of pure ferrihydrite, may change the aggregation state of coprecipitates during reduction to a larger extent than possible for pure Fe oxides.

Coprecipitated OM is generally considered more stable than adsorbed OM, since Fe-OM coprecipitates display decreased desorption in comparison to adsorption complexes at similar C contents, which is assumed to be a precursor for decomposition (Pan et al., 2016). If they are more prone to microbial reduction, however, coprecipitated OM is more likely to be mobilized than adsorbed OM, and thus more prone to decomposition.

5.6 Impact of electron transfer mechanism on microbial Fe reduction

In addition to the properties of Fe-organic associations, including the type of OM present, the microbial reduction of both adsorption complexes and coprecipitates may further depend on the Fe respiration pathways of the Fe-reducing bacteria. *Shewanella* species have been shown to excrete molecules acting as electron shuttles rather than transferring electrons via direct contact to the mineral (Kotloski and Gralnick, 2013; von Canstein et al., 2008), whereas *Geobacter* species have been suggested to transfer electrons by both direct contact to the Fe oxyhydroxide and by using conductive nanowires (Boesen and Nielsen, 2013; Malvankar et al., 2011).

The initial reduction rates of the pure Fe oxyhydroxides by both *Shewanella putrefaciens* and *Geobacter metallireducens* increased with rising SSA (study II, Fig. 10). The responses

of each type of microorganism to OM in relation to Fe reduction, however, differed considerably.

For both adsorption complexes (study II) and coprecipitates (study I), the microbial Fe reduction by *Shewanella putrefaciens* was governed by OM-derived electron shuttling. Using OM-derived exogenous electron-shuttling compounds is energetically more favorable for an microorganism than producing endogenous electron-shuttling molecules themselves.

In spite of several studies reporting *Geobacter* species to be able to reduce extracellular quinone moieties (Scott et al., 1998) and humic acid (Jiang and Kappler, 2008; Lovley et al., 1996) without Fe present in solution, both adsorbed and coprecipitated OM caused a decrease in reduction by *Geobacter metallireducens* in comparison to each respective pure Fe oxide. The discrepancy between the cited publications and our studies not being indicative of electron shuttling playing a major role for microbial Fe reduction by *Geobacter metallireducens*, can most likely be attributed to the missing influence of surface coverage and aggregation in studies with pure dissolved organic compounds.

To assess the ability of both *Shewanella putrefaciens* and *Geobacter metallireducens* to reduce OM-derived organic moieties which might act as electron-shuttling compounds, all types of NOM were incubated with each respective microorganism while monitoring the production of CO₂ according to equation 1.2 and 1.3 in section 1.2 (study II, Fig. 8). While this method is not suitable for quantifying the exact electron shuttling capacity for each respective OM, it still displayed the different capabilities of both types of microorganisms to transfer electrons to the different types of OM used in our experiments. The production of CO₂ during the incubation of dissolved OM was generally significantly smaller for *Geobacter metallireducens* than for *Shewanella putrefaciens*.

Despite a slight accelerating influence of electron shuttling, not even a NOM concentration of 50 mg C L⁻¹ was large enough to outweigh the aggregation-induced inhibition of Fe reduction by *Geobacter metallireducens* in comparison to pure Fe oxyhydroxides, which is an

uncharacteristically large concentration of free dissolved OM in many Fe-reducing soil environments. Thus, a considerably larger concentration of electron-shuttling compounds in plant-derived water-extractable OM seemed to be required to noticeably stimulate Fe reduction by *Geobacter metallireducens* than by *Shewanella putrefaciens*.

The Fe reduction by *Geobacter metallireducens* was mainly controlled by the particle size of the adsorption complexes and coprecipitates. For the reduction of adsorption complexes with small C loadings and larger particle sizes by *Shewanella putrefaciens*, it was not possible to differentiate whether aggregation outweighed the stimulation of reduction via electron shuttling or whether the concentration of electron-shuttling molecules was *per se* not large enough. In contrast to *Geobacter metallireducens*, however, OM-induced aggregation did not result in smaller reduction rates in comparison to the pure Fe oxides in our experiments with *Shewanella putrefaciens*. Aggregation-induced decreased Fe reduction rates found for ferrihydrite-humic acid adsorption complexes by *Shewanella putrefaciens* (Amstaetter et al., 2012) were most likely caused by larger Fe concentrations rather than by OM-induced aggregation.

5.7 Ligand-promoted dissolution

Not only bacteria, but fungi and graminaceous plants as well exude Fe-chelating siderophores into the soil solution (Neilands, 1957; Roemheld, 1991; Takagi, 1976; Winkelmann, 1992) to increase the availability of otherwise poorly soluble Fe oxyhydroxides. While low molecular weight organic (LMWO) acids common in soil like oxalate, citrate, malonate and ascorbate have been suggested to increase dissolution rates of Fe oxyhydroxides by the siderophore desferrioxamine-B (DFOB) due to synergistic effects (Cheah et al., 2003; Mikutta and Kretzschmar, 2008; Reichard et al., 2007; Wang et al., 2015), the impact of more complex, heterogeneous soil OM adsorbed to or coprecipitated with Fe oxyhydroxides was

not addressed systematically in the past. To elucidate the effect of EPS and NOM on siderophore-promoted dissolution of Fe-OM associations in relation to (i) surface site coverage and/or pore blockage, (ii) aggregation state, (iii) charge characteristics, and (iv) crystallinity, ferrihydrite-OM adsorption complexes and coprecipitates were subjected to DFOB-induced dissolution at pH 7 and pH 4.

Irrespective of the type of OM, at pH 7, the initial Fe dissolution rates of the adsorption complexes generally decreased along with increasing C loadings and thus decreasing SSA (study III, Fig. 4), which agrees with previous abiotic dissimilatory reduction experiments conducted with similar samples (Eusterhues et al., 2014). However, pure ferrihydrite exhibited one of the smallest dissolution rates despite displaying the largest SSA, thus pointing towards a combined effect of both surface coverage and degree of aggregation indicated by the particle size seemed likely. At pH 4, the ligand-promoted dissolution of pure ferrihydrite was elevated by 50 % in comparison to pH 7 (study III, Fig. 5), which could be ascribed to the faster recovery of the surface site after detachment of the Fe atom due to a faster protonation at lower pH (Wieland, 1988) and the smaller particle size of ferrihydrite in comparison to pH 7. In contrast to dissolution at pH 7, adsorption of OM resulted in decreased initial dissolution rates in comparison to ferrihydrite for all types of OM (study III, Figure 5) with a similar pattern of decreasing initial dissolution rates with increasing C loading. In comparison to pH 7, desorption of OM at pH 4 was negligible (study III, Table 1), whereas at pH 7, up to 20 % of the OM was desorbed upon suspension of the adsorption complexes in background electrolyte (Table 1) thus diminishing the influence of OM-induced surface site blockage. Overall, a smaller available mineral surface area in combination with larger particle sizes thus accounted for the smaller dissolution rates of the adsorption complexes at pH 4.

The impact of coprecipitated OM on ligand-promoted dissolution generally followed the same trends as adsorbed OM (study III, Fig. 4 and 5). At pH 7, the initial dissolution rates of

the Fe-OM coprecipitates significantly surpassed the dissolution of pure ferrihydrite, whereas at pH 4, dissolution of the EPS and beech Oi coprecipitate was significantly smaller. The spruce Oa coprecipitate represented an exception, considerably exceeding the dissolution rates of all samples at both pH 4 and pH 7. Since the XRD-derived disturbance of the mineral structure was most pronounced for the spruce Oa coprecipitate (study I, Fig. 3) and less crystalline and generally irregular structures are preferentially dissolved (Schwertmann, 1984), the considerably larger dissolution rates for the spruce Oa coprecipitate can most likely be attributed to its more defective structure.

Overall, the OM-induced inhibition of siderophore-promoted dissolution seemed to be more pronounced at pH 4 than at pH 7. Microorganisms that prefer circumneutral conditions and acquire Fe via chelating compounds should thus be less affected. Particularly the rhizosphere, however, usually exhibits lower pH values, as organic acids and protons are released into the soil via plant roots (April and Keller, 1990; Bonneville et al., 2011; Brantley et al., 2011). Since top soils usually exhibit larger OM contents (Kalbitz et al., 2000), acquisition of Fe by plants releasing siderophores into the soil might therefore be inhibited by adsorbed OM to some extent.

5.8 Microbial reduction vs. mediated electrochemical reduction

One major drawback of examining microbial as well as abiotic Fe reduction kinetics lies in the usual necessity of applying indirect measurements to determine Fe(II) contents and thus decoupling the quantification of the reduced species from the actual experiment. The novel analytical approach of mediated electrochemical reduction (MER) allows for continuous monitoring of the changing electron acceptor capacity during sample reduction at a constant redox potential (Sander et al., 2015). Despite this, no previous studies examining the mediated electrochemical reduction as of Fe-OM coprecipitates existed before. The MER of pure ferrihydrite and the coprecipitates was conducted at two different reduction potentials E_h

(-0.49 V and -0.28 V) using four different mediators (cyanoviologen (1,1'-bis(cyanomethyl)-4,4'-bipyridyl) (CV), riboflavin 5'-monophosphate sodium salt (RF), diquat dibromide monohydrate (1,1'-ethylene-2,2'-bipyridyl) (DQ), and zwitterionic viologen (4,4'-bipyridinium-1,1'-bis(2-ethylsulfonate)) (ZiV)).

The electron accepting capacity (EAC; i.e., the number of electrons transferred to a mass unit of analyte) of ferrihydrite and the coprecipitates determined by MER were approximately equal to the Fe(III) content determined by acidic digestion (study I, Fig. 4a), thus confirming the applicability of MER to Fe-OM coprecipitates.

Pseudo-first-order rate constants for the MER of coprecipitates showing similar C contents were larger than those of pure ferrihydrite and decreased exponentially with increasing particle sizes of the coprecipitates (study I, Fig. 4). This trend indicates that the electron transfer rate of the coprecipitates was dictated by the aggregate size and not related to SSA. The rates of electron transfer to coprecipitates containing a larger amount of OM, however, were no longer correlated to their particle size. Instead, electron transfer rates increased along with increasing C contents, pointing towards reduction rates being controlled by the more defective crystal structure induced by increasing OM contents of the coprecipitates.

The total EAC of the coprecipitates determined by MER did not depend on the electron transfer mediator used (study I, Fig. 4). The pseudo-first-order rate constants, however, increased with decreasing potential applied to the working electrode. At the same time, mediators containing sulfonate (ZiV) or phosphate groups (RF) caused decreased electron transfer rates initiated by sorption of the mentioned groups to ferrihydrite surfaces (Stumm, 1997). The chemical structure of the electron transfer mediator might thus exert a larger influence on electrochemical reduction kinetics than the electrochemical potential difference between the sample and the working electrode.

Analogous to microbial Fe reduction by *Geobacter metallireducens*, electrochemical reduction of ferrihydrite and the Fe-OM coprecipitates was thus affected by both aggregation state and crystallinity, whereas no influence of surface passivation was detected. In contrast to reduction by *Shewanella putrefaciens*, the electron-shuttling capacity of coprecipitated OM exerted no noticeable influence on electrochemical reduction. While MER thus offers an accurate way to determine the EAC of Fe-OM coprecipitates, our results suggest that the electrochemical stability of Fe-OM coprecipitates cannot easily be used to deduce their durability under natural soil conditions, as different electron transfer mechanisms applied by different genera of microorganisms result in different parameters impacting the reactivity and therefore stability of coprecipitates.

6 CONCLUSIONS AND OUTLOOK

The general objective of this thesis was to systematically assess the impact of the composition and concentration of both adsorbed and coprecipitated naturally occurring OM on microbial, ligand-promoted, and electrochemical reduction and dissolution of Fe-organic associations. Seeking to elucidate these processes, our study was the first one to...

- (i) prepare adsorption complexes with defined C contents for microbial reduction in addition to quantifying both adsorbed and easily desorbable C,
- (ii) systematically assess the particle size in suspension and the specific surface area of adsorption complexes in relation to microbial reduction,
- (iii) combine different types of plant- and microbially-derived OM in relation to microbial Fe reduction as opposed to using OM fractions,
- (iv) examine the impact of both plant- and microbially-derived coprecipitated OM on microbial reduction with regard to its composition and in comparison to adsorbed OM,
- (v) conduct microbial Fe reduction experiments with both *Shewanella putrefaciens* and *Geobacter metallireducens* using the same samples for both species applying the same experimental conditions,
- (vi) explore the effect of more complex, heterogeneous natural organic matter adsorbed to Fe oxyhydroxide on siderophore-promoted dissolution, and
- (vii) apply MER to Fe-organic associations.

While none of the initially stated hypotheses had to be rejected entirely, most of them had to be modified to some extent:

- H1** Dissolved organic matter enhances microbial reduction of Fe oxyhydroxides by *Shewanella putrefaciens* by providing redox active electron-shuttling compounds with a minor contribution by complexation of Fe(II, III).
- H2** Adsorbed and coprecipitated organic matter inhibits microbial reduction of Fe oxyhydroxides by blocking surface sites to some degree for microbial Fe reduction by *Geobacter metallireducens*. The particle or aggregation size may be a more suitable parameter to assess the bioavailable surface area than the BET-derived SSA.
- H3** Organic matter inhibits the transformation of Fe oxyhydroxides during microbial Fe reduction in comparison to pure Fe oxyhydroxides most likely by blocking readsorption sites for Fe(II).
- H4** Ferrihydrite-organic matter coprecipitates are more prone to microbial reduction than ferrihydrite-organic matter adsorption complexes due to their more defective crystal structure.
- H5** Fe-reducing bacteria using different electron transfer mechanisms are affected by adsorbed and coprecipitated OM to differing degrees. Microbial reduction of Fe-organic associations by *Shewanella putrefaciens* is mainly controlled by the concentration of electron-shuttling molecules provided by OM, whereas microbial reduction of Fe-organic associations by *Geobacter metallireducens* is mainly controlled by the OM-induced stabilization of aggregates.
- H6** Ligand-promoted dissolution of ferrihydrite is inhibited by adsorbed and coprecipitated organic matter via surface site blockage at pH 4, whereas the stabilization of aggregates by sorbed OM at pH 7 rather results in enhanced dissolution.
- H7** Mediated electrochemical reduction assesses the redox state of ferrihydrite and ferrihydrite-organic matter coprecipitates. Their stability against electrochemical reduction does not necessarily mirror their stability against microbial reductive mobilization.

Experiments aiming to explore distinct processes of a system as complex as the soil always have to be interpreted with some extra precaution, particularly bearing in mind that in spite of all the advances in analytical techniques, the actual structure of both ferrihydrite and soil organic matter has not been resolved to this day. Nevertheless, the findings of this thesis suggest that the influence of OM on the stability of Fe-organic associations against microbial mobilization in soils cannot easily be assessed without considering the heterogeneous composition of soil OM and the microbial soil community.

Experiments using pure Fe oxyhydroxides found huge impacts on Fe mobilization under flow through conditions (Liang et al., 2008; Roden et al., 2000), flow interruption cycles (Carstens et al., 2017), and redox oscillations (Thompson et al., 2006). Ideally, these experimental conditions should be combined with the experimental approach of our study to move yet another tiny step towards the main goal of understanding the microbially-mediated transformation and mobilization of Fe-organic associations in the soil.

References

- Amstaetter, K., Borch, T., Kappler, A., 2012. Influence of humic acid imposed changes of ferrihydrite aggregation on microbial Fe(III) reduction. *Geochim. Cosmochim. Acta* 85, 326–341. doi:10.1016/j.gca.2012.02.003
- April, R., Keller, D., 1990. Mineralogy of the rhizosphere in forest soils of the eastern United States. *Biogeochemistry*. doi:10.1007/BF00002714
- Boesen, T., Nielsen, P., 2013. Molecular dissection of bacterial nanowires. *MBio* 4, e00270-13. doi:10.1128/mBio.00270-13. Copyright
- Bonneville, S., Morgan, D.J., Schmalenberger, A., Bray, A., Brown, A., Banwart, S.A., Benning, L.G., 2011. Tree-mycorrhiza symbiosis accelerate mineral weathering: Evidences from nanometer-scale elemental fluxes at the hypha-mineral interface. *Geochim. Cosmochim. Acta* 75, 6988–7005. doi:10.1016/j.gca.2011.08.041
- Brantley, S.L., Megonigal, J.P., Scatena, F.N., Balogh-Brunstad, Z., Barnes, R.T., Bruns, M.A., Van Cappellen, P., Dontsova, K., Hartnett, H.E., Hartshorn, A.S., Heimsath, A., Herndon, E., Jin, L., Keller, C.K., Leake, J.R., Mcdowell, W.H., Meinzer, F.C., Mozdzer, T.J., Petsch, S., Pett-Ridge, J., Pregitzer, K.S., Raymond, P.A., Riebe, C.S., Shumaker, K., Sutton-Grier, A., Walter, R., Yoo, K., 2011. Twelve testable hypotheses on the geobiology of weathering. *Geobiology* 9, 140–165. doi:10.1111/j.1472-4669.2010.00264.x
- Carstens, J.F., Bachmann, J., Neuweiler, I., 2017. Effects of flow interruption on transport and retention of iron oxide colloids in quartz sand. *Colloids Surfaces A Physicochem. Eng. Asp.* 520, 532–543. doi:10.1016/j.colsurfa.2017.02.003
- Cheah, S.-F., Kraemer, S.M., Cervini-Silva, J., Sposito, G., 2003. Steady-state dissolution kinetics of goethite in the presence of desferrioxamine B and oxalate ligands: implications for the microbial acquisition of iron. *Chem. Geol.* 198, 63–75. doi:10.1016/S0009-2541(02)00421-7
- Chorover, J., Amistadi, M.K., 2001. Reaction of forest floor organic matter at goethite, birnessite and smectite surfaces. *Geochim. Cosmochim. Acta* 65, 95–109.
- Eusterhues, K., Hädrich, A., Neidhardt, J., Küsel, K., Keller, T.F., Jandt, K.D., Totsche, K.U., 2014. Reduction of ferrihydrite with adsorbed and coprecipitated organic matter: microbial reduction by *Geobacter bremensis* vs. abiotic reduction by Na-dithionite. *Biogeosciences* 11, 4953–4966. doi:10.5194/bg-11-4953-2014
- Eusterhues, K., Wagner, F.E., Häusler, W., Hanzlik, M., Knicker, H., Totsche, K.U., Kögel-Knabner, I., Schwertmann, U., 2008. Characterization of ferrihydrite-soil organic matter coprecipitates by X-ray diffraction and Mössbauer spectroscopy. *Environ. Sci. Technol.* 42, 7891–7.
- Hansel, C.M., Benner, S.G., Fendorf, S., 2005. Competing Fe (II)-induced mineralization pathways of ferrihydrite. *Environ. Sci. Technol.* 39, 7147–53.
- Hansel, C.M., Benner, S.G., Neiss, J., Dohnalkova, A., Kukkadapu, R.K., Fendorf, S., 2003. Secondary mineralization pathways induced by dissimilatory iron reduction of ferrihydrite under advective flow. *Geochim. Cosmochim. Acta* 67, 2977–2992. doi:10.1016/S0016-7037(03)00276-X
- Henneberry, Y.K., Kraus, T.E.C., Nico, P.S., Horwath, W.R., 2012. Structural stability of coprecipitated natural organic matter and ferric iron under reducing conditions. *Org. Geochem.* 48, 81–89. doi:10.1016/j.orggeochem.2012.04.005
- Illés, E., Tombácz, E., 2006. The effect of humic acid adsorption on pH-dependent surface charging and aggregation of magnetite nanoparticles. *J. Colloid Interface Sci.* 295, 115–123. doi:10.1016/j.jcis.2005.08.003
- Jiang, J., Kappler, A., 2008. Kinetics of microbial and chemical reduction of humic substances: implications for electron shuttling. *Environ. Sci. Technol.* 42, 3563–9.

- Jones, A.M., Collins, R.N., Rose, J., Waite, T.D., 2009. The effect of silica and natural organic matter on the Fe(II)-catalysed transformation and reactivity of Fe(III) minerals. *Geochim. Cosmochim. Acta* 73, 4409–4422. doi:10.1016/j.gca.2009.04.025
- Kaiser, K., Guggenberger, G., 2003. Mineral surfaces and soil organic matter. *Eur. J. Soil Sci.* 54, 219–236.
- Kalbitz, K., Schwesig, D., Rethemeyer, J., Matzner, E., 2005. Stabilization of dissolved organic matter by sorption to the mineral soil. *Soil Biol. Biochem.* 37, 1319–1331. doi:10.1016/j.soilbio.2004.11.028
- Kalbitz, K., Schwesig, D., Schmerwitz, J., Kaiser, K., Haumaier, L., Glaser, B., Ellerbrock, R., Leinweber, P., 2003. Changes in properties of soil-derived dissolved organic matter induced by biodegradation. *Soil Biol. Biochem.* 35, 1129–1142. doi:10.1016/S0038-0717(03)00165-2
- Kalbitz, K., Solinger, S., Park, J.-H., Michalzik, B., Matzner, E., 2000. Controls on the Dynamics of Dissolved Organic Matter in Soils: a Review. *Soil Sci.* 165, 277–304. doi:10.1097/00010694-200004000-00001
- Kotloski, N.J., Gralnick, J.A., 2013. Flavin electron shuttles dominate extracellular electron transfer by *Shewanella oneidensis*. *MBio* 4, 10–13. doi:10.1128/mBio.00553-12
- Kukkadapu, R.K., Zachara, J.M., Fredrickson, J.K., Kennedy, D.W., 2004. Biotransformation of two-line silica-ferrihydrite by a dissimilatory Fe(III)-reducing bacterium: formation of carbonate green rust in the presence of phosphate. *Geochim. Cosmochim. Acta* 68, 2799–2814. doi:10.1016/j.gca.2003.12.024
- Liang, L., Hofmann, A., Gu, B., 2008. Ligand-induced dissolution and release of ferrihydrite colloids. *Geochim. Cosmochim. Acta* 64, 2027–2037.
- Lovley, D.R., Coates, J.D., Blunt-Harris, E.L., Phillips, E.J.P., Woodward, J.C., 1996. Humic substances as electron acceptors for microbial respiration. *Nature* 382, 445–448.
- Malvankar, N.S., Vargas, M., Nevin, K.P., Franks, A.E., Leang, C., Kim, B.-C., Inoue, K., Mester, T., Covalla, S.F., Johnson, J.P., Rotello, V.M., Tuominen, M.T., Lovley, D.R., 2011. Tunable metallic-like conductivity in microbial nanowire networks. *Nat. Nanotechnol.* 6, 573–579. doi:10.1038/nnano.2011.119
- Mikutta, C., Kretzschmar, R., 2008. Synthetic coprecipitates of exopolysaccharides and ferrihydrite. Part II: Siderophore-promoted dissolution. *Geochim. Cosmochim. Acta* 72, 1128–1142. doi:10.1016/j.gca.2007.11.034
- Neilands, J.B., 1957. Some aspects of microbial iron metabolism. *Anal. Biochem.* 21, 220–230.
- Nevin, K.P., Lovley, D.R., 2002. Mechanisms for Fe(III) oxide reduction in sedimentary environments. *Geomicrobiol. J.* 19, 141–159. doi:10.1080/01490450252864253
- O’Loughlin, E.J., Gorski, C.A., Cook, R.E., Kemner, K.M., Boyanov, M.I., Scherer, M.M., 2010. Effects of oxyanions and natural organic matter on the bioreduction of lepidocrocite (γ -FeOOH) and the formation of secondary mineralization products. *Environ. Sci. Technol.* 44, 4570–4576. doi:10.1021/es100294w
- Ona-Nguema, G., Morin, G., Wang, Y., Menguy, N., Juillot, F., Olivi, L., Aquilanti, G., Abdelmoula, M., Ruby, C., Bargar, J.R., Guyot, F., Calas, G., Brown, G.E., 2009. Arsenite sequestration at the surface of nano-Fe(OH)₂, ferrous-carbonate hydroxide, and green-rust after bioreduction of arsenic-sorbed lepidocrocite by *Shewanella putrefaciens*. *Geochim. Cosmochim. Acta* 73, 1359–1381. doi:10.1016/j.gca.2008.12.005
- Pan, W., Kan, J., Inamdar, S., Chen, C., Sparks, D., 2016. Dissimilatory microbial iron reduction release DOC (dissolved organic carbon) from carbon-ferrihydrite association. *Soil Biol. Biochem.* 103, 232–240. doi:10.1016/j.soilbio.2016.08.026
- Piepenbrock, A., Dippon, U., Porsch, K., Appel, E., Kappler, A., 2011. Dependence of microbial magnetite formation on humic substance and ferrihydrite concentrations. *Geochim. Cosmochim. Acta* 75, 6844–6858. doi:10.1016/j.gca.2011.09.007

- Reichard, P.U., Kretzschmar, R., Kraemer, S.M., 2007. Dissolution mechanisms of goethite in the presence of siderophores and organic acids. *Geochim. Cosmochim. Acta* 71, 5635–5650. doi:10.1016/j.gca.2006.12.022
- Ritchie, J.D., Perdue, E.M., 2003. Proton-binding study of standard and reference fulvic acids, humic acids, and natural organic matter. *Geochim. Cosmochim. Acta* 67, 85–93. doi:10.1016/S0016-7037(02)01044-X
- Roden, E.E., 2003. Fe(III) oxide reactivity toward biological versus chemical reduction. *Environ. Sci. Technol.* 37, 1319–1324. doi:10.1021/es026038o
- Roden, E.E., Urrutia, M.M., 1999. Ferrous iron removal promotes microbial reduction of crystalline iron(III) oxides. *Environ. Sci. Technol.* 33, 1847–1853. doi:10.1021/es9809859
- Roden, E.E., Urrutia, M.M., Mann, C.J., 2000. Bacterial reductive dissolution of crystalline Fe (III) oxide in continuous-flow column reactors. *Appl. Environ. Microbiol.* 66, 1062–1065. doi:10.1128/AEM.66.3.1062-1065.2000.Updated
- Roemheld, V., 1991. The Role of phytosiderophores in aquisition of iron and other micronutrients in graminaceous species: an ecological approach. *Plant Soil* 130, 127–134.
- Royer, R.A., Burgos, W.D., Fisher, A.S., Jeon, B.-H., Unz, R.F., Dempsey, B. a, 2002. Enhancement of hematite bioreduction by natural organic matter. *Environ. Sci. Technol.* 36, 2897–904. doi:10.1021/es015735y
- Sander, M., Hofstetter, T.B., Gorski, C.A., 2015. Electrochemical analyses of redox-active iron minerals: A review of non-mediated and mediated approaches. *Environ. Sci. Technol.* 49, 5862–5878. doi:10.1021/acs.est.5b00006
- Scheel, T., Dörfel, C., Kalbitz, K., 2007. Precipitation of dissolved organic matter by aluminum stabilizes carbon in acidic forest soils. *Soil Sci. Soc. Am. J.* 71, 64–74. doi:10.2136/sssaj2006.0111
- Schneider, M.P.W., Scheel, T., Mikutta, R., van Hees, P., Kaiser, K., Kalbitz, K., 2010. Sorptive stabilization of organic matter by amorphous Al hydroxide. *Geochim. Cosmochim. Acta* 74, 1606–1619. doi:10.1016/j.gca.2009.12.017
- Schwertmann, U., 1984. The influence of aluminium on iron oxides: IX. Dissolution of Al-goethites in 6 M HCl. *Clay Miner.* 19, 9–19. doi:10.1180/claymin.1984.019.1.02
- Scott, D.T., McKnight, D.M., Blunt-Harris, E.L., Kolesar, S.E., Lovley, D.R., 1998. Quinone moieties act as electron acceptors in the reduction of humic substances by humics-reducing microorganisms. *Environ. Sci. Technol.* 32, 2984–2989. doi:10.1021/es980272q
- Shimizu, M., Zhou, J., Schröder, C., Obst, M., Kappler, A., Borch, T., 2013. Dissimilatory reduction and transformation of ferrihydrite-humic acid coprecipitates. *Environ. Sci. Technol.* 47, 13375–84. doi:10.1021/es402812j
- Stumm, W., 1997. Reactivity at the mineral-water interface: dissolution and inhibition. *Colloids and Surfaces* 120, 143–166.
- Takagi, S., 1976. Naturally occurring iron-chelating compounds in oat- and rice-root washings. *Soil Sci. Plant Nutr.* 22, 423–433. doi:10.1080/00380768.1976.10433004
- Thompson, A., Chadwick, O.A., Rancourt, D.G., Chorover, J., 2006. Iron-oxide crystallinity increases during soil redox oscillations. *Geochim. Cosmochim. Acta* 70, 1710–1727. doi:10.1016/j.gca.2005.12.005
- Tipping, E., Woof, C., Rigg, E., Harrison, A.F., Ineson, P., Taylor, K., Benham, D., Poskitt, J., Rowland, A.P., R, B., Harkness, D.D., 1999. Climatic influences on the leaching of dissolved organic matter from upland UK moorland soils, investigated by a field manipulation experiment. *Environ. Int.* 25, 83–95. doi:10.1016/S0160-4120(98)00098-1
- von Canstein, H., Ogawa, J., Shimizu, S., Lloyd, J.R., 2008. Secretion of flavins by *Shewanella* species and their role in extracellular electron transfer. *Appl. Environ.*

- Microbiol. 74, 615–23. doi:10.1128/AEM.01387-07
- Wang, Z., Schenkeveld, W.D.C., Kraemer, S.M., Giammar, D.E., 2015. Synergistic effect of reductive and ligand-promoted dissolution of goethite. *Environ. Sci. Technol.* 49, 7236–7244. doi:10.1021/acs.est.5b01191
- Waychunas, G., Rea, B., Fuller, C., Davis, J., 1993. Surface chemistry of ferrihydrite: Part 1. EXAFS studies of the geometry of coprecipitated and adsorbed arsenate. *Geochim. Cosmochim. Acta.* doi:10.1016/0016-7037(93)90567-G
- Winkelmann, G., 1992. Structures and functions of fungal siderophores containing hydroxamate and complexone type iron binding ligands. *Mycol. Res.* 96, 529–534. doi:10.1016/S0953-7562(09)80976-3

Acknowledgements

First of all, I would like to thank my supervisors Professor Dr. Georg Guggenberger and Professor Dr. Robert Mikutta, without whom this work would never have been possible, and Professor Dr. Francois Holtz for kindly taking on the role of a chairman.

Furthermore, I am deeply indebted to the lab experts of the Institute of Soil Science, especially Roger-Michael Klatt, Pieter Wiese, Ulrike Pieper, Hilal Alemdar, and Dr. Poldi Sauheidl; my colleagues at the Institute of Soil Science, especially Dr. Susanne Woche, Dr. Birgit Schampera, Sandra Meyer-Stüve, Dr. Katharina Leiber-Sauheidl, Dr. Stefan Dultz, and Dr. Jens Boy; the Microbiology Group at the BGR, especially Dr. Axel Schippers, Dr. Reiner Dohrmann, Gudrun Mengel-Jung, and Cornelia Struckmeyer; the Institute of Biogeochemistry and Pollutant Dynamics at the ETH Zurich, especially Dr. Michael Sander; the Institute of Organic Chemistry, especially Dr. Alexander Marchanka; my industrious student helpers Patrick Liebmann, Markus Koch, Fabian Kalks, Marie Rinne, Britta Osterkamp, and Alexander Schek; the Soil Physics Coffee Support Group, Jiem Krüger and Timo Leinemann; little Timo and his mother Annika Dechêne; and last but by no means least my office mates and all around wonderful human beings Joanna & Christian Weiss and Anja Freund.

Most of all, I am more than grateful for the moral support of my awesome friends and family.

Lebenslauf

Persönliche Angaben

Name: Christine Poggenburg
Geburtsdatum: 04.09.1985
E-Mail: poggenburg@ifbk.uni-hannover.de

Berufserfahrung

seit 09/2017 Wissenschaftliche Mitarbeiterin am Institut für Bodenkunde Hannover als Bearbeiterin des Projektes „Characterization of structure and properties of bioorganoclays - perspective hybrid materials“

04/2016 – 08/2017 Wissenschaftliche Mitarbeiterin am Institut für Bodenkunde Hannover als Bearbeiterin des Projektes „Global comparison of the biogenic weathering rates of mycorrhiza“

03/2012 – 03/2016 Wissenschaftliche Mitarbeiterin am Institut für Bodenkunde Hannover als Bearbeiterin des Projektes „Microbially-mediated transformation and mobilization of Fe-organic associations in the critical zone“

Ausbildung

03/2012 – 07/2017 Promotionsstudentin am Institut für Bodenkunde Hannover

10/2005 – 02/2012 Studium der Geowissenschaften an der Leibniz Universität Hannover
Abschluss: Diplom

09/1998 – 06/2005 Gymnasium Isernhagen
Abschluss: Abitur

Studienbezogene Tätigkeiten

08-09/2010 Praktikum an der Bundesanstalt für Geowissenschaften und Rohstoffe im Arbeitsbereich „Stofflicher Bodenschutz, Bodenanalytik“ des Fachbereichs B 2.4 (Boden als Ressource)

04/2009 – 09/2009 Wissenschaftliche Hilfskraft für Dr. Stefan Dultz, Institut für Bodenkunde, Leibniz Universität Hannover

11/2007 – 06/2008 Wissenschaftliche Hilfskraft für Heinz Hunfeld, Institut für angewandte Biotechnologie der Tropen, Georg-August-Universität Göttingen

06/2007 – 11/2007 Wissenschaftliche Hilfskraft an der Bundesanstalt für Geowissenschaften und Rohstoffe im Referat B 3.22 (Strukturgeologie)

08/2007 Praktikum an der Bundesanstalt für Geowissenschaften und Rohstoffe in den Referaten B 3.23 (Meeresgeologie, Tiefseebergbau), B 3.25 (Stratigraphie, Sammlungen), B 4.11 (Organische Geochemie, Organische Petrographie)

Publications

Poggenburg C., Mikutta R., Sander M., Schippers A., Marchanka A., Dohrmann R. and Guggenberger G. (2016) Microbial reduction of ferrihydrite-organic matter coprecipitates by *Shewanella putrefaciens* and *Geobacter metallireducens* in comparison to mediated electrochemical reduction. *Chem. Geol.* **447**, 133-147, doi: 10.1016/j.chemgeo.2016.09.031.

Poggenburg C., Mikutta R., Schippers A., Dohrmann R. and Guggenberger G. (2018) Impact of Natural Organic Matter Coatings on the Microbial Reduction of Iron Oxides. *Geochim. Cosmochim. Acta* **224**, 223-248, doi: 10.1016/j.gca.2018.01.004.

Poggenburg C., Mikutta R., Liebmann P., Koch M. and Guggenberger G.
Impact of soil organic matter on siderophore-promoted dissolution of ferrihydrite-organic associations at different pH
Submitted for publication in Organic Geochemistry